Looking for new physics beyond the Standard Model through flavour transitions

A thesis

submitted to the

Tata Institute of Fundamental Research, Mumbai
for the degree of Doctor of Philosophy
in Physics

by

Diptimoy Ghosh

Department of Theoretical Physics
Tata Institute of Fundamental Research
Mumbai

Submitted on April 19, 2012

Final version accepted on July 17, 2012

Declaration

This thesis is a presentation of my original research work. Wherever contributions of others are involved, every effort is made to indicate this clearly, with due reference to the literature, and acknowledgement of collaborative research and discussions.

The work was done under the guidance of Professor Amol Dighe, at the Tata Institute of Fundamental Research, Mumbai.

Diptimoy Ghosh

In my capacity as supervisor of the candidate's thesis, I certify that the above statements are true to the best of my knowledge.

Amol Dighe

Date

Acknowledgment

It has been a pleasure to work under the supervision of Prof. Amol Dighe, and I want to thank him for all the advice and time he has given me. I am extremely thankful to him for his constant support, encouragement and guidance.

I would also like to thank all my collaborators for their kind co-operation and continuous support. I am truly thankful to all the former and present students of the Department of Theoretical Physics with whom I have shared the office and who helped me a lot day in and day out. I would like to take this opportunity to thank all the faculty members and the non-academic members of our department.

Finally without the support and love of my parents, my brother, my wife and my friends it would have been impossible for me to finish this thesis work. I am thankful to all of them.

List of Publications

The papers included in this thesis are marked with a star (∗).

Articles in Refereed Journals [1–8]:

[1] ∗A. K. Alok, A. Dighe, D. Ghosh, D. London, J. Matias, M. Nagashima and A. Szynkman, "New-physics contributions to the forward-backward asymmetry in $B \to K * \mu^+\mu^-$," JHEP **1002**, 053 (2010) [arXiv:0912.1382 [hep-ph]].

[2] ∗B. Bhattacherjee, A. Dighe, D. Ghosh and S. Raychaudhuri, "Do new data on $B^+ \to \tau^+\nu_\tau$ decays point to an early discovery of supersymmetry at the LHC?," Phys. Rev. D **83**, 094026 (2011) [arXiv:1012.1052 [hep-ph]].

[3] B. Bhattacherjee, S. S. Biswal and D. Ghosh, "Top quark forward-backward asymmetry at Tevatron and its implications at the LHC," Phys. Rev. D **83**, 091501 (2011) [arXiv:1102.0545 [hep-ph]].

[4] S. Descotes-Genon, D. Ghosh, J. Matias and M. Ramon, "Exploring New Physics in the C7-C7' plane," JHEP **1106**, 099 (2011) [arXiv:1104.3342 [hep-ph]].

[5] A. Dighe, D. Ghosh, A. Kundu and S. K. Patra, "Reconciling anomalous measurements in $B_s - \bar{B}_s$ mixing: the role of CPT-conserving and CPT-violating new physics," Phys. Rev. D **84**, 056008 (2011) [arXiv:1105.0970 [hep-ph]].

[6] ∗A. K. Alok, A. Datta, A. Dighe, M. Duraisamy, D. Ghosh and D. London, "New Physics in $b \to s\mu^+\mu^-$: CP-Conserving Observables," JHEP **1111**, 121 (2011) [arXiv:1008.2367 [hep-ph]].

[7] ∗A. K. Alok, A. Datta, A. Dighe, M. Duraisamy, D. Ghosh and D. London, "New Physics in $b \to s\mu^+\mu^-$: CP-Violating Observables," JHEP **1111**, 122 (2011) [arXiv:1103.5344 [hep-ph]].

[8] A. Dighe, D. Ghosh, R. M. Godbole and A. Prasath, "Large mass splittings for fourth generation fermions allowed by LHC Higgs exclusion," Phys. Rev. D **85**, 114035 (2012) [arXiv:1204.3550 [hep-ph]].

Preprints in arXiv [9–14]:

[9] D. Ghosh, M. Guchait and D. Sengupta, "Higgs Signal in Chargino-Neutralino Production at the LHC," [arXiv:1202.4937 [hep-ph]].

[10] P. Byakti and D. Ghosh, "Magic Messengers in Gauge Mediation and signal for 125 GeV boosted Higgs boson," [arXiv:1204.0415 [hep-ph]].

[11] D. Ghosh, M. Guchait, S. Raychaudhuri and D. Sengupta, "How Constrained is the cMSSM?," [arXiv:1205.2283 [hep-ph]].

[12] A. Datta, M. Duraisamy and D. Ghosh, "Diagnosing New Physics in $b \to c\,\tau\,\nu_\tau$ decays in the light of the recent BaBar result," [arXiv:1206.3760 [hep-ph]].

[13] A. Dighe and D. Ghosh, "How large can the branching ratio of $B_s \to \tau^+\tau^-$ be ?," [arXiv:1207.1324 [hep-ph]].

[14] D. Ghosh and D. Sengupta, "Searching the sbottom in the four lepton channel at the LHC," [arXiv:1209.4310 [hep-ph]].

Articles in Conference Proceedings [15, 16]:

[15] A. Dighe, A. Giri, R. Dutta, N. Gaur, T. Gershon, D. Ghosh, X. -G. He and G. W. S. Hou *et al.*, "B physics: WHEPP-XI working group report," Pramana **76**, 729 (2011).

[16] S. Descotes-Genon, D. Ghosh, J. Matias and M. Ramon, "Exploring New Physics in C7-C7'," PoS EPS **-HEP2011**, 170 (2011) [arXiv:1202.2172 [hep-ph]].

Contents

Thesis Synopsis
Looking for new physics beyond the Standard Model through flavour transitions

Diptimoy Ghosh
Thesis advisor : Amol Dighe
Department of Theoretical Physics
Tata Institute of Fundamental Research, Mumbai, India

A Introduction

The term flavour was first used in particle physics in the context of the quark model of hadrons. Flavour physics denotes physics of transitions among the three generations of Standard Model (SM) fermions. In the standard model all the flavour and CP violation arise solely through the Cabibbo-Kobayashi-Maskawa (CKM) matrix.

The SM flavour Lagrangian, in the mass basis, is given by (in the unitary gauge),

$$\begin{aligned}\mathcal{L}_m^F = &\left(\overline{q^i} \not{D}\, q^j \delta_{ij}\right)_{\rm NC} + \left(\overline{u_L}\,\overline{c_L}\,\overline{t_L}\right)\begin{pmatrix} y_u & 0 & 0 \\ 0 & y_c & 0 \\ 0 & 0 & y_t \end{pmatrix}\begin{pmatrix} u_R \\ c_R \\ t_R \end{pmatrix}(v+h) + (u,c,t) \leftrightarrow (d,s,b) \\ &+ \frac{g_2}{\sqrt{2}}\overline{u_{Li}}\gamma^\mu V_{ij} d_{Lj} W_\mu^+ + \text{h.c.},\end{aligned} \tag{1}$$

where the subscript NC stands for neutral current interaction for the gluons, the photon and the Z gauge bosons, $W^\pm$ stands for the charged electroweak gauge bosons, h is the physical Higgs field, $v \sim 176\,\text{GeV}$, y_i are the Yukawa couplings, g_2 is the weak coupling constant and V is the CKM matrix.

To emphasize the physical transitions associated with the CKM matrix, it is usually written as

$$V = \begin{pmatrix} V_{ud} & V_{us} & V_{ub} \\ V_{cd} & V_{cs} & V_{cb} \\ V_{td} & V_{ts} & V_{tb} \end{pmatrix}, \tag{2}$$

so that the entries are labeled by the quark flavours.

Interesting constraints come from the orthogonality of columns (or rows) of the unitary CKM matrix. Taking the first and third columns of V, one has

$$V_{ud}V_{ub}^* + V_{cd}V_{cb}^* + V_{td}V_{tb}^* = 0\,. \tag{3}$$

Equation (3) says that the three terms in the sum trace out a triangle on the complex plane – the unitarity triangle, shown in Fig. 1.

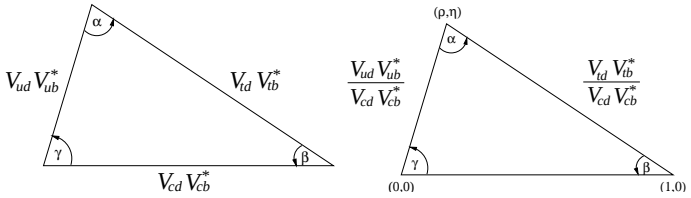

Figure 1: The unitarity triangle. The figure on the left directly expresses Eq. (3). The rescaled version on the right shows the triangle in the plane (ρ, η) which is defined later in the text.

The lengths of the sides are simply $|V_{ud}V_{ub}^*|$, etc., and the angles are

$$\alpha = \arg\left[-\frac{V_{td}V_{tb}^*}{V_{ud}V_{ub}^*}\right], \qquad \beta = \arg\left[-\frac{V_{cd}V_{cb}^*}{V_{td}V_{tb}^*}\right], \qquad \gamma = \arg\left[-\frac{V_{ud}V_{ub}^*}{V_{cd}V_{cb}^*}\right]. \tag{4}$$

The notation $\beta \equiv \phi_1$, $\alpha \equiv \phi_2$, $\gamma \equiv \phi_3$ is also used. By construction $\alpha + \beta + \gamma = \pi$. The area of the triangle is defined as $|J|/2$ where J is called the Jarlskog invariant. In fact, there are five more unitarity triangles, all with area $|J|/2$.

A convenient parameterization of the CKM matrix is due to Wolfenstein. It stems from the observation that the measured matrix obeys a hierarchy, with diagonal elements close to 1, and progressively smaller elements away from the diagonal. It has four parameters λ, A, ρ, and η . From experiment $\lambda \approx 0.22$, $A \approx 0.8$, and $\sqrt{\rho^2+\eta^2} \approx 0.4$, so it is phenomenologically useful to expand V in powers of λ:

$$V = \begin{pmatrix} 1-\frac{1}{2}\lambda^2 & \lambda & A\lambda^3(\rho - i\eta) \\ -\lambda & 1-\frac{1}{2}\lambda^2 & A\lambda^2 \\ A\lambda^3(1-\rho-i\eta) & -A\lambda^2 & 1 \end{pmatrix} + \mathcal{O}(\lambda^4)\,. \tag{5}$$

The Jarlskog invariant can now be expressed as $J = A^2\lambda^6\eta \approx (7\times10^{-5})\eta$. The unitarity triangle in Eq. (3) is special, because its three sides are all of order $A\lambda^3$. The other triangles are all long and thin, with sides $(\lambda, \lambda, A\lambda^5)$ (e.g., for the kaon) or $(\lambda^2, \lambda^2, A\lambda^4)$ (e.g., for the B_s meson).

The rich phenomenology of weak decays has always been a source of information about the nature of elementary particle interactions. Despite the impressive success of the CKM picture of flavour changing interactions in which the GIM mechanism for

the suppression of flavour changing neutral currents (FCNC) plays a very important role, there are many open questions of theoretical and experimental nature that should be answered before we can claim to have a theory of flavour. Weak decays of hadrons containing heavy quarks are now being employed for precision tests of the Standard Model and measurements of its parameters. In particular, they offer the most direct way to determine the weak mixing angles, to test the unitarity of the CKM matrix, and to explore the physics of CP violation. The existing tensions in some of the corners of the SM and still a rather big room for new physics (NP) contributions in rare decays of mesons and leptons and CP-violating observables give us hopes that indeed several phenomena required to answer at least some of these questions could be discovered in this decade. On the other hand, hadronic weak decays also serve as a probe of that part of strong-interaction phenomenology which is least understood: the confinement of quarks and gluons inside hadrons.

As far as high precision experiments are concerned a number of selected processes and observables will play the leading role in learning about the NP. This selection is based on the sensitivity to NP and theoretical cleanness. The former can be increased with the increased precision of experiments and the latter can improve with the progress in theoretical calculations, in particular the non-perturbative ones like the lattice simulations. The decay modes involving $b \to s\mu^+\mu^-$ transitions and the decay $B^+ \to \tau\nu_\tau$ are two important modes that are very sensitive to NP. Clearly, there are other modes in flavour physics but the ones above will play very crucial role in our search for the theory of flavour. Having experimental results on these decays and observables with sufficient precision accompanied by improved theoretical calculations will exclude several presently studied models reducing thereby our exploration of short distance scales to a few avenues. We will study the above two modes in detail in this thesis.

A.1 Operator Product Expansion(OPE)

To predict the decay rate of a B meson into some final state f, one must calculate the transition amplitude $\mathcal{M}$ for $B \to f$. In general there are many contributions to $\mathcal{M}$, each of which is, at the quark level, pictorially represented by Feynman diagrams such as those in Fig. 2. The theoretical tool for the calculation of the amplitude is the operator product expansion (OPE). Schematically the decay amplitude $\mathcal{M}$ is expressed as

$$\mathcal{M} = -\frac{4\,G_F}{\sqrt{2}}\,V \sum_j C_j(\mu)\,\langle f|O_j(\mu)|B\rangle \left[1 + \mathcal{O}\left(\frac{m_b^2}{M_W^2}\right)\right], \tag{6}$$

where μ is a renormalization scale. All dependence on heavy masses $M \gg \mu$ such as m_t, M_W or the masses of new undiscovered heavy particles is contained in C_j – the wilson coefficients. The Hamiltonian for $\Delta B = 1$ and $\Delta S = 1$ transitions consists of

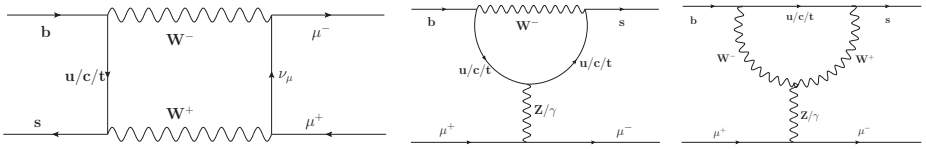

Figure 2: Standard Model W exchange box diagram and penguin diagram with internal top quark loop for the decay $b \to s\mu^+\mu^-$.

many operators,

$$\begin{aligned}
O_1^c &= [\bar{s}_L^\alpha \gamma_\mu c_L^\beta]\,[\bar{c}_L^\beta \gamma^\mu b_L^\alpha],\; O_1^u = [\bar{s}_L^\alpha \gamma_\mu u_L^\beta]\,[\bar{u}_L^\beta \gamma^\mu b_L^\alpha],\; O_2^c = [\bar{s}_L^\alpha \gamma_\mu c_L^\alpha]\,[\bar{c}_L^\beta \gamma^\mu b_L^\beta], \\
O_2^u &= [\bar{s}_L^\alpha \gamma_\mu u_L^\alpha]\,[\bar{u}_L^\beta \gamma^\mu b_L^\beta],\; O_3 = \sum_{q=u,d,s,c,b} [\bar{s}_L^\alpha \gamma_\mu b_L^\alpha]\,[\bar{q}_L^\beta \gamma^\mu q_L^\beta], \\
O_4 &= \sum_{q=u,d,s,c,b} [\bar{s}_L^\alpha \gamma_\mu b_L^\beta]\,[\bar{q}_L^\beta \gamma^\mu q_L^\alpha],\; O_5 = \sum_{q=u,d,s,c,b} [\bar{s}_L^\alpha \gamma_\mu b_L^\alpha]\,[\bar{q}_R^\beta \gamma^\mu q_R^\beta], \\
O_6 &= \sum_{q=u,d,s,c,b} [\bar{s}_L^\alpha \gamma_\mu b_L^\beta]\,[\bar{q}_R^\beta \gamma^\mu q_R^\alpha],\; O_8 = \frac{g}{16\pi^2}\, m_b\, [\bar{s}_L \sigma^{\mu\nu} G^a_{\mu\nu} T^a b_R]\,.
\end{aligned} \tag{7}$$

Some of these operators are depicted in Fig. 3. In O_8, $G^a_{\mu\nu}$ is the chromomagnetic field strength tensor. The operators are grouped into classes, based on their origin: O_1 and O_2 are called current-current operators, O_3 through O_6 are called four-quark penguin operators, and O_8 is called the chromomagnetic penguin operator.

In some cases, especially when isospin breaking plays a role, one also needs to consider penguin diagrams which are of higher order in the electroweak fine structure constant α_{ew}. They give rise to the electroweak penguin operators:

$$\begin{aligned}
O_7 &= \frac{e}{16\pi^2}\, m_b\, [\bar{s}_L^\alpha\, \sigma^{\mu\nu} F_{\mu\nu}\, b_R^\alpha]\,, \\
O_7^{\rm ew} &= \frac{3}{2} \sum_{q=u,d,s,c,b} e_q\, [\bar{s}_L^\alpha \gamma_\mu b_L^\alpha]\,[\bar{q}_R^\beta \gamma^\mu q_R^\beta]\,, O_8^{\rm ew} = \sum_{q=u,d,s,c,b} \frac{3}{2} e_q\, [\bar{s}_L^\alpha \gamma_\mu b_L^\beta]\,[\bar{q}_R^\beta \gamma^\mu q_R^\alpha]\,, \\
O_9^{\rm ew} &= \frac{3}{2} \sum_{q=u,d,s,c,b} e_q\, [\bar{s}_L^\alpha \gamma_\mu b_L^\alpha]\,[\bar{q}_L^\beta \gamma^\mu q_L^\beta]\,, O_{10}^{\rm ew} = \sum_{q=u,d,s,c,b} \frac{3}{2} e_q\, [\bar{s}_L^\alpha \gamma_\mu b_L^\beta]\,[\bar{q}_L^\beta \gamma^\mu q_L^\alpha]\,.
\end{aligned} \tag{8}$$

Here $F^{\mu\nu}$ is the electromagnetic field strength tensor, and e_q denotes the charge of quark q. The magnetic (penguin) operator O_7 is of key importance for the radiative decay $b \to s\gamma$. For semileptonic decays the following additional operators occur:

$$\begin{aligned}
O_9 &= \frac{e^2}{16\pi^2}\, [\bar{s}_L\, \gamma_\mu\, b_L]\,[\bar{\ell}\, \gamma^\mu\, \ell]\,, \qquad\qquad O_{10} = \frac{e^2}{16\pi^2}\, [\bar{s}_L\, \gamma_\mu\, b_L]\,[\bar{\ell}\, \gamma^\mu \gamma_5\, \ell]\,, \\
O_{11} &= \frac{e^2}{32\pi^2 \sin^2\theta_W}\, [\bar{s}_L\, \gamma_\mu\, b_L]\,[\bar{\nu}_L\, \gamma^\mu\, \nu_L]\,.
\end{aligned} \tag{9}$$

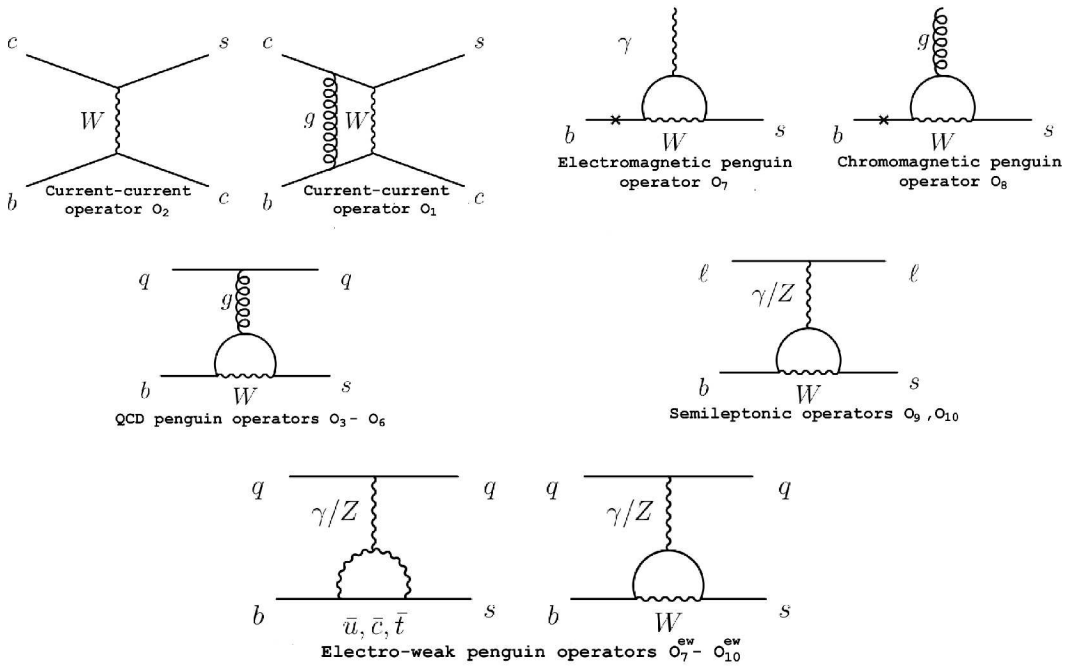

Figure 3: Quark level diagrams for some of the effective operators of (7),(8),(9).

The operators introduced above are sufficient to describe nonleptonic transitions in the Standard Model to order G_F. In extensions of the Standard Model, on the other hand, the short distance structure can be very different. Additional operators with new Dirac structures, whose standard Wilson coefficients vanish, could also enter the effective Hamiltonian.

B New Physics in $b \to s\mu^+\mu^-$:CP-Conserving Observables

The decay $b \to s\mu^+\mu^-$ is extremely versatile with the possibility to measure, for instance, the differential decay rate in bins of leptons' invariant mass. One can also construct asymmetries, like the well-known forward-backward asymmetry (AFB), with differing sensitivity to NP effects. A full angular analysis of $B \to K^*(\to K\pi)\mu^+\mu^-$ would give access to a multitude of observables. In this section we will study the CP-conserving observables in different $b \to s\mu^+\mu^-$ modes.

Within the SM, the effective Hamiltonian for the quark-level transition $b \to s\mu^+\mu^-$

is

$$\mathcal{H}_{\rm eff}^{SM} = -\frac{4G_F}{\sqrt{2}}\,V_{ts}^*V_{tb}\left\{\sum_{i=1}^{6}C_i(\mu)\mathcal{O}_i(\mu) + C_7\,\frac{e}{16\pi^2}\,[\bar{s}\sigma_{\mu\nu}(m_sP_L+m_bP_R)b]\,F^{\mu\nu}\right.$$
$$\left. + C_9\,\frac{\alpha_{em}}{4\pi}\,(\bar{s}\gamma^\mu P_Lb)\,\bar{\mu}\gamma_\mu\mu + C_{10}\,\frac{\alpha_{em}}{4\pi}\,(\bar{s}\gamma^\mu P_Lb)\,\bar{\mu}\gamma_\mu\gamma_5\mu\right\}\,, \qquad (10)$$

where $P_{L,R}=(1\mp\gamma_5)/2$. The operators $\mathcal{O}_i$ $(i=1,..6)$ correspond to the P_i in Ref. [17], and $m_b=m_b(\mu)$ is the running b-quark mass in the $\overline{\rm MS}$ scheme. We use the SM Wilson coefficients as given in Ref. [18]. In the magnetic dipole operator with the coefficient C_7, we neglect the term proportional to m_s.

We now add new physics to the effective Hamiltonian and check their impact on $b\to s\mu^+\mu^-$,

$$\mathcal{H}_{\rm eff}(b\to s\mu^+\mu^-) = \mathcal{H}_{\rm eff}^{SM} + \mathcal{H}_{\rm eff}^{VA} + \mathcal{H}_{\rm eff}^{SP} + \mathcal{H}_{\rm eff}^{T}\,, \qquad (11)$$

where $\mathcal{H}_{\rm eff}^{SM}$ is given by Eq. (10), while

$$\mathcal{H}_{\rm eff}^{VA} = -\frac{4G_F}{\sqrt{2}}\,\frac{\alpha_{em}}{4\pi}\,V_{ts}^*V_{tb}\left\{R_V\,(\bar{s}\gamma^\mu P_Lb)\,\bar{\mu}\gamma_\mu\mu + R_A\,(\bar{s}\gamma^\mu P_Lb)\,\bar{\mu}\gamma_\mu\gamma_5\mu\right.$$
$$\left. + R'_V\,(\bar{s}\gamma^\mu P_Rb)\,\bar{\mu}\gamma_\mu\mu + R'_A\,(\bar{s}\gamma^\mu P_Rb)\,\bar{\mu}\gamma_\mu\gamma_5\mu\right\}\,, \qquad (12)$$

$$\mathcal{H}_{\rm eff}^{SP} = -\frac{4G_F}{\sqrt{2}}\,\frac{\alpha_{em}}{4\pi}\,V_{ts}^*V_{tb}\left\{R_S\;(\bar{s}P_Rb)\;\bar{\mu}\mu + R_P\;(\bar{s}P_Rb)\;\bar{\mu}\gamma_5\mu\right.$$
$$\left. + R'_S\;(\bar{s}P_Lb)\;\bar{\mu}\mu + R'_P\;(\bar{s}P_Lb)\;\bar{\mu}\gamma_5\mu\right\}\,, \qquad (13)$$

$$\mathcal{H}_{\rm eff}^{T} = -\frac{4G_F}{\sqrt{2}}\frac{\alpha_{em}}{4\pi}V_{ts}^*V_{tb}\Big\{C_T(\bar{s}\sigma_{\mu\nu}b)\bar{\mu}\sigma^{\mu\nu}\mu + iC_{TE}(\bar{s}\sigma_{\mu\nu}b)\bar{\mu}\sigma_{\alpha\beta}\mu\;\epsilon^{\mu\nu\alpha\beta}\Big\} \qquad (14)$$

are the new contributions. Here, $R_V, R_A, R'_V, R'_A, R_S, R_P, R'_S, R'_P, C_T$ and C_{TE} are the NP effective couplings. In the following section we will consider only real NP couplings and concentrate only on CP conserving observables.

B.1 Constraints on NP couplings

The constraints on the NP couplings in $b\to s\mu^+\mu^-$ come mainly from the upper bound on the branching ratio $B(\bar{B}_s^0\to\mu^+\mu^-)$ and the measurements of the total branching ratios $B(\bar{B}_d^0\to X_s\mu^+\mu^-)$ and $B(\bar{B}_d^0\to\bar{K}\mu^+\mu^-)$ [19–23].

For $R_{V,A}$, the allowed parameter space is the region between two ellipses:

$$1.0 \lesssim \frac{|R_V+3.6|^2}{(4.7)^2} + \frac{|R_A-4.0|^2}{(4.8)^2}\,, \quad \frac{|R_V+2.8|^2}{(6.5)^2} + \frac{|R_A-4.1|^2}{(6.6)^2} \lesssim 1\,, \qquad (15)$$

while for $R'_{V,A}$, the allowed region is the intersection of an annulus and a circle:

$$22.2 \lesssim |R'_V+3.6|^2 + |R'_A-4.0|^2 \lesssim 56.6\,, \quad |R'_V|^2 + |R'_A|^2 \lesssim 17\,. \qquad (16)$$

For the SP operators, the present upper bound on $B(\bar{B}_s^0 \to \mu^+\mu^-)$ provides the limit

$$|R_S - R'_S|^2 + |R_P - R'_P|^2 \lesssim 0.44 \ . \tag{17}$$

This constitutes a severe constraint on the NP couplings if only $R_{S,P}$ or $R'_{S,P}$ are present. However, if both types of operators are present, these bounds can be evaded due to cancellations between the $R_{S,P}$ and $R'_{S,P}$. In that case, $B(\bar{B}_d^0 \to X_s\mu^+\mu^-)$ and $B(\bar{B}_d^0 \to \bar{K}\mu^+\mu^-)$ can still bound these couplings. The stronger bound is obtained from the measurement of the latter quantity, which yields

$$|R_S|^2 + |R_P|^2 \lesssim 9 \ , \quad R_S \approx R'_S \ , \quad R_P \approx R'_P \ . \tag{18}$$

Finally, the constraints on the NP tensor operators come entirely from $B(\bar{B}_d^0 \to X_s\mu^+\mu^-)$. When only the T operators are present,

$$|C_T|^2 + 4|C_{TE}|^2 \lesssim 1.0 \ . \tag{19}$$

Our main results are summarized below.

B.2 $\bar{B}_s^0 \to \mu^+\mu^-$

The SM prediction for the branching ratio is $B(\bar{B}_s^0 \to \mu^+\mu^-) = (3.35 \pm 0.32) \times 10^{-9}$ [24]. The Tevatron gives an upper bound on its branching ratio (BR) of 4.7×10^{-8} at 90% C.L. [19–21]. Our analysis shows that
(i)Both VA and SP operators can suppress $B(\bar{B}_s^0 \to \mu^+\mu^-)$ significantly below the SM prediction.
(ii)While VA operators can only marginally enhance $B(\bar{B}_s^0 \to \mu^+\mu^-)$ above 10^{-8}, making the decay accessible at the Tevatron in an optimistic scenario, the SP operators can enhance the branching ratio even up to the present experimental bound.

B.3 $\bar{B}_d^0 \to X_s\mu^+\mu^-$

The BR of $\bar{B}_d^0 \to X_s\mu^+\mu^-$ in both the low-q^2 and high-q^2 regions has been measured experimentally [22, 23]. The SM predictions for $B(\bar{B} \to X_s\,\mu^+\,\mu^-)$ in the low-q^2 and high-q^2 regions are $(1.59 \pm 0.11) \times 10^{-6}$ and $(0.24 \pm 0.07) \times 10^{-6}$, respectively [25].

The SM predicts a positive zero crossing for A_{FB} in $\bar{B}_d^0 \to X_s\mu^+\mu^-$ in the low-q^2 region, i.e. for q^2 less than (greater than) the crossing point, the value of A_{FB} is negative (positive). The NNLO prediction [25] for the zero of $A_{FB}(q^2)$ is (taking $m_b = 4.8$ GeV) $(q^2)_0 = (3.5 \pm 0.12)\,\mathrm{GeV}^2$.This quantity has not yet been measured. Fig. 4 shows $A_{FB}(q^2)$ for $\bar{B}_d^0 \to X_s\mu^+\mu^-$ in the presence of NP in the form of $R_{V,A}$ couplings, which are the ones that can most influence these observables. We observe that
(i)The NP VA couplings can enhance A_{FB} up to 30% at low q^2, make it have either sign,

and even make the zero crossing disappear altogether. Enhancement or suppression of the DBR by a factor of 2 is possible.
(ii)At high q^2, however, A_{FB} can only be suppressed.
(iii)The $R'_{V,A}$ couplings can only affect A_{FB} mildly.
(iv)If SP or T couplings are individually present, their contribution to A_{FB} is either absent or suppressed by m_μ/m_b. However if both SP and T operators are present, their interference term is not suppressed and some enhancement of A_{FB} is possible.

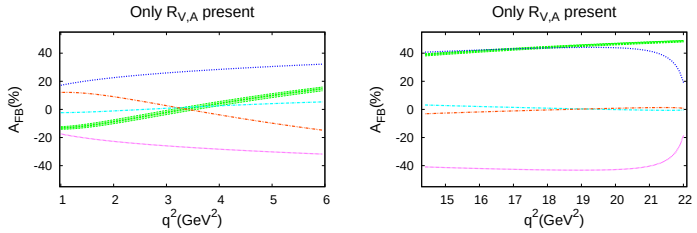

Figure 4: The left (right) panels of the figure show A_{FB} for $\bar{B}^0_d \to X_s\mu^+\mu^-$ in the low-q^2 (high-q^2) region, in the scenario where only (R_V, R_A) terms are present. The band corresponds to the SM prediction; its width is due to the uncertainties in the input parameters. The lines show predictions for some representative values of NP parameters.

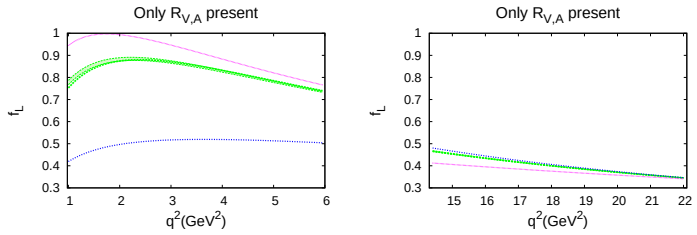

Figure 5: The left (right) panels of the figure show f_L for $\bar{B}^0_d \to X_s\mu^+\mu^-$ in the low-q^2 (high-q^2) region, in the scenario where only (R_V, R_A) terms are present. The same conventions as in Fig. 4 are used.

Polarization fractions f_L and f_T

In Ref. [26] it was pointed out that, besides the dilepton invariant mass spectrum and the forward-backward asymmetry, a third observable can be obtained from $\bar{B}^0_d \to$

$X_s\mu^+\mu^-$, namely the double differential decay width:

$$\frac{d^2B}{dz\,d\cos\theta} = \frac{3}{8}\Big[(1+\cos^2\theta)H_T(z) + 2\cos\theta H_A(z) + 2(1-\cos^2\theta)H_L(z)\Big] \,. \qquad (20)$$

The polarization fractions f_L and f_T can be defined as

$$f_L = \frac{H_L(z)}{H_L(z)+H_T(z)} \,, \qquad f_T = \frac{H_T(z)}{H_L(z)+H_T(z)} \,. \qquad (21)$$

In the SM, f_L can be as large as 0.9 at low q^2, and it decreases to about 0.3 at high q^2.

Fig. 5 shows that when only $R_{V,A}$ couplings are present, in the low-q^2 region f_L can be suppressed substantially, or even enhanced up to 1. A similar effect – small enhancement or a factor of two suppression – is possible at high q^2. The suppression at low-q^2 is typically correlated with an enhancement at high-q^2. The effect of $R'_{V,A}$ couplings is similar, but much milder, as expected. SP and T operators, individually or together, can only have an marginal effect on f_L.

B.4 $\bar{B}_s^0 \to \mu^+\mu^-\gamma$

This decay has not been detected as yet. The SM prediction for the BR in the range $q^2 \le 9.5$ GeV^2 and $q^2 \ge 15.9$ GeV^2 is $\approx 18.9\times10^{-9}$ [27]. Our analysis shows that

(i)In the presence of $R_{V,A}$ couplings, the maximum allowed value of DBR can be 2-3 times larger than the SM prediction. The BR can also be suppressed below the SM prediction due to destructive interference. In the low-q^2 region, the suppression can be large. The features of the zero-crossing predicted by the SM can be affected: it can be positive or negative, can take place at any value of q^2, and can disappear altogether. As expected, the impact of $R'_{V,A}$ couplings is much milder. In particular, the zero-crossing is always positive and in the low-q^2 region.
(ii)The SP operators do not contribute to the amplitude of $\bar{B}_s^0 \to \mu^+\mu^-\gamma$ and hence do not play any role in the decay.
(iii)With new tensor couplings, an enhancement of the DBR by up to a factor of 3 in comparison to the SM prediction is possible. Tensors can only suppress A_{FB} from its SM value.

B.5 $\bar{B}_d^0 \to \bar{K}\mu^+\mu^-$

The total branching ratio of $\bar{B}_d^0 \to \bar{K}\mu^+\mu^-$ has been measured to be [21] $B(\bar{B}_d^0 \to \bar{K}\mu^+\mu^-) = \left(4.5^{+1.2}_{-1.0}\right)\times10^{-7}$, which is consistent with the SM prediction [28] $B(\bar{B}_d^0 \to \bar{K}\mu^+\mu^-)_{\rm SM} = (3.5\pm1.2)\times10^{-7}$. We find that

(i) New VA couplings alone cannot give rise to A_{FB}, which vanishes in the SM in any case.
(ii)If both the primed and unprimed SP couplings are present simultaneously, the

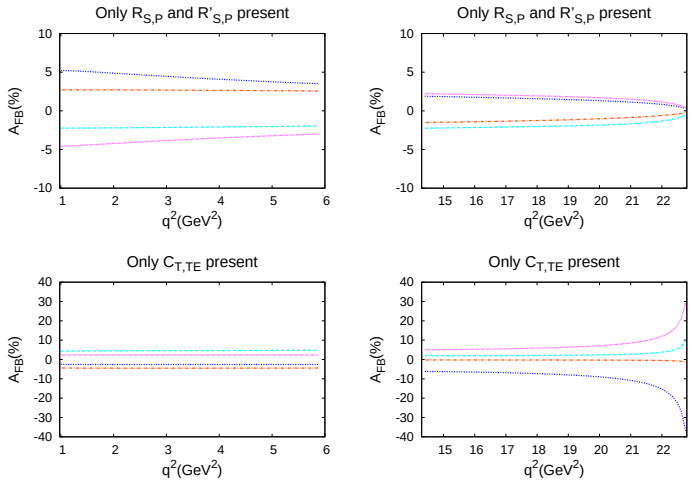

Figure 6: The left (right) panels of the figure show A_{FB} for $\bar{B}^0_d \to \bar{K}\mu^+\mu^-$ in the low-q^2 (high-q^2) region, in the scenario where only NP SP(above) and T(below) couplings are present. The lines show predictions for some representative values of NP parameters.

constraints on them are weakened. In such a situation, the peak value of A_{FB} in the low-q^2 (high-q^2) can become $\sim 5\%$ ($\sim 3\%$). This may be seen in Fig. 6. The DBR also is significantly affected only if both the primed and unprimed SP couplings are present: it can be enhanced by up to a factor of 3.
(iii)$A_{FB}(q^2)$ can be enhanced up to 5-6% in almost the entire q^2 region in the presence of T couplings. Moreover, at $q^2 \gtrsim 21$ GeV^2, the peak value of $A_{FB}(q^2)$ reaches a larger value ($\sim 30\%$).
(iv)When SP and T couplings are present simultaneously, their interference can have a large impact on A_{FB} which can be more than 30% in the whole high-q^2 region.

B.6 $\bar{B}^0_d \to \bar{K}^*\mu^+\mu^-$

The decay $\bar{B}^0_d \to \bar{K}^*\mu^+\mu^-$, with $\bar{K}^*$ decaying to $\bar{K}\pi$, has four particles in the final state. This implies that there are three physical angles (see Fig. 7)that can specify the relative directions of these four final-state particles. The differential decay rate as a function of these three angles has much more information than just the forward-backward asymmetry.

Differential branching ratio and forward-backward asymmetry

In Fig. 8 we show the A_{FB} in the presence of both the $R_{V,A}$ and $R'_{V,A}$ couplings. Our analysis shows that (i) If only $R_{V,A}$ couplings are present, A_{FB} can be enhanced at low

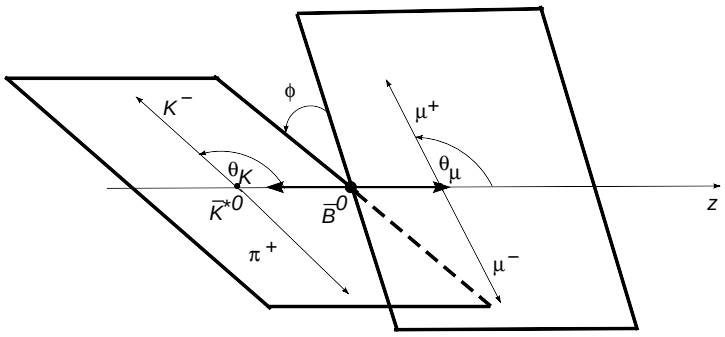

Figure 7: The description of the angles $\theta_{\mu,K}$ and ϕ in the angular distribution of $\bar{B} \to \bar{K}^*(\to \bar{K}\pi)\mu^+\mu^-$ decay.

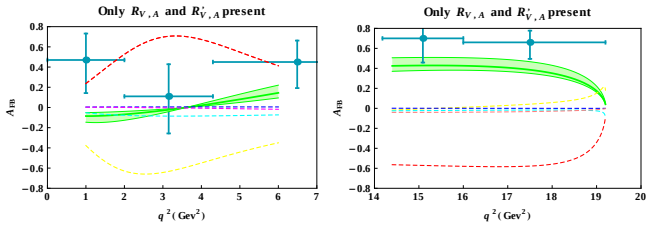

Figure 8: The left (right) panels of the figure show A_{FB} and DBR for $\bar{B}^0_d \to \bar{K}^*\mu^+\mu^-$ in the low-q^2 (high-q^2) region, in the scenario where both (R_V, R_A) and (R'_V, R'_A) terms are present. The band corresponds to the SM prediction; its width is due to the uncertainties in the input parameters. The lines show predictions for some representative values of NP parameters. For comparison, the experimental data are also displayed.

q^2, while keeping it positive, so that there is no zero crossing. On the other hand, if only $R'_{V,A}$ couplings are present, A_{FB} can become large and positive at high q^2.
(ii)New SP couplings by themselves cannot significantly affect either the DBR or the A_{FB} predictions of the SM. New T couplings in general tend to enhance DBR significantly, by up to a factor of 2 but can not enhance the A_{FB}.
(iii)When SP and T couplings are present simultaneously, additional contributions to A_{FB} that are not suppressed by m_μ/m_B are possible. As a result, A_{FB} obtained with this combination can be marginally enhanced as compared to the case with only T operators. It is then possible to have no zero crossing. However, the magnitude of A_{FB} cannot be large in the high-q^2 region.

Polarization fraction f_L

The longitudinal and transverse polarization fractions, f_L and f_T, respectively, are defined as

$$f_L = \frac{A_L}{A_L + A_T} , \quad f_T = \frac{A_T}{A_L + A_T} , \tag{22}$$

where A_L and A_T are the longitudinal and transverse polarization amplitudes. In the SM, f_L can be as large as 0.9 at low q^2, and it decreases to about 0.3 at high q^2. We observe that
(i)New VA couplings can suppress f_L substantially: it can almost vanish in some allowed parameter range.
(ii)New SP couplings cannot change the value of f_L outside the range allowed by the SM. This may be attributed to the strong constraints on the values of these couplings.
(iii)New T couplings tend to suppress f_L, except at $q^2 \approx$ 1-2 GeV^2, where the value of f_L cannot be less than 0.5.
(iv) Since both VA and T couplings tend to suppress f_L, their combined effect results in a similar behaviour.

Angular asymmetries $A_T^{(2)}$ and A_{LT}

The CP-conserving transverse asymmetry $A_T^{(2)}$ can be defined through the double differential decay rate

$$\frac{d^2\Gamma}{dq^2 d\phi} = \frac{1}{2\pi}\frac{d\Gamma}{dq^2}\Big[1 + f_T\left(A_T^{(2)}\cos 2\phi + A_T^{(im)}\sin 2\phi\right)\Big] . \tag{23}$$

Here $A_T^{(im)}$ depends on the imaginary part of a certain combination of amplitudes and can be used to construct CP-violating observables. In the low-q^2 region, which corresponds to the LEET limit, $A_T^{(2)} \approx 0$ in the SM and is independent of form factors up to corrections of order Λ_{QCD}/E_{K^*}, Λ_{QCD}/m_b and α_s, i.e. the hadronic uncertainty is small. This can be seen in Fig. 9. The longitudinal-transverse asymmetry A_{LT} is defined through

$$\frac{d^2\Gamma_{LT}}{dq^2 d\phi} = \frac{d\Gamma}{dq^2}\left(A_{LT}\cos\phi + A_{LT}^{(im)}\sin\phi\right) , \tag{24}$$

where

$$\frac{d^2\Gamma_{LT}}{dq^2 d\phi} = \int_0^1 d\cos\theta_K \frac{d^3\Gamma}{dq^2 d\cos\theta_K d\phi} - \int_{-1}^0 d\cos\theta_K \frac{d^3\Gamma}{dq^2 d\cos\theta_K d\phi} . \tag{25}$$

Just like A_{FB}, the quantity A_{LT} also has a zero crossing which is independent of form factors in the LEET limit. Note that the zero crossing of A_{LT} is different from that

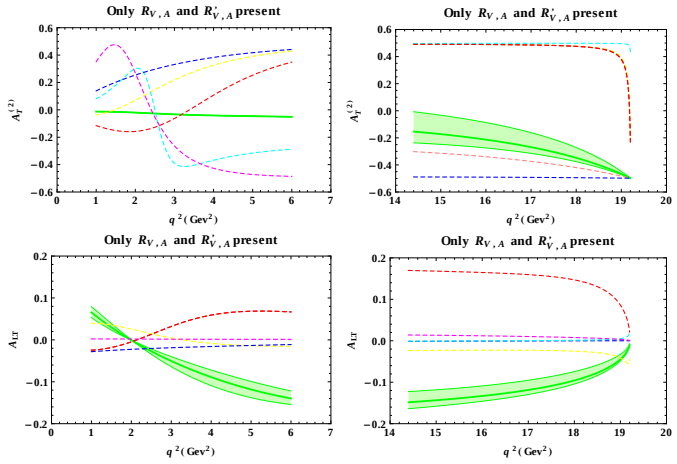

Figure 9: The left (right) panels of the figure show $A_T^{(2)}$ and A_{LT} for $\bar{B}_d^0 \to \bar{K}^* \mu^+ \mu^-$ in the low-q^2 (high-q^2) region, in the scenario where both (R_V, R_A) and (R'_V, R'_A) terms are present. The same conventions as in Fig. 8 are used.

of A_{FB}. Fig. 9 demonstrates that the zero crossing of A_{LT} has a very small hadronic uncertainty. Except at very low q^2, the magnitude of A_{LT} is generally suppressed by new VA couplings. The primed VA couplings can be constrained by A_{LT} better than the unprimed VA couplings. In both cases, the value of A_{LT} can be anywhere in the q^2 range, and can be positive or negative. In particular, there may or may not be a zero crossing, and if there is, its position can be different from that of the SM.

New VA couplings can affect $A_T^{(2)}$ significantly: they can enhance its magnitude by a large amount, change its sign, and change its q^2-dependence. The zero-crossing point may be at a value of q^2 different from that predicted by the SM.

New SP couplings do not affect $A_T^{(2)}$, and A_{LT} qualitatively behaves similarly to the SM. New T couplings in general tend to suppress the magnitudes of both asymmetries.

C New Physics in $b \to s\mu^+\mu^-$:CP-Violating Observables

In the SM the CP-violating observables in $b \to s\mu^+\mu^-$ are extremely small, $< 1\%$. Hence, measurement of any such signal at the level of more than a few percent would be a clear signature of new physics.

For non-zero CP-violation, existence of both the weak and strong phases are necessary. In the SM $C_9^{\rm eff}$ has a non trivial strong phase because of intermediate $c\bar{c}$ states. Since the SM operator $(C_9^{\rm eff})$ is of VA type, the NP operator must also be VA in order to generate a significant direct CP asymmetry through SM-NP interference. Other

NP operators can also interfere with the SM, but the effect is suppressed by m_μ/m_b, and hence expected to be very small. In this section we consider the CP-violating observables in $b \to s\mu^+\mu^-$ and study the impact of NP lorentz structures on them.

C.1 $\bar{B}_s^0 \to \mu^+\mu^-$

The measurement of either of these CP asymmetries requires the measurement of muon polarization, which will be an impossible task for the upcoming experiments [29]. And even if this were doable, the lack of any sources for different strong phases in the two CP-conjugate final states implies that the direct CP asymmetry would vanish even with NP. We therefore do not study CP violation in $\bar{B}_s^0 \to \mu^+\mu^-$.

C.2 $\bar{B}_d^0 \to X_s\mu^+\mu^-$

The CP asymmetry in the differential branching ratio (DBR) of $\bar{B}_d^0 \to X_s\mu^+\mu^-$ is defined as

$$A_{\rm CP}(q^2) = \frac{(dB/dz) - (d\overline{B}/dz)}{(dB/dz) + (d\overline{B}/dz)}\,, \tag{26}$$

where $z \equiv q^2/m_b^2$, and dB/dz and $d\overline{B}/dz$ are the DBRs of $\bar{B}_d^0 \to X_s\mu^+\mu^-$ and its CP-conjugate $B_d^0 \to X_s\mu^+\mu^-$, respectively. The expression for (dB/dz) has been given in Ref. [29]. The CP asymmetry in the forward-backward asymmetry A_{FB} is defined as

$$\Delta A_{FB}(q^2) \equiv A_{FB}(q^2) - \overline{A}_{FB}(q^2)\,, \tag{27}$$

where the definition of A_{FB} is given in Ref. [29], and $\overline{A}_{FB}$ is the analogous quantity for the CP-conjugate decay.
(i)When only $R_{V,A}$ couplings are present, $A_{\rm CP}(q^2)$ can be enhanced up to $\pm 6\%$ at low q^2. On the other hand, its value at high q^2 can be as high as $\pm 12\%$.
(ii)In the presence of $R_{V,A}$ couplings, ΔA_{FB} can be enhanced up to 3% at low q^2. At high q^2, the enhancement can be up to 12%.
(iii) When only $R'_{V,A}$ couplings are present, $A_{\rm CP}(q^2)$ cannot be enhanced above the SM value. They can only affect the DBR, which may be enhanced by up to 50%. The impact of $R'_{V,A}$ couplings on ΔA_{FB} is negligible ($< 1\%$).

C.3 $\bar{B}_s^0 \to \mu^+\mu^-\gamma$

Fig. 10 shows $A_{\rm CP}(q^2)$ and $\Delta A_{FB}(q^2)$ for $\bar{B}_s^0 \to \mu^+\mu^-\gamma$ in the presence of new VA couplings. Our analysis shows that
(i)When only $R_{V,A}$ couplings are present, at low q^2 the magnitude of $A_{\rm CP}(q^2)$ can be enhanced up to $\pm 30\%$ at certain q^2 values. At high q^2, the magnitude of $A_{\rm CP}(q^2)$ is almost independent of q^2, and can be enhanced to about $\pm 13\%$.

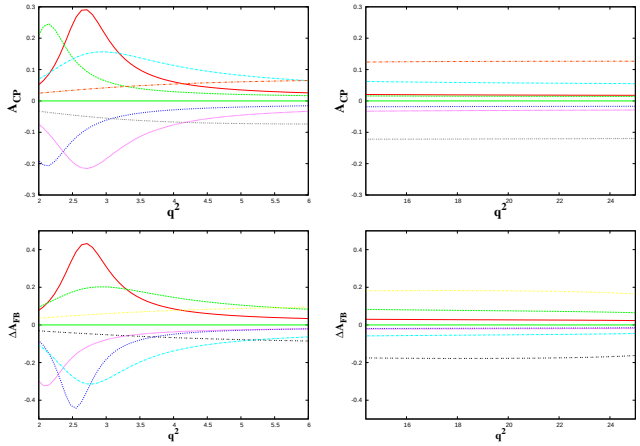

Figure 10: The left (right) panels of the figure show $A_{\rm CP}(q^2)$ and ΔA_{FB} for $\bar{B}_s^0 \to \mu^+\mu^-\gamma$ in the low-q^2 (high-q^2) region, in the scenario where only (R_V, R_A) couplings are present.

(ii)When only $R'_{V,A}$ couplings are present, $A_{\rm CP}(q^2)$ cannot be enhanced in magnitude to more than 1.5% at low q^2, or more than 3% at high q^2.
(iii)The behaviour of $\Delta A_{FB}(q^2)$ is similar to that of $A_{CP}(q^2)$. This quantity can be enhanced up to 40% for some values in the low-q^2 region. It can be as high as 18% throughout the high-q^2 region. The impact of $R'_{V,A}$ couplings is negligible ($< 1\%$).

C.4 $\bar{B}_d^0 \to \bar{K}\mu^+\mu^-$

(i)When only $R_{V,A}$ couplings are present, $A_{\rm CP}(q^2)$ can be enhanced up to $\pm 7\%$ at low q^2. On the other hand, its value at high q^2 can be as high as $\pm 12\%$.
(ii)When only $R'_{V,A}$ couplings are present, $A_{\rm CP}(q^2)$ can be enhanced up to $\pm 4\%$ at low q^2. On the other hand, its value at high q^2 can be as high as $\pm 12\%$.
(iii)New VA couplings do not contribute to ΔA_{FB}.

C.5 $\bar{B}_d^0 \to \bar{K}^*\mu^+\mu^-$

Direct CP asymmetries in the DBR and A_{FB}

(i)If only $R_{V,A}$ couplings are present, $A_{CP}(q^2)$ can be enhanced up to $\pm$ 5% at low q^2, and up to $\pm$ 14 % at high q^2. $\Delta A_{FB}(q^2)$ can be enhanced up to $\pm$ 3% at low q^2, and up to $\pm$ 11 % at high q^2.
(ii)If only $R'_{V,A}$ couplings are present, $A_{CP}(q^2)$ can be enhanced up to $\pm$ 3% at low q^2, and up to $\pm$ 7% at high q^2. $\Delta A_{FB}(q^2)$ can be enhanced up to $\pm$ 1% at low q^2, and up to ± 4 % at high q^2.

(iii)When both primed and unprimed VA couplings are present, $A_{CP}(q^2)$ can be enhanced up to $\pm$ 9% at low q^2, and up to $\pm$ 14 % at high q^2. $\Delta A_{FB}(q^2)$ can be enhanced up to $\pm$ 6% at low q^2, and up to $\pm$ 19 % at high q^2.

Direct CP asymmetry $\Delta f_L(q^2)$ in the polarization fraction f_L

(i)If only $R_{V,A}$ couplings are present, $\Delta f_L(q^2)$ can be enhanced up to $\pm$ 2% at very low q^2. On the other hand, $\Delta f_L(q^2)$ is almost the same as the SM at high q^2.
(ii)If only $R'_{V,A}$ couplings are present, $\Delta f_L(q^2)$ can be enhanced up to $\pm$2% at both low and high q^2.
(iii) When both primed and unprimed VA couplings are present, $\Delta f_L(q^2)$ can be enhanced up to $\pm$9% at low q^2, and up to $\pm$6% at high q^2.

Direct CP asymmetries in the angular asymmetries $A_T^{(2)}$ and A_{LT}

Fig. 11 shows $\Delta A_T^{(2)}$ for $\bar{B}_d^0 \to \bar{K}^*\mu^+\mu^-$ in the presence of new VA couplings. we observe that
(i)If only $R_{V,A}$ couplings are present, $\Delta A_T^{(2)}$ cannot be enhanced more than $\pm$1% at both low and high q^2.
(ii)If only $R'_{V,A}$ couplings are present, $\Delta A_T^{(2)}$ can be enhanced up to $\pm$4% at low q^2, and up to $\pm$6% high q^2.
(iii)When both primed and unprimed VA couplings are present, $\Delta A_T^{(2)}$ can be enhanced up to $\pm$11% at low q^2, and up to $\pm$13% at high q^2.
(iv)With VA couplings we find that these couplings cannot enhance $\Delta A_{LT}(q^2)$ to more than 3% at both low and high q^2.

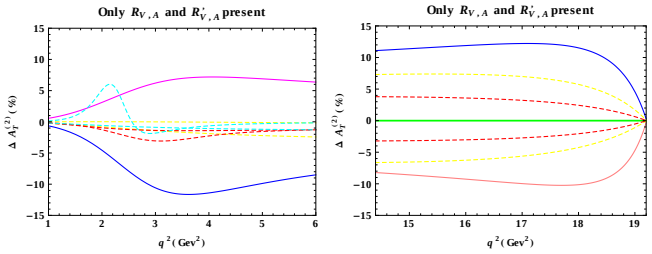

Figure 11: The left (right) panels of the figure show $\Delta A_T^{(2)}(q^2)$ for $\bar{B}_d^0 \to \bar{K}^*\mu^+\mu^-$ in the low-q^2 (high-q^2) region, in the scenario where both (R_V, R_A) and (R'_V, R'_A) terms are present. The green line corresponds to the SM prediction. The other lines show predictions for some representative values of NP parameters.

CP-violating triple-product asymmetries $A_T^{(im)}(q^2)$ and $A_{LT}^{(im)}(q^2)$

Fig. 12 shows $A_T^{(im)}(q^2)$ for $\bar{B}_d^0 \to \bar{K}^*\mu^+\mu^-$ in the presence of new VA couplings.If only $R_{V,A}$ couplings are present, $A_T^{(im)}(q^2)$ can be enhanced up to 5% at low q^2 and can have

either sign. On the other hand, $A_T^{(im)}(q^2)$ is almost same as the SM prediction ($\simeq 0$) at high q^2. If only $R'_{V,A}$ couplings are present, $A_T^{(im)}(q^2)$ can be enhanced up to 49% at low q^2, and up to 46% at high q^2. It can have either sign at both low and high q^2. When both primed and unprimed VA couplings are present, the results for $A_T^{(im)}(q^2)$ are almost the same as those obtained with only $R'_{V,A}$ couplings (see Fig. 12).

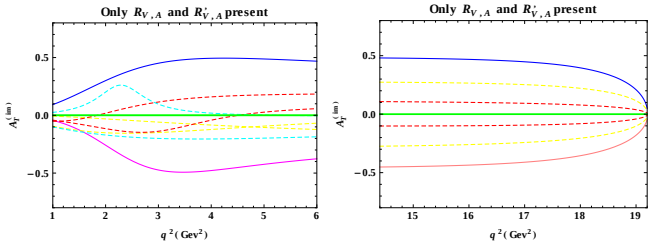

Figure 12: The left (right) panels of the figure show $A_T^{(im)}(q^2)$ for $\bar{B}_d^0 \to \bar{K}^* \mu^+ \mu^-$ in the low-q^2 (high-q^2) region, in the scenario where both (R_V, R_A) and (R'_V, R'_A) terms are present. The same conventions as in Fig. 11 are used.

If only $R_{V,A}$ couplings are present, $A_{LT}^{(im)}(q^2)$ can be enhanced up to 6% at very low q^2, and up to 3% at high q^2. It can have either sign at both low and high q^2. If only $R'_{V,A}$ couplings are present, $A_{LT}^{(im)}(q^2)$ can be enhanced up to 8% at low and high q^2. It can have either sign at both low and high q^2. When both primed and unprimed VA couplings are present, $A_{LT}^{(im)}(q^2)$ can be enhanced up to 11% at low and high q^2. It can have either sign at both low and high q^2. In principle, $A_{LT}^{(im)\bar{B}(B)}$ can be generated due to NP SP-T interference. However, we find that the effect is tiny: $A_{LT}^{(im)}(q^2)$ can be enhanced up to 0.2% at low q^2 and can have either sign; $A_{LT}^{(im)}(q^2)$ is same as the SM ($\simeq 0$) at high q^2.

D The $B^+ \to \tau^+ \nu_\tau$ anomaly and constraints on Supersymmetric Models

The purely leptonic tree level decay $B^+ \to \tau^+ \nu_\tau$ is sensitive to charged Higgs boson ($H^\pm$) at the tree level and thus provide valuable probes of such particles which are complementary to constraints provided by loop-induced decays. Importantly, in supersymmetric (SUSY) models the loop-induced decays are particularly sensitive to the sparticle spectrum and the assumptions made for the SUSY breaking sector, and thus the purely leptonic decays offer a more model-independent probe of parameters in the Higgs sector. The unprecedented data samples provided by the B factories have enabled the first measurements of this decay mode despite its relatively small branching ratio and challenging signature.

In the SM, the branching ratio is given by the tree-level formula

$$\mathrm{BR}(B^+ \to \tau^+\nu_\tau)_{\mathrm{SM}} = \frac{G_F^2 m_B m_\tau^2}{8\pi}\left(1-\frac{m_\tau^2}{m_B^2}\right)^2 f_B^2\,|V_{ub}|^2\,\tau_B\ , \tag{28}$$

where G_F is the Fermi constant, τ_B is the B^+ lifetime, $f_B = 192.8 \pm 9.9$ MeV [30] is the B^+ decay constant, and m_B, m_τ are the masses of B^+, τ^+, respectively. Here $|V_{ub}| = (3.52 \pm 0.11) \times 10^{-3}$ is the relevant CKM matrix element, obtained through the combined fit [31,32] to all the data excluding the $B^+ \to \tau^+\nu_\tau$ measurements. The SM prediction, including higher-order corrections, is

$$\mathrm{BR}(B^+ \to \tau^+\nu_\tau)_{\mathrm{SM}} = (0.81 \pm 0.15) \times 10^{-4}\ . \tag{29}$$

The experimental world average is [33]

$$\mathrm{BR}(B^+ \to \tau^+\nu_\tau)_{\mathrm{exp}} = (1.68 \pm 0.31) \times 10^{-4}\ . \tag{30}$$

Clearly, this measurement deviates significantly from the SM prediction given in Eq. (6.3). Defining $R^{\mathrm{exp}}_{\tau\nu_\tau}$ to be [34,35]

$$R^{\mathrm{exp}}_{\tau\nu_\tau} \equiv \frac{\mathrm{BR}(B^+ \to \tau^+\nu_\tau)_{\mathrm{exp}}}{\mathrm{BR}(B^+ \to \tau^+\nu_\tau)_{\mathrm{SM}}}\ , \tag{31}$$

and using Eqs. (29) and (30), we get

$$R^{\mathrm{exp}}_{\tau\nu_\tau} = 2.07 \pm 0.54\ , \tag{32}$$

which indicates a $\sim 2\sigma$ deviation. Following Ref. [34], we characterize the NP models that could potentially explain this anomaly by a quantity $R^{\mathrm{NP}}_{\tau\nu_\tau}$, defined as

$$R^{\mathrm{NP}}_{\tau\nu_\tau} \equiv \frac{\mathrm{BR}(B^+ \to \tau^+\nu_\tau)_{\,\mathrm{SM+NP}}}{\mathrm{BR}(B^+ \to \tau^+\nu_\tau)_{\mathrm{SM}}}\ , \tag{33}$$

where the subscript SM+NP represents the net branching ratio in the NP scenario, including the SM contribution. The 95% C.L. allowed range for $R^{\mathrm{NP}}_{\tau\nu_\tau}$ then works out to

$$0.99 < R^{\mathrm{NP}}_{\tau\nu_\tau} < 3.14\,, \tag{34}$$

which essentially means that NP models with positive contributions are favored by the data and those with negative contributions are quite strongly disfavored. In two-Higgs doublet models, of which the cMSSM is an example – the branching ratio of $B^+ \to \tau^+\nu_\tau$ is given by [36]

$$\mathrm{BR}(B^+ \to \tau^+\nu_\tau)_{\mathrm{NP}} = \frac{G_F^2 m_B m_\tau^2}{8\pi}\left(1-\frac{m_\tau^2}{m_B^2}\right)^2 f_B^2\,|\widetilde{V}_{ub}|^2\,\tau_B\left(1-\tan^2\beta\frac{m_B^2}{M_+^2}\right)^2. \tag{35}$$

In the above formula $|\widetilde{V}_{ub}|$ is the value of $|V_{ub}|$ obtained in the context of the NP model, which in general will be different from $|V_{ub}|$ obtained from the data in the context of the SM. In order to get rid of this uncertainty in the CKM parameter, we restrict ourselves to the determination of $|V_{ub}|$ through only those measurements that are independent of NP. Such a fit is called the fit to the universal unitarity triangle (UUTfit) [37], and it uses only (i) the measurements of $|V_{ub}/V_{cb}|$ from semileptonic B decays, (ii) the ratio of mass differences in the B_s and B_d systems: $|\Delta M_s/\Delta M_d|$, and (iii) the measurement of $\sin 2\beta$ from the time-dependent CP asymmetry in $B_d \to J/\psi K^{(*)}$. The UUTfit value of $|V_{ub}|$ comes out as [31]

$$|V_{ub}|_{\rm UUTfit} = (3.50 \pm 0.12) \times 10^{-3} \ , \tag{36}$$

which is actually very close to the global fit value. Once $|V_{ub}|$ is chosen in this "model-independent" way, we can take $|\widetilde{V}_{ub}| = |V_{ub}|_{\rm UUTfit}$, and hence the theoretical MFV prediction for $R^{\rm NP}_{\tau\nu}$ at the tree level becomes

$$R^{\rm NP}_{\tau\nu_\tau}|_{\rm tree} = \left(1 - \tan^2\beta \frac{m_B^2}{M_+^2}\right)^2 \ . \tag{37}$$

If higher-order corrections are included then this ratio gets modified [38] to a form

$$R^{\rm NP}_{\tau\nu_\tau} = \left(1 - \frac{\tan^2\beta}{1 + \tilde{\epsilon}_0 \, \tan\beta} \frac{m_B^2}{M_+^2}\right)^2 \ , \tag{38}$$

where $\tilde{\epsilon}_0$ encodes all the higher-order corrections. The impact of the experimental data on MFV models with a charged Higgs boson, as discussed above, can be clearly discerned from Fig. 13(a), where we plot the value of $R^{NP}_{\tau\nu_\tau}$ as a function of the charged Higgs boson mass. Clearly, high $\tan\beta$ and low charged higgs mass is required for the solution of the $B^+ \to \tau^+\nu_\tau$ problem. Fig. 13(b) shows how severely the parameter space is ruled out with the current data as compared to the 2008 measurement.

D.1 Constraining the cMSSM

Here we list briefly the theoretical, collider and low enrgy constraints other than the $B^+ \to \tau^+\nu_\tau$ branching ratio. These are (i)Requirement of correct electroweak symmetry breaking, (ii)Requirement of neutral LSP, (iii)Nondiscovery in direct searches [20] at the CERN LEP and Fermilab Tevatron of predicted particles, most notably the light Higgs boson h^0 and the lighter chargino $\widetilde{\chi}_1^+$, and (iv)Indirect bounds coming from the measurements of (a) the anomalous magnetic moment of the muon, (b) the rate of the radiative decay $B_d \to X_s\gamma$, and (c) the BR for the leptonic decay $B_s \to \mu^+\mu^-$. We now analyse the constraints on the m_0–$m_{1/2}$ plane, keeping A_0 floating between -2 TeV and $+2$ TeV. In our analysis, a point in the m_0–$m_{1/2}$ plane, for a given $\tan\beta$, is taken

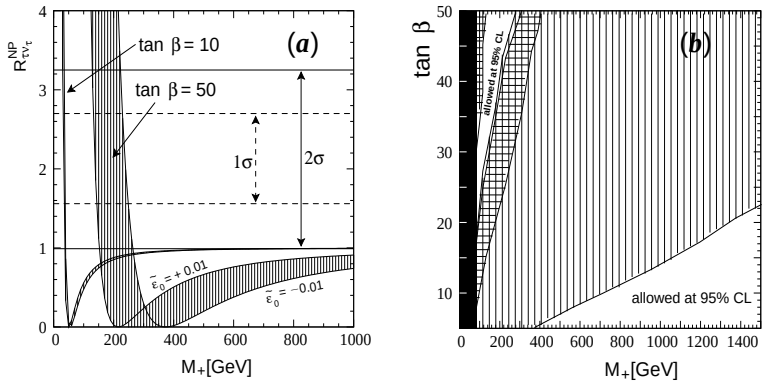

Figure 13: (a) The dependence of $R^{NP}_{\tau\nu_\tau}$ on the mass M_+ of the charged Higgs boson in MFV models for two values $\tan\beta = 10$ and 50, and (b) the 95% C.L. constraints on the M_+–$\tan\beta$ plane. The vertically hatched regions in (a) correspond to higher order corrections varying between $\tilde{\epsilon}_0 = -0.01$ and $+0.01$, while the 1σ (2σ) experimental measurements of $R^{NP}_{\tau\nu_\tau}$ are shown by horizontal broken (solid) lines. The dark band in (b) corresponds to the LEP bound. The large, vertically hatched region in (b) is disallowed by the recent (2010) $R^{NP}_{\tau\nu_\tau}$ constraint, while the horizontally hatched region is disallowed by the 2008 data.

to be allowed at 95% C.L. by a given constraint if we can find any value of A_0, lying in the range -2 TeV $\leq A_0 \leq 2$ TeV, for which the given constraint is satisfied. Our results are exhibited in Fig. 14. We now plot, in the left panel of Fig. 15, the same constraints in the plane of A_0 and $m_{1/2}$, keeping m_0 fixed at the value $m_0 = 150$ GeV, for $\tan\beta = 10$. The very first prediction one would naturally demand from a specific point or region in the cMSSM parameter space is whether this can adequately explain the dark-matter content of the Universe as a relic density of LSP's. The CMBR data indicate a relic density $\Omega h^2 = 0.1123 \pm 0.007$ at 95% C.L. [39]. In general, SUSY models with a low-lying mass spectrum, such as the one in question, tend to predict too large a density of LSP's unless these are coannihilated by some reaction with a substantial crosssection. This leads to a restriction on the cMSSM parameter space, which, given the accuracy of the CMBR data, confines us, more or less, to a line passing through the four-dimensional parameter space. The dark-matter requirement is known to favor large negative values of A_0 [40–42], and it is rather gratifying to see that this line passes right through the allowed region in the parameter space discovered in this work – which seems to indicate that a SUSY explanation of dark-matter may indeed be the correct one. The line consistent with the dark-matter requirement[1] is shown by red dots on both panels in Fig. 15 and may be seen to pass clearly through the allowed region, favoring a narrow range of A_0 around -1.25 TeV and $\tan\beta$ in the range $9 - 11$. In order to make a clear prediction about the LHC signals, we choose the following

[1]We do not go so far as to call it a constraint, though this is not unheard of in the literature.

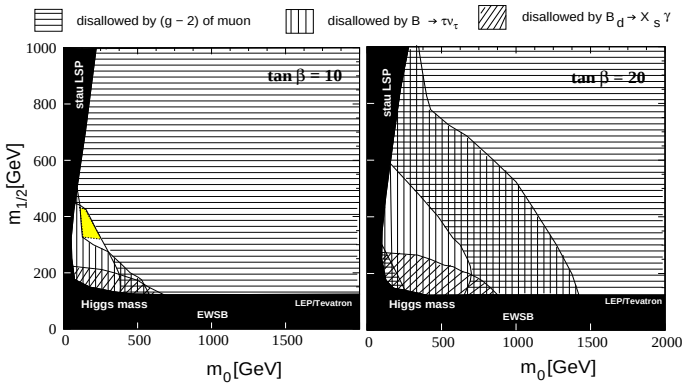

Figure 14: The 95% C.L. constraints on the m_0–$m_{1/2}$ plane, for $\tan\beta = 10$ (left panel) and $\tan\beta = 20$ (right panel). The trilinear coupling A_0 is kept floating over the range $(-2, +2)$ TeV. Horizontal (vertical) hatching indicates regions ruled out by the measurement of the muon $(g-2)/2$ ($BR(B^+ \to \tau^+\nu_\tau)$). We take $\mu > 0$ in this and all subsequent plots. Regions are considered disallowed only if they remain disallowed for all values of A_0 in the given range. This weakens the constraints enough for a small allowed region to appear in the left panel ($\tan\beta = 10$). The yellow/light gray region is simultaneously consistent with *all* constraints at 95% C.L.

benchmark point in the cMSSM parameter space:

$$m_0 = 150 \text{ GeV} , \quad m_{1/2} = 400 \text{ GeV} , \quad A_0 = -1250 \text{ GeV} , \quad \tan\beta = 10 , \quad \mu > 0 . \tag{39}$$

At this benchmark point, we get the central values of the observables to be $\text{BR}(B \to X_s\gamma) = 2.64 \times 10^{-4}, R_{\tau\nu}^{NP} = 0.993$, and $a_\mu = 13.0 \times 10^{-10}$. Clearly, all of these are consistent with the measurements to within 2σ, though $R_{\tau\nu}^{NP}$ only barely survives the 2σ bound.

We now discuss the cMSSM mass spectrum expected with this benchmark point. The lightest Higgs boson h^0 is predicted to have a mass around 119 GeV, and hence must be detected through the rare decay $h^0 \to \gamma\gamma$, which is unlikely in the 7 TeV run.The heavy Higgs bosons, including the H^+, will lie in the range 835–840 GeV, which is again kinematically inaccessible in the 7 TeV run.The gluino mass, however, is as high as 934 GeV and the squark masses mostly populate the range 800–900 GeV, except for the $\widetilde{b}_1$, with mass around 719 GeV, and a light stop $\widetilde{t}_1$ which lies as low as 393 GeV. An immediate consequence of these large squark and gluino masses is that the sparticle production cross section at the LHC will be on the low side: at 7 TeV it will be around 0.4 pb at the leading order (LO), while at 14 TeV, it will have the much healthier value of 5.2 pb at LO. About 60% of these crosssections come from squark pair production, of which roughly half is due to $\widetilde{t}_1\widetilde{t}_1^*$ production alone. The $\widetilde{t}_1$ will decay to a top quark and a neutralino with a BR $\sim 2/3$, and hence, a possible signal would be a top-enriched final state with large missing transverse energy (MET).

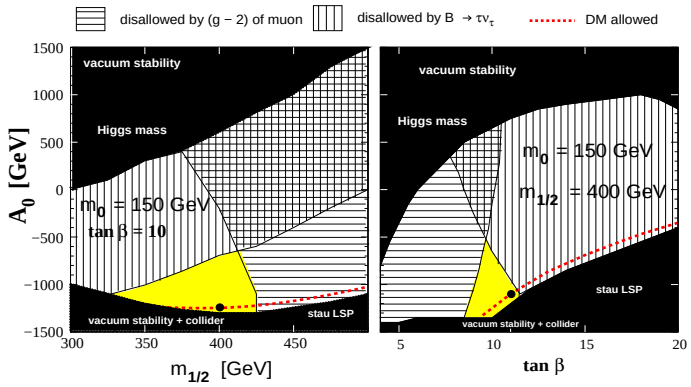

Figure 15: Further constraints on the cMSSM parameter space. The left panel shows constraints on the $m_{1/2}$–A_0 plane, for $m_0 = 150$ GeV and $\tan\beta = 10$. The right panel shows, similarly, constraints on the $\tan\beta$–A_0 plane for $m_0 = 150$ GeV and $m_{1/2} = 400$ GeV. Notations and conventions are the same as in Fig. 14. The dotted (red) line represents the dark-matter-compatible region, and the black dot superposed on it is a benchmark point chosen for LHC studies.

However, the enormous $t\bar{t}$ background to this process must be taken into consideration when studying this signal. The other traditional signals for SUSY – cascade decays of the gluino or squarks to charginos and heavy neutralinos, ending up in multileptons, jets, and MET – in this case provide τ-rich final states because of the low-lying $\widetilde{\tau}_1$. It may be noted that the entire parameter space allowed by low-energy constraints at 95% C.L., including our golden point, lies just outside the 5σ discovery limit of ATLAS [43].

D.2 NUHM : explaining $B^+ \to \tau^+\nu_\tau$

In the previous analysis, we have seen that the combination of constraints on the cMSSM parameter space leads to the prediction of a small value of $\tan\beta$ and hence, according to Fig. 13(b), the charged Higgs boson is necessarily heavy. Comparison with Fig. 13(a) readily shows that in this limit, the model is only just consistent with the $B^+ \to \tau^+\nu_\tau$ constraint at 95% C.L. However, if we take the position that the 2σ discrepancy between the SM and the experimental result should be *explained* by a positive NP contribution, then the cMSSM fails the test, for it actually tends to diminish the SM prediction, and barely survives exclusion in a decoupling limit. This bare survival, by the skin of its teeth, as it were, is the proximate cause of the stringent constraints on the cMSSM parameter space discussed in the previous section.

As the cMSSM is the SUSY model with the maximum number of simplifying assumptions (and hence the minimum number of free parameters), it is interesting to ask if the relaxation of one or more of these assumptions could lead to a SUSY model which actually explains, rather than merely remains consistent with, the $B^+ \to \tau^+\nu_\tau$ discrep-

ancy. Since the NP effect in $B^+ \to \tau^+\nu_\tau$ involves the scalar sector of the cMSSM, an obvious option would be to consider a model where the parameters of the Higgs sector are given a greater degree of flexibility than in the highly constrained cMSSM.

In this context, an obvious choice of model is the so-called The nonuniversal Higgs-mass (NUHM) model which is an extension of the cMSSM where the Higgs-mass parameters m_{H_1} and m_{H_2} are delinked from the universal scalar mass parameter m_0 at the GUT scale and are allowed to vary freely [44]. At the electroweak scale, these two extra parameters m_{H_1} and m_{H_2} are usually traded for the Higgsino mixing parameter μ and the pseudoscalar Higgs boson mass m_A. This model, therefore, has *six* parameters, viz. $m_0, m_{1/2}, \mu, M_A, A_0$ and $\tan\beta$. While an exhaustive study of the NUHM parameter

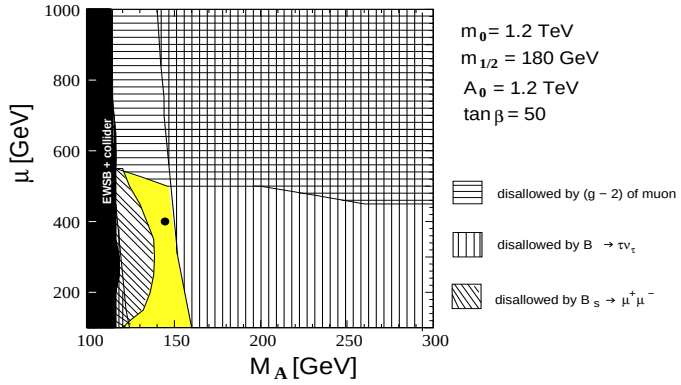

Figure 16: Constraints on the M_A–μ parameter space in the NUHM model. Notations and conventions are the same as in the previous plots, except that now there is a significant constraint from $B_s \to \mu^+\mu^-$ rather than $B_d \to X_s\gamma$. The yellow/light gray region is allowed by all the constraints, and the black dot inside it is a benchmark point chosen for LHC studies.

space vis-á-vis the present set of constraints would require a separate work in itself, it is interesting to see if the NUHM model can at all provide regions in parameter space which are consistent with all the constraints, and can simultaneously provide a NP explanation of the $B^+ \to \tau^+\nu_\tau$ discrepancy. To illustrate that this is, in fact, possible, we show in Fig. 16 the regions allowed by the different constraints in the m_A–μ plane, keeping all the other parameters fixed at

$$m_0 = 1.2 \text{ TeV} , \qquad m_{1/2} = 180 \text{ GeV} , \qquad A_0 = 1.2 \text{ TeV} , \qquad \tan\beta = 50 . \tag{40}$$

As before, to be precise about the LHC signals, we choose a benchmark point, which has the fixed parameter choices of Eq. (40) as well as

$$M_A = 145 \text{ GeV} , \qquad \mu = 400 \text{ GeV} , \tag{41}$$

which is indicated in Fig. 16 by a small black dot in the middle of the allowed (yellow/light gray) patch. The central values of the observables at this point are BR($B \to$

$X_s\gamma) = 3.50 \times 10^{-4}, R_{\tau\nu}^{NP} = 1.24, \mathrm{BR}(B_s \to \mu^+\mu^-) = 3.22 \times 10^{-8}, a_\mu = 12.8 \times 10^{-10}$, all of which are well within the 2σ range of the respective measurements. We note that the relic density of LSP's at this point is not enough to saturate the CMBR requirements, which means that this model is not ruled out by the latter, but is not a solution to that problem either.

We reiterate that NUHM models which explain the $B^+ \to \tau^+\nu_\tau$ discrepancy and, at the same time, remain consistent with the data on $B_s \to \mu^+\mu^-$, will generically come with light gauginos, and lead to collider signals somewhat similar to those discussed above. However, what we have studied is just one portion of the NUHM parameter space, inasmuch as we fixed m_0 and A_0 to very large values. A more comprehensive scan over the NUHM parameter space might reveal more patches consistent with all the constraints, and some of these may lead to collider signals which are different from those discussed in the context of our benchmark point. The detailed exploration of the NUHM parameter space in this context calls for a separate study.

E Conclusions

Flavour-changing neutral current (FCNC) processes are expected to be incisive probes of new physics. In the SM, they occur only at loop level, and hence are suppressed. This may allow the new-physics (NP) effects to be identifiable. Of course, since we have no clue about what form the NP takes, the observations from a variety of processes are necessary. In this thesis, we have focussed on the processes that involve the effective transition $b \to s\mu^+\mu^-$. While specific models of NP may be used and their effect on the relevant observables studied, we have chosen to explore the NP in a model-independent way, in terms of the Lorentz structures of the NP operators that contribute to the effective $b \to s\mu^+\mu^-$ Hamiltonian. We have performed a general analysis that includes NP vector-axial vector (VA), scalar-pseudoscalar (SP), and/or tensor (T) operators. We have considered both CP conserving as well as CP violationg observables. In the remaining part of this thesis we have investigated the departure of the branching ratio of $B^+ \to \tau^+\nu_\tau$ from its SM value and the resulting constraints on MFV models. Though improved values for f_B from lattice and $|V_{ub}|$ from tree level decays will be important to confirm any true departure from SM, in any case, values of $\mathrm{Br}(B^+ \to \tau^+\nu_\tau)$ significantly above 1×10^{-4} will signal NP contributions either in this decay or somewhere else.

In the transition $b \to s\mu^+\mu^-$ new VA operators are the ones that influence the observables strongly in most cases. They typically can interfere with the SM terms constructively or destructively, thus enhancing or suppressing the differential branching ratios by up to factors of 2 or 3. They also are able to enhance almost all the asymmetries, the notable exception being A_{FB} in $\bar{B}_d^0 \to \bar{K}\mu^+\mu^-$, where the VA operators cannot contribute. But for most other observables, this kind of NP can potentially be observed. This can be traced to the large magnitudes of the NP couplings still al-

lowed by data, which in turn can be traced to the possibility of interference between the new VA operators with the SM operators that allows more freedom for the new VA couplings. Typically, the $R_{V,A}$ couplings are constrained more weakly than the $R'_{V,A}$ couplings, since the corresponding operators have the same structure as those of the SM, allowing strong destructive interferences. Consequently, the operators with $R_{V,A}$ couplings are more likely to show themselves over and above the SM background. We point out that the exception to this rule is the A_{FB} in $\bar{B}^0_d \to \bar{K}^*\mu^+\mu^-$ at large q^2, where the $R'_{V,A}$ couplings can cause a larger enhancement.

The SP operators, on the other hand, are handicapped by the stringent constraints from the upper bound on $B(\bar{B}^0_s \to \mu^+\mu^-)$. If only $R_{S,P}$ or $R'_{S,P}$ couplings are present, the constraints become even more severe. It is for this reason that, even when the SP contributions are unsuppressed by m_μ/m_b, they are not often large enough to stand apart from the SM background. The couplings of the T operators, viz. C_T and C_{TE}, are not as suppressed as those of the SP operators. Therefore, they typically contribute significantly to the DBRs. However, the interference terms of these operators with the SM operators often suffer from the m_μ/m_b helicity suppression, and hence they tend to suppress the magnitudes of the asymmetries. It is crucial to understand this SM background, which makes it imperative to use observables whose values are predicted reasonably accurately within the SM.

The main source of the SM uncertainties is the hadronic matrix elements, whose theoretical calculations often have errors of the order of tens of percent. We have handled this on many levels. First, we have tried to identify observables that will not be very sensitive to the hadronic uncertainties. For example in $\bar{B}^0_d \to \bar{K}\mu^+\mu^-$, the SM prediction for the forward-backward asymmetry is simply zero, independent of any hadronic elements. Also, while the differential branching ratios may be strongly dependent on the hadronic matrix elements, the forward-backward asymmetries are less so. Furthermore, the large-energy effective theory (LEET) limits can be used to control the uncertainties in the low-q^2 region for observables like A_{FB} and $A_T^{(2)}$. For example, certain observables, such as the zero-crossing of A_{FB} in $\bar{B}^0_d \to \bar{K}^*\mu^+\mu^-$, can be shown to be robust under form-factor uncertainties in the LEET limit. The new observable A_{LT} in $\bar{B}^0_d \to \bar{K}^*\mu^+\mu^-$ that is introduced in this paper also has a zero crossing in the SM with small hadronic uncertainties. These measurements can even be used to extract the parameters of the NP operators, to a very good approximation.

In the last part of this thesis, we have shown that the combined effect many low-energy measurements – those consistent with the SM (e.g. the branching ratios of $B_d \to X_s\gamma$ and $B_s \to \mu^+\mu^-$) as well as those showing deviations from the SM (e.g. the anomalous magnetic moment of the muon, and the branching ratio of the $B^+ \to \tau^+\nu_\tau$) – results not only in indicating new physics, but also in pinpointing the relevant new physics parameters. In particular, we have pointed out that the latest measurement of $B^+ \to \tau^+\nu_\tau$ branching ratio has a large impact on a large class of NP models, especially those which include a charged Higgs boson H^+. In fact, the decay $B^+ \to \tau^+\nu_\tau$, by

itself, can constrain most of the models with minimal flavour violation that involve an H^+. This is because the latest measurement gives a branching ratio $\sim 2\sigma$ more than the SM prediction. If this discrepancy is to be explained by a MFV model, one needs very light charged Higgs bosons ($M_+ \lesssim 200$ GeV) and large $\tan\beta$ ($\gtrsim 20$). On the other hand, a heavy charged Higgs boson ($M_+ \gtrsim 300$ GeV) and a small $\tan\beta$ can be barely consistent with the data to within 2σ, but cannot be considered an explanation for the gap between theory and experiment. This is a general result that can be applied to any member of the MFV models, and we choose to apply it to the constrained MSSM, which is motivated by mSUGRA and is one of the most predictive SUSY models. Our results indicate a rather specific region of parameter space which is allowed by all the low energy measurements. We also discuss the specific signals at the LHC which can be used to look for SUSY in that parameter space.

We will finish by saying that flavour physics is a very rich field which necessarily will be a prominent part of a future theory of fundamental interactions both at large and short distance scales. Flavour Physics is characterized by a fruitful interplay between theory and experiments. This has led to many significant discoveries and developments. B physics has the potential to determine many important parameters of the electroweak theory and to test the Standard Model at low energies. At the same time, through the study of CP violation it provides a window to physics beyond the Standard Model. Indeed, there is a fair chance that such New Physics will be seen in the present collider experiment like the Large Hadron Collider and also in the high-luminosity experiments to come in future.

Bibliography:

[17] C. Bobeth, M. Misiak, and J. Urban, *Photonic penguins at two loops and m_t-dependence of $BR(B \to X_s l^+ l^-)$*, *Nucl. Phys.* **B574** (2000) 291–330, [hep-ph/9910220].

[18] W. Altmannshofer et al., *Symmetries and Asymmetries of $B \to K^* \mu^+ \mu^-$ Decays in the Standard Model and Beyond*, *JHEP* **01** (2009) 019, [arXiv:0811.1214].

[19] **CDF** Collaboration, T. Aaltonen et al., *Search for $B_s^0 \to \mu^+ \mu^-$ and $B_d^0 \to \mu^+ \mu^-$ decays with $2fb^{-1}$ of p anti-p collisions*, *Phys. Rev. Lett.* **100** (2008) 101802, [arXiv:0712.1708].

[20] **Particle Data Group** Collaboration, C. Amsler et al., *Review of particle physics*, *Phys. Lett.* **B667** (2008) 1–1340.

[21] **Heavy Flavor Averaging Group** Collaboration, E. Barberio et al., *Averages of b-hadron and c-hadron Properties at the End of 2007*, arXiv:0808.1297.

[22] **BABAR** Collaboration, B. Aubert et al., *Measurement of the $B \to X_s l^+ l^-$ branching fraction with a sum over exclusive modes*, *Phys. Rev. Lett.* **93** (2004) 081802, [hep-ex/0404006].

[23] **Belle** Collaboration, M. Iwasaki et al., *Improved measurement of the electroweak penguin process $B \to X_s l^+ l^-$*, *Phys. Rev.* **D72** (2005) 092005, [hep-ex/0503044].

[24] M. Blanke, A. J. Buras, D. Guadagnoli, and C. Tarantino, *Minimal Flavour Violation Waiting for Precise Measurements of Delta M_s, $S_{\psi\phi}$, A^s_{SL}, $|V_{ub}|$, gamma and $B^0_{s,d} \to \mu^+\mu^-$*, *JHEP* **10** (2006) 003, [hep-ph/0604057].

[25] T. Huber, T. Hurth, and E. Lunghi, *Logarithmically Enhanced Corrections to the Decay Rate and Forward Backward Asymmetry in $\bar{B} \to X_s l^+ l^-$*, *Nucl. Phys.* **B802** (2008) 40–62, [arXiv:0712.3009].

[26] K. S. M. Lee, Z. Ligeti, I. W. Stewart, and F. J. Tackmann, *Extracting short distance information from $b \to s l^+ l^-$ effectively*, *Phys. Rev.* **D75** (2007) 034016, [hep-ph/0612156].

[27] D. Melikhov and N. Nikitin, *Rare radiative leptonic decays $B_{d,s} \to l^+ l^- \gamma$*, *Phys. Rev.* **D70** (2004) 114028, [hep-ph/0410146].

[28] A. Ali, E. Lunghi, C. Greub, and G. Hiller, *Improved model independent analysis of semileptonic and radiative rare B decays*, *Phys. Rev.* **D66** (2002) 034002, [hep-ph/0112300].

[29] A. K. Alok et al., *New Physics in $b \to s\mu^+\mu^-$: CP-Conserving Observables*, arXiv:1008.2367.

[30] J. Laiho, E. Lunghi, and R. S. Van de Water, *Lattice QCD inputs to the CKM unitarity triangle analysis*, *Phys. Rev.* **D81** (2010) 034503, [arXiv:0910.2928].

[31] **UTfit collaboration** Collaboration, M. Bona et al., *An Improved Standard Model Prediction Of $BR(B \to \tau\nu)$ And Its Implications For New Physics*, *Phys. Lett.* **B687** (2010) 61–69, [arXiv:0908.3470].

[32] **CKMfitter Group** Collaboration, J. Charles et al., *CP violation and the CKM matrix: Assessing the impact of the asymmetric B factories, updated results and plots available at: http://ckmfitter.in2p3.fr* , *Eur. Phys. J.* **C41** (2005) 1–131, [hep-ph/0406184].

[33] S. T'Jampens (CKMFitter Collaboration), Talk at ICHEP 2010,.

[34] G. Isidori and P. Paradisi, *Hints of large tan(beta) in flavour physics*, *Phys. Lett.* **B639** (2006) 499–507, [hep-ph/0605012].

[35] J. R. Ellis, S. Heinemeyer, K. A. Olive, A. M. Weber, and G. Weiglein, *The Supersymmetric Parameter Space in Light of B- physics Observables and Electroweak Precision Data*, *JHEP* **08** (2007) 083, [arXiv:0706.0652].

[36] W.-S. Hou, *Enhanced charged Higgs boson effects in $B^- \to \tau\bar{\nu_\tau}$, $\mu\bar{\nu_\mu}$ and $b \to \tau\,\bar{\nu_\tau} + X$*, *Phys. Rev.* **D48** (1993) 2342–2344.

[37] A. J. Buras, P. Gambino, M. Gorbahn, S. Jager, and L. Silvestrini, *Universal unitarity triangle and physics beyond the standard model*, *Phys. Lett.* **B500** (2001) 161–167, [hep-ph/0007085].

[38] A. G. Akeroyd and S. Recksiegel, *The effect of H^{+-} on $B^{+-} \to \tau^{+-}\nu_\tau$ and $B^{+-} \to \mu^{+-}\nu_\mu$*, *J. Phys.* **G29** (2003) 2311–2317, [hep-ph/0306037].

[39] E. Komatsu et al., *Seven-Year Wilkinson Microwave Anisotropy Probe (WMAP) Observations: Cosmological Interpretation*, arXiv:1001.4538.

[40] V. A. Bednyakov, S. G. Kovalenko, H. V. Klapdor-Kleingrothaus, and Y. Ramachers, *Is SUSY accessible by direct dark matter detection?*, *Z. Phys.* **A357** (1997) 339–347, [hep-ph/9606261].

[41] J. R. Ellis, K. A. Olive, Y. Santoso, and V. C. Spanos, *High-Energy Constraints on the Direct Detection of MSSM Neutralinos*, *Phys. Rev.* **D69** (2004) 015005, [hep-ph/0308075].

[42] U. Chattopadhyay, D. Das, A. Datta, and S. Poddar, *Non-zero trilinear parameter in the mSUGRA model - dark matter and collider signals at Tevatron and LHC*, *Phys. Rev.* **D76** (2007) 055008, [arXiv:0705.0921].

[43] **ATLAS collaboration** Collaboration, J. Dietrich, *The ATLAS discovery reach for SUSY models with early data*, arXiv:1005.2034.

[44] V. Berezinsky et al., *Neutralino dark matter in supersymmetric models with nonuniversal scalar mass terms*, *Astropart. Phys.* **5** (1996) 1–26, [hep-ph/9508249].

Chapter 1

Introduction

It is now common knowledge that matter is made from atoms, which stick together to form molecules. There are simple substances like water which is made of simple molecules containing only two or three atoms. More complicated objects like animals are made from more complicated molecules such as proteins and DNA, and contain millions of atoms, which stick together to make cells, tissue, fur and brains. There are around a hundred different types of atoms known as elements, from hydrogen to uranium, catalogued by chemists in the periodic table. Chemistry of these elements can be understood by learning the properties of 3 particles – proton, neutron and electron, and the influence of the electromagnetic force. In the same spirit, the Standard Model (SM) [45, 46] describes the chemistry of all the fundamental particles known till date. The theories and discoveries of thousands of physicists over the past century have resulted in a remarkable insight into the fundamental structure of matter: all the visible matter in the Universe is found to be made from twelve fundamental matter particles, their interactions governed by four fundamental forces carried by force carriers called gauge bosons. Seven of these particles – charm, bottom, top, tau neutrino, W, Z and gluon were predicted by the Standard Model before they were observed experimentally! There is one additional particle predicted by the Standard Model called the Higgs, which has not yet been observed. Our best understanding of how these twelve matter particles and three of the forces are related to each other is encapsulated in the Standard Model of particles and forces. Developed in the early 1970s, it has successfully explained a large number of experimental results and precisely predicted a wide variety of phenomena. Over time and through many experiments by many physicists, the Standard Model has become established as a well-tested theory.

The SM consists of three types of fields, the spin one fields, the spin half fields and a spin zero field. The spin-one fields are described by introducing gauge redundancies in the fields that appear in the Lagrangian. This means that a particular symmetry of the Lagrangian is treated as a redundancy, i.e., two field configurations related by that symmetry transformation are identified with the same physical state. The spectrum of spin-one particles is described by the lie algebra of gauge redundancies $\mathrm{SU(3)_C \times SU(2)_W \times U(1)_Y}$ where C stands for 'Color', W stands for 'Weak' and Y stands for 'hYpercharge'. The number of spin-one particles turns out to be the dimension of

the adjoint representation which works out to be $(3^2-1)=8$ for $SU(3)_C$, $(2^2-1)=3$ for $SU(2)_W$ and 1 for $U(1)_Y$.

The spin-half sector of the SM can be conveniently discussed in terms of the Weyl fields which are irreducible representation (1/2,0) of the Lorentz lie-algebra $SO(3,1)$. These fileds lie in particular representations of the lie-algebra of the SM gauge group,

$$Q \equiv (3,2)_{1/6},\ U_c \equiv (\bar{3},1)_{-2/3},\ D_c \equiv (\bar{3},1)_{1/3},\ L \equiv (1,2)_{-1/2},\ E_c \equiv (1,1)_{+1}, \qquad (1.1)$$

where the first number in the bracket is the $SU(3)_C$ representation and the second number refers to the $SU(2)_W$ representation. The number outside the bracket is the Hypercharge of the multiplet. In the SM there are 3 copies of each of these irreducible representations. These correspond to three generations of spin-half fields. The fields which transform non-trivially under $SU(3)_C$ are called quarks and the fields which are singlets of $SU(3)_C$ are called Leptons.

The spin zero sector of the SM contains only one field, the Higgs field which lie in the representation $(1,2)_{1/2}$ of the SM lie-algebra. Till now the Higgs particle which is last missing part for the experimental confirmation of the SM, has escaped the direct detection at high energy colliders.

The local gauge invariance of SM implies that all the spin-one gauge bosons have to be massless and should carry long range forces. As we have experimentally observed massive gauge bosons which mediate the short range weak force, there must be something beyond the local gauge symmetry which can generate masses of these gauge bosons. This was achieved with the help of spontaneous symmetry breaking through the Higgs mechanism [47]. In the Higgs mechanism the local gauge symmetry is spontaneously broken by the Vacuum Expectation Value (VEV) of the scalar Higgs $SU(2)_W$ doublet of the SM. This is a superconductivity-like phase transition, the electroweak phase transition which removes some of the spin-one bosons from the low energy spectrum (by making them masive) reducing the gauge algebra to $SU(3)_C \times U(1)_{em}$ where 'em' refers to electromagnetism. This can be compared with the Meissner effect in Superconductivity. This at low energies is followed by another phase transition: the confinement phase transition[1], which again removes some more spin-one fields from the low energy spectrum reducing the gauge algebra to electromagnetism only. Another unique property of the SM is that the lie-algebra representation (R_{SM}) for the matter fields is chiral i.e., the representation $R_{SM} \otimes R_{SM}$ does not have any trivial subrepresentation. This means that the gauge invariance also forbids masses for all the fermions. After the symmetry breaking these fermions acquire masses due to their couplings, called the Yukawa couplings, to the Higgs field.

Spontaneously broken non-abelian Yang-Mills gauge theories were also proved to be renormalizable in the early seventies [48]. The reason why physicists prefer renor-

[1]One of the most important physics experiment that aims to study this phase transition from the de-confined phase called the Quark Gluon Plasma to the confined phase of Mesons and Hadrons is the so called Relativistic Heavy Ion Collider (RHIC in short).

malizable field theories is that they are more predictive. Renormalizability allows us to make precise predictions for measurable quantities also in higher orders of the perturbative expansion. A renormalizable field theory's predictions only depend on a finite number of low-energy parameters that may be determined by a comparison with the experiments. With a fixed value of the low-energy parameters such as the couplings and masses, a renormalizable theory may be uniquely extrapolated to arbitrarily high scales and it remains predictive at arbitrarily high scales.

On the other hand, in the modern way to understanding quantum field theory as an effective field theory, the theory includes all renormalizable (relevant and marginal) operators, which give the largest contribution to any low energy process, but when we are interested in either high precision or high energy processes, we have to systematically include non-renormalizable terms as well, which come from some more complete theory at a higher energy scale. This also means that if we postulate that the new physics only occurs at some extremely high scale Λ, all effects of the new physics are suppressed by positive powers of $1/\Lambda$. This assumption makes life controllable. However, nothing guarantees that we immediately get the right description that is valid to an arbitrarily high energy scale. By studying particle physics at ever higher energy scales, we may equally well unmask just another layer of the onion that would break down at slightly higher energies and needs to be fixed by another layer.

Another important triumph for the structure of the SM was the absence of axial vector anomalies among the gauge currents, which is a fundamental consistency check on any chiral gauge theories. Technically this means that the fermionic measure appearing in the path-integral is gauge-invariant. Though individual multiplets in Eq. 1.1 contribute non-trivially to the anomaly, when the contributions from all the multiplets in a generation are summed up, the anomalies cancel each other quite miraculously. This cancellation happens within each fermionic generation of the SM.

Both, the Higgs mechanism and the proof of renormalizability were the foundations of the application of local gauge theories to describe short range weak interactions and the starting point of the formulation of the SM. As was mentioned before, the spontaneous breaking of gauge symmetry needs the introduction of at least one scalar particle – the Higgs. At this point it is worth mentioning that the single-Higgs model is an extremely economical way to perturbatively unitarize the theory and also accomplish the symmetry breaking [2]. In extensions of SM, more number of Higgs doublets can also be realized. There are two interesting virtues of the weakly-interacting Higgs model: (i) it is calculable, and (ii) it is so far phenomenologically successful, as it is consistent with the LEP and SLD electroweak precision data [49]. Both calculability (which results from perturbativity) and the success in passing the precision tests follow from the Higgs boson being light. It is however well known that an elementary light scalar is unstable under radiative corrections, its mass receives quadratically divergent

[2]But we know that in another similar physical system, the QCD, it is not the solution that Nature has chosen.

corrections, which makes a light Higgs scalar highly unnatural in the absence of some symmetry which protects its mass (like the chiral symmetry for fermions). An old and still attractive idea is that the Higgs boson might be a bound state of a new strongly interacting dynamics not much above the weak scale. Being composite, it would solve the SM hierarchy problem if the scale of the strong dynamics is not too high, as quantum corrections to its mass are now saturated at the compositeness scale. Significant theoretical progress on the construction of these theories has recently come from the intriguing connection between gravity in certain higher dimensional curved spacetimes and strongly coupled gauge theories [50].

A quite remarkable and intriguing property of SM is that all the fermion representations repeat themselves thrice in what are called generations. The only difference from one generation to another is the masses of the fermions. Flavor physics denotes physics of transitions among these three generations of Standard Model fermions and that the fermions of different generations have different masses plays a crucial role here. A unique property built in the structure of the SM is that there are tree level flavour-changing charged current processes, but there are no flavour changing tree level current interactions, due to the famous Glashow-Iliopoulos-Maiani (GIM) mechanism [51]. In fact, the charmed quark was predicted to explain the lack of flavour-changing neutral currents (FCNC). The FCNC processes happen only through loop diagrams in the SM and therefore their rates are suppressed. As unknown heavy particles can propagate and make their existance feel through loops, flavour physics can probe such new physics (NP) through loop corrections, before those NP particles themselves are produced on-shell in energy frontier experiments. For example, the mass of charm quark was successfully predicted from Δm_K before it was discovered in 1975 [52]. The large mixing observed in the neutral B system led to the speculation that the top quark must be quite heavier than the rest of the quarks [53, 54], and the rate of radiative B decays [55] predicted the correct ballpark for top quark mass before its direct discovery.

Flavor physics is also intimately connected with the origin of fermion masses. In the limit of vanishing masses the flavour physics is trivial –no intergenerational transitions occur since weak and mass eigenbases coincide with each other. It is the misalignment of weak and mass eigenstates or the mismatch between the basis states in which Yukawa terms in the up and down sectors are diagonal that makes flavour physics interesting. In the quark sector of SM this mismatch is described by a single unitary matrix - the Cabibbo-Kobayashi-Maskawa (CKM) matrix [56, 57]. In the lepton sector, on the other hand, flavour violation is described by the Pontecorvo-Maki-Nakagawa-Sakata (PMNS) [58–60] matrix. The Charge-Parity (CP) violation in the SM is also closely related to flavour physics. It crucially relies on the fact that there are (at least) three generations of fermions. In the Standard Model the CP violation in the quark sector, in neutral K and B meson systems, has been observed experimentally and it is well accounted by the CKM mechanism and no CP violation has been measured yet in the lepton sector.

In this context, another important question is to ask whether the standard model of particle physics combined with the standard model of cosmology can explain the value of the observed Baryon Asymmetry of the Universe (BAU). This has been answered in recent years and, surprisingly, the answer does not refer to the role the CKM phase may play in these explanatory attempts. Theoretical progress in understanding the SM electroweak phase transition in the early universe in conjunction with the experimental lower bound on the mass of the SM Higgs boson, $m_h > 114$ GeV, leads to the conclusion: no! But even in models beyond SM, the existence of new sources of CP violation beyond the CKM picture is required to be able to account for the observed BAU through baryogenesis [61, 62] and hence it is important to investigate possible new source of CP violation in both the quark and the lepton sectors.

The rich phenomenology of weak decays of Hadrons and Mesons has always been a source of information about the nature of elementary particle interactions. The CKM picture which was borne out of experimental necessity, has been able to explain with good accuracy all the empirical observations in the flavour sector till date. But despite the impressive success of the CKM picture where the GIM mechanism plays a very crucial role, there are many avenues where existence of new physics contribution can not be ruled out. In particular, weak decays of hadrons containing heavy quarks are good candidates for precision tests of the Standard Model and measurements of its parameters. They offer the most direct way to determine the weak mixing angles, to test the unitarity of the CKM matrix, and to explore the physics of CP violation.

A number of selected processes and observables have played a leading role in learning about the quantum mechanical structure of the SM through high precision experiments. This selection is based on the sensitivity to NP and theoretical cleanness. The former can be increased with the increased precision of experiments and the latter can improve with the progress in theoretical calculations, in particular the non-perturbative methods like the lattice simulations. In this regard, the flavour-changing semileptonic decay, $b \to s l^+ l^-$ is an ideal choice especially because its amplitude is very sensitive to the presence of heavy quarks, scaling as $\text{mass}^2_{\text{quark}}$. This mode is useful because apart from Branching Ratios (BR) it also provides a great deal of other observables like dilepton invariant mass spectrum, forward-backward asymmetry etc. The full angular distribution of all the final state particles in case of exclusive decays like $B \to K^* l^+ l^-$ contains large number of terms which can be used to form various asymmetries. In general, these asymmetries are sensitive to different Lorentz Structures of the underlying Lagrangian in different ways and therefore can be used to identify the nature of NP.

An important issue here is to realize that the claim of existence of NP in some observable can only be made in an unambiguous way only if the SM prediction for that observable is known reasonably precisely. This is where hadronic uncertainties come into picture. The theory predictions are more reliable for the inclusive modes. For the exclusive modes the uncertainties are larger mainly because of their dependence

on form factors, which are manifestly properties of bound states and therefore of non-perturbative character. This is why it is extremely important to construct observables which are less prone to hadronic uncertainties. The different asymmetries fall into this category because they are ratios of certain quantities and theoretical uncertainties are expected to cancel to a good extent. Similarly vanishing of certain quantities are sometimes relates to the presence of some (approximate) symmetries of the theory and thus are useful to look for new physics. The CP violating effects in this $b \to s$ mode is also expected to be extremely tiny in the SM. Hence, CP violating asymmetries are good places to verify whether any dynamics beyond the the CKM picture is at work.

As opposed to the $b \to s$ transitions which is a loop process, the theoretically much cleaner tree level decays probe individual entries of the CKM matrix directly and hence are indispensable for the vindication of the CKM structure. The leptonic decay $B^+ \to \tau\nu_\tau$ is one such example which directly probes the (1,3) element of the CKM matrix, V_{ub}. As the decay rate of this process is also proportional to the B meson decay constant f_B, precise lattice calculation of f_B is also required to determine the value of V_{ub}. Recently, the directly measured branching fraction for this decay has shown a considerable deviation from the global fit prediction and this deviation persists then that would call for possible NP explanations.

Indeed there is big room for new physics (NP) contributions in rare decays of mesons and also in CP-violating observables. With more and more data on these decays and observables accompanied by improved theoretical calculations will possibly exclude several of presently studied models. There are two approaches one can take to study the effect of new physics on a particular process. One approach is to choose a specific microscopic model and examine the possible ways one one can get deviations from SM. This in turn can also restrict the parameter space of that Model. The other approach is to abandon specific models and write down all possible operators respecting only the Lorentz Symmetry (and may be the SM gauge symmetry). This would allow us to make model independent statements about how these operators are constrained, which can also be translated to bounds on specific couplings or specific combination of couplings in a particular Model. In this thesis, for the $b \to s l^+ l^-$ mode we follow the second approach and for the $B^+ \to \tau\nu_\tau$ mode we restrict our discussion to Supersymmetric Models. Theoretical analysis of these modes requires a familiarity with the flavour structure of the SM as well as with the language of effective theories. Therefore, in the next two chapters we will review the necessary concepts of the Standard Model CKM mechanism and the notion of effective theories respectively. In Chapter 4 we shall consider the CP conserving observables in the decay modes involving the $b \to s l^+ l^-$ transition, while the CP violating observables will be presented in Chapter 5. The repercussion of the measurement of the branching ratio of $B^+ \to \tau\nu_\tau$ and the latest CKM Global Fit on the parameter spaces of the Supersymmetric model will be taken up in Chapter 6. We will close our journey in Chapter 7 with a critical summary of

our findings along with some concluding remarks.

Bibliography:

[45] S. L. Glashow, "Partial Symmetries of Weak Interactions," Nucl. Phys. **22**, 579 (1961).

[46] S. Weinberg, "A Model of Leptons," Phys. Rev. Lett. **19**, 1264 (1967).

[47] P. W. Higgs, "Broken Symmetries and the Masses of Gauge Bosons," Phys. Rev. Lett. **13**, 508 (1964).

[48] G. 't Hooft and M. J. G. Veltman, "Combinatorics of gauge fields," Nucl. Phys. B **50**, 318 (1972).

[49] J. Alcaraz [ALEPH and CDF and D0 and DELPHI and L3 and OPAL and SLD Collaboration], "Precision Electroweak Measurements and Constraints on the Standard Model," arXiv:0911.2604 [hep-ex].

[50] C. Csaki, J. Hubisz and P. Meade, "TASI lectures on electroweak symmetry breaking from extra dimensions," hep-ph/0510275.

[51] S. L. Glashow, J. Iliopoulos and L. Maiani, "Weak Interactions with Lepton-Hadron Symmetry," Phys. Rev. D **2**, 1285 (1970).

[52] M. K. Gaillard, B. W. Lee and J. L. Rosner, "Search for Charm," Rev. Mod. Phys. **47**, 277 (1975).

[53] J. R. Ellis, J. S. Hagelin and S. Rudaz, "Reexamination of the Standard Model in the Light of B Meson Mixing," Phys. Lett. B **192**, 201 (1987).

[54] I. I. Y. Bigi and A. I. Sanda, "From a New Smell to a New Flavor: B (d) anti-B (d) Mixing, CP Violation and New Physics," Phys. Lett. B **194**, 307 (1987).

[55] N. G. Deshpande, P. Lo, J. Trampetic, G. Eilam and P. Singer, "$B \to K^* \gamma$ and the Top Quark Mass," Phys. Rev. Lett. **59**, 183 (1987).

[56] N. Cabibbo, "Unitary Symmetry and Leptonic Decays," Phys. Rev. Lett. **10**, 531 (1963).

[57] M. Kobayashi and T. Maskawa, "CP Violation in the Renormalizable Theory of Weak Interaction," Prog. Theor. Phys. **49**, 652 (1973).

[58] B. Pontecorvo, "Mesonium and antimesonium," Sov. Phys. JETP **6**, 429 (1957) [Zh. Eksp. Teor. Fiz. **33**, 549 (1957)].

[59] Z. Maki, M. Nakagawa and S. Sakata, "Remarks on the unified model of elementary particles," Prog. Theor. Phys. **28**, 870 (1962).

[60] B. Pontecorvo, "Neutrino Experiments and the Problem of Conservation of Leptonic Charge," Sov. Phys. JETP **26**, 984 (1968) [Zh. Eksp. Teor. Fiz. **53**, 1717 (1967)].

[61] A. Riotto, "Theories of baryogenesis," hep-ph/9807454.

[62] W. Bernreuther, "CP violation and baryogenesis," Lect. Notes Phys. **591**, 237 (2002) [hep-ph/0205279].

Chapter 2

The CKM Paradigm

The fantastic performance of the two asymmetric B-factories, the Belle and BaBar, in the last decade has led to a significant progress in our understanding of the flavour sector of the SM. The CKM mechanism which was put forward as an ansatz in 1970's, is now a well established theory and any new physics can only be a correction to it. Be it a simple tree level or a more complicated rare decay or some CP asymmetry, the CKM structure has consistently explained all experimental numbers with sufficient accuracy. Quite interestingly, a single phase in the CKM matrix could accommodate both the small CP violation in the K system as well as comparatively large CP violation in the B system.

In this chapter we will recapitulate some of the basic virtues of the Standard Model CKM picture and set up some notations. This would be useful for our arguments from time to time in the subsequent chapters.

2.1 The Flavour parameters of the SM

The masses and mixings of quarks have a common origin in the Standard Model (SM). They arise from the Yukawa interactions with the SU(2) doublet Higgs,

$$\mathcal{L}_Y = -Y^d_{ij}\bar{Q}_i\Phi D_j - Y^u_{ij}\bar{Q}_i\,\epsilon\,\Phi^* U_j + \text{h.c.}, \tag{2.1}$$

where $Y^{u,d}$ are $3\times$ 3 complex matrices, Φ is the Higgs field, i, j are generation labels, and ϵ is the 2×2 antisymmetric tensor. Q_i are left-handed quark doublets, and D_j and U_j are right-handed down- and up-type quark singlets, respectively, in the flavour eigenstate basis. When Φ acquires a vacuum expectation value, $<\Phi>= (0, v/\sqrt{2})^T$, it yields mass terms for the quarks. In general, the matrices $Y^{u,d}$ have off-diagonal elements which lead to flavour violationg processes. The physical states (mass eigenstates) are obtained by diagonalizing $Y^{u,d}$.

From Eq. 2.1 we can see that the SM lagrangian has two Yukawa matrices $Y^{u,d}$. As both Y^u and Y^d are in general complex 3×3 matrices, naively one might think that the number of the SM flavour parameters is given by 18 real and 18 imaginary ones. However, a closer look into the structure of SM shows that some of the parameters

which appear in the Yukawa matrices are unphysical. A simple way to understand this is to realize the fact that a flavour basis transformation,

$$\mathrm{Q} \to \mathrm{V_Q Q}\,, \qquad \mathrm{U} \to \mathrm{V_U U}\,, \qquad \mathrm{D} \to \mathrm{V_D D}\,, \tag{2.2}$$

leaves the SM Lagrangian invariant, apart from redefinition of the Yukawas,

$$\mathrm{Y_u} \to \mathrm{V_Q Y^u V_U^\dagger}\,, \qquad \mathrm{Y^d} \to \mathrm{V_Q Y^d V_D^\dagger}\,, \tag{2.3}$$

where $\mathrm{V_i}$ are 3×3 unitary matrices. Each of the three rotation matrices $\mathrm{V_{Q,U,D}}$ contains three real parameters corresponding to the three rotation generators of the subgroup SO(3) and six imaginary ones corresponding to the remaining generators of U(3). The elements of $\mathrm{V_{Q,U,D}}$ can now be chosen appropriately to eliminate some of the parameters of $\mathrm{Y_{u,d}}$.

Let us identify all the flavour parameters of the SM in a systematic way. After the symmetry breaking of the Higgs field $\langle\Phi\rangle = (0, v/\sqrt{2})^{\mathrm{T}}$, Eq. 2.1 gives the mass term for the d-type quarks:

$$\mathcal{L}(\mathrm{d}) = -\frac{\mathrm{v}}{\sqrt{2}}[\mathrm{Y^d_{ij}}\bar{\mathrm{d}}_{\mathrm{Li}}\mathrm{d}_{\mathrm{Rj}} + \mathrm{h.c.}]\,. \tag{2.4}$$

Here $\mathrm{Y^d_{ij}}$ is a 3×3 complex matrix. Such a matrix can always be put into real diagonal form with the help of two unitary matrices, so that we can write,

$$\mathrm{Y^d} = \mathrm{D_L^\dagger \hat{m}^d D_R}\,, \tag{2.5}$$

where $\mathrm{\hat{m}^d}$ is a real diagonal matrix, and $\mathrm{D_L}$, $\mathrm{D_R}$ are unitary matrices. If the diagonal elements are distinct, as appears experimentally to be the case, $\mathrm{D_L}$, $\mathrm{D_R}$ are unique, except that both may be multiplied on the left by the same phase factor matrix,

$$\begin{pmatrix} \mathrm{e}^{\mathrm{i}\alpha_1} & 0 & 0 \\ 0 & \mathrm{e}^{\mathrm{i}\alpha_2} & 0 \\ 0 & 0 & \mathrm{e}^{\mathrm{i}\alpha_3} \end{pmatrix}\,.$$

Similarly for the u quarks, on symmetry breaking, Eq. 2.1 gives the u-quark mass terms,

$$\mathcal{L}(\mathrm{u}) = -\frac{\mathrm{v}}{\sqrt{2}}[\mathrm{Y^u_{ij}}\bar{\mathrm{u}}_{\mathrm{Li}}\mathrm{u}_{\mathrm{Rj}} + \mathrm{h.c.}] \tag{2.6}$$

It can be brought into real diagonal form in a similar way:

$$\mathrm{Y^u} = \mathrm{U_L^\dagger \hat{m}^u U_R}\,, \tag{2.7}$$

where $\mathrm{U_L}$ and $\mathrm{U_R}$ are unitary matrices, and $\mathrm{\hat{m}_u}$ is diagonal. $\mathrm{U_L}$ and $\mathrm{U_R}$ may be both multiplied on the left by a phase factor matrix, say

$$\begin{pmatrix} \mathrm{e}^{\mathrm{i}\beta_1} & 0 & 0 \\ 0 & \mathrm{e}^{\mathrm{i}\beta_2} & 0 \\ 0 & 0 & \mathrm{e}^{\mathrm{i}\beta_3} \end{pmatrix}\,.$$

It is useful to define the 'true' quark fields for which the mass matrices are diagonal:

$$\begin{aligned} \mathrm{d'_{Li}} &= \mathrm{D_{L\,ij} d_{Lj}}\ ,\ \mathrm{d'_{Ri}} = \mathrm{D_{R\,ij} d_{Rj}}, \\ \mathrm{u'_{Li}} &= \mathrm{U_{L\,ij} u_{Lj}}\ ,\ \mathrm{u'_{Ri}} = \mathrm{U_{R\,ij} u_{Rj}}. \end{aligned} \tag{2.8}$$

Dropping the primes, the SM flavour Lagrangian in the mass basis is given by,

$$\begin{aligned} \mathcal{L}^{\mathrm{F}}_{\mathrm{m}} = & \left(\overline{\mathrm{u_L}}\,\overline{\mathrm{c_L}}\,\overline{\mathrm{t_L}}\right) \begin{pmatrix} \mathrm{y_u} & 0 & 0 \\ 0 & \mathrm{y_c} & 0 \\ 0 & 0 & \mathrm{y_t} \end{pmatrix} \begin{pmatrix} \mathrm{u_R} \\ \mathrm{c_R} \\ \mathrm{t_R} \end{pmatrix} (v+h) + (\mathrm{u,c,t}) \leftrightarrow (\mathrm{d,s,b}) \\ & + \frac{g_2}{\sqrt{2}} \overline{\mathrm{u_{Li}}} \gamma^{\mu} \mathrm{V^{CKM}_{ij}} \mathrm{d_{Lj}} \mathrm{W^{+}_{\mu}} + \mathrm{h.c.}, \end{aligned} \tag{2.9}$$

where $\mathrm{W^{\pm}}$ stands for the charged electroweak gauge bosons, h is the physical Higgs field, $\mathrm{v} \sim 246\,\mathrm{GeV}$, $\mathrm{m_i} = \mathrm{y_i v}/\sqrt{2}$ and $\mathrm{V^{CKM}}$ is the CKM matrix:

$$\mathrm{V^{CKM}} = \mathrm{U_L D_L^{\dagger}}. \tag{2.10}$$

There is a freedom in defining $\mathrm{V^{CKM}}$ in that we can permute between the various generations. This permutation ambiguity for ordering the CKM entries is removed by arranging the fields in Eq. (2.9) according to their masses in the increasing order. The elements of $\mathrm{V^{CKM}}$ are therefore written as follows:

$$\mathrm{V^{CKM}} = \begin{pmatrix} \mathrm{V_{ud}} & \mathrm{V_{us}} & \mathrm{V_{ub}} \\ \mathrm{V_{cd}} & \mathrm{V_{cs}} & \mathrm{V_{cb}} \\ \mathrm{V_{td}} & \mathrm{V_{ts}} & \mathrm{V_{tb}} \end{pmatrix}. \tag{2.11}$$

Here the entries are labeled by the quark flavours. The vertex at which a b-quark decays to a $\mathrm{W^-}$ and c-quark is proportional to $\mathrm{V_{cb}}$; similarly, the vertex at which a c-quark decays to a $\mathrm{W^+}$ and s-quark is proportional to $\mathrm{V^*_{cs}}$.

Since the product of two unitary matrices is unitary, $\mathrm{V^{CKM}}$ is a 3×3 unitary matrix. A 3×3 unitary matrix is specified by $3^2 = 9$ parameters, so we apparently have nine parameters to be measured experimentally. But using the six arbitrary phases in the matrices $\mathrm{D_L}$ and $\mathrm{U_L}$, five out of the nine parameters can be removed. One can only remove five parameters and not six because in the CKM matrix only phase differences appear and only five independent phase differences can be constructed out of the six phases. We are now in a position to count and identify the physical parameters of the Flavor sector of SM. There are 6 masses for the up and down type quarks. The CKM matrix, on the other hand, has 4 independent parameters, 3 of them are angles and the remaining one is a phase –the sole source of CP violation in the SM.

So to make the long story short, the charged current interactions are the only terms in the SM Lagrangian which are not invariant under the vectorial $\mathrm{U(1)^6}$ transformations on the quark fields (as evident from Eq. (2.9)),

$$\mathrm{u_i} \to \mathrm{e^{i\beta_i} u_i}\ ,\ \mathrm{d_i} \to \mathrm{e^{i\alpha_i} d_i}. \tag{2.12}$$

The diagonal part of this transformation corresponds to the classically conserved baryon current, while the non-diagonal, $U(1)^5$, part of the transformation can be used to remove 5 out of the 6 phases, leaving the CKM matrix with a single physical phase.

It is worth mentioning here that though both the Baryon number(B) and the Lepton number(L) are classically conserved quantum numbers in the renormalisable Lagrangian of the Standard Model, quantum mechanically both B and L are anomalous and the associated currents have a non zero divergence induced by instanton effects, which are of the form $\partial_\mu j^\mu_{B,L} = a\, W^{\mu\nu}\tilde{W}_{\mu\nu} + b\, B^{\mu\nu}\tilde{B}_{\mu\nu}$, where $W^{\mu\nu}$ and $B^{\mu\nu}$ are the field strength tensors of the SU(2) and U(1) gauge fields and a, b are some numerical coefficients. It turns out that though both B and L are violated quantum mechanically (B - L) is a true conserved quantity. This is also the reason behind why neutrino mass can not be generated in the SM even by non-perturbative effects.

2.2 CP Violation and the Unitarity Triangle

It is clear from the definition of the CKM matrix V^{CKM} in the previous section that it is a measure of the mis-allignment of the flavour eigenstates of the up and down type quarks. Hence, all the flavour and CP violation in the SM arise solely through the CKM matrix. It alone governs the interaction strength and mixing of all the charged current interactions in the SM. In theories beyond the SM, there can be in general, other sources of flavour and CP violation. But if V^{CKM} is the only source of CP violation (for example, in any Minimal Flavour Violating (MFV) models which will be discussed later), there are many relations between CP-conserving and CP violating observables. This is a remarkable property of the CKM picture of CP violation: measuring a number of CP conserving quantities can tell us whether all CP violation is predicted by the same quantity in the SM. This property stems from the fact that the CKM matrix V^{CKM} is by definition a unitary matrix in the flavour space.

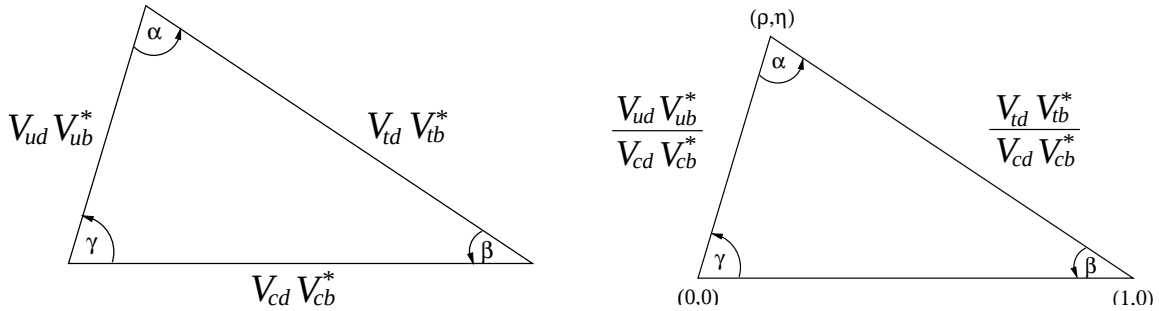

Figure 2.1: (Left panel) The unitarity triangle directly expressing Eq. (2.13) in pictorial form. (Right panel) The rescaled version of the Unitarity Triangle in the (ρ, η) plane, which is discussed later in the text.

Because V^{CKM} is unitary, $|V_{ud}|^2+|V_{us}|^2+|V_{ub}|^2 = 1$, and similarly for all other rows and columns. These constraints can be used to obtain information about unmeasured or poorly measured elements of V^{CKM}. For example, because $|V_{cb}|$ and $|V_{ub}|$ are known to be small, $|V_{tb}|$ should be very close to 1—if, indeed, there are only three generations. By similar arguments, $|V_{ts}|$ and $|V_{td}|$ must also be small. More interesting constraints come from the orthogonality of columns (or rows) of V^{CKM}. For example, taking the first and third columns of V^{CKM}, one has

$$V_{ud}V_{ub}^* + V_{cd}V_{cb}^* + V_{td}V_{tb}^* = 0\,. \tag{2.13}$$

Equation (2.13) is a sum of three complex numbers that add up to zero. One can draw these complex numbers as vectors in the complex plane, and since they sum up to zero they will have to form a closed triangle. Because it is a consequence of the unitarity property of V^{CKM}, this triangle is called the "unitarity triangle", shown in the left panel of Fig. 2.1. The lengths of the sides are $|V_{ud}V_{ub}^*|$, $|V_{cd}V_{cb}^*|$ and $|V_{td}V_{tb}^*|$. The relative angles between two sides are the arguments of the ratios of these complex numbers

$$\alpha = \arg\left[-\frac{V_{td}V_{tb}^*}{V_{ud}V_{ub}^*}\right], \qquad \beta = \arg\left[-\frac{V_{cd}V_{cb}^*}{V_{td}V_{tb}^*}\right], \qquad \gamma = \arg\left[-\frac{V_{ud}V_{ub}^*}{V_{cd}V_{cb}^*}\right]. \tag{2.14}$$

An equivalent notation $\beta \equiv \phi_1$, $\alpha \equiv \phi_2$, $\gamma \equiv \phi_3$ is also used in the literature. By definition, $\alpha+\beta+\gamma = \pi$. One can normalize one of the sides to length one and turn it such that it lies on the real axis. The resulting triangle is what we see in the right panel of Fig. 2.1.

In fact, here are five more unitarity triangles which come from the orthogonality of other rows and columns. The unitarity triangles are extremely useful because they provide a simple and vivid summary of the CKM mechanism. The area of all these unitarity triangles can be shown to be equal and denoted by $|J|/2$. A good confirmation of the CKM mechanism is to check whether the lengths and angles determined through the measurements of various decays, mixing rates and CP asymmetries are consistent with each other. Furthermore, when one combines independent measurements—from the B, B_s, K, and D systems, all triangles should have the same area. If there are non-CKM contributions beyond the SM then there should be conflicts among the different independent measurements because the interpretation of rates and asymmetries as measurements of the sides and angles of the unitarity triangles will no longer hold.

The size of the CP violation can be written in terms of a rephasing invariant (independent of the phase redefinitions of the quark fields) quantity involving the commutator of the up and down type mass matrices,

$$\det C = \det[\hat{m}^u\hat{m}^{u\dagger}, \hat{m}^d\hat{m}^{d\dagger}] = -2iF_uF_dJ. \tag{2.15}$$

where

$$\mathrm{F_u} = (\mathrm{m_u^2} - \mathrm{m_c^2})(\mathrm{m_c^2} - \mathrm{m_t^2})(\mathrm{m_t^2} - \mathrm{m_u^2})\,, \tag{2.16}$$

$$\mathrm{F_d} = (\mathrm{m_d^2} - \mathrm{m_s^2})(\mathrm{m_s^2} - \mathrm{m_b^2})(\mathrm{m_b^2} - \mathrm{m_d^2})\,, \tag{2.17}$$

$$\mathrm{J} = \mathrm{Im}[\mathrm{V_{ij}V_{kj}^*\,V_{k\ell}V_{i\ell}^*}] \sum_{\mathrm{m}} \varepsilon_{\mathrm{ikm}} \sum_{\mathrm{n}} \varepsilon_{\mathrm{j\ell n}}\,. \tag{2.18}$$

The definition of J is valid for all combinations of i, j, k, and ℓ. J is called the Jarlskog invariant [63].

Ignoring the Θ term of QCD (which leads to the so-called strong CP problem, for a review see [64]), the CP violation in the SM from the CKM mechanism is solely determined by the determinant $\det \mathrm{C}$. It is clear from the definition of J that for CP violation in the SM, complex nature of the CKM matrix is necessary. This reminds us that CP violation stems from complex couplings. It is also important to notice that there is no CP violation unless $\mathrm{F_u}$, $\mathrm{F_d}$, and J are all different from zero. Hence all the up and down type quarks have to be non-degenerate in mass so as to have non zero CP violation in the SM.

2.3 Parameterization of CKM Matrix

The fact that there are only three real and one imaginary physical parameters in V can be made manifest by choosing an explicit parametrization. A general unitary matrix can be constructed as a product of rotation matrices and unitary matrices made up of phase factors. There is no unique parameterisation of the KM matrix by this method. The one advocated by the Particle Data Group (PDG) [65] is

$$\begin{aligned}
\mathrm{V^{CKM}} &= \begin{pmatrix} 1 & 0 & 0 \\ 0 & c_{23} & s_{23} \\ 0 & -s_{23} & c_{23} \end{pmatrix} \begin{pmatrix} e^{-i\delta/2} & 0 & 0 \\ 0 & 1 & 0 \\ 0 & 0 & e^{i\delta/2} \end{pmatrix} \begin{pmatrix} c_{13} & 0 & s_{13} \\ 0 & 1 & 0 \\ -s_{13} & 0 & c_{13} \end{pmatrix} \times \\
&\quad \begin{pmatrix} e^{i\delta/2} & 0 & 0 \\ 0 & 1 & 0 \\ 0 & 0 & e^{-i\delta/2} \end{pmatrix} \begin{pmatrix} c_{12} & s_{12} & 0 \\ -s_{12} & c_{12} & 0 \\ 0 & 0 & 1 \end{pmatrix} \\
&= \begin{pmatrix} c_{12}c_{13} & s_{12}c_{13} & s_{13}e^{-i\delta_{13}} \\ -s_{12}c_{23} - c_{12}s_{23}s_{13}e^{i\delta_{13}} & c_{12}c_{23} - s_{12}s_{23}s_{13}e^{i\delta_{13}} & s_{23}c_{13} \\ s_{12}s_{23} - c_{12}c_{23}s_{13}e^{i\delta_{13}} & -c_{12}s_{23} - s_{12}c_{23}s_{13}e^{i\delta_{13}} & c_{23}c_{13} \end{pmatrix}
\end{aligned} \tag{2.19}$$

where $c_{ij} = \cos\theta_{ij}$ and $s_{ij} = \sin\theta_{ij}$. Each angle is here labelled with the indices corresponding to the mixing of two families, so that $\theta_{ij} = 0$ would indicate that families i and j are decoupled; all these angles can always be chosen to lie in the first quadrant and the phase of δ_{13} is chosen so that $0 \leq \delta_{13} < 2\pi$.

Using the parameterization of Eq. (2.19) the Jarlskog invariant can be writen as

$$\mathrm{J} = \mathrm{c}_{12}\mathrm{c}_{23}\mathrm{c}_{13}^2\mathrm{s}_{12}\mathrm{s}_{23}\mathrm{s}_{13}\sin\delta_{13}\,. \tag{2.20}$$

From the above explicit expression the fact of the disappearance of CP violation with the vanishing of any mixing angle θ_{ij} is manifest. On the other hand the product of all three mixing angles appears in J, so that the hierarchical structure of the CKM matrix, with relatively small inter-family mixing, suppresses any CP-violating amplitude even for $\delta = \pi/2$. So the CKM matrix must not only have complex entries, but also non-trivial mixing; otherwise the KM phase δ_{13} can be removed. From Eq. 2.18 one can also see that at least four different quarks (real or virtual) must be involved for a process to exhibit CP violation.

In nature the mixing angles are such that the matrix elements of $\mathrm{V}^{\mathrm{CKM}}$ have very different magnitudes. In 1983 it was realized that the bottom quark decays predominantly to charm quark so that $|\mathrm{V_{cb}}| \gg |\mathrm{V_{cb}}|$. Wolfenstein then noticed that $|\mathrm{V_{cb}}| \sim |\mathrm{V_{us}}|^2$ and introduced an approximate parameterization of $\mathrm{V}^{\mathrm{CKM}}$. It is approximate in the sense that the unitarity only holds approximately. The Wolfenstein parameterization [66] which has become popular till then and has been used extensively in phenomenological studies has the following form,

$$\mathrm{V}^{\mathrm{CKM}} = \begin{pmatrix} 1-\frac{1}{2}\lambda^2 & \lambda & A\lambda^3(\rho - i\eta) \\ -\lambda & 1-\frac{1}{2}\lambda^2 & A\lambda^2 \\ A\lambda^3(1-\rho-i\eta) & -A\lambda^2 & 1 \end{pmatrix} + \mathcal{O}(\lambda^4)\,. \tag{2.21}$$

It has four real parameters λ, A, ρ, and η all of which should be determined experimentally. From experiments $\lambda \approx 0.22$, $A \approx 0.8$, and $\sqrt{\rho^2+\eta^2} \approx 0.4$, so it was indeed phenomenologically useful to expand $\mathrm{V}^{\mathrm{CKM}}$ in powers of λ.

The above approximate form of the $\mathrm{V}^{\mathrm{CKM}}$ can also be derived from the exact parameterization of Eq. 2.19 by setting

$$\lambda \equiv \mathrm{s}_{12}\,, \qquad \mathrm{A} \equiv \mathrm{s}_{23}/\lambda^2\,, \qquad \rho + \mathrm{i}\eta \equiv \mathrm{s}_{13}\mathrm{e}^{\mathrm{i}\delta_{13}}/\mathrm{A}\lambda^3\,. \tag{2.22}$$

The Wolfenstein parametrization is indeed a good approximation to the actual numerical values. That is, the CKM matrix is very close to a unit matrix with off diagonal terms that are small. The order of magnitude of each element can be read from the power of λ. Each up-type quark preferably couples to the down-type quark of the same family, and to other ones with couplings which are smaller, the more the two families are distant; indeed the off-diagonal elements are of order λ between generations 1 and 2, λ^2 between 2 and 3 and λ^3 between 1 and 3 : $|\theta_{12}| \gg |\theta_{23}| \gg |\theta_{13}|$ in the parameterisation of Eq. 2.19. One can easily check that the unitarity relations – normalisation of each row and column of $\mathrm{V}^{\mathrm{CKM}}$ and orthogonality of each pair of rows and columns is satisfied up to order λ^3. An expansion of $\mathrm{V}^{\mathrm{CKM}}$ up to a higher power of λ must be made if better experimental accuracy is reached. Another observation is

that $\eta/\rho \sim \mathcal{O}(1)$ shows that CP is not even an approximate symmetry of the SM: the smallness of CP-violating effects is just due to the small mixing angles which appear together with the complex phase δ_{13} in the expression for specific observables, rather than a necessity. Conversely, it should be observed that the CP-violating parameter η can be determined also from experiments on CP-conserving processes, since the CKM matrix is uniquely determined by the moduli of its elements; for example if A is known the knowledge of $|\mathrm{V_{ub}}|$ and $|\mathrm{V_{td}}|$ gives ρ and η. The knowledge of the moduli of the CKM matrix elements is thus sufficient to put a limit on the amount of CP violation in the SM.

It is important to note that the position in which complex terms appear in the CKM matrix is not physically significant, as in different parametrizations the complex phase shifts to different matrix elements. Clearly, the physics should not depend on the choice of the parametrization, and quantities must be identified which are insensitive to such choice; again, CP violation will only be present if a complex term appears which cannot be made real with any choice of arbitrary phases. The Jarlskog invariant J, as was already mentioned before is such a rephasing invariant quantity and hence a measure of true CP violation.

The Jarlskog invariant can now be expressed $\mathrm{J} = \mathrm{A}^2\lambda^6\eta \approx (7 \times 10^{-5})\eta$. It is also clear from the above expression that the CKM CP violation is small not only because δ_{13} is small but also because flavour violation in the SM is suppressed, empirically, by powers of λ.

The unitarity triangle which we wrote in Eq. (2.13) is special, because its three sides are all of order $\mathrm{A}\lambda^3$. The angles α, β, γ of the triangle defined in Eq. 2.14 can be easily expressed in terms of the parameters of the Wolfenstein Parameterisation as [1]

$$\alpha = \tan^{-1}\left(\frac{\bar{\eta}}{\bar{\eta}^2 + \bar{\rho}(\bar{\rho}-1)}\right), \quad \beta = \tan^{-1}\left(\frac{\bar{\eta}}{1-\bar{\rho}}\right), \quad \gamma = \tan^{-1}\left(\frac{\bar{\eta}}{\bar{\rho}}\right). \tag{2.23}$$

The triangle formed from the orthogonality of the first and third rows also has this property, but it is not accessible, because the top quark decays before the mesons needed to measure the angles are bound:

$$\mathrm{V_{td}V_{ud}^*} + \mathrm{V_{ts}V_{us}^*} + \mathrm{V_{tb}V_{ub}^*} = 0\,. \tag{2.24}$$

The other triangles are all long and thin, with sides $(\lambda, \lambda, A\lambda^5)$ (e.g., for the Kaon system)

$$\mathrm{V_{ud}V_{us}^*} + \mathrm{V_{cd}V_{cs}^*} + \mathrm{V_{td}V_{ts}^*} = 0\,, \tag{2.25}$$

or $(\lambda^2, \lambda^2, A\lambda^4)$ (e.g., for the $\mathrm{B_s}$ meson),

$$\mathrm{V_{us}V_{ub}^*} + \mathrm{V_{cs}V_{cb}^*} + \mathrm{V_{ts}V_{tb}^*} = 0\,. \tag{2.26}$$

[1] The replacements $\rho \to \bar{\rho} = \rho(1-\lambda^2/2)$ and $\eta \to \bar{\eta} = \eta(1-\lambda^2/2)$ improve the accuracy of the Unitarity Triangle apex.

In Eq. (2.26) the third term is much smaller than the other two. This makes the angle

$$\beta_s = \arg\left[-\frac{V_{ts}V_{tb}^*}{V_{cs}V_{cb}^*}\right] = \lambda^2\eta + \mathcal{O}(\lambda^4) \tag{2.27}$$

very small, of order one degree. Therefore, the CP asymmetry in for example, $B_s \to J/\psi\phi$ is expected to be smaller in the SM than the corresponding asymmetry in the B decays. The precise measurement of β_s is thus important to identify the existence of any NP. Furthermore, this asymmetry is also sensitive to new physics in $B_s^0 - \bar{B}_s^0$ mixing. The Tevatron experiments have discovered and precisely quantified $B_s^0 - \bar{B}_s^0$ mixing oscillations [67–69] whose frequency is in good agreement with the Standard Model prediction, and presented first determinations of the associated CP-violating phase from tagged analyses of $B_s \to J/\psi\phi$ decays [70, 71]. Recently, possible New Physics in the $B_s^0 - \bar{B}_s^0$ mixing amplitude has received considerable attention after the Tevatron measurement of dimuon charge asymmetry which disagrees with the Standard Model prediction by more than 3 standard deviations [72]. The most recent measurement of β_s and the width difference of the $B_s^0 - \bar{B}_s^0$ system by the LHCb collaboration [73] is though in good agreement with the SM prediction.

The orthogonality of the first two rows of the CKM matrix gives the unitarity triangle for the D system,

$$V_{ud}V_{cd}^* + V_{us}V_{cs}^* + V_{ub}V_{cb}^* = 0\,. \tag{2.28}$$

The three sides of this triangle are of order $(\lambda, \lambda, A\lambda^5)$ and thus it is even thinner than the one for the B_s system. This makes its determination in the current flavour physics experiments extremely challenging but a non-zero measurement of the CP asymmetry in the D system would be clear sign of new physics.

2.4 The Global CKM fit

The CKM matrix elements are fundamental parameters of the SM and should be determined as precisely as possible from experiments. The measurements of CP asymmetries, mixing, semileptonic, and rare decays give us valuable information about the the magnitudes and phases of these parameters.

CP-violation measurements in B-meson decays provide direct information on the angles of the unitarity triangle. These overconstraining measurements serve to improve the determination of the CKM elements, or to reveal effects also beyond the SM. The $b \to c\bar{c}s$ decays to CP eigenstates ($B^0 \to$ charmonium $K^0_{S,L}$) are the theoretically cleanest examples, measuring the angle β ($\sin(2\beta)$, to be more precise). Since α is the phase between $V_{tb}^*V_{td}$ and $V_{ub}^*V_{ud}$, only time-dependent CP asymmetries in $b \to u\bar{u}d$ decay dominated modes can directly measure $\sin(2\alpha)$. Since $b \to d$ penguin amplitudes have a different CKM phase than $b \to u\bar{u}d$ tree amplitudes, and their

magnitudes are of the same order, the penguin contribution can be sizable, which makes the determination of α complicated. To date, α has been measured in $B \to \pi\pi$, $\rho\pi$ and $\rho\rho$ decay modes. The angle γ does not depend on CKM elements involving the top quark, so it can be measured in tree level B decays. This is an important distinction from the measurements of α and β, and implies that the measurements of γ are unlikely to be affected by physics beyond the SM. The angle γ has been measured from the $B \to DK$ and $B \to D\pi$ modes.

The average directly measured values of these three angles are [74] :

$$\alpha = 89.0^{+4.4^\circ}_{-4.2}\,,\ \beta = 21.38^{+0.79^\circ}_{-0.77}\,,\ \gamma = 68^{+10^\circ}_{-11}\,. \tag{2.29}$$

Details of these measurements along with references can be found in [75]. An important

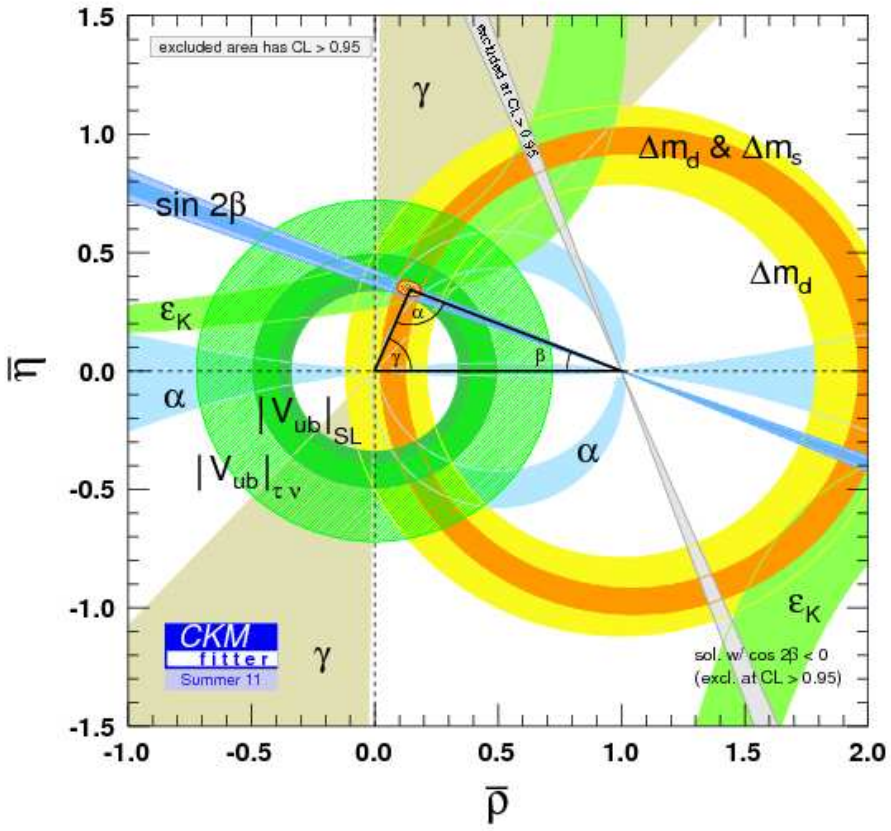

Figure 2.2: Global fit to the unitarity triangle based on all available data. [74]

goal of flavour physics is to overconstrain the CKM elements from various independent

measurements. Many measurements can be conveniently displayed and compared in the $\bar{\rho}, \bar{\eta}$ plane and if the SM CKM picture is the correct one then the different measurements should give unique values of $\bar{\rho}$ and $\bar{\eta}$. One should remember that processes dominated by loop contributions in the SM are sensitive to new physics, and can be used to extract CKM elements only if the SM is assumed. Even then, this is an extremely challenging task for both experimentalists and theorists because SM has a large number of parameters which are not predicted from theory. On top of that theoretical calculations are often plagued with large uncertainties because of the strong interaction. Fig. 2.2 is the most recent compilation of all the results from different flavour physics experiments. What we see here are many bounds all overlapping at one small area in the $\bar{\rho} - \bar{\eta}$ plane. It is worth mentioning that not all the observables in flavour physics can be used as inputs for the global fit, due to limitations on our experimental and theoretical knowledge on these quantities. Only those quantities are used which enjoy good theoretical control and also good accuracy in their measurements.

We can see clearly from Fig. 2.2 that several independent measurements are consistent with each other for values of $\bar{\rho}, \bar{\eta}$ lying in very small region. This confirms that the Cabibbo-Kobayashi-Maskawa mechanism is at least the dominant source of flavour and CP violation in flavour-changing processes. Indeed the Nobel prize was awarded to Kobayashi and Maskawa in 2008 because it is now experimentally proven that the CKM phase is the one which explains the observed CP violation in Nature.

Bibliography:

[63] C. Jarlskog, "Commutator Of The Quark Mass Matrices In The Standard Electroweak Model And Phys. Rev. Lett. **55**, 1039 (1985).

[64] R. D. Peccei, "The Strong CP problem and axions," Lect. Notes Phys. **741**, 3 (2008) [hep-ph/0607268].

[65] K. Nakamura *et al.* [Particle Data Group], "Review of particle physics," J. Phys. G **37**, 075021 (2010).

[66] L. Wolfenstein, "Parametrization Of The Kobayashi-Maskawa Matrix," Phys. Rev. Lett. **51**, 1945 (1983).

[67] V. M. Abazov *et al.* [D0 Collaboration], "First direct two-sided bound on the B_s^0 oscillation frequency," Phys. Rev. Lett. **97**, 021802 (2006) [hep-ex/0603029].

[68] A. Abulencia *et al.* [CDF - Run II Collaboration], "Measurement of the $B_s^0 - \bar{B}_s^0$ Oscillation Frequency," Phys. Rev. Lett. **97**, 062003 (2006) [hep-ex/0606027].

[69] A. Abulencia *et al.* [CDF Collaboration], "Observation of $B_s^0 - \bar{B}_s^0$ Oscillations," Phys. Rev. Lett. **97**, 242003 (2006) [hep-ex/0609040].

[70] T. Aaltonen *et al.* [CDF Collaboration], "First Flavor-Tagged Determination of Bounds on Mixing-Induced CP Violation in $B_s^0 \to J/\psi\phi$ Decays," Phys. Rev. Lett. **100**, 161802 (2008) [arXiv:0712.2397 [hep-ex]].

[71] V. M. Abazov *et al.* [D0 Collaboration], "Measurement of B_s^0 mixing parameters from the flavour-tagged decay $B_s^0 \to J/\psi\phi$," Phys. Rev. Lett. **101**, 241801 (2008) [arXiv:0802.2255 [hep-ex]].

[72] V. M. Abazov *et al.* [D0 Collaboration], "Evidence for an anomalous like-sign dimuon charge asymmetry," Phys. Rev. Lett. **105**, 081801 (2010) [arXiv:1007.0395 [hep-ex]].

[73] "Tagged time-dependent angular analysis of $B_s^0 \to J/\psi\phi$ decays at LHCb," LHCb-CONF-2012-002

[74] J. Charles *et al.* [CKMfitter Group], "CP violation and the CKM matrix: Assessing the impact of the asymmetric B Eur. Phys. J. C **41**, 1 (2005) [arXiv:hep-ph/0406184].

[75] D. Asner *et al.* [Heavy Flavor Averaging Group Collaboration], "Averages of b-hadron, c-hadron, and τ-lepton Properties," arXiv:1010.1589 [hep-ex].

Chapter 3

Effective Theory Formalism

Einstein once said that most un-understandable thing about the universe is that it is understandable. But the main reason it is understandable is that the universe separates itself into different pieces or layers. Each layer is characterized by a different scale or size, that can be studied and modeled independently of the other layers. For example, typical scales might be the size of the observable universe, a galaxy, the solar system, the earth, people, the atom, the nucleus or the Plank length. One does not have to understand the universe as a whole, one can study it one piece or layer at a time. Dynamics at low energies (or large distances) does not depend on the details of the dynamics at high energies (or short distances). Hence, low energy physics can be described using an effective Hamiltonian that contains only a few degrees of freedom, ignoring additional degrees of freedom present at higher energies. This is the essence of Effective Field Theories(EFT) [76]. An EFT is an approximate theory, that includes appropriate degrees of freedom to describe physical phenomena occurring at a chosen length scale, while ignoring substructure and degrees of freedom at shorter distances (or, equivalently, at higher energies). As a simple example, the multipole expansion in electrodynamics works because the substructure or short-distance details of charge distribution are not important while calculating the field at far away distances. Similarly, one does not need to worry about the sizes and shapes of the planets, when studying orbital motions in the Solar System. Another text-book example is the calculation of the energy levels of the Hydogen atom. Only the mass and charge of the proton are necessary for the calculation and the quark structure of proton is unimportant for this purpose. But one should also keep in mind that the above statement is true only if the answer which has some theoretical uncertainty is sufficient. By sufficient we mean that the experimental accuracy is worse than the theoretical uncertainty. Of course, a more accurate calculation of the energy levels, including the hyperfine splitting, requires that we also know the spin and magnetic moment of the proton to a good precision. More details of the proton structure are needed as we require a more accurate answer for the energy levels.

That the dynamics at high energies is unimportant for the description of low energy phenomena is a subtle statement and needs some clarification. For this purpose we will closely follow the excellent discussion presented in the lecture note by Aneesh V.

Manohar [77]. To be precise, it is not true that energy levels of Hydrogen atom does not depend on the mass of the top quark. If we keep the electromagnetic coupling constant fixed at high energies then a change in the top mass changes the low energy value of the electromagnetic coupling constant according to the equation [77]: $m_t d(1/\alpha)/dm_t = -1/3\pi$. In fact, the top quark mass also contributes to the proton mass, $m_p \propto m_t^{2/27}$. In spite of this fact that both α and m_p are dependent on the top quark mass m_t still, for the calculation of Hydrogen atom energy levels the value of m_t is irrelevant because in Schrodinger equation both α and m_p are input parameters whose values have to be obtained by fitting to the experimentally observed energy levels. "The value of m_t is irrelevant for atomic physics if the Schrodinger equation is treated as a low energy theory whose parameters α, m_e , m_p are determined from low energy experiments" [77].

If there is a single mass scale M in the microscopic theory, then the effective field theory can be seen as an expansion in $\frac{1}{M}$. The construction of an effective field theory accurate to some power of $\frac{1}{M}$ requires a new set of free parameters at each order of the expansion in $\frac{1}{M}$. This technique is useful for scattering or other processes where the maximum momentum scale k satisfies the condition $\frac{k}{M} \ll 1$. Since effective field theories are not valid at small length scales, they need not be renormalizable. Indeed, the ever expanding number of parameters at each order in $\frac{1}{M}$ required for an effective field theory means that they are generally not renormalizable in the same sense as quantum electrodynamics which requires only the renormalization of three parameters. This observation about decoupling of large energy scales also follows from the equations of mechanics, electrodynamics, or quantum mechanics. But calculations in field theory require extra care because of the fact that integration over loop momenta involves all scales [78, 79]. The effective field theory expansion breaks down if one introduces a mass-dependent subtraction scheme such as a momentum space cutoff. However, this is only a superficial obstacle as this problem can be cured if one uses a mass-independent subtraction scheme, such as dimensional regularization and minimal subtraction. The decoupling of heavy states is, of course, the reason for building high-energy accelerators. If quantum field theories were sensitive to all energy scales, it would be sufficient more useful to increase the precision of low-energy experiments instead of building large colliders. There are many precision calculations that agree with experiments in spite of neglecting the contribution from heavy particles. At the time of the original calculation of the anomalous magnetic moment of the electron, by Schwinger, weak interactions were not understood. Yet the result based on only the photon contribution agreed with the experiment within a few percent [80].

There are many more examples of EFTs. Here we mention some of them very briefly.

• The best-known example of is the Fermi theory of beta decay. This theory was developed during the early study of weak decays of nuclei when only the hadrons and leptons undergoing weak decay were known. This theory posited a pointlike interaction between the four fermions involved in these reactions. The theory had great

phenomenological success and was eventually understood to arise from the gauge theory of electroweak interactions, which forms a part of the standard model of particle physics. In this more fundamental theory, the interactions are mediated by a flavour-changing gauge boson, the $W^{\pm}$. The immense success of the Fermi theory was because the W particle has mass of about 80 GeV, whereas the early experiments were all done at an energy scale of less than 10 MeV.

• Another famous example is the BCS theory of superconductivity. Here the underlying theory is of electrons in a metal interacting with lattice vibrations called phonons. The phonons cause attractive interactions between some electrons, causing them to form Cooper pairs. The length scale of these pairs is much larger than the wavelength of phonons, making it possible to neglect the dynamics of phonons and construct a theory in which two electrons effectively interact at a point. This theory has had remarkable success in describing and predicting the results of experiments.

• The effective field theory of low energy QCD, the so called chiral perturbation theory which deals with the interactions of hadrons with pions or kaons, which are the Goldstone bosons of spontaneous chiral symmetry breaking. The expansion parameter is the pion energy/momentum.

• For hadrons containing one heavy quark (such as the bottom or charm), an effective field theory which expands in powers of the quark mass, called the heavy-quark effective theory (HQET), has been found useful. For hadrons containing two heavy quarks, an effective field theory which expands in powers of the relative velocity of the heavy quarks, called non-relativistic QCD (NRQCD), has been found useful, especially when used in conjunctions with lattice QCD.

There are many ways EFTs are useful. If the full theory is not known then EFTs can be usesd to parameterize the unknown interactions and estimate their relative importance. On the other hand, even if the full theory is known sometimes the calculations are very complicated and EFTs often simplify calculations. Complex computations can be broken into several easier tasks.

Before we end the discussion on EFTs we should stress a few points. EFTs are nonrenormalizable as they contain operators of mass dimension higher than four. In order to maintain a consistent expansion in the inverse of large mass scales and preserve power counting arguments it is mandatory to use a mass independent regularisation scheme so that the renormalization scale only appears in dimensionless ratios inside logarithms and does not alter power counting. In the effective lagrangian, not only higher dimensional terms get contributions from the heavy particles, in general, the heavy states also contribute to the renormalizable terms. But sometimes the contribution of the heavy particles to a renormalizable operator is unobservable because the effect of existence of the heavy particles is only to redefine the coefficient of the operator which is determined from experiments instead of being predicted by the theory. On the other hand the coefficients of the higher-dimensional operators are suppressed by inverse powers of the heavy masses. These coefficients decrease as one increases the

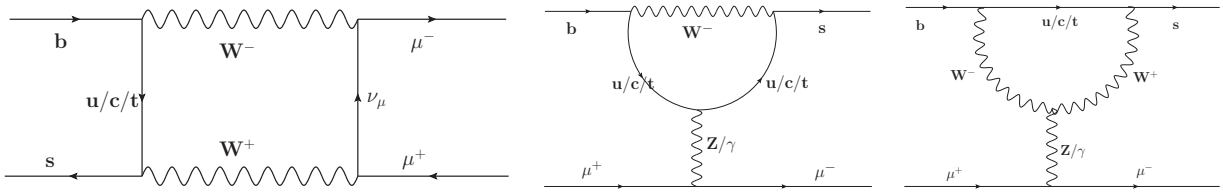

Figure 3.1: Standard Model W exchange box diagram and penguin diagram with internal top quark for the decay $b \to s\mu^+\mu^-$.

masses of the heavy particles.

3.1 Effective Hamiltonian for B Meson Decays

The mass of B meson is much smaller than the Weak interaction gauge bosons as well as the top quark; hence we can switch to an effective field theory for the description of its properties. At the quark level there are many contributions to the amplitude $\mathcal{M}$ for the decay rate of a B meson into some final state f. These are pictorially represented by Feynman diagrams like those shown in Fig. 3.1 which represents for example, the decay $B_s \to \mu^+\mu^-$ in the SM.

Unlike the leptons, quarks feel strong interactions whose strength depends on the distance scales at which it is probed. Due to the crucial property of asymptotic freedom, the strong interaction can be described perturbatively at short distances much smaller than $1/\Lambda_{\rm QCD}$ [81–86]. Higher order QCD corrections can be taken into account by dressing the lowest order diagrams in Fig. 3.1 with gluons. Over a distance scale of order $1/\Lambda_{\rm QCD}$, however, quarks and gluons hadronize and QCD becomes nonperturbative [87] so that it should be treated differently. One theoretical tool for this is the operator product expansion(OPE) [88] which allows to separate the short distance(SD) and long distance(LD) contributions to the weak decay amplitudes. Schematically the decay amplitude $\mathcal{M}$ is expressed as

$$\mathcal{M} = -\frac{4\,\mathrm{G_F}}{\sqrt{2}}\,\mathrm{V_{CKM}} \sum_j \mathrm{C_j}(\mu)\,\langle \mathrm{f}|\mathrm{O_j}(\mu)|\mathrm{B}\rangle \left[1 + \mathcal{O}\left(\frac{\mathrm{m_b^2}}{\mathrm{M_W^2}}\right)\right]. \tag{3.1}$$

Here $\mathrm{G_F}$ is the Fermi constant and $\mathrm{O_i}$ are the relevant local operators which govern the decay in question. The local operators $\mathrm{O_i}$ are built out of light quarks, lepton, photon and gluon fields. The scale μ is a renormalization scale. Physics from distances shorter than μ^{-1} is contained in the Wilson coefficients $\mathrm{C_j}$, and physics from distances longer than μ^{-1} is accounted for by the hadronic matrix elements $\langle \mathrm{f}|\,\mathrm{O_j}\,|\mathrm{B}\rangle$ of the local operators $\mathrm{O_j}$. The CKM factor $\mathrm{V_{CKM}}$ and the Wilson coefficients $\mathrm{C_j}$ determine the strength with which a given operator enters the effective Hamiltonian. In principle,

there are infinitely many terms in the OPE, but higher dimension operators yield contributions suppressed by powers of m_b^2/m_W^2. From a practical point of view, therefore, the sum in (3.1) ranges over operators of dimension five and six. All dependence on masses of heavy particles $M \gg \mu$ such as m_t, M_W or the masses of new undiscovered heavy particles is contained in C_j. On the other hand, the matrix element $\langle f|O_j|B\rangle$ of the $B \to f$ transition contains information about non perturbative dynamics from scales, such as Λ_{QCD}, that are below μ. Therefore, they can only be evaluated using some nonperturbative methods. There are many approaches such as QCD sum rules [91–94], lattice calculations [89, 90], 1/N expansion [95–99], chiral perturbation theory etc. In addition heavy quark effective theory (HQET) [100–102] and heavy quark expansions (HQE) have been widely used for B decays. In spite of the excellent progress in these non-pertubative techniques, especially in lattice gauge theory, the problem is not yet solved satisfactorily.

One can view the Wilson Coefficients C_j's in Eq. (3.1) as effective coupling constants and the O_j's in Eq. (3.1) as the corresponding interaction vertices. Thus one can write the effective Hamiltonian in the form

$$\mathcal{H} = \frac{4\,G_F}{\sqrt{2}}\,V_{CKM}\sum_j C_j\,O_j + \text{h.c.} \tag{3.2}$$

The Effective Hamiltonian in Eq. (3.2) reproduces the Standard Model result modulo corrections which are of order $\mathcal{O}\left(\frac{m_b^2}{M_W^2}\right)$ compared to Eq. (3.2). The flavour structure of the set of operators O_j needed to describe a particular physical process depends on the process itself.

Note that, in this thesis, as we are interested in flavour transitions we will only consider operators which contain some fermionic fields. There is another class of operators in the SM which do not contain any quark or lepton field, that is, these operators consist only of gauge and Higgs fields. Clearly, these operators are irrelevant with respect to flavour physics, but they have been used to parameterize new physics effects in the gauge sector. Such operators originate whenever heavy fields directly couple only to the SM gauge fields and the Higgs doublet. These operators are "universal" in the sense that they universally affect all quarks and leptons through fermion couplings to the SM gauge fields. Sometimes such operators are referred to as "oblique". In fact, one may reformulate the analysis of Peskin and Takeuchi [103] in terms of this class of dimension six operators [104].

The Effective Hamiltonian for $\Delta B = 1$ and $\Delta S = 1$ transitions consist of many

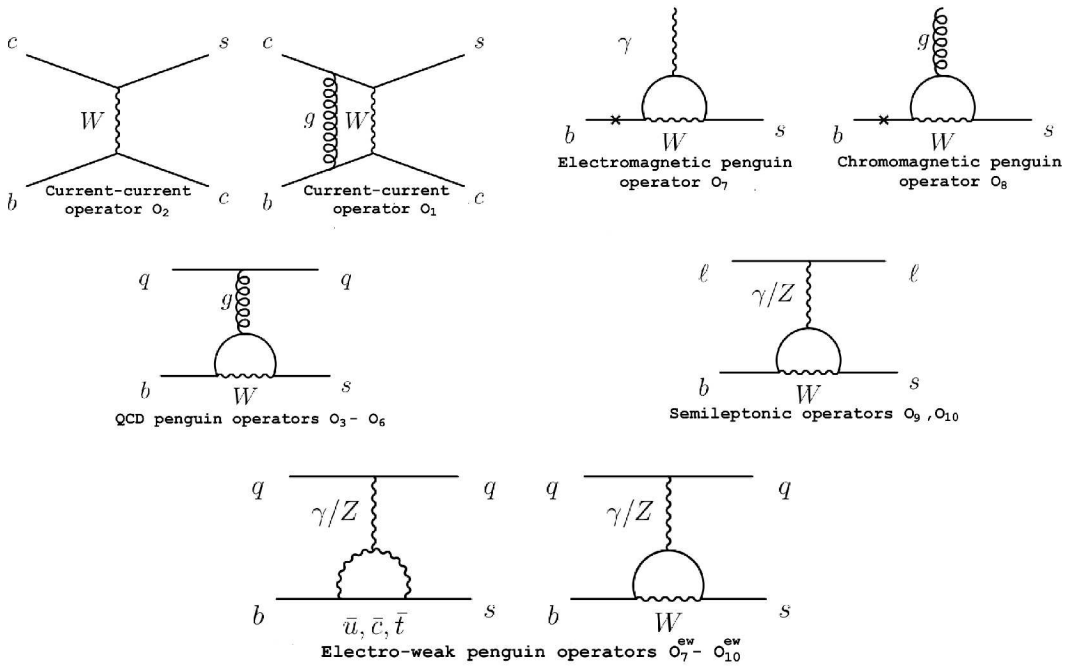

Figure 3.2: Quark level diagrams for some of the effective operators of (3.3),(3.4),(3.5).

operators. The corresponding operator basis reads (for a recent review see [105])

$$\begin{aligned}
O_1^c &= [\bar{s}_L^\alpha \gamma_\mu c_L^\beta]\,[\bar{c}_L^\beta \gamma^\mu b_L^\alpha],\; O_1^u = [\bar{s}_L^\alpha \gamma_\mu u_L^\beta]\,[\bar{u}_L^\beta \gamma^\mu b_L^\alpha],\; O_2^c = [\bar{s}_L^\alpha \gamma_\mu c_L^\alpha]\,[\bar{c}_L^\beta \gamma^\mu b_L^\beta], \\
O_2^u &= [\bar{s}_L^\alpha \gamma_\mu u_L^\alpha]\,[\bar{u}_L^\beta \gamma^\mu b_L^\beta],\; O_3 = \sum_{q=u,d,s,c,b} [\bar{s}_L^\alpha \gamma_\mu b_L^\alpha]\,[\bar{q}_L^\beta \gamma^\mu q_L^\beta], \\
O_4 &= \sum_{q=u,d,s,c,b} [\bar{s}_L^\alpha \gamma_\mu b_L^\beta]\,[\bar{q}_L^\beta \gamma^\mu q_L^\alpha],\; O_5 = \sum_{q=u,d,s,c,b} [\bar{s}_L^\alpha \gamma_\mu b_L^\alpha]\,[\bar{q}_R^\beta \gamma^\mu q_R^\beta], \\
O_6 &= \sum_{q=u,d,s,c,b} [\bar{s}_L^\alpha \gamma_\mu b_L^\beta]\,[\bar{q}_R^\beta \gamma^\mu q_R^\alpha],\; O_8 = \frac{g}{16\pi^2}\, m_b\, [\bar{s}_L \sigma^{\mu\nu} G_{\mu\nu}^a T^a b_R]\,.
\end{aligned} \tag{3.3}$$

The Feynman diagrams leading to these operators are shown in in Fig. 3.2. The operators have different names depending on the structural form. O_1 and O_2 are called current-current operators, O_3 through O_6 are called four-quark penguin operators, and O_8 is called the chromomagnetic penguin operator. In O_8, $G_{\mu\nu}^a$ is the chromomagnetic field strength tensor. The operators in (3.3) arise from the lowest order in the electroweak coupling constant , i.e., diagrams involving a single W bosons plus QCD corrections to it. In case of isospin breaking transitions the above set of operators are not sufficient and one also needs to extend the set to include penguin diagrams which are of higher order in the electroweak fine structure constant α_{ew}. They give rise to

the electroweak penguin operators:

$$\begin{aligned} O_7 &= \frac{e}{16\pi^2}\, m_b\, [\bar{s}_L^\alpha\, \sigma^{\mu\nu} F_{\mu\nu}\, b_R^\alpha]\,, \\ O_7^{\rm ew} &= \frac{3}{2}\sum_{q=u,d,s,c,b} e_q\, [\bar{s}_L^\alpha \gamma_\mu b_L^\alpha]\, [\bar{q}_R^\beta \gamma^\mu q_R^\beta]\,, O_8^{\rm ew} = \sum_{q=u,d,s,c,b} \frac{3}{2} e_q\, [\bar{s}_L^\alpha \gamma_\mu b_L^\beta]\, [\bar{q}_R^\beta \gamma^\mu q_R^\alpha]\,, \\ O_9^{\rm ew} &= \frac{3}{2}\sum_{q=u,d,s,c,b} e_q\, [\bar{s}_L^\alpha \gamma_\mu b_L^\alpha]\, [\bar{q}_L^\beta \gamma^\mu q_L^\beta]\,, O_{10}^{\rm ew} = \sum_{q=u,d,s,c,b} \frac{3}{2} e_q\, [\bar{s}_L^\alpha \gamma_\mu b_L^\beta]\, [\bar{q}_L^\beta \gamma^\mu q_L^\alpha]\,. \end{aligned} \tag{3.4}$$

Here $F^{\mu\nu}$ is the electromagnetic field strength tensor, and e_q denotes the charge of quark q. The magnetic (penguin) operator O_7 is also of key importance for the radiative decay $b \to s\gamma$.

For semileptonic decays some more operators need to be considered which are of the form

$$\begin{aligned} O_9 &= \frac{e^2}{16\pi^2}\, [\bar{s}_L\, \gamma_\mu\, b_L]\, [\bar{\ell}\, \gamma^\mu\, \ell]\,, \qquad\qquad O_{10} = \frac{e^2}{16\pi^2}\, [\bar{s}_L\, \gamma_\mu\, b_L]\, [\bar{\ell}\, \gamma^\mu \gamma_5\, \ell]\,, \\ O_{11} &= \frac{e^2}{32\pi^2 \sin^2\theta_W}\, [\bar{s}_L\, \gamma_\mu\, b_L]\, [\bar{\nu}_L\, \gamma^\mu\, \nu_L]\,. \end{aligned} \tag{3.5}$$

Hence the effective Hamiltonian for radiative $b \to s$ transitions reads

$$\mathcal{H}_{\rm eff} = -\frac{4G_F}{\sqrt{2}} \left(\lambda_t^{(s)} \mathcal{H}_{\rm eff}^{(t)} + \lambda_u^{(s)} \mathcal{H}_{\rm eff}^{(u)} \right) + h.c., \tag{3.6}$$

with the CKM matrix combinations $\lambda_q^{(s)} = V_{qb} V_{qs}^*$, and

$$\begin{aligned} \mathcal{H}_{\rm eff}^{(t)} &= C_1 \mathcal{O}_1^c + C_2 \mathcal{O}_2^c + \sum_{i=3}^{11} C_i \mathcal{O}_i + \sum_{i=7}^{10} C_i^{\rm ew} \mathcal{O}_i^{\rm ew}, \\ \mathcal{H}_{\rm eff}^{(u)} &= C_1 (\mathcal{O}_1^c - \mathcal{O}_1^u) + C_2 (\mathcal{O}_2^c - \mathcal{O}_2^u). \end{aligned} \tag{3.7}$$

Note that the unitarity relation $\lambda_u^{(s)} + \lambda_c^{(s)} + \lambda_t^{(s)} = 0$ has been used in Eq.3.6. The contribution of $\mathcal{H}_{\rm eff}^{(u)}$ is usually dropped for being doubly Cabibbo-suppressed with respect to that of $\mathcal{H}_{\rm eff}^{(t)}$.

The Wilson coefficients $\rm C_i$ at the low scale are calculated in two steps. At first, some physical quantities (like amplitudes) in the full theory are compared to those calculated in the effective theory(containing only the light fields) to extract the Wilson coefficients at the high scale $\mu_h \sim m_W$ where both the theories are expected to work. This step is called the "matching" of the full theory onto the effective theory. The scale at which this is done is called the matching scale. The weak scale perturbative matching is performed in a mass-independent scheme such as $\overline{MS}$, giving the Wilson

coefficients expanded in powers of $\alpha_s(\mu_h)$ and $\alpha_{\rm em}(\mu_h)$

$$C_i(\mu_h) = C_i^{(0)} + \frac{\alpha_s(\mu_h)}{4\pi} C_i^{(1)}(\mu_h) + \left(\frac{\alpha_s(\mu_h)}{4\pi}\right)^2 C_i^{(2)}(\mu_h) + \frac{\alpha_{\rm em}(\mu_h)}{4\pi} C_i^{(1e)}(\mu_h) + \cdots \tag{3.8}$$

One should note that, $\alpha_s(\mu)$ is small enough in the full range of relevant short distance scales of $\mathcal{O}(M_W)$ down to O(1 GeV) to serve as a reasonable expansion parameter. Both the hard gluons and electroweak loops are included in the matching calculation. Here $C_i^{(0)}$ is the tree level contribution which vanishes for all operators except the operator O_2. Till date, the matching conditions at $\mu = m_W$ have been calculated with two loop accuracy [106].

Because of the presence of vastly different scales in the problem($M_W \gg m_b$) large logarithms appear in the calculation. This is a general property of Quantum Field Theories. The presence of such large logarithms $\ln(M_W/\mu)$ multiplying $\alpha_s(\mu)$ (where $\mu = \mathcal{O}(1GeV)$) in the calculation of the coefficients $C_i(\mu, M_W)$ spoils the validity of the usual perturbation series. This problem is cured by performing a renormalization group analysis which allows an efficient summation of logarithmic terms to all orders in perturbation theory. Hence in the second step, the Wilson coefficients are evolved from μ_h down to the relevant scale in the problem (say, $\mu \sim m_b$) by solving the Renormalization Group Equations(RGE)

$$\mu \frac{d}{d\mu} C(\mu)_i = (\hat{\gamma})_{ji} C(\mu)_j, \tag{3.9}$$

where $\hat{\gamma}$ is called the anomalous dimension matrix which is also expanded as

$$\hat{\gamma} = \frac{\alpha_s}{4\pi}\hat{\gamma}_s^{(0)} + \frac{\alpha_s^2}{(4\pi)^2}\hat{\gamma}_s^{(1)} + \frac{\alpha_{\rm em}}{4\pi}\hat{\gamma}_{\rm em}^{(0)} + \cdots . \tag{3.10}$$

Two loop matching requires the inclusion of anomalous dimensions matrix in the renormalization group equations to three loop $\mathcal{O}\alpha_s^3$ accuracy which have been calculated in [107–109]. In this way the usual perturbation theory is replaced by the renormalization group improved perturbation theory in which the leading order (LO) corresponds to summing the leading logarithmic terms $\sim (\alpha_s(\mu)\ln(M_W/\mu))^n$. Then at next-to-leading order (NLO), all terms of the form $\sim \alpha_s(\mu)(\alpha_s(\mu)\ln(M_W/\mu))^n$ are summed in addition,and so on.

Another important point is the choice of the scale μ. In principle, the value of μ is arbitrary. In order that the final result is μ-independent, it must be that the μ-dependence of the short distance coefficients $C_i(\mu)$ has to cancel the μ-dependence of the long distance matrix element $\langle Q_i(\mu)\rangle$. However, in order to cancel the μ -dependence completely large number of terms in the OPE have to be calculated which

is, in practice, an impossible task. Hence, in real calculations there is always some μ dependence which reduces as we go to more and more higher orders. Although μ is in principle arbitrary, it is customary to choose μ to be of the order of the mass of the decaying hadron. For example, in B meson decays μ is chosen to $\mathcal{O}(m_b)$. For the estimation of theoretical uncertainty due to scale dependence, conventionally μ is varied from $m_b/2$ to $2m_b$ in calculations. For D meson decays it is $\mathcal{O}(m_c)$ but in the case of K decays the typical choice is $\mu = \mathcal{O}(1 - 2 \text{ GeV})$ instead of $\mathcal{O}(m_K)$, which is much too low for any perturbative calculation of the couplings C_i.

There is also a question of renormalization scheme dependence of the coefficients $C_i(\mu)$. One of the type of scheme dependences is the manner in which γ_5 is defined in $D = 4 - 2\varepsilon$ dimensions implying for instance the three schemes: Naive Dimensional Regularization(NDR), t'Hooft Veltmann(HV) and Dimensional Reduction(DRED). In dimensional regularization D=4 dimensional space-time is analytically continued to D $= 4 - 2\varepsilon$ which requires the generalization of the Dirac algebra to D $\neq 4$ dimensions. In the naive dimensional regularization (NDR) scheme γ_5 is assumed to anticommute with the D dimensional Dirac matrices. This leads to inconsistencies in the evaluation of closed Fermi lines. For example calculations adopting the NDR scheme are not able to reproduce chiral anomalies correctly. Several schemes which consistently define the Dirac algebra have been proposed having in common complicated and tedious algebraic manipulations. For example in the 't Hooft-Veltman (HV) scheme γ_5 anticommutes with the 4-dimensional parts of the Dirac matrices and commutes with the elements of the (D - 4) dimensional subspace of the Dirac matrices. However, in many practical calculations the appearance of Dirac traces containing γ_5 can be avoided and hence NDR scheme can be used. The related technical issues with original references are discussed in detail in [110]. The numerical values for the renormalization group improved Wilson coefficients can be found in [110, 111].

So in brief, the steps of the calculation for the radiative B decays can be summarized as follows:

- At first, the Wilson coefficients are determined by matching the full theory and the effective theory amplitudes at the electroweak scale $\mu \sim M_W$. This is equivalent to integrating out the heavy degrees of freedom in the path integral.

- The Wilson coefficients are then renormalization group evolved down to the relevant low energy scale $\mu \sim m_b$. This step resums the large logarithms to all orders in the strong coupling constant α_s. This is reminiscent of a renormalization group improved perturbation theory.

- Physical observables of our interest such as branching ratios and various asymmetries are now calculated in the effective theory which requires the evaluation of matrix elements of the effective theory operators between the physical states. For precise predictions the inclusion of the corresponding bremsstrahlung corrections is also essential.

3.2 Beyond the Standard Model

The Standard Model can always be thought as the renormalizable part of an Effective Theory which can be obtained from an underlying microscopic theory which is valid at a scale(say, Λ) much larger than the Electroweak scale. It is well established by diverse experimental efforts over many decades that the Standard Model is a successful effective theory of particle interactions valid up to the high scale Λ which is the ultraviolet cut-off of the SM. But the value of Λ is still unknown. In some sense, the goal of the particle physics experiments is to find evidence of a finite Λ because in the limit of $\Lambda \to \infty$ all the NP effects beyond the SM will go to zero. We have already probed such a NP through the experimental observation of Neutrino mass, but the scale of NP for that is expected to be very high $\sim 10^8$ GeV. Similarly the lower bound on proton lifetime has pushed the scale Baryon(B) and Lepton(L) number violating interactions close to the GUT scale. On the other hand, a natural solution of the higgs mass hierarchy problem requires that Λ should be $\mathcal{O}$(TeV). Stringent bounds also come from meson mixing. In we do not assume any non generic flavour structure then $K^0 - \bar{K}^0$ mass difference sets a lower bound of about at least 10^2 TeV [112] on the new physics scale if fine tuning is avoided. In the context of NP models like Supersymmetry or Technicolour, this is also referred to as the "flavour problem". A detail compilation of these bounds (and also from B_d, B_s and D systems) can be found in [112]. So if we demand NP to emerge in the TeV scale then the structure of that should be highly non trivial. For example, B, L, have to be at least approximate symmetries of the new underlying theory at the TeV scale. The new theory must also be approximately CP conserving because the CP violation observed in nature is beautifully accounted for by the CKM picture (The case of BAU is still not clear though). The flavour sector of the NP should also be highly non generic.

To study the effect of NP on B decays in a model independent fashion, the same effective Hamiltonian approach as described above can be used. As in the SM, NP contribution to the B decays can also be parameterised in terms of effective Wilson coefficients at the weak scale. The effect of NP on the Wilson coefficients can be categorised in two types. First, it shifts the values of the SM Wilson coefficients away from the SM values

$$\lambda_p^{(q)} C_i = \lambda_p^{(q)} C_i^{\rm SM} + C_i^{\rm NP}. \tag{3.11}$$

Second, NP contributions can also enlarge the basis of the operators, for instance by introducing operators of opposite chirality, or even introducing operators with scalar and tensor interactions. We will see the effect of introducing such new operators in detail in the subsequent chapters. The evolution of the new Wilson Coefficients from the weak scale to the lower scales is determined by the SM. Note that in general, the NP contribution to the Wilson coefficients will not respect the CKM hierarchy of the SM Wilson coefficients and can also have new weak phases in them.

To discuss the effect of $C_i^{\rm NP}$ on a specific process we do not at all need to refer to a particular model. But just to give an example of a specicfic kind of new physics which can generate the $C_i^{\rm NP}$s, let us consider the $b \to s$ FCNC transition discussed before. While in the SM these are dominated by one-loop contributions with the exchange of a virtual W and the top quark, in Supersymmetry several competing sources of FCNC are present. To begin with, in SUSY models the Higgs sector is richer than in the SM, since at least two Higgs doublets must be present both for theoretical and phenomenological reasons. Consequently, there exists at least one physical charged scalar $H^{\pm}$ which can be exchanged in the one-loop contributions to $b \to s$, together with an up quark. This will generate new scalar operators for the $b \to s$ transition with some NP Wilson coefficients. The SM Wilson coefficients C_7 and C_8 will also get modified by these new charged Higgs contributions. The second obvious source of FCNC comes from the supersymmetrization of the W and the charged Higgs contribution, where the up quark is replaced by an up squark and W^- and H^- are respectively replaced by their SUSY partners wino and higgsino. To be more precise, since wino and higgsino are only gauge eigenstates, the eigenstates of the 2×2 charged fermion mass matrix, the so-called charginos have actually to be considered. A less obvious source of FCNC, peculiar of SUSY theories, comes from the flavour changing vertices quark-squark-neutralino or quark-squark-gluino. This is due to a characteristic renormalization effect of the quark and squark mass matrices when the effective low-energy Lagrangian is derived. Depending on the masses of the SUSY particles all these new contributions will modify the SM wilson coefficients in different ways. But, given the complexity of the above FCNC contributions it is phenomenologically useful to exactly define the particular SUSY model in which the analysis of rare B-processes is to be performed.

3.3 Minimal Flavor Violation:An Organizing Principle

It is clear from the discussion in the previous section that there is already good experimental evidence that some powerful organizing principle must govern the Flavour sector of the New Physics underlying the SM. A key virtue of that organizing prinple should be that the structure of FCNC processes present in the SM has to be preserved. Such a scenario goes under the name of Minimal Flavour violation(MFV). We know that in the SM without Yukawa interactions there is a global flavour symmetry SU(3)^5:

$$SU(3)_Q \times SU(3)_U \times SU(3)_D \times SU(3)_L \times SU(3)_E.$$

Yukawa interactions break this symmetry and give rise to all the flavour violation. In MFV, all flavour violating interactions are generated only by the SM Yukawa couplings and hence are governed solely by the CKM matrix with the CKM phase being the only source of CP violation, in particular there are no FCNC processes at the tree level. One

should note that MFV does not refer to a particular model, in fact, it arises naturally as a low energy limit of a sizable class of models like supersymmetric models with gauge or anomaly mediation [113–115]. In the case of MSSM, the MFV hypothesis is valid when all the supersymmetry breaking soft scalar masses are universal and the trilinear soft terms are proportional to Yukawa couplings, at an arbitrary high-energy scale (one should keep in mind that MFV is not an RG invariant statement but taken to be valid at the high scale).

In this thesis we shall consider the minimal supergravity model (mSUGRA) which also falls in the category of MFV. Apart from rare B-processes we will also consider the anomalous magnetic moment of muon and the tree level decay $B^+ \to \tau^+\nu_\tau$ to identify regions in the mSUGRA parameter space which are favoured by data. As far as the muon anomalous magnetic moment is concerned, there is a growing consensus that the SM prediction for the hadronic vacuum polarization contributions to the anomalous dipole moment of the muon based on data on $e^+e^- \to \gamma^* \to$ hadrons (from CMD2, SND, KLOE, B-factories) is more reliable, which again elevates the discrepancy between the measurement of $g_\mu - 2$ and its SM prediction to the level of ~ 3.5 standard deviations.[1] On the other hand, the decay $B^+ \to \tau^+\nu_\tau$ is theoretically clean and on the experimental side, there are a few independent determinations of the branching ratio (using different techniques) which are all consistent with each other. In addition to these, constraints also come from the by now quite accurate determination of the relic density of Dark Matter particles under the standard assumption that all DM is formed by lightest superparticles(LSPs). A detailed study of the five dimensional parameter space of the mSUGRA model in view of the above experimental data along with the information obtained from the direct collider searches will be discussed in great detail in chapter 6.

Bibliography:

[76] S. Weinberg, "Phenomenological Lagrangians," Physica A **96**, 327 (1979).

[77] A. V. Manohar, "Effective field theories," In *Schladming 1996, Perturbative and nonperturbative aspects of quantum field theory* 311-362 [hep-ph/9606222].

[78] K. G. Wilson and J. B. Kogut, "The Renormalization group and the epsilon expansion," Phys. Rept. **12**, 75 (1974).

[1] The hadronic light-by-light contributions cannot be computed from first principles and hence are model dependent.

[79] T. Appelquist and J. Carazzone, "Infrared Singularities and Massive Fields," Phys. Rev. D **11**, 2856 (1975).

[80] J. S. Schwinger, "On Quantum electrodynamics and the magnetic moment of the electron," Phys. Rev. **73**, 416 (1948).

[81] D. J. Gross and F. Wilczek, "Ultraviolet behavior of non-abelian gauge theories," Phys. Rev. Lett. **30**, 1343 (1973).

[82] H. D. Politzer, "Reliable perturbative results for strong interactions?," Phys. Rev. Lett. **30**, 1346 (1973).

[83] D. J. Gross, "The discovery of asymptotic freedom and the emergence of QCD," Proc. Nat. Acad. Sci. **102**, 9099 (2005) [Int. J. Mod. Phys. A **20**, 5717 (2005 RMPHA,77,837-849.2005)].

[84] H. D. Politzer, "The dilemma of attribution," Proc. Nat. Acad. Sci. **102**, 7789 (2005) [Int. J. Mod. Phys. A **20**, 5741 (2005 RMPHA,77,851-856.2005)].

[85] F. Wilczek, "Asymptotic freedom: From paradox to paradigm," Proc. Nat. Acad. Sci. **102**, 8403 (2005) [Int. J. Mod. Phys. A **20**, 5753 (2005 RMPHA,77,857-870.2005)] [arXiv:hep-ph/0502113].

[86] G. 't Hooft, "When was asymptotic freedom discovered? or The rehabilitation of quantum Nucl. Phys. Proc. Suppl. **74**, 413 (1999) [arXiv:hep-th/9808154].

[87] Y. Nambu, "The Confinement Of Quarks," Sci. Am. **235N5**, 48 (1976).

[88] K. G. Wilson and W. Zimmermann, "Operator Product Expansions And Composite Field Operators In The General Commun. Math. Phys. **24**, 87 (1972).

[89] R. Gupta, "Calculations of hadronic matrix elements using lattice QCD," In Baton Rouge 1993, Proceedings, High performance computing and its applications in the physical sciences 131-153. and Los Alamos Nat. Lab. - LA-UR-93-2496 (93/08,rec.Aug.) 22 p. C [hep-lat/9308002].

[90] J. Laiho, E. Lunghi and R. S. Van de Water, "Lattice QCD inputs to the CKM unitarity triangle analysis," Phys. Rev. D **81**, 034503 (2010) [arXiv:0910.2928 [hep-ph]].

[91] V. A. Novikov, L. B. Okun, M. A. Shifman, A. I. Vainshtein, M. B. Voloshin and V. I. Zakharov, "Charmonium And Gluons: Basic Experimental Facts And Theoretical Phys. Rept. **41**, 1 (1978).

[92] M. A. Shifman, "Vacuum structure and QCD sum rules," *Amsterdam, Netherlands: North-Holland (1992) 516 p. (Current physics: sources and comments, 10)*

[93] E. de Rafael, "An Introduction to sum rules in QCD: Course," hep-ph/9802448.

[94] P. Colangelo and A. Khodjamirian, "QCD sum rules, a modern perspective," In *Shifman, M. (ed.): At the frontier of particle physics, vol. 3* 1495-1576 [hep-ph/0010175].

[95] G. 't Hooft, "A planar diagram theory for strong interactions," Nucl. Phys. B **72**, 461 (1974).

[96] E. Witten, "Baryons In The 1/N Expansion," Nucl. Phys. B **160**, 57 (1979).

[97] S. R. Das, "Some Aspects Of Large N Theories," Rev. Mod. Phys. **59**, 235 (1987).

[98] T. D. Cohen, "Chiral and large-Nc limits of quantum chromodynamics and models of the Rev. Mod. Phys. **68**, 599 (1996).

[99] E. E. Jenkins, "Large-N_c Baryons," Ann. Rev. Nucl. Part. Sci. **48**, 81 (1998) [arXiv:hep-ph/9803349].

[100] A. G. Grozin, "Introduction to the heavy quark effective theory. part 1," hep-ph/9908366.

[101] T. Mannel, "Review of heavy quark effective theory," In *St. Goar 1996, Heavy quarks at fixed target* 107-129 [hep-ph/9611411].

[102] M. B. Wise, "Heavy quark physics," arXiv:hep-ph/9805468.

[103] M. E. Peskin and T. Takeuchi, "A New constraint on a strongly interacting Higgs sector," Phys. Rev. Lett. **65**, 964 (1990).

[104] H. Georgi, "Effective Field Theory And Electroweak Radiative Corrections," Nucl. Phys. B **363**, 301 (1991).

[105] A. J. Buras, "Climbing NLO and NNLO Summits of Weak Decays," arXiv:1102.5650 [hep-ph].

[106] C. Bobeth, M. Misiak and J. Urban, "Photonic penguins at two loops and m(t) dependence of $BR[B \to X_s l^+ l^-]$," Nucl. Phys. B **574**, 291 (2000) [hep-ph/9910220].

[107] P. Gambino, M. Gorbahn and U. Haisch, "Anomalous dimension matrix for radiative and rare semileptonic B decays up to three loops," Nucl. Phys. B **673**, 238 (2003) [hep-ph/0306079].

[108] M. Gorbahn, U. Haisch and M. Misiak, "Three-loop mixing of dipole operators," Phys. Rev. Lett. **95**, 102004 (2005) [hep-ph/0504194].

[109] M. Gorbahn and U. Haisch, "Effective Hamiltonian for non-leptonic $|\Delta F| = 1$ decays at NNLO in QCD," Nucl. Phys. B **713**, 291 (2005) [hep-ph/0411071].

[110] A. J. Buras, "Weak Hamiltonian, CP violation and rare decays," hep-ph/9806471.

[111] G. Buchalla, A. J. Buras and M. E. Lautenbacher, "Weak decays beyond leading logarithms," Rev. Mod. Phys. **68**, 1125 (1996) [hep-ph/9512380].

[112] O. Gedalia and G. Perez, "TASI 2009 Lectures - Flavor Physics," arXiv:1005.3106 [hep-ph].

[113] M. Dine, A. E. Nelson and Y. Shirman, "Low-energy dynamical supersymmetry breaking simplified," Phys. Rev. D **51**, 1362 (1995) [hep-ph/9408384].

[114] M. Dine, A. E. Nelson, Y. Nir and Y. Shirman, "New tools for low-energy dynamical supersymmetry breaking," Phys. Rev. D **53**, 2658 (1996) [hep-ph/9507378].

[115] L. Randall and R. Sundrum, "Out of this world supersymmetry breaking," Nucl. Phys. B **557**, 79 (1999) [hep-th/9810155].

Chapter 4

New Physics in $b \to s\mu^+\mu^-$: CP-Conserving Observables

4.1 Introduction

In recent years, there have been quite a few measurements of quantities in B decays which differ from the predictions of the Standard Model (SM) by $\sim 2\sigma$. For example, in $B \to \pi K$, the SM has some difficulty in accounting for all the experimental measurements [117]. The measured indirect (mixing-induced) CP asymmetry in some $b \to s$ penguin decays is found not to be identical to that in $B^0_d \to J/\psi K_S$ [118–120], counter to the expectations of the SM. While the SM predicts that the indirect CP asymmetry in $\bar{B}^0_s \to J/\psi\phi$ should be $\simeq 0$, the measurement of this quantity by the CDF and DO / collaborations shows a deviation from the SM [121]. One naively expects the ratio of transverse and longitudinal polarizations of the decay products in $B \to \phi K^*$ to be $f_T/f_L \ll 1$, but it is observed that $f_T/f_L \simeq 1$ [122, 123]. It may be possible to explain this value of f_T/f_L within the SM, but this is not certain. Finally, the recent observation of the anomalous dimuon charge asymmetry by the D$\emptyset$ collaboration [124] also points towards some new physics in B_s mixing that affects the lifetime difference and mixing phase involved therein (for example, see Ref. [125]). Though none of the measurements above show a strong enough deviation from the SM to claim positive evidence for new physics (NP), they are intriguing since (i) the effects are seen in several different B decay channels, (ii) use a number of independent observables, and (iii) all involve $b \to s$ transitions.

A further hint has recently been seen in the leptonic decay channel: in the exclusive decay $\bar{B}^0_d \to \bar{K}^*\mu^+\mu^-$, the forward-backward asymmetry (A_{FB}) has been found to

This chapter is based on JHEP **1111**, 121 (2011) by Ashutosh Kumar Alok, Alakabha Datta, Amol Dighe, Murugeswaran Duraisamy, Diptimoy Ghosh and David London [116]. The analytic expressions for the decay rates and asymmetries existed partly (for a subset of new operators) in the literature. I have brought all the earlier results together in a consistent notation and completed them using all the Lorentz Structures. All the numerical analysis for the modes $\bar{B}^0_s \to \mu^+\mu^-\gamma, \bar{B}^0_d \to \bar{K}\mu^+\mu^-$, and $\bar{B}^0_d \to X_s\mu^+\mu^-$ were performed by me with some initial help from Ashutosh Kumar Alok.

deviate somewhat from the predictions of the SM [126–129] [1].

This is interesting since it is a CP-conserving process, whereas most of the other effects involve CP violation. Motivated by this hint of NP in $\bar{B}^0_d \to \bar{K}^*\mu^+\mu^-$, we explore the consequences of such NP in related decays. We do not restrict ourselves to any particular model, but work in the framework of effective operators with different Lorentz structures.

If NP affects $\bar{B}^0_d \to \bar{K}^*\mu^+\mu^-$, it must be present in the decay $b \to s\mu^+\mu^-$, and will affect the related decays $\bar{B}^0_s \to \mu^+\mu^-$, $\bar{B}^0_d \to X_s\mu^+\mu^-$, $\bar{B}^0_s \to \mu^+\mu^-\gamma$, and $\bar{B}^0_d \to \bar{K}\mu^+\mu^-$. The analyses of these decays in the context of the SM as well as in some NP models have been performed in the literature: $\bar{B}^0_s \to \mu^+\mu^-$ [131–141], $\bar{B}^0_d \to X_s\mu^+\mu^-$ [142–151], $\bar{B}^0_s \to \mu^+\mu^-\gamma$ [152–160], $\bar{B}^0_d \to \bar{K}\mu^+\mu^-$ [148, 161–167], $\bar{B}^0_d \to \bar{K}^*\mu^+\mu^-$ [168–183]. Correlations between some of these modes have been studied in Refs. [184–186].

In this chapter, we consider the addition of NP vector-axial vector (VA), scalar-pseudoscalar (SP), and tensor (T) operators that contribute to $b \to s\mu^+\mu^-$, and compute their effects on the above decays. Our aim here is not to obtain precise predictions, but rather to obtain an understanding of how the NP affects the observables, and to establish which Lorentz structure(s) can provide large deviations from the SM predictions. Some of these effects have already been examined by some of us: for example, new VA and SP operators in $\bar{B}^0_s \to \mu^+\mu^-$ [137], new VA and SP operators in $\bar{B}^0_s \to \mu^+\mu^-\gamma$ [159], the correlation between $\bar{B}^0_s \to \mu^+\mu^-$ and $\bar{B}^0_d \to \bar{K}\mu^+\mu^-$ with SP operators [185, 186], large forward-backward asymmetry in $\bar{B}^0_d \to \bar{K}\mu^+\mu^-$ from T operators [165], and the contribution of all Lorentz structures to $\bar{B}^0_d \to \bar{K}^*\mu^+\mu^-$, with a possible explanation of the A_{FB} anomaly [178]. Here we perform a combined study of all of these decay modes with all the Lorentz structures, consolidating and updating some of the earlier conclusions, and adding many new results and insights. Such a combined analysis, performed here for the first time, is crucial for obtaining a consistent picture of the bounds on NP and the possible effect of NP on the observables of interest. While observables like the differential branching ratio (DBR) and $A_{FB}(q^2)$ by themselves are sensitive to NP, we also examine the correlations between them in the context of NP Lorentz structures.

A full angular distribution of $\bar{B}^0_d \to \bar{K}^*\mu^+\mu^-$ allows us access to many independent observables, and hence to multiple avenues for probing NP. We present here the full angular distribution, including all the NP Lorentz structures, for this decay mode. This leads to the identification of observables that could be significantly influenced by specific Lorentz structures of NP. In addition to the DBR and A_{FB}, we also examine the longitudinal polarization fraction f_L and the angular asymmetry $A_T^{(2)}$, introduced recently in Ref. [173]. We further analyze the longitudinal-transverse asymmetry A_{LT}, which, as we will argue, has very small hadronic uncertainties.

[1] While this paper was written much earlier, the recent LHCb measurement has brought it down close to the SM prediction [130].

Hadronic uncertainties often are the main source of error in the calculation of SM predictions of a quantity, and make the positive identification of NP rather difficult. In this chapter, for $\bar{B}_d^0 \to \bar{K}\mu^+\mu^-$ we use the form factors from light-cone sum rules. For $\bar{B}_d^0 \to \bar{K}^*\mu^+\mu^-$, we use the form factors obtained in the QCD factorization framework at low q^2 [169], and those using the light-cone sum rules at high q^2 [161]. The latest next-to-leading order (NLO QCD) corrections [187] have not been included. These corrections would affect the central values of the SM predictions to a small extent, while also decreasing the renormalization-scale uncertainty. However, since our primary interest is looking for observables for which the NP effects are large, a LO analysis is sufficient at this stage. In our figures, we display bands for the SM predictions that include the form-factor uncertainties as claimed by the respective authors.

In addition to the form-factor uncertainties, the SM prediction bands also include the uncertainties due to quark masses, Cabibbo-Kobayashi-Maskawa (CKM) matrix elements and meson decay constants. In our figures, these bands are overlaid with some examples of the allowed values of these observables when NP contributions are included. This allows the scaling of these uncertainties to be easily visualized. It turns out that in many cases, the results with the NP can be significantly different from those without the NP, even taking into account inflated values for the hadronic uncertainties. We identify and emphasize such observables. We also show that the hadronic uncertainties in several of these observables are under control, especially when the invariant mass of the muon pair is small and one can use the limit of large-energy effective theory (LEET). This makes such observables excellent probes of new physics. Also, since all the observables are shown as functions of q^2, we have the information not just about the magnitudes of the observables, but also about their shape as a function of q^2, where some of the uncertainties are expected to cancel out.

In this chapter, we restrict ourselves to real values for all the NP couplings, and study only the CP-conserving observables[2]. In section 4.2, we examine the various SM and NP $b \to s\mu^+\mu^-$ operators, and give the current constraints on the NP couplings. The effects of the NP operators on the observables of the decays are discussed in the following sections: $\bar{B}_s^0 \to \mu^+\mu^-$ (Sec. 4.3), $\bar{B}_d^0 \to X_s\mu^+\mu^-$ (Sec. 4.4), $\bar{B}_s^0 \to \mu^+\mu^-\gamma$ (Sec. 4.5), $\bar{B}_d^0 \to \bar{K}\mu^+\mu^-$ (Sec. 4.6), and $\bar{B}_d^0 \to \bar{K}^*\mu^+\mu^-$ (Sec. 4.7). Our notation in these sections clearly distinguishes the contributions from VA, SP and T operators and their interference terms, which offers many insights into their impact on modifying the observables. We give the details of the calculations involved in sections 4.4–4.7 in the appendices I-IV, respectively, for the sake of completeness and in order to have a clear consistent notation for this combined analysis. In Sec. 4.8, we summarize our findings and discuss their implications. In particular, we point out the measurements which will allow one to distinguish among the different classes of NP operators, and thus clearly identify which type of new physics is present.

[2]The CP-violating observables [188], with complex values of the couplings, are treated in the following chapter.

4.2 $b \to s\mu^+\mu^-$ Operators

4.2.1 Standard Model and New Physics: effective Hamiltonians

Within the SM, the effective Hamiltonian for the quark-level transition $b \to s\mu^+\mu^-$ is

$$\begin{aligned}\mathcal{H}_{\rm eff}^{SM} &= -\frac{4G_F}{\sqrt{2}}\,V_{ts}^*V_{tb}\left\{\sum_{i=1}^{6}C_i(\mu)\mathcal{O}_i(\mu) + C_7\,\frac{e}{16\pi^2}\,[\bar{s}\sigma_{\mu\nu}(m_sP_L + m_bP_R)b]\,F^{\mu\nu}\right.\\ &\left. + C_9\,\frac{\alpha_{em}}{4\pi}\,(\bar{s}\gamma^\mu P_L b)\,\bar{\mu}\gamma_\mu\mu + C_{10}\,\frac{\alpha_{em}}{4\pi}\,(\bar{s}\gamma^\mu P_L b)\,\bar{\mu}\gamma_\mu\gamma_5\mu\right\}, \qquad (4.1)\end{aligned}$$

where $P_{L,R} = (1\mp\gamma_5)/2$. The operators $\mathcal{O}_i$ ($i = 1, ..6$) correspond to the P_i in Ref. [147], and $m_b = m_b(\mu)$ is the running b-quark mass in the $\overline{\rm MS}$ scheme. We use the SM Wilson coefficients as given in Ref. [177]. In the magnetic dipole operator with the coefficient C_7, we neglect the term proportional to m_s.

The operators O_i, i = 1-6, can contribute indirectly to $b \to s\mu^+\mu^-$ and their effects can be included in an effective Wilson coefficient as [177]

$$\begin{aligned}C_9^{\rm eff} &= C_9(m_b) + h(z,\hat{m}_c)\left(\frac{4}{3}C_1 + C_2 + 6\,C_3 + 60\,C_5\right)\\ &- \frac{1}{2}h(z,\hat{m}_b)\left(7C_3 + \frac{4}{3}C_4 + 76C_5 + \frac{64}{3}C_6\right)\\ &- \frac{1}{2}h(z,0)\left(C_3 + \frac{4}{3}C_4 + 16\,C_5 + \frac{64}{3}C_6\right) + \frac{4}{3}C_3 + \frac{64}{9}C_5 + \frac{64}{27}C_6\ . \qquad (4.2)\end{aligned}$$

Here $z \equiv q^2/m_b^2$, and $\hat{m}_q \equiv m_q/m_b$ for all quarks q. The function $h(z,\hat{m})$ represents the one-loop correction to the four-quark operators O_1-O_6 and is given by [143, 177]

$$\begin{aligned}h(z,\hat{m}) &= -\frac{8}{9}\ln\frac{m_b}{\mu_b} - \frac{8}{9}\ln\hat{m} + \frac{8}{27} + \frac{4}{9}x \qquad (4.3)\\ &-\frac{2}{9}(2+x)|1-x|^{1/2}\begin{cases}\left(\ln\left|\frac{\sqrt{1-x}+1}{\sqrt{1-x}-1}\right| - i\pi\right), & \text{for } x \le 1\ ,\\ 2\arctan\frac{1}{\sqrt{x-1}}, & \text{for } x > 1\ ,\end{cases}\end{aligned}$$

where $x \equiv 4\hat{m}^2/z$. In the numerical analysis, the renormalization scale μ_b is varied between $m_b/2$ and $2m_b$. Note that in the high-q^2 region one can perform an operator product expansion (OPE) in $1/Q$ with $Q = (m_b\sqrt{q^2})$ [189,190]. Numerically the results of Refs. [189,190] differ little from those in Eq. (4.2) and so we use the above expression for the entire range of q^2. An analysis of $b \to s\mu^+\mu^-$ where the OPE in the high-q^2 region is used can be found in Refs. [180, 182].

We now add new physics to the effective Hamiltonian for $b \to s\mu^+\mu^-$, so that it becomes

$$\mathcal{H}_{\rm eff}(b \to s\mu^+\mu^-) = \mathcal{H}_{\rm eff}^{SM} + \mathcal{H}_{\rm eff}^{VA} + \mathcal{H}_{\rm eff}^{SP} + \mathcal{H}_{\rm eff}^{T} \ , \tag{4.4}$$

where $\mathcal{H}_{\rm eff}^{SM}$ is given by Eq. (4.1), while

$$\begin{aligned}
\mathcal{H}_{\rm eff}^{VA} &= -\frac{4G_F}{\sqrt{2}}\,\frac{\alpha_{em}}{4\pi}\,V_{ts}^*V_{tb}\Big\{R_V\,(\bar{s}\gamma^\mu P_L b)\,\bar{\mu}\gamma_\mu\mu + R_A\,(\bar{s}\gamma^\mu P_L b)\,\bar{\mu}\gamma_\mu\gamma_5\mu \\
&\qquad + R'_V\,(\bar{s}\gamma^\mu P_R b)\,\bar{\mu}\gamma_\mu\mu + R'_A\,(\bar{s}\gamma^\mu P_R b)\,\bar{\mu}\gamma_\mu\gamma_5\mu\Big\} \ , \qquad (4.5)\\
\mathcal{H}_{\rm eff}^{SP} &= -\frac{4G_F}{\sqrt{2}}\,\frac{\alpha_{em}}{4\pi}\,V_{ts}^*V_{tb}\Big\{R_S\,(\bar{s}P_R b)\,\bar{\mu}\mu + R_P\,(\bar{s}P_R b)\,\bar{\mu}\gamma_5\mu \\
&\qquad + R'_S\,(\bar{s}P_L b)\,\bar{\mu}\mu + R'_P\,(\bar{s}P_L b)\,\bar{\mu}\gamma_5\mu\Big\} \ , \qquad (4.6)\\
\mathcal{H}_{\rm eff}^{T} &= -\frac{4G_F}{\sqrt{2}}\,\frac{\alpha_{em}}{4\pi}\,V_{ts}^*V_{tb}\Big\{C_T(\bar{s}\sigma_{\mu\nu}b)\bar{\mu}\sigma^{\mu\nu}\mu + iC_{TE}(\bar{s}\sigma_{\mu\nu}b)\bar{\mu}\sigma_{\alpha\beta}\mu\,\epsilon^{\mu\nu\alpha\beta}\Big\} \qquad (4.7)
\end{aligned}$$

are the new contributions. Here, $R_V, R_A, R'_V, R'_A, R_S, R_P, R'_S, R'_P, C_T$ and C_{TE} are the NP effective couplings. We do not consider NP in the form of the $O_7 = \bar{s}\sigma^{\alpha\beta}P_R b\,F_{\alpha\beta}$ operator or its chirally-flipped counterpart $O'_7 = \bar{s}\sigma^{\alpha\beta}P_L b\,F_{\alpha\beta}$. This is because there has been no hint of NP in the radiative decays $\bar{B} \to X_s\gamma, \bar{K}^{(*)}\gamma$ [161], which imposes strong constraints on $|C_7^{\rm eff}|$. This by itself does not rule out the possibility of a flipped-sign $C_7^{\rm eff}$ scenario. However this solution can be ruled out at 3σ from the decay rate of $\bar{B} \to X_s\ell^+\ell^-$ if there are no NP effects in C_9 and C_{10} [191]. Thus, NP effects exclusively in C_7 cannot provide large deviations from the SM. The impact of O'_7 on the forward-backward asymmetry in $\bar{B}^0_d \to \bar{K}^*\mu^+\mu^-$, together with other observables, was studied in Ref. [176].

Note that the operators with coefficients R_V and R_A have the same Lorentz structure as those in the SM involving C_9 and C_{10}, respectively [see Eq. (4.1)], so that any measurement will be sensitive only to the combinations $(C_9 + R_V)$ or $(C_{10} + R_A)$. For simplicity, in our numerical analysis of the observables of various decays, these couplings are taken to be real. As a consequence, the results in this chapter would be the same if the corresponding CP-conjugate decays were considered. However, for completeness, the expressions allow for a complex-coupling analysis.

When calculating the transition amplitudes, for the leptonic part we use the notation

$$\begin{aligned}
&L^\mu \equiv \langle\mu^+(p_+)\mu^-(p_-)|\bar{\mu}\gamma^\mu\mu|0\rangle \ , \qquad && L^{\mu 5} \equiv \langle\mu^+(p_+)\mu^-(p_-)|\bar{\mu}\gamma^\mu\gamma^5\mu|0\rangle \ , \\
&L \equiv \langle\mu^+(p_+)\mu^-(p_-)|\bar{\mu}\mu|0\rangle \ , && L^5 \equiv \langle\mu^+(p_+)\mu^-(p_-)|\bar{\mu}\gamma^5\mu|0\rangle \ , \\
&L^{\mu\nu} \equiv \langle\mu^+(p_+)\mu^-(p_-)|\bar{\mu}\sigma^{\mu\nu}\mu|0\rangle \ . &&
\end{aligned} \tag{4.8}$$

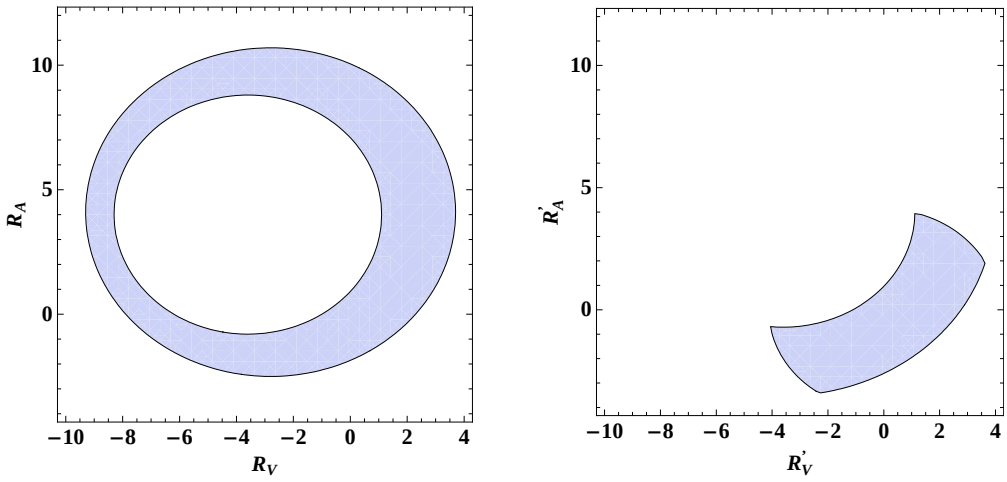

Figure 4.1: The constraints on the couplings R_V, R_A (left panel) and R'_V, R'_A (right panel) when only primed or unprimed couplings are present.

4.2.2 Constraints on NP couplings

The constraints on the NP couplings in $b \to s\mu^+\mu^-$ come mainly from the upper bound on the branching ratio $B(\bar{B}_s^0 \to \mu^+\mu^-)$ and the measurements of the total branching ratios $B(\bar{B}_d^0 \to X_s\mu^+\mu^-)$ and $B(\bar{B}_d^0 \to \bar{K}\mu^+\mu^-)$ [192–196]:

$$B(\bar{B}_s^0 \to \mu^+\mu^-) \;<\; 4.7 \times 10^{-8} \quad (90\%\ \text{C.L.})\,, \tag{4.9}$$

$$B(\bar{B}_d^0 \to X_s\mu^+\mu^-) \;=\; \begin{cases} (1.60 \pm 0.50) \times 10^{-6} & (\text{low } q^2) \\ (0.44 \pm 0.12) \times 10^{-6} & (\text{high } q^2) \end{cases}\,, \tag{4.10}$$

$$B(\bar{B}_d^0 \to \bar{K}\mu^+\mu^-) \;=\; \left(4.5^{+1.2}_{-1.0}\right) \times 10^{-7}\,, \tag{4.11}$$

where the low-q^2 and high-q^2 regions correspond to 1 GeV$^2 \le q^2 \le 6$ GeV^2 and $q^2 \ge 14.4$ GeV^2, respectively, where q^2 is the invariant mass squared of the two muons. The constraints from the first two quantities above have been derived in Ref. [178]. Here we also include the additional constraints from $B(\bar{B}_d^0 \to \bar{K}\mu^+\mu^-)$. The three decays above provide complementary information about the NP operators. For the SM predictions here, we use the latest NNLO calculations. Note that the measurements for $B(\bar{B}_d^0 \to \bar{K}^*\mu^+\mu^-)$ are also available [127,197]. However, the form-factor uncertainties in $\bar{B}_d^0 \to \bar{K}^*\mu^+\mu^-$ are rather large, and as a result the constraints due to this decay mode are subsumed in those from the other three modes.

The constraints on the new VA couplings come mainly from $B(\bar{B}_d^0 \to X_s\mu^+\mu^-)$ and $B(\bar{B}_d^0 \to \bar{K}\mu^+\mu^-)$. Their precise values depend on which NP operators are assumed to be present. For example, if only $R_{V,A}$ or only $R'_{V,A}$ couplings are present, the constraints on these couplings take the form shown in Fig. 4.1. For $R_{V,A}$, the allowed parameter

space is the region between two ellipses:

$$1.0 \lesssim \frac{|R_V + 3.6|^2}{(4.7)^2} + \frac{|R_A - 4.0|^2}{(4.8)^2} \ , \quad \frac{|R_V + 2.8|^2}{(6.5)^2} + \frac{|R_A - 4.1|^2}{(6.6)^2} \lesssim 1 \ , \tag{4.12}$$

while for $R'_{V,A}$, the allowed region is the intersection of an annulus and a circle:

$$22.2 \lesssim |R'_V + 3.6|^2 + |R'_A - 4.0|^2 \lesssim 56.6 \ , \quad |R'_V|^2 + |R'_A|^2 \lesssim 17 \ . \tag{4.13}$$

If both $R_{V,A}$ and $R'_{V,A}$ are present, the constraints on them get individually weakened to

$$\frac{|R_V + 2.8|^2}{(6.5)^2} + \frac{|R_A - 4.1|^2}{(6.6)^2} \lesssim 1 \ , \tag{4.14}$$

and

$$|R'_V|^2 + |R'_A|^2 \lesssim 40 \ , \tag{4.15}$$

respectively[3].

For the SP operators, the present upper bound on $B(\bar{B}^0_s \to \mu^+\mu^-)$ provides the limit

$$|R_S - R'_S|^2 + |R_P - R'_P|^2 \lesssim 0.44^4 \ , \tag{4.16}$$

where we have used $f_{B_s} = (238.8 \pm 9.5)\,\text{MeV}$ [198] and $|V^*_{ts}V_{tb}| = 0.0407 \pm 0.0010$ [193]. This constitutes a severe constraint on the NP couplings if only $R_{S,P}$ or $R'_{S,P}$ are present. However, if both types of operators are present, these bounds can be evaded due to cancellations between the $R_{S,P}$ and $R'_{S,P}$. In that case, $B(\bar{B}^0_d \to X_s\mu^+\mu^-)$ and $B(\bar{B}^0_d \to \bar{K}\mu^+\mu^-)$ can still bound these couplings. The stronger bound is obtained from the measurement of the latter quantity, which yields

$$|R_S|^2 + |R_P|^2 \lesssim 9 \ , \quad R_S \approx R'_S \ , \quad R_P \approx R'_P \ . \tag{4.17}$$

Finally, the constraints on the NP tensor operators come entirely from $B(\bar{B}^0_d \to X_s\mu^+\mu^-)$. When only the T operators are present,

$$|C_T|^2 + 4|C_{TE}|^2 \lesssim 1.0 \ . \tag{4.18}$$

Although the bounds presented in this section for VA, SP and T couplings are obtained by taking one kind of Lorentz structure at a time, in our numerical analysis for scenarious where we consider combinations of two or more kinds of Lorentz structres, we

[3]Note: the constraints on $R_{V,A}$ obtained here are milder than those obtained in Ref. [159] using $B(\bar{B}^0_d \to (\bar{K}\,, \bar{K}^*)\,\mu^+\,\mu^-)$. This is because Ref. [159] had neglected the interference terms between the SM and new physics VA operators. Their inclusion relaxes the stringent constraints therein.

[4](Written in July 2012) Note that, the latest LHCb data has strengthened this limit to $|R_S - R'_S|^2 + |R_P - R'_P|^2 \lesssim 0.04$. This will make the allowed contributions from the scalar and pseudoscalar operators extremely small.

use the allowed parameter space obtained by considering the corresponding combined Lorentz structures.

We now analyze the $b \to s\mu^+\mu^-$ modes in detail and present our results. As explained in the Introduction, the figures have the SM prediction bands overlaid with the predictions for specific allowed values of NP couplings. The SM band is generated by varying the form factors within their ranges as predicted by the respective authors, while the CKM matrix elements, quark masses and meson decay constants are varied within their 1.6σ allowed values.

4.3 $\bar{B}_s^0 \to \mu^+\mu^-$

In this section we examine the NP contributions to $\bar{B}_s^0 \to \mu^+\mu^-$. Within the SM, $\bar{B}_s^0 \to \mu^+\mu^-$ is chirally suppressed. The SM prediction for the branching ratio is $B(\bar{B}_s^0 \to \mu^+\mu^-) = (3.35 \pm 0.32) \times 10^{-9}$ [138]. The Tevatron gives an upper bound on its branching ratio (BR) of 4.7×10^{-8} at 90% C.L. [192, 239, 240]. This decay can be observed at the Tevatron only if NP enhances its BR above 10^{-8}. LHCb is the only experiment which will probe $B(\bar{B}_s^0 \to \mu^+\mu^-)$ down to its SM value. It has the potential for a 3σ observation (5σ discovery) of $\bar{B}_s^0 \to \mu^+\mu^-$ with $\sim 2\,\text{fb}^{-1}$ ($\sim 6\,\text{fb}^{-1}$) of data [199]. LHCb therefore has the potential to observe either an enhancement or a suppression of $B(\bar{B}_s^0 \to \mu^+\mu^-)$. It can observe $\bar{B}_s^0 \to \mu^+\mu^-$ as long as its BR is above 1.0×10^{-9}.

4.3.1 Branching ratio

The transition amplitude for $\bar{B}_s^0 \to \mu^+\mu^-$ is given by

$$\begin{aligned} i\mathcal{M}(\bar{B}_s^0 \to \mu^+\mu^-) &= (-i)\frac{1}{2}\left[-\frac{4G_F}{\sqrt{2}}\frac{\alpha_{em}}{4\pi}(V_{ts}^* V_{tb})\right] \times \\ &\left\{ \left\langle 0\left|\bar{s}\gamma_\mu\gamma_5 b\right|\bar{B}_s^0(p)\right\rangle (-C_{10}^{\text{eff}} - R_A + R'_A)L^{5\mu} \right. \\ &+ \left. \left\langle 0\left|\bar{s}\gamma_5 b\right|\bar{B}_s^0(p)\right\rangle \left[(R_S - R'_S)L + (R_P - R'_P)L^5\right] \right\}, \end{aligned} \tag{4.19}$$

where $L^{5\mu}$, L and L^5 are defined in Eq. (4.8). Using the matrix elements [131]

$$\left\langle 0\left|\bar{s}\gamma_\mu\gamma_5 b\right|\bar{B}_s^0(p)\right\rangle = i\,p_\mu\,f_{B_s}\,, \quad \left\langle 0\left|\bar{s}\gamma_5 b\right|\bar{B}_s^0(p)\right\rangle = -i\,f_{B_s}\frac{m_{B_s}^2}{m_b + m_s}\,, \tag{4.20}$$

the calculation of the BR gives

$$B(\bar{B}_s^0 \to \mu^+\mu^-) = \frac{G_F^2 \alpha_{em}^2 m_{B_s}^5 f_{B_s}^2 \tau_{B_s}}{64\pi^3} |V_{tb}V_{ts}^*|^2 \sqrt{1-\frac{4m_\mu^2}{m_{B_s}^2}} \times \left\{ \left(1-\frac{4m_\mu^2}{m_{B_s}^2}\right) \left| \frac{R_S - R_S'}{m_b+m_s} \right|^2 + \left| \frac{R_P - R_P'}{m_b+m_s} + \frac{2m_\mu}{m_{B_s}^2}(C_{10} + R_A - R_A') \right|^2 \right\}. \quad (4.21)$$

Clearly, NP in the form of tensor operators does not contribute to $\bar{B}_s^0 \to \mu^+\mu^-$. From Eq. (4.21) and the constraints on NP couplings obtained in Sec. 4.2.2, one can study the effect of new VA and SP couplings.

Since the NP contribution from VA operators is suppressed by a factor of $\sim m_\mu/m_b$ compared to that from the SP operators, the effect of SP operators dominates. Both VA and SP operators can suppress $B(\bar{B}_s^0 \to \mu^+\mu^-)$ significantly below the SM prediction. However while VA operators can only marginally enhance $B(\bar{B}_s^0 \to \mu^+\mu^-)$ above 10^{-8}, making the decay accessible at the Tevatron in an optimistic scenario, the SP operators can enhance the branching ratio even up to the present experimental bound. Indeed, the strongest limit on the SP couplings comes from this decay. This strong limit prevents the SP operators from expressing themselves in many other observables, as we shall see later in this chapter.

4.3.2 Muon polarization asymmetry

The longitudinal polarization asymmetry of muons in $\bar{B}_s^0 \to \mu^+\mu^-$ is defined as

$$A_{LP} = \frac{N_R - N_L}{N_R + N_L}\,, \quad (4.22)$$

where $N_R\,(N_L)$ is the number of μ^-'s emerging with positive (negative) helicity. A_{LP} is a clean observable that is not suppressed by m_μ/m_{B_s} only if the NP contribution is in the form of SP operators, such as in an extended Higgs sector.

A_{LP} for the most general NP is [186]

$$A_{LP} = \frac{2\sqrt{1-\frac{4m_\mu^2}{m_{B_s}^2}}\ \mathrm{Re}\left[\left(\frac{R_S-R_S'}{m_b+m_s}\right)\left(\frac{R_P-R_P'}{m_b+m_s} + \frac{2m_\mu}{m_{B_s}^2}(C_{10}+R_A-R_A')\right)\right]}{\left(1-\frac{4m_\mu^2}{m_{B_s}^2}\right)\left|\frac{R_S-R_S'}{m_b+m_s}\right|^2 + \left|\frac{R_P-R_P'}{m_b+m_s} + \frac{2m_\mu}{m_{B_s}^2}(C_{10}+R_A-R_A')\right|^2}\,. \quad (4.23)$$

From the above equation, we see that A_{LP} can be nonzero if and only if $R_S - R_S' \neq 0$, i.e. there must be a contribution from NP SP operators. (Within the SM, SP couplings are negligibly small, so that $A_{LP} \simeq 0$.)

The present upper bound on $B(\bar{B}_s^0 \to \mu^+\mu^-)$ puts no constraint on A_{LP}, and it can be as large as 100% [186]. A_{LP} can be maximal even if $B(\bar{B}_s^0 \to \mu^+\mu^-)$ is close to its SM prediction. Therefore, in principle A_{LP} can serve as an important tool to probe NP of the SP form. However, in order to measure its polarization, the muon must decay within the detector. This is not possible due to the long muon lifetime ($c\tau$ for the muon is 659 m). Hence in practice, this quantity is not measurable at current detectors.

4.4 $\bar{B}_d^0 \to X_s\mu^+\mu^-$

The BR of $\bar{B}_d^0 \to X_s\mu^+\mu^-$ in the low-q^2 and high-q^2 regions has been measured to be [195, 196]

$$B(\bar{\mathrm{B}} \to X_s\ell^+\ell^-)_{\text{low } q^2} = \begin{cases} \left(1.49 \pm 0.50^{+0.41}_{-0.32}\right) \times 10^{-6}\,, & \text{(Belle)}\,, \\ (1.8 \pm 0.7 \pm 0.5) \times 10^{-6}\,, & \text{(BaBar)}\,, \\ (1.60 \pm 0.50) \times 10^{-6}\,, & \text{(Average)}\,. \end{cases} \tag{4.24}$$

$$B(\bar{B} \to X_s\ell^+\ell^-)_{\text{high } q^2} = \begin{cases} \left(0.42 \pm 0.12^{+0.06}_{-0.07}\right) \times 10^{-6}\,, & \text{(Belle)}\,, \\ \left(0.50 \pm 0.25^{+0.08}_{-0.07}\right) \times 10^{-6}\,, & \text{(BaBar)}\,, \\ (0.44 \pm 0.12) \times 10^{-6}\,, & \text{(Average)}\,. \end{cases} \tag{4.25}$$

The SM predictions for $B(\bar{B} \to X_s\,\mu^+\,\mu^-)$ in the low-q^2 and high-q^2 regions are $(1.59 \pm 0.11) \times 10^{-6}$ and $(0.24 \pm 0.07) \times 10^{-6}$, respectively [149].

Apart from the measurement of the total BR of $\bar{B}_d^0 \to X_s\mu^+\mu^-$, which has already been used to restrict the VA and T operators in Sec. 4.2.2, the differential branching ratio (DBR) as a function of q^2 also contains valuable information that can help us detect NP. In particular, the SM predicts a positive zero crossing for A_{FB} in $\bar{B}_d^0 \to X_s\mu^+\mu^-$ in the low-q^2 region, i.e. for q^2 less than (greater than) the crossing point, the value of A_{FB} is negative (positive). This zero crossing is sufficiently away from the charm resonances so that its value can be determined perturbatively to an accuracy of $\sim 5\%$. The NNLO prediction [149] for the zero of $A_{FB}(q^2)$ is (taking $m_b = 4.8$ GeV)

$$(q^2)_0 = (3.5 \pm 0.12)\,\text{GeV}^2\,. \tag{4.26}$$

This quantity has not yet been measured. However, estimates show that a precision of about 5% could be obtained at a Super-B factory [200]. A deviation from the zero crossing point predicted above will be a clear signal of NP.

4.4.1 Differential branching ratio and forward-backward asymmetry

After including all the NP interactions, and neglecting terms suppressed by m_μ/m_b and m_s/m_b, the total differential branching ratio $\mathrm{d}B/\mathrm{d}z$ is given by

$$\left(\frac{\mathrm{d}B}{\mathrm{d}z}\right)_{\text{Total}} = \left(\frac{\mathrm{d}B}{\mathrm{d}z}\right)_{\text{SM}} + B_0\Big[B_{SM\text{-}VA} + B_{VA} + B_{SP} + B_T\Big]\,, \tag{4.27}$$

where the quantities B depend on the SM and NP couplings and kinematic variables. The complete expressions for these quantities are given in Appendix I. The subscripts denote the Lorentz structure(s) contributing to that term.

The forward-backward asymmetry in $\bar{B}_d^0 \to X_s\mu^+\mu^-$ is

$$A_{FB}(q^2) = \frac{\int_0^1 d\cos\theta_\mu \frac{d^2B}{dq^2 d\cos\theta_\mu} - \int_{-1}^0 d\cos\theta_\mu \frac{d^2B}{dq^2 d\cos\theta_\mu}}{\int_0^1 d\cos\theta_\mu \frac{d^2B}{dq^2 d\cos\theta_\mu} + \int_{-1}^0 d\cos\theta_\mu \frac{d^2B}{dq^2 d\cos\theta_\mu}}\,, \tag{4.28}$$

where θ_μ is the angle between the μ^+ and the $\bar{B}^0$ in the dimuon center-of-mass frame. We can write A_{FB} in the form

$$A_{FB}(q^2) = \frac{N(z)}{\mathrm{d}B/\mathrm{d}z}\,, \tag{4.29}$$

where the numerator is given by

$$N(z) = B_0\Big[N_{SM} + N_{SM\text{-}VA} + N_{VA} + N_{SP\text{-}T}\Big]\,. \tag{4.30}$$

The terms suppressed by m_μ/m_b and m_s/m_b have been neglected as before. Again for the detailed expressions, we refer the reader to Appendix I.

Fig. 4.2 shows $A_{FB}(q^2)$ and the DBR for $\bar{B}_d^0 \to X_s\mu^+\mu^-$ in the presence of NP in the form of $R_{V,A}$ couplings, which are the ones that can most influence these observables. Enhancement or suppression of the DBR by a factor of 2 is possible. The NP couplings can enhance A_{FB} up to 30% at low q^2, make it have either sign, and even make the zero crossing disappear altogether. At high q^2, however, A_{FB} can only be suppressed. The $R'_{V,A}$ couplings can only affect these observables mildly: a 50% enhancement in DBR is possible (no suppression), but A_{FB} can only be marginally enhanced and a positive zero crossing in the q^2 = 2-4 GeV^2 region is maintained. The mild effect of $R'_{V,A}$ couplings as compared to the $R_{V,A}$ couplings is a generic feature for almost all observables. This may be attributed to the bounds on the magnitudes of these couplings: from Sec. 4.2.2, while $|R_{V,A}| < 10$, the values of $|R'_{V,A}| < 5$.

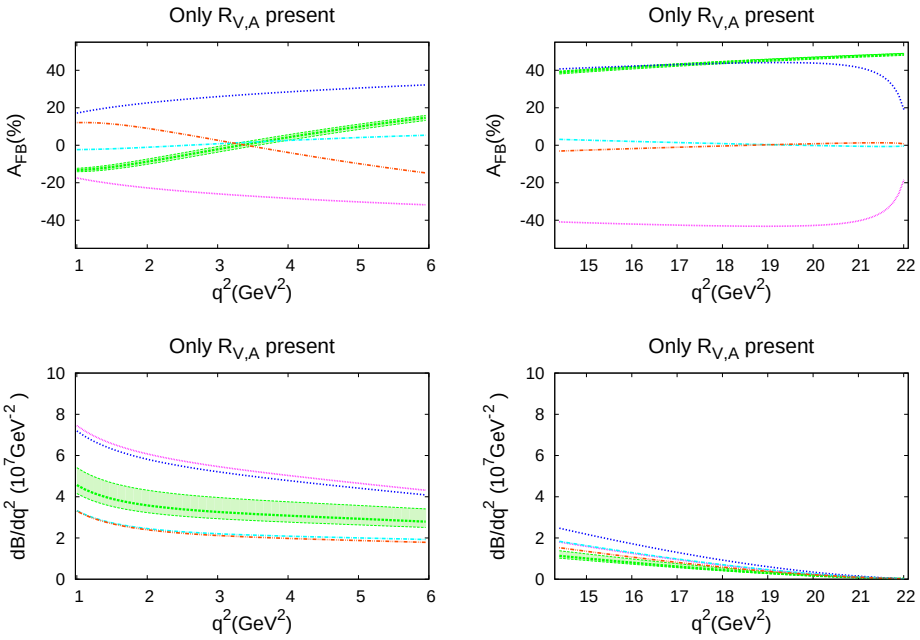

Figure 4.2: The left (right) panels of the figure show A_{FB} and DBR for $\bar{B}_d^0 \to X_s \mu^+ \mu^-$ in the low-q^2 (high-q^2) region, in the scenario where only (R_V, R_A) terms are present. The band corresponds to the SM prediction and its uncertainties; the lines show predictions for some representative values of NP parameters (R_V, R_A). For example, the blue curves in the low-q^2 and high-q^2 regions correspond to $(-6.85, 8.64)$ and $(-9.34, 8.85)$, respectively.

Eq. (4.30) shows that if SP or T couplings are individually present, their contribution to A_{FB} is either absent or suppressed by m_μ/m_b. In such a case, though they can enhance the DBR (marginally for SP, by up to a factor of 2 for T), A_{FB} is suppressed in general (marginally for SP, significantly for T). However if both SP and T operators are present, their interference term is not suppressed and some enhancement of A_{FB} is possible. This still is not significant, since the magnitude of the SP couplings is highly constrained from $\bar{B}_s^0 \to \mu^+ \mu^-$ measurements. A positive zero crossing in the low-q^2 region is always maintained. This may be seen in Fig. 4.3.

4.4.2 Polarization fractions f_L and f_T

In Ref. [150] it was pointed out that, besides the dilepton invariant mass spectrum and the forward-backward asymmetry, a third observable can be obtained from $\bar{B}_d^0 \to$

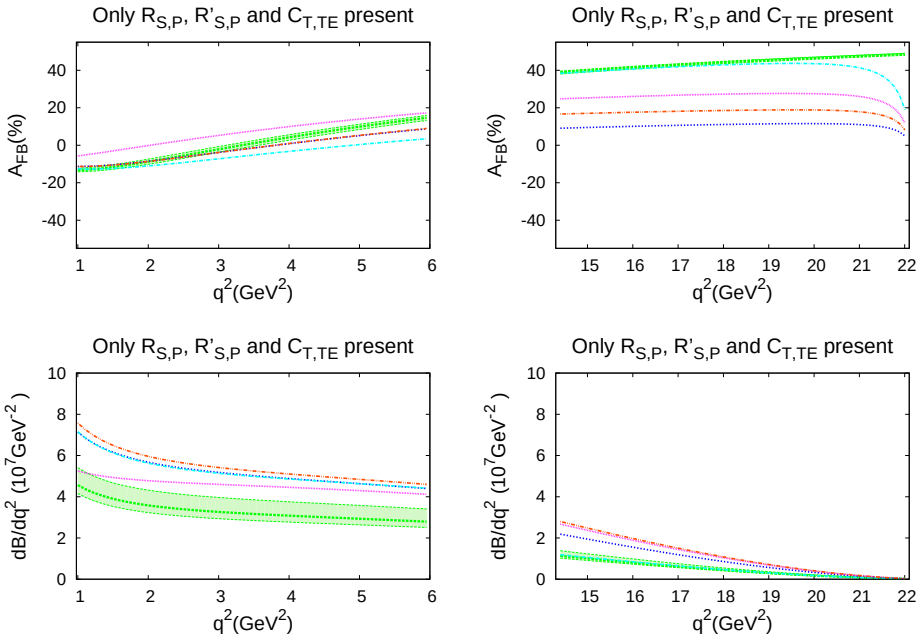

Figure 4.3: The left (right) panels of the figure show A_{FB} and DBR for $\bar{B}_d^0 \to X_s\mu^+\mu^-$ in the low-q^2 (high-q^2) region, in the scenario where both SP and T terms are present. The band corresponds to the SM prediction and its uncertainties; the lines show predictions for some representative values of NP parameters $(R_S, R_P, R'_S, R'_P, C_T, C_{TE})$. For example, the magenta curves in the low-q^2 and high-q^2 regions correspond to $(-1.23, -1.79, -0.86, -1.85, 0.27, -0.36)$ and $(-1.23, -0.23, -1.35, 0.08, 1.37, 0.01)$, respectively.

$X_s\mu^+\mu^-$, namely the double differential decay width:

$$\frac{d^2B}{dz\, d\cos\theta_\mu} = \frac{3}{8}\Big[(1+\cos^2\theta_\mu)H_T(z) + 2\cos\theta_\mu H_A(z) + 2(1-\cos^2\theta_\mu)H_L(z)\Big] \ . \quad (4.31)$$

The functions $H_i(z)$ do not depend on $\cos\theta_\mu$. The sum $H_L(z) + H_T(z)$ gives the differential branching ratio dB/dz, while the forward-backward asymmetry is given by $3\,H_A/4(H_L+H_T)$. Splitting dB/dz into longitudinal and transverse parts separates the contributions with different q^2 dependences, providing a third independent observable. This does not require measuring any additional kinematical variable – q^2 and $\cos\theta_\mu$ are sufficient. Including all the NP interactions, and neglecting terms suppressed by m_μ/m_b and m_s/m_b, $H_L(z)$ and $H_T(z)$ are given by

$$H_L(z) = H_L^{SM}(z) + H_L^{SM-VA}(z) + H_L^{VA}(z) + H_L^{SP}(z) + H_L^{T}(z) \ , \quad (4.32)$$

$$H_T(z) = H_T^{SM}(z) + H_T^{SM-VA}(z) + H_T^{VA}(z) + H_T^{SP}(z) + H_T^{T}(z) \ , \quad (4.33)$$

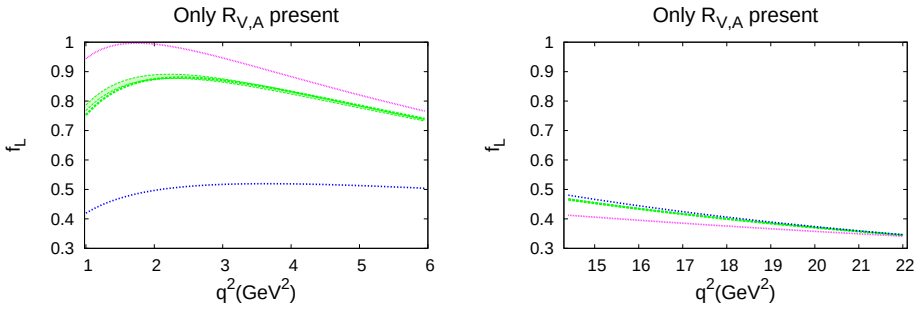

Figure 4.4: The left (right) panels of the figure show f_L for $\bar{B}^0_d \to X_s\mu^+\mu^-$ in the low-q^2 (high-q^2) region, in the scenario where only (R_V, R_A) terms are present. The band corresponds to the SM prediction and its uncertainties; the lines show predictions for some representative values of NP parameters (R_V, R_A). For example, the blue curves in the low-q^2 and high-q^2 regions correspond to $(-8.14, 5.75)$ and $(1.87, 4.85)$, respectively.

where the H functions are given in Appendix I. The superscripts indicate the Lorentz structures contributing to the term. The polarization fractions f_L and f_T can be defined as

$$f_L = \frac{H_L(z)}{H_L(z) + H_T(z)} , \qquad f_T = \frac{H_T(z)}{H_L(z) + H_T(z)} . \tag{4.34}$$

In the SM, f_L can be as large as 0.9 at low q^2, and it decreases to about 0.3 at high q^2.

Fig. 4.4 shows that when only $R_{V,A}$ couplings are present, in the low-q^2 region f_L can be suppressed substantially, or even enhanced up to 1. A similar effect – small enhancement or a factor of two suppression – is possible at high q^2. The suppression at low-q^2 is typically correlated with an enhancement at high-q^2. The effect of $R'_{V,A}$ couplings is similar, but much milder, as expected. SP and T operators, individually or together, can only have an marginal effect on f_L.

4.5 $\bar{B}^0_s \to \mu^+\mu^-\gamma$

In this section we examine the NP contributions to the radiative leptonic decay $\bar{B}^0_s \to \mu^+\mu^-\gamma$. This decay has not been detected as yet. The SM prediction for the BR in the range $q^2 \leq 9.5$ GeV^2 and $q^2 \geq 15.9$ GeV^2 is $\approx 18.9 \times 10^{-9}$ [157]. Although this decay needs the emission of an additional photon as compared to $\bar{B}^0_s \to \mu^+\mu^-$, which would suppress the BR by a factor of α_{em}, the photon emission also frees it from helicity suppression, making its BR much larger than $\bar{B}^0_s \to \mu^+\mu^-$.

This decay has contributions from many channels [152–155, 157, 158]: (i) direct emission of real or virtual photons from valence quarks of the $\bar{B}^0_s$, (ii) real photon

emitted from an internal line of the $b \to s$ loop, (iii) weak annihilation due to the axial anomaly, and (iv) bremsstrahlung from leptons in the final state. The photon emission from the $b \to s$ loop is suppressed by m_b^2/m_W^2 [153], and the weak annihilation is further suppressed by Λ_{QCD}/m_b [157]. These two contributions can then be neglected. The bremsstrahlung contribution is suppressed by m_μ/m_b, and dominates only at extremely low photon energies due to the infrared divergence. The virtual photon emission dominates in the low-q^2 region around the ϕ resonance. If we choose the regions 2 GeV$^2 \le q^2 \le 6$ GeV^2 and 14.4 GeV$^2 \le q^2 \le 25$ GeV^2 as the low-q^2 and high-q^2 regions, respectively, then the dominating contribution comes from the diagrams in which the final-state photon is emitted either from the b or the s quark. Then the $\bar{B}_s^0 \to \mu^+\mu^-\gamma$ decay is governed by the effective Hamiltonian describing the $b \to s\mu^+\mu^-$ transition, as given in Eq. (4.1), and our formalism is applicable. Here we consider the the DBR and A_{FB} in $\bar{B}_s^0 \to \mu^+\mu^-\gamma$.

4.5.1 Differential branching ratio and forward-backward asymmetry

We begin with the differential branching ratio. The SP operators do not contribute to the amplitude of $\bar{B}_s^0 \to \mu^+\mu^-\gamma$ and hence do not play any role in the decay.

In terms of the dimensionless parameter $x_\gamma = 2E_\gamma/m_{B_s}$, where E_γ is the photon energy in the $\bar{B}_s^0$ rest frame, one can calculate the double differential decay rate to be

$$\frac{\mathrm{d}^2\Gamma}{\mathrm{d}x_\gamma \mathrm{d}(\cos\theta_\mu)} = \frac{1}{2m_{B_s}} \frac{2v\, m_{B_s}^2 x_\gamma}{(8\pi)^3} \mathcal{M}^\dagger \mathcal{M} \,, \tag{4.35}$$

where $v \equiv \sqrt{1 - 4m_\mu^2/[m_{B_s}^2(1-x_\gamma)]}$. From Eq. (4.35) we get the DBR to be

$$\begin{aligned} \frac{\mathrm{d}B}{\mathrm{d}x_\gamma} &= \tau_{B_s} \int_{-1}^{1} \frac{\mathrm{d}^2\Gamma}{\mathrm{d}x_\gamma \mathrm{d}(\cos\theta_\mu)} \,\mathrm{d}\cos\theta_\mu \\ &= \tau_{B_s} \left[\frac{1}{2m_{B_s}} \frac{2vm_{B_s}^2}{(8\pi)^3}\right] \left[\frac{1}{4}\, \frac{16G_F^2}{2} \frac{\alpha_{em}^2}{16\pi^2} |V_{tb}V_{ts}^*|^2 e^2\right] \Theta \,. \end{aligned} \tag{4.36}$$

Here the quantity Θ has the form

$$\Theta = \frac{2}{3}\, m_{B_s}^4\, x_\gamma^3 \Big[X_{VA} + X_T + X_{VA\text{-}T}\Big] \,, \tag{4.37}$$

where the X terms are given in Appendix II. The subscripts of the X terms denote the Lorentz structure(s) contributing to that term. For the sake of brevity, we have included the SM contributions in X_{VA}.

The normalized forward-backward asymmetry of muons in $\bar{B}_s^0 \to \mu^+\mu^-\gamma$ is defined as

$$A_{FB}(q^2) = \frac{\displaystyle\int_0^1 d\cos\theta_\mu \frac{d^2B}{dq^2 d\cos\theta_\mu} - \int_{-1}^0 d\cos\theta_\mu \frac{d^2B}{dq^2 d\cos\theta_\mu}}{\displaystyle\int_0^1 d\cos\theta_\mu \frac{d^2B}{dq^2 d\cos\theta_\mu} + \int_{-1}^0 d\cos\theta_\mu \frac{d^2B}{dq^2 d\cos\theta_\mu}} \ , \tag{4.38}$$

where θ_μ is the angle between the three-momentum vectors of the $\bar{B}_s^0$ and the μ^+ in the dimuon center-of-mass frame. The calculation of A_{FB} gives

$$A_{FB}(q^2) \ = \ \frac{1}{\Theta}\left(2m_{B_s}^4 v\ x_\gamma^3\right)\left[Y_{VA} + Y_{VA\text{-}T}\right] , \tag{4.39}$$

with the Y terms are defined in Appendix II.

The details of the calculation are given in Appendix II. For the numerical calculations, we use the matrix elements given in Ref. [156]. The parameters involved in the form factor calculations are chosen in such a way that the LEET relations between form factors are satisfied to a 10% accuracy [156]. In our numerical analysis we take the errors in these form factors to be $\pm 10\%$.

Within the SM, $A_{FB}(q^2)$ is predicted to vanish around $q^2 \approx 4.3$ GeV^2 (i.e. $x_\gamma \approx 0.85$) [156], and the crossing is predicted to be negative. It is therefore interesting to see the effects of various NP operators and their combinations on A_{FB}. In the extreme LEET limit, using the form-factor relations given in Ref. [156], one can easily see that the A_{FB} is independent of the form factors. In Fig. 4.5 we see large bands in the SM predictions of A_{FB} in the low q^2 region. One may tend to interpret these as large corrections to the LEET limit, however this would be somewhat misleading, as we take the errors in the form factors, due to corrections from the LEET limit, to be uncorrelated. In realistic models, LEET corrections to the form factors will be correlated, leading to a smaller uncertainty band for A_{FB} in the SM.

Fig. 4.5 also shows A_{FB} and DBR in the presence of NP in the form of $R_{V,A}$ couplings. With the large allowed values of $|R_{V,A}|$ and the absence of any helicity suppression, we expect VA operators to have a significant impact on the observables. As can be seen from the figure, the maximum allowed value of DBR can be 2-3 times larger than the SM prediction. The BR can also be suppressed below the SM prediction due to destructive interference. In the low-q^2 region, the suppression can be large. The features of the zero-crossing predicted by the SM can be affected: it can be positive or negative, can take place at any value of q^2, and can disappear altogether. As expected, the impact of $R'_{V,A}$ couplings is much milder. In particular, the zero-crossing is always positive and in the low-q^2 region.

With new tensor couplings, an enhancement of the DBR by up to a factor of 3 in comparison to the SM prediction is possible. Moreover, in the limit of neglecting

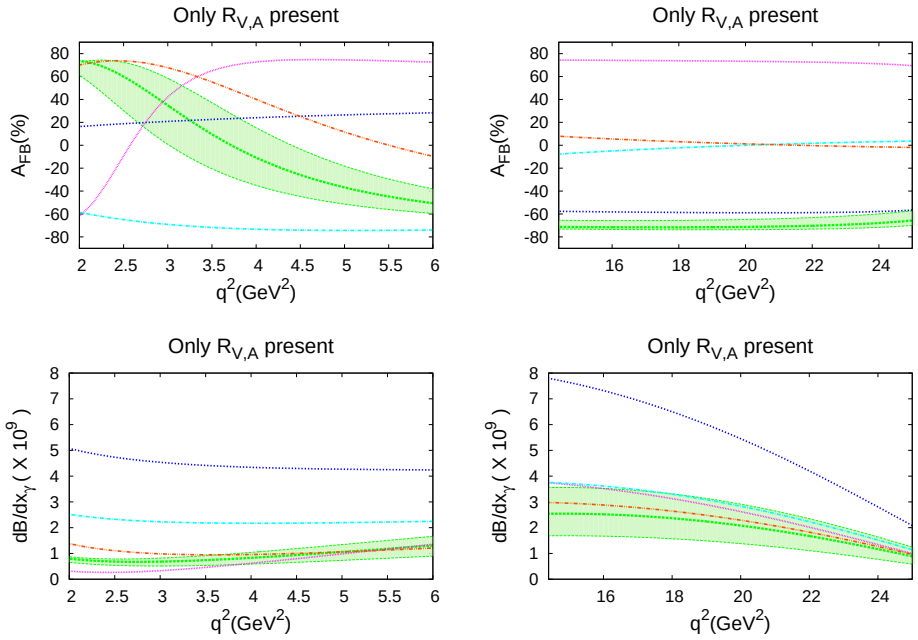

Figure 4.5: The left (right) panels of the figure show A_{FB} and DBR for $\bar{B}_s^0 \to \mu^+\mu^-\gamma$ in the low-q^2 (high-q^2) region, in the scenario where only (R_V, R_A) terms are present. Note that here $q^2 = m_B^2(1 - x_\gamma)$. The band corresponds to the SM prediction and its uncertainties; the lines show predictions for some representative values of NP parameters (R_V, R_A). For example, the magenta curves in the low-q^2 and high-q^2 regions correspond to $(2.47, 7.08)$ and $(-7.14, -0.42)$, respectively.

the muon mass, T operators do not contribute to the Y-terms in Eq. (4.39); their contribution is only to Θ. As a result, they can only suppress A_{FB} from its SM value.

When all NP operators are allowed, we find that $B(\bar{B}_s^0 \to \mu^+\mu^-\gamma)$ can be enhanced by a factor of 4, or it can be suppressed significantly. The shape of $A_{FB}(q^2)$ is determined by the new VA couplings, while its magnitude can be suppressed if the T couplings are significant.

4.6 $\bar{B}_d^0 \to \bar{K}\mu^+\mu^-$

The decay mode $\bar{B}_d^0 \to \bar{K}\mu^+\mu^-$ is interesting primarily because the forward-backward asymmetry of muons is predicted to vanish in the SM. This is due to the fact that the hadronic matrix element for the $\bar{B}_d^0 \to \bar{K}$ transition does not have any axial-vector contribution. A_{FB} can have a nonzero value only if it receives a contribution from new physics in the form of SP or T operators. Thus, the information from this decay

is complementary to that from the other decays considered earlier, which were more sensitive to new physics VA operators.

The total branching ratio of $\bar{B}_d^0 \to \bar{K}\mu^+\mu^-$ has been measured to be [194]

$$B(\bar{B}_d^0 \to \bar{K}\mu^+\mu^-) = \left(4.5^{+1.2}_{-1.0}\right) \times 10^{-7} \,, \tag{4.40}$$

which is consistent with the SM prediction [148]

$$B(\bar{B}_d^0 \to \bar{K}\mu^+\mu^-)_{\rm SM} = (3.5 \pm 1.2) \times 10^{-7} \,. \tag{4.41}$$

The integrated asymmetry, $\langle A_{FB}\rangle$, has been measured by BaBar [201] and Belle [126, 202] to be

$$\langle A_{FB}\rangle = (0.15^{+0.21}_{-0.23} \pm 0.08) \quad \text{(BaBar)} \,, \tag{4.42}$$

$$\langle A_{FB}\rangle = (0.10 \pm 0.14 \pm 0.01) \quad \text{(Belle)}. \tag{4.43}$$

These measurements are consistent with zero. However, within 2σ they can be as large as $\sim 40\%$. Experiments such as the LHC or a future Super-B factory will increase the statistics by more than two orders of magnitude. For example, at ATLAS at the LHC, after analysis cuts the number of $\bar{B}_d^0 \to \bar{K}\mu^+\mu^-$ events is expected to be ~ 4000 with 30 fb^{-1} of data [203]. Thus, $\langle A_{FB}\rangle$ can soon be probed to values as low as 5%. With higher statistics, one will even be able to measure A_{FB} as a function of the invariant dimuon mass squared q^2. This can provide a stronger handle on this quantity than just its average value $\langle A_{FB}\rangle$.

The effect of NP on $\langle A_{FB}\rangle$ and the $A_{FB}(q^2)$ distribution in $\bar{B}_d^0 \to \bar{K}\mu^+\mu^-$ was studied in Refs. [164] and [165] respectively. In the latter, it was shown that simultaneous new-physics SP and T operators can lead to a large enhancement of $A_{FB}(q^2)$ in the high-q^2 region. However, NP effects due to other operators were not studied. Here we present a complete analysis of the effect of NP on the $A_{FB}(q^2)$ distribution in $\bar{B}_d^0 \to \bar{K}\mu^+\mu^-$ by taking into account all possible NP operators and their combinations. In addition, we study the possible zero crossing of $A_{FB}(q^2)$ and the correlations between the DBR and A_{FB} features.

4.6.1 Differential branching ratio and forward-backward asymmetry

The differential branching ratio for this mode is given by

$$\frac{dB}{dz} \;=\; B_0' \, \phi^{1/2} \, \beta_\mu \left[X'_{VA} + X'_{SP} + X'_T + X'_{VA\text{-}SP} + X'_{VA\text{-}T} \right] , \tag{4.44}$$

where the normalization factor B_0', the phase factor ϕ and the X' terms are given in Appendix III. The subscripts for the X' terms denote the Lorentz structure(s) contributing to that term.

The normalized forward-backward asymmetry for the muons in $\bar{B}_d^0 \to \bar{K}\mu^+\mu^-$ is defined as

$$A_{FB}(q^2) = \frac{\displaystyle\int_0^1 d\cos\theta_\mu \frac{d^2B}{dq^2 d\cos\theta_\mu} - \int_{-1}^0 d\cos\theta_\mu \frac{d^2B}{dq^2 d\cos\theta_\mu}}{\displaystyle\int_0^1 d\cos\theta_\mu \frac{d^2B}{dq^2 d\cos\theta_\mu} + \int_{-1}^0 d\cos\theta_\mu \frac{d^2B}{dq^2 d\cos\theta_\mu}} \,, \tag{4.45}$$

where θ_μ is the angle between the three-momenta of the $\bar{B}_d^0$ and the μ^+ in the dimuon center-of-mass frame. The calculation of $A_{FB}(q^2)$ gives

$$A_{FB}(q^2) = \frac{2B_0' \beta_\mu \phi}{dB/dz}\left[Y'_{VA\text{-}SP} + Y'_{VA\text{-}T} + Y'_{SP\text{-}T}\right] \tag{4.46}$$

where the Y terms are given in Appendix III.

The largest source of uncertainty in the calculations are the $\bar{B} \to \bar{K}$ form factors. As these cannot be calculated from first principles within QCD, one has to rely on models. In the numerical calculations, we use the form factors as calculated in Ref. [161] in the framework of QCD light-cone sum rules; the details are given in Appendix III. There are, however, certain limits in which relations between form factors can be rigorously obtained. In the large energy (LEET) limit, these relations are valid up to α_s, $1/E_K$ and $1/m_b$ corrections [166, 167].

In the LEET limit, using the form-factor relations in Eq. (III.51), one can verify that A_{FB} is independent of the form factors. This is quite useful as it implies that the measurement of A_{FB} can be used to extract the parameters of the new-physics operators without form-factor uncertainties in this limit.

In the low-energy, large q^2, region one can also derive relations between form factors in the heavy-quark limit [189, 190]. However, these relations do not completely eliminate the form-factor dependence of the calculated quantities, and hence we do not consider these relations. An analysis where these relations have been used in the context of $b \to s\mu^+\mu^-$ can be found in Refs. [180, 182].

From Eq. (4.46), clearly new VA couplings alone cannot give rise to A_{FB}, which vanishes in the SM in any case. Note that this is one of the few cases where the VA couplings fail to influence an asymmetry significantly, in spite of the large allowed values of the couplings. This is because the argument about the hadronic matrix element $\bar{B}_d^0 \to \bar{K}$ not having any axial-vector contribution stays valid even in the presence of NP. The DBR can, however, be enhanced by up to a factor of 2, or marginally suppressed.

The contribution of SP operators through the $Y'_{VA\text{-}SP}$ terms can give rise to A_{FB}, where the VA contribution comes from the SM operators. The effect is rather small when only $R_{S,P}$ or only $R'_{S,P}$ couplings are present, due to the strong constraints on their values. The peak value of A_{FB} in the low-q^2 region stays below the percent level,

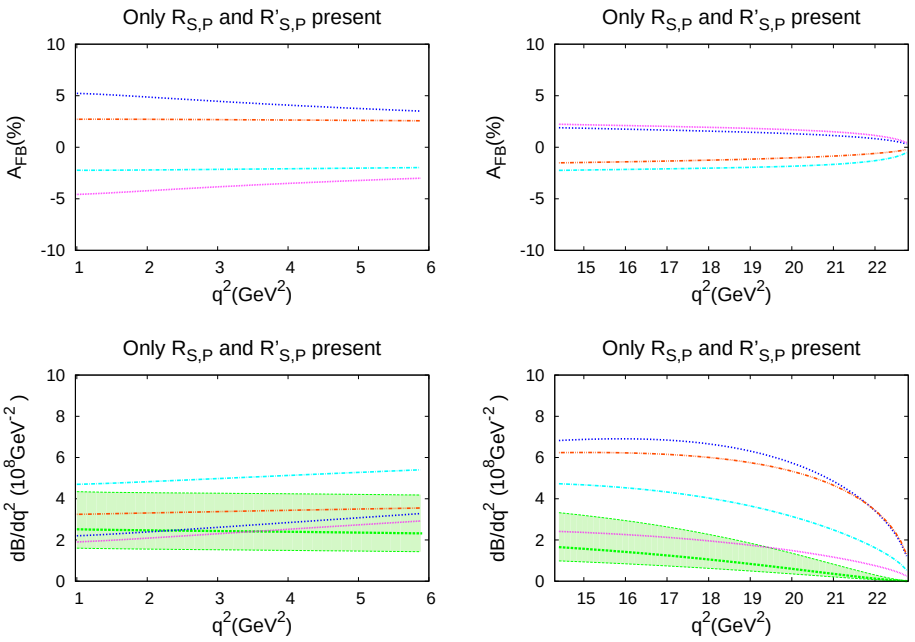

Figure 4.6: The left (right) panels of the figure show A_{FB} and DBR for $\bar{B}_d^0 \to \bar{K}\mu^+\mu^-$ in the low-q^2 (high-q^2) region, in the scenario where all NP SP couplings are present. The band corresponds to the SM prediction and its uncertainties; the lines show predictions for some representative values of NP parameters (R_S, R_P, R'_S, R'_P) . For example, the blue curves in the low-q^2 and high-q^2 regions correspond to $(-2.50, 6.18, -2.84, -5.64)$ and $(-2.41, 1.86, -2.07, 1.42)$, respectively.

while in the the high-q^2 region it can be enhanced up to 2% at the extreme end point ($q^2 \gtrsim 22$ GeV^2), which is virtually impossible to observe. However if both the primed and unprimed SP couplings are present simultaneously, the constraints on them are weakened. In such a situation, the peak value of A_{FB} in the low-q^2 (high-q^2) can become $\sim 5\%$ ($\sim 3\%$). This may be seen in Fig. 4.6. It is also observed that A_{FB} is always positive or always negative, i.e. there is no zero crossing. The DBR also is significantly affected only if both the primed and unprimed SP couplings are present: it can be enhanced by up to a factor of 3.

New T couplings are also expected to give rise to A_{FB} through the $Y'_{VA\text{-}T}$ terms in Eq. (III.53). It is observed from Fig. 4.7 that $A_{FB}(q^2)$ can be enhanced up to 5-6% in almost the entire q^2 region. Moreover, at $q^2 \gtrsim 21$ GeV^2, the peak value of $A_{FB}(q^2)$ reaches a larger value ($\sim 30\%$). The value of $A_{FB}(q^2)$ is always positive or always negative, i.e. there is no zero crossing point. The DBR values do not go significantly outside the SM-allowed range.

When VA and T couplings are present simultaneously, a DBR enhancement of up

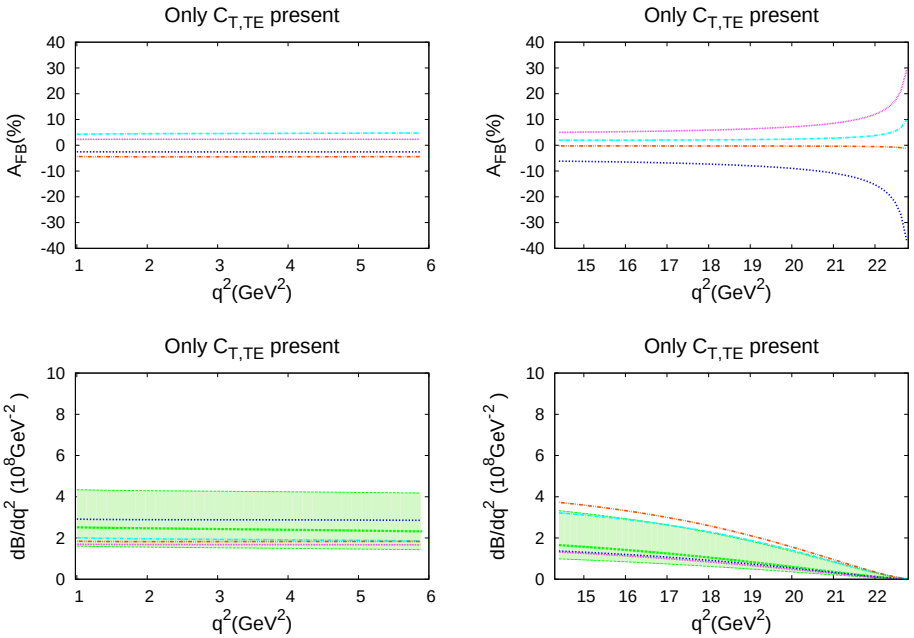

Figure 4.7: The left (right) panels of the figure show A_{FB} and DBR for $\bar{B}_d^0 \to \bar{K}\mu^+\mu^-$ in the low-q^2 (high-q^2) region, in the scenario where only T terms are present. The band corresponds to the SM prediction and its uncertainties; the lines show predictions for some representative values of NP parameters (C_T, C_{TE}). For example, the blue curves in the low-q^2 and high-q^2 regions correspond to $(0.30, 0.37)$ and $(0.49, 0.57)$, respectively.

to a factor of 2 is possible, while A_{FB} can be large only at extremely high q^2. On the other hand, when SP and T couplings are present simultaneously, their interference can have a large impact on A_{FB}. The interference term $Y'_{SP\text{-}T}$ that contributes to A_{FB} is not suppressed by m_μ/m_b, and therefore a large A_{FB} is possible, as can be seen from Fig. 4.8. This is also the only combination of NP couplings where a zero crossing may occur. Among the asymmetries considered in this chapter, this is the one where the SP and T operators can have the largest impact. The DBR can also be enhanced by up to a factor of 2-3 at large q^2 due to the simultaneous presence of primed and unprimed SP operators.

4.7 $\bar{B}_d^0 \to \bar{K}^*\mu^+\mu^-$

The measurement of the forward-backward asymmetry in $\bar{B}_d^0 \to \bar{K}^*\mu^+\mu^-$ by the Belle collaboration [126, 127], which showed a deviation from the SM prediction, indicates

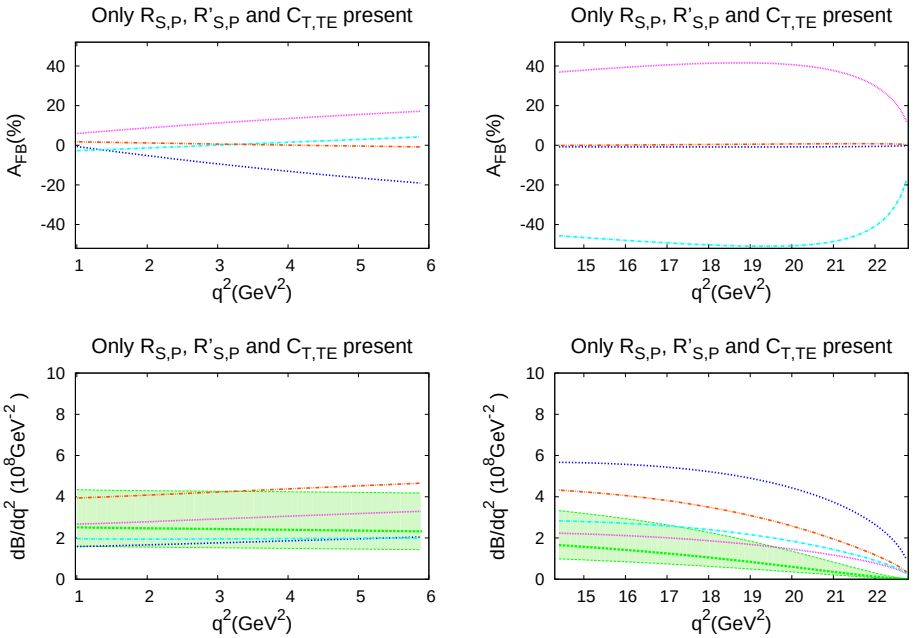

Figure 4.8: The left (right) panels of the figure show A_{FB} and DBR for $\bar{B}_d^0 \to \bar{K}\mu^+\mu^-$ in the low-q^2 (high-q^2) region, in the scenario where both SP and T terms are present. The band corresponds to the SM prediction and its uncertainties; the lines show predictions for some representative values of NP parameters $(R_S, R_P, R'_S, R'_P, C_T, C_{TE})$. For example, the magenta curves in the low-q^2 and high-q^2 regions correspond to $(-0.09, -2.24, 0.16, -2.14, -0.33, -0.40)$ and $(-0.40, 1.87, -0.59, 1.88, -0.34, 0.66)$, respectively.

the possibility of the presence of new physics. According to the SM, A_{FB} is $\leq 20\%$ and negative at low q^2, has a zero crossing at $q^2 \approx 4$ GeV^2, and is positive but $\leq 40\%$ for larger q^2 values. The experiment showed the asymmetry to be positive throughout the range of q^2 – consequently no zero crossing – and $A_{FB} \approx 60\%$ at large q^2 values. This has generated a special interest in this decay.

There have already been a number of theoretical studies, both within the SM [168, 169, 176] and in specific NP scenarios [173, 174, 177, 178], focusing on the branching fraction and A_{FB} of $\bar{B}_d^0 \to \bar{K}^*\mu^+\mu^-$. For example, Ref. [175] has pointed out that $A_{FB}(q^2)$ is a sensitive probe of NP that affects the SM Wilson coefficients. Other observables based on the K^* spin amplitudes of this decay are at present under active theoretical and experimental analysis [173, 174, 176]. Finally, more challenging observables, such as the polarized lepton forward-backward asymmetry [162, 163, 171, 172], have also been considered, though the measurement of this quantity is still lacking.

In the coming years, the LHCb experiment will collect around 3000 events of $\bar{B}_d^0 \to$

$\bar{K}^*\mu^+\mu^-$ per fb^{-1} in the full range of q^2. An integrated luminosity of 2 fb^{-1} already would allow the extraction of the SM zero of A_{FB} (if it is there) with a precision of ± 0.5 GeV^2 [204]. Indeed, a dataset of 100 pb^{-1} would already improve the world precision obtained by Babar, Belle and CDF. These measurements would also permit many of the additional tests for NP mentioned above.

The decay $\bar{B}^0_d \to \bar{K}^*\mu^+\mu^-$, with $\bar{K}^*$ decaying to $\bar{K}\pi$, has four particles in the final state. This implies that there are three physical angles that can specify the relative directions of these four final-state particles. The differential decay rate as a function of these three angles has much more information than just the forward-backward asymmetry. Indeed, A_{FB} is just one of the observables that can be derived from the complete angular analysis of this decay. In this section we also consider other CP-conserving observables.

4.7.1 Angular analysis

The complete angular distribution in $\bar{B}^0_d \to \bar{K}^*\mu^+\mu^-$ has been calculated in Refs. [205, 206] within the SM. In this section, we calculate the angular distribution in the presence of NP, which is a new result. The full transition amplitude for $\bar{B}(p_B) \to \bar{K}^*(p_{K^*}, \epsilon^*)\mu^+(p_\mu^+)\mu^-(p_\mu^-)$ is

$$\begin{aligned} i\mathcal{M}(\bar{B}^0_d \to \bar{K}^*\mu^+\mu^-) &= (-i)\frac{1}{2}\left[\frac{4\,G_F}{\sqrt{2}}\frac{\alpha_{em}}{4\pi}(V_{ts}^*V_{tb})\right]\times \\ &\quad [M_{V\mu}L^\mu + M_{A\mu}L^{\mu 5} + M_S L + M_P L^5 + M_{T\mu\nu}L^{\mu\nu} + iM_{E\mu\nu}L_{\alpha\beta}\epsilon^{\mu\nu\alpha\beta}] \end{aligned} \quad (4.47)$$

where the L's are defined in Eq. (4.8). The M's are given in Appendix IV.

The complete three-angle distribution for the decay $\bar{B} \to \bar{K}^*(\to \bar{K}\pi)\mu^+\mu^-$ can be expressed in terms of q^2, two polar angles θ_μ, θ_K, and the angle between the planes of the dimuon and $K\pi$ decays, ϕ. These angles are described in Fig. 4.9. We choose the momentum and polarization four-vectors of the K^* meson in the dimuon rest frame as

$$\begin{aligned} &p_{K^*} = (E_{K^*}, 0, 0, |\vec{p}_{K^*}|)\ , \\ &\varepsilon(0) = \frac{1}{m_{K^*}}(|\vec{p}_{K^*}|, 0, 0, E_{K^*})\ , \quad \varepsilon(\lambda = \pm 1) = \mp\frac{1}{\sqrt{2}}(0, 1, \pm i, 0)\ , \end{aligned} \quad (4.48)$$

with

$$E_{K^*} = \frac{m_B^2 - m_{K^*}^2 - q^2}{2\sqrt{q^2}}, \quad |\vec{p}_{K^*}| = \sqrt{E_{K^*}^2 - m_{K^*}^2}\ . \quad (4.49)$$

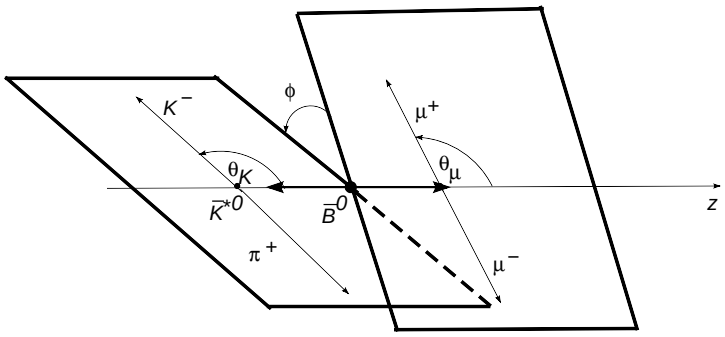

Figure 4.9: The description of the angles $\theta_{\mu,K}$ and ϕ in the angular distribution of $\bar{B} \to \bar{K}^*(\to \bar{K}\pi)\mu^+\mu^-$ decay.

The three-angle distribution can be obtained using the helicity formalism:

$$\frac{d^4\Gamma}{dq^2 d\cos\theta_\mu d\cos\theta_K d\phi} = N_F \times$$
$$\Big\{ \quad \cos^2\theta_K\Big(I_1^0 + I_2^0\cos 2\theta_\mu + I_3^0\cos\theta_\mu\Big) + \sin^2\theta_K\Big(I_1^T + I_2^T\cos 2\theta_\mu + I_3^T\cos\theta_\mu$$
$$+I_4^T\sin^2\theta_\mu\cos 2\phi + I_5^T\sin^2\theta_\mu\sin 2\phi\Big) + \sin 2\theta_K\Big(I_1^{LT}\sin 2\theta_\mu\cos\phi$$
$$+I_2^{LT}\sin 2\theta_\mu\sin\phi + I_3^{LT}\sin\theta_\mu\cos\phi + I_4^{LT}\sin\theta_\mu\sin\phi\Big)\Big\}\,, \qquad (4.50)$$

where the normalization factor N_F is

$$N_F \;=\; \frac{3\alpha_{em}^2 G_F^2 |V_{ts}^* V_{tb}|^2 |\vec{p}_{K^*}^{\,\mathcal{B}}|\beta_\mu}{2^{14}\pi^6 m_B^2} Br(K^* \to K\pi)\,. \qquad (4.51)$$

Here $\beta_\mu = \sqrt{1-4m_\mu^2/q^2}$, and $|\vec{p}_{K^*}^{\,\mathcal{B}}|$ is the magnitude of the K^* momentum in the B-meson rest frame:

$$|\vec{p}_{K^*}^{\,\mathcal{B}}| \;=\; \frac{1}{2m_B}\sqrt{m_B^4 + m_{K^*}^4 + q^4 - 2[q^2 m_B^2 + m_{K^*}^2(m_B^2+q^2)]}\,. \qquad (4.52)$$

The twelve angular coefficients I depend on the couplings, kinematic variables and form factors, and are given in Appendix IV. In this chapter we concentrate on the CP-conserving observables: the DBR, the forward-backward asymmetry A_{FB}, the polarization fraction f_L, and the asymmetries $A_T^{(2)}$ and A_{LT}.

The theoretical predictions for the relevant $B \to K^*$ form factors are rather uncertain in the region ($7\ \text{GeV}^2 \le q^2 \le 12\ \text{GeV}^2$) due to nearby charmed resonances.

The predictions are relatively more robust in the lower and higher q^2 regions. We therefore concentrate on calculating the angular distribution in the low-q^2 ($1\ \text{GeV}^2 \leq q^2 \leq 6\ \text{GeV}^2$) and the high-$q^2$ ($q^2 \geq 14.4\ \text{GeV}^2$) regions. For numerical calculations, we follow Ref. [178] for the form factors: in the low-q^2 region, we use the form factors obtained using QCD factorization, while in the high-q^2 region, we use the form factors calculated in the light-cone sum-rule approach.

4.7.2 Differential branching ratio and forward-backward asymmetry

The forward-backward asymmetry for the muons is defined by

$$A_{FB}(q^2) = \frac{\int_0^1 d\cos\theta_\mu \frac{d^2\Gamma}{dq^2 d\cos\theta_\mu} - \int_{-1}^0 d\cos\theta_\mu \frac{d^2\Gamma}{dq^2 d\cos\theta_\mu}}{\int_0^1 d\cos\theta_\mu \frac{d^2\Gamma}{dq^2 d\cos\theta_\mu} + \int_{-1}^0 d\cos\theta_\mu \frac{d^2\Gamma}{dq^2 d\cos\theta_\mu}} \,. \tag{4.53}$$

It can be obtained by integrating over the two angles θ_K and ϕ in Eq. (4.50). We obtain the double differential decay rate as

$$\frac{d^2\Gamma}{dq^2 d\cos\theta_\mu} = \frac{8\pi N_F}{3}\Big[\frac{1}{2}\Big(I_1^0 + I_2^0\cos 2\theta_\mu + I_3^0\cos\theta_\mu\Big) + \Big(I_1^T + I_2^T\cos 2\theta_\mu + I_3^T\cos\theta_\mu\Big)\Big] \,. \tag{4.54}$$

Further integration over the angle θ_μ gives the differential decay rate. The contribution of the NP operators to the differential branching ratio and forward-backward asymmetry of $\bar{B}_d^0 \to \bar{K}^*\mu^+\mu^-$ was examined in detail in Ref. [178]. We do not reproduce the analysis here, but only give the results below.

If only $R_{V,A}$ couplings are present, A_{FB} can be enhanced at low q^2, while keeping it positive, so that there is no zero crossing as indicated by the recent data [126–129]. However, an enhancement at high q^2, also indicated by the same data, is not possible. On the other hand, if only $R'_{V,A}$ couplings are present, A_{FB} can become large and positive at high q^2, but then it has to be large and negative at low q^2. These couplings are therefore unable to explain the positive values of A_{FB} at low q^2. Thus, in order to reproduce the current $\bar{B}_d^0 \to \bar{K}^*\mu^+\mu^-$ experimental data, one needs both unprimed and primed NP VA operators. The NP coupling values that come closest to the data typically correspond to suppressed DBR at low q^2. (See Fig. 4.10.) But it is also possible to have a large A_{FB} (up to 60%) in the entire q^2 region while being consistent with the SM prediction for the DBR. At present, the errors on the measurements are quite large. However, if future experiments reproduce the current central values with greater precision, this will put important constraints on any NP proposed to explain the data.

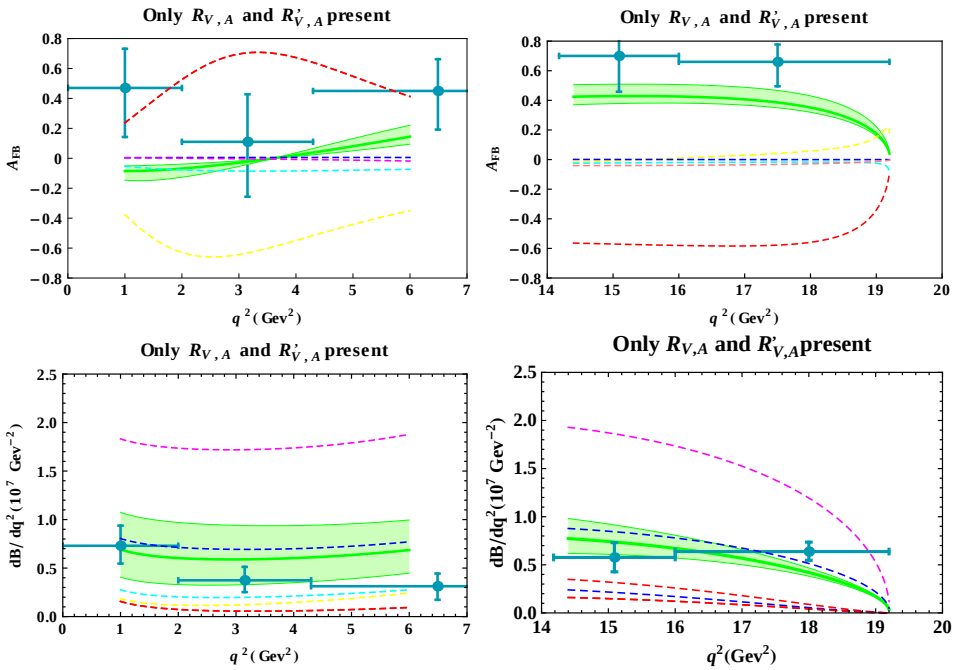

Figure 4.10: The left (right) panels of the figure show A_{FB} and DBR for $\bar{B}^0_d \to \bar{K}^* \mu^+ \mu^-$ in the low-q^2 (high-q^2) region, in the scenario where both (R_V, R_A) and (R'_V, R'_A) terms are present. The band corresponds to the SM prediction and its uncertainties; the lines show predictions for some representative values of NP parameters (R_V, R_A, R'_V, R'_A). For example, the red curves for A_{FB} in the low and high q^2 regions correspond to $(-1.55, 1.75, 6.16, 1.73)$ and $(-5.79, 1.10, 0.47, -3.34)$, respectively. The pink curves for DBR in the low-q^2 and high-q^2 regions correspond to $(1.96, -4.09, 4.61, 0.13)$. For comparison, the experimental data are also displayed in blue cross lines.

New SP couplings by themselves cannot significantly affect either the DBR or the A_{FB} predictions of the SM. New T couplings in general tend to enhance DBR significantly, by up to a factor of 2, while not contributing any additional terms to the asymmetry. As a result, the magnitude of A_{FB} is suppressed. The zero crossing can be anywhere in the entire q^2 range, or it may disappear altogether. However, whenever it is present, it is always a SM-like (positive) crossing. When SP and T couplings are present simultaneously, additional contributions to A_{FB} that are not suppressed by m_μ/m_B are possible. As a result, A_{FB} obtained with this combination can be marginally enhanced as compared to the case with only T operators. It is then possible to have no zero crossing. However, the magnitude of A_{FB} cannot be large in the high-q^2 region.

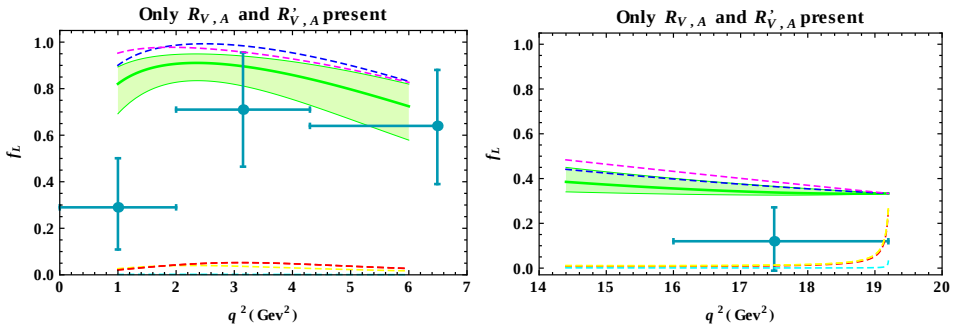

Figure 4.11: The left (right) panel of the figure shows f_L for $\bar{B}^0_d \to \bar{K}^* \mu^+ \mu^-$ in the low-q^2 (high-q^2) region, in the scenario where both (R_V, R_A) and (R'_V, R'_A) terms are present. For example, the blue curves in the low-q^2 and high-q^2 regions correspond to $(1.64, -0.90, 4.27, -0.91)$ and $(1.96, -4.09, 4.61, 0.13)$, respectively. For comparison, the experimental data are also displayed in blue cross lines.

4.7.3 Polarization fraction f_L

The differential decay rate and K^* polarization fractions can be found by integrating over the three angles in Eq. (4.50) to get

$$\frac{d\Gamma}{dq^2} = \frac{8\pi N_F}{3}(A_L + A_T) , \tag{4.55}$$

where the longitudinal and transverse polarization amplitudes A_L and A_T are obtained from Eq. (4.54):

$$A_L = \left(I_1^0 - \frac{1}{3} I_2^0\right), \quad A_T = 2\left(I_1^T - \frac{1}{3} I_2^T\right) . \tag{4.56}$$

It can be seen from the expressions for the I's in Appendix IV [see Eq. (IV.69)] that SP couplings cannot affect A_T. The longitudinal and transverse polarization fractions, f_L and f_T, respectively, are defined as

$$f_L = \frac{A_L}{A_L + A_T} , \quad f_T = \frac{A_T}{A_L + A_T} . \tag{4.57}$$

In the SM, f_L can be as large as 0.9 at low q^2, and it decreases to about 0.3 at high q^2. As can be seen from Fig. 4.11, new VA couplings can suppress f_L substantially: it can almost vanish in some allowed parameter range.

New SP couplings cannot change the value of f_L outside the range allowed by the SM. This may be attributed to the strong constraints on the values of these couplings. New T couplings tend to suppress f_L, except at $q^2 \approx$ 1-2 GeV^2, where the value of f_L cannot be less than 0.5 as may be seen from Fig. 4.12. Since both VA and T couplings tend to suppress f_L, their combined effect results in a similar behavior.

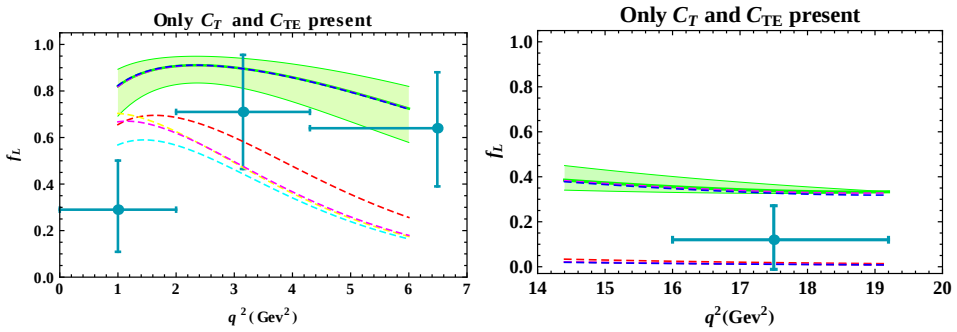

Figure 4.12: The left (right) panel of the figure shows f_L for $\bar{B}_d^0 \to \bar{K}^* \mu^+ \mu^-$ in the low-q^2 (high-q^2) region, in the scenario where only new T couplings are present. The band corresponds to the SM prediction and its uncertainties; the lines show predictions for some representative values of NP parameters (C_T, C_{TE}). For example, the red curves in the low-q^2 and high-q^2 regions correspond to $(0.66, -0.14)$ and $(0.3, -0.46)$, respectively.

4.7.4 Angular asymmetries $A_T^{(2)}$ and A_{LT}

In this subsection we consider the two angular asymmetries $A_T^{(2)}$ and A_{LT}. The first quantity was discussed before in Ref. [173], while A_{LT} is introduced here for the first time.

The CP-conserving transverse asymmetry $A_T^{(2)}$ can be defined through the double differential decay rate

$$\frac{d^2\Gamma}{dq^2 d\phi} = \frac{1}{2\pi}\frac{d\Gamma}{dq^2}\Big[1 + f_T\left(A_T^{(2)}\cos 2\phi + A_T^{(im)}\sin 2\phi\right)\Big] . \tag{4.58}$$

Here $A_T^{(im)}$ depends on the imaginary part of a certain combination of amplitudes and can be used to construct CP-violating observables. We will not consider it any further in this work. The asymmetry $A_T^{(2)}$ can be obtained by integrating over the two polar angles θ_μ and θ_K in Eq. (4.50). It can be expressed as

$$A_T^{(2)} = \frac{4I_4^T}{3A_T}. \tag{4.59}$$

We observe that $A_T^{(2)}$ cannot be affected by SP couplings.

In the SM,

$$A_T^{(2)} \approx \frac{4\beta_\mu^2\Big(|A_\perp^V|^2 - |A_\parallel^V|^2 + |A_\perp^A|^2 - |A_\parallel^A|^2\Big)}{3A_T} . \tag{4.60}$$

The transversity amplitudes $A_{\parallel,\perp}$ are defined through Eqs. (IV.65) and (IV.66) given in Appendix IV. At leading order in Λ_{QCD}/E_{K^*}, Λ_{QCD}/m_b and α_s (the LEET limit), one can use the form-factor relations of Refs. [166, 167] and neglect terms of $\mathcal{O}(m_{K^*}^2/m_B^2)$ to obtain

$$A_V^+ \approx 0 \quad , \qquad A_A^+ \approx 0 \; . \tag{4.61}$$

Thus, in the low-q^2 region,

$$A_\parallel^i \approx \frac{A_i^-}{\sqrt{2}} \quad , \qquad A_\perp^i \approx -\frac{A_i^-}{\sqrt{2}} \quad \text{for} \quad i = V, A \; , \tag{4.62}$$

which corresponds to the LEET limit. $A_T^{(2)} \approx 0$ in the SM and is independent of form factors up to corrections of order Λ_{QCD}/E_{K^*}, Λ_{QCD}/m_b and α_s, i.e. the hadronic uncertainty is small. This can be seen in Figs. 4.13 and 4.14. This indicates that corrections to the LEET limit are small, and makes $A_T^{(2)}$ an excellent observable to look for new-physics effects [173].

We now examine the longitudinal-transverse asymmetry A_{LT}, defined by

$$A_{LT} \;=\; \frac{\int_{-\pi/2}^{\pi/2} d\phi (\int_0^1 d\cos\theta_K \frac{d^3\Gamma}{dq^2 d\phi d\cos\theta_K} - \int_{-1}^0 d\cos\theta_K \frac{d^3\Gamma}{dq^2 d\phi d\cos\theta_K})}{\int_{-\pi/2}^{\pi/2} d\phi (\int_0^1 d\cos\theta_K \frac{d^3\Gamma}{dq^2 d\phi d\cos\theta_K} + \int_{-1}^0 d\cos\theta_K \frac{d^3\Gamma}{dq^2 d\phi d\cos\theta_K})} \; . \tag{4.63}$$

One can compare A_{LT} to A_{FB}. In A_{FB} the angle ϕ is integrated over its entire range, while in A_{LT} ϕ is only integrated over the range $(-\pi/2, \pi/2)$. This choice of integration range eliminates all terms which depend on the imaginary part of combinations of amplitudes in the angular distribution. (These eliminated terms can be used to construct CP-violating observables and will not be discussed here.) In A_{LT} only the CP-conserving parts of the angular distribution survive. Note that, in the CP-conserving limit, A_{LT} is the same as the observable S_5 defined in Ref. [177], apart from a normalization constant. The quantity A_{LT} can also be expressed in terms of the observables $A_T^{(3)}$ and $A_T^{(4)}$ defined in Ref. [176]. However, A_{LT} is easily extracted from the angular distribution and has different properties in the LEET limit than $A_T^{(3)}$ and $A_T^{(4)}$.

Using Eq. (4.50), the asymmetry A_{LT} can be expressed as

$$A_{LT} \;=\; \frac{I_3^{LT}}{2(A_L + A_T)}. \tag{4.64}$$

We observe from Eq. (IV.70) that A_{LT} depends on the VA couplings, as well as on V-S, S-TE, and P-T interference terms. In the SM,

$$A_{LT} \;=\; \frac{\beta_\mu \mathrm{Re}[A_{0,VA}^L (A_\perp^{V*} - A_\perp^{A*}) - A_{0,VA}^R (A_\perp^{V*} + A_\perp^{A*})]}{\sqrt{2}(A_L + A_T)} \; . \tag{4.65}$$

Now, in the LEET limit, $A_{V,A}^{+} \approx 0$. Hence, in this limit,

$$A_{LT}^{LEET} \propto \frac{\mathrm{Re}[A_V^0 A_A^{-*} + A_A^0 A_V^{-*}]}{A_L + A_T} . \tag{4.66}$$

From this it can be shown that the SM predicts $A_{LT} = 0$ at

$$q^2 \approx -\frac{C_7^{eff} m_b m_B^2}{C_7^{eff} m_b + C_9^{eff} m_B} \approx 1.96 \text{ GeV}^2 . \tag{4.67}$$

Thus, just like A_{FB}, the quantity A_{LT} also has a zero crossing which is independent of form factors in the LEET limit. Note that the zero crossing of A_{LT} is different from that of A_{FB}. Figs. 4.13 and 4.14 also demonstrate that the zero crossing of A_{LT} has a very small hadronic uncertainty. This indicates small corrections to the LEET limit, making the position of the zero crossing of A_{LT} a robust prediction of the SM. This quantity would therefore be very useful in searching for new-physics effects.

New VA couplings can affect $A_T^{(2)}$ significantly: they can enhance its magnitude by a large amount, change its sign, and change its q^2-dependence. The zero-crossing point may be at a value of q^2 different from that predicted by the SM.

Since A_{LT} here is identical to the observable S_5 in Refs. [177, 183] in the CP-conserving limit (apart from a normalization factor), the zero-crossing in both of these observables is expected to take place at the same q^2. Indeed, the results agree at LO, while the NLO corrections can shift the q^2 at the zero-crossing to $q^2 = 2.24^{+0.06}_{-0.08}$ [177]. Note that the deviation due to new VA couplings can be much larger than the effects due to NLO corrections.

Except at very low q^2, the magnitude of A_{LT} is generally suppressed by new VA couplings. The primed VA couplings can be constrained by A_{LT} better than the unprimed VA couplings. In both cases, the value of A_{LT} can be anywhere in the q^2 range, and can be positive or negative. In particular, there may or may not be a zero crossing, and if there is, its position can be different from that of the SM.

New SP couplings do not affect $A_T^{(2)}$, and A_{LT} qualitatively behaves similarly to the SM. New T couplings in general tend to suppress the magnitudes of both asymmetries (see Fig. 4.14).

4.8 Discussion and Summary

Flavor-changing neutral current (FCNC) processes are expected to be incisive probes of new physics. In the SM, they occur only at loop level, and hence are suppressed. This may allow the new-physics (NP) effects to be identifiable. Of course, since we have no clue about what form the NP takes, the observations from a variety of processes are necessary. In this chapter, we have focussed on the processes that involve the effective transition $b \to s\mu^+\mu^-$.

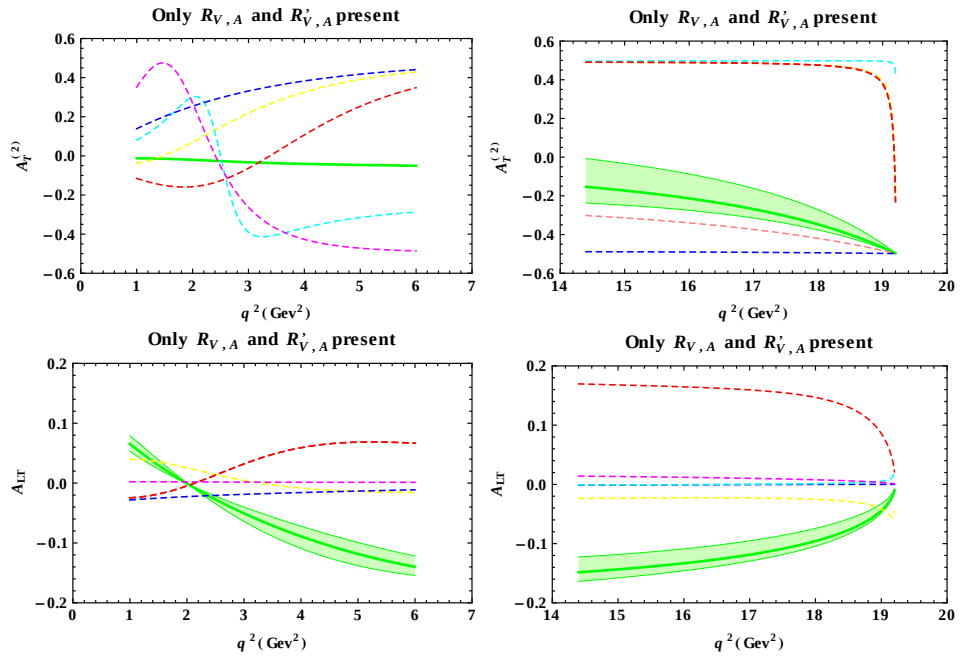

Figure 4.13: The left (right) panels of the figure show $A_T^{(2)}$ and A_{LT} for $\bar{B}_d^0 \to \bar{K}^* \mu^+ \mu^-$ in the low-q^2 (high-q^2) region, in the scenario where both (R_V, R_A) and (R'_V, R'_A) terms are present. The band corresponds to the SM prediction and its uncertainties; the lines show predictions for some representative values of NP parameters (R_V, R_A, R'_V, R'_A). For example, the pink curves for $A_T^{(2)}$ in the low-q^2 and high-q^2 regions correspond to $(1.96, -4.09, 4.61, 0.13)$ and $(1.64, -0.90, 4.27, -0.91)$, respectively. The red curves for A_{LT} in the low-q^2 and high-q^2 regions correspond to $(-1.55, 1.75, 6.16, 1.73)$ and $(-5.79, 1.10, 0.47, -3.33)$, respectively.

The transition $b \to s\mu^+\mu^-$ is responsible for many decay modes such as $\bar{B}_s^0 \to \mu^+\mu^-$, $\bar{B}_d^0 \to X_s\mu^+\mu^-$, $\bar{B}_s^0 \to \mu^+\mu^-\gamma$, $\bar{B}_d^0 \to \bar{K}\mu^+\mu^-$, $\bar{B}_d^0 \to \bar{K}^*\mu^+\mu^-$. While some of these processes (e.g. $\bar{B}_s^0 \to \mu^+\mu^-$) have not yet been observed, the upper bounds on their branching ratios have already yielded strong constraints on NP. Some of these processes have been observed and the measurements of their branching fractions, as well as of additional observables such as the forward-backward asymmetries, are available. Indeed, the recently-observed muon forward-backward asymmetry in $\bar{B}_d^0 \to \bar{K}^*\mu^+\mu^-$ has been found to deviate slightly from the SM predictions. If this is in fact due to the presence of NP, such NP should contribute to all the other decays involving the effective transition $b \to s\mu^+\mu^-$. The effects of this NP on these decay modes would be correlated, and hence a combined analysis of all these decay modes would be invaluable in discerning the type of NP present.

While specific models of NP may be used and their effect on the relevant observables

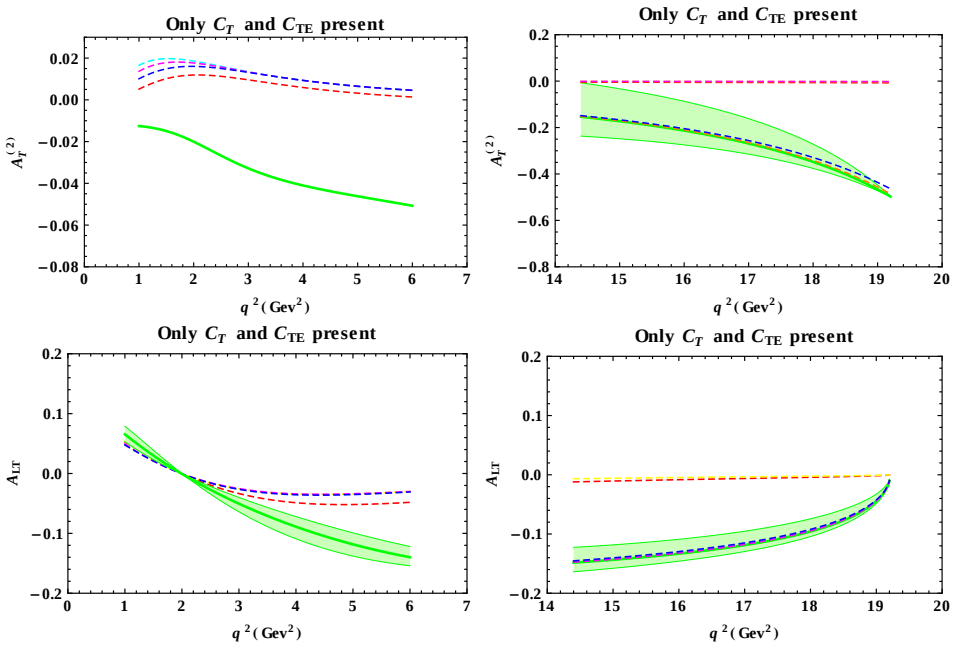

Figure 4.14: The left (right) panels of the figure show $A_T^{(2)}$ and A_{LT} for $\bar{B}_d^0 \to \bar{K}^* \mu^+ \mu^-$ in the low-q^2 (high-q^2) region, in the scenario where only new T couplings are present. The band corresponds to the SM prediction and its uncertainties; the lines show predictions for some representative values of NP parameters (C_T, C_{TE}). For example, the blue curves for $A_T^{(2)}$ in the low-q^2 and high-q^2 regions correspond to $(0.3, -0.46)$ and $(-0.005, 0.014)$, respectively. The red curves for A_{LT} in the low-q^2 and high-q^2 regions correspond to $(0.3, -0.46)$ and $(0.66, -0.14)$, respectively.

studied, we have chosen to explore the NP in a model-independent way, in terms of the Lorentz structures of the NP operators that contribute to the effective $b \to s\mu^+\mu^-$ Hamiltonian. We have performed a general analysis that includes NP vector-axial vector (VA), scalar-pseudoscalar (SP), and/or tensor (T) operators. We have computed the effects of such NP operators, individually and in all combinations, on these decays. We have taken the couplings to be real and have considered the CP-conserving observables in this chapter; the CP-violating observables are discussed in the next chapter. The aim is to find NP signals, and using them, to identify the Lorentz structure of the NP. As the first step towards this goal, we calculate the constraints on the NP couplings, and, keeping the couplings within these bounds, we look for the observables where the NP signal can potentially stand out above the SM background.

It is crucial to understand this SM background, which makes it imperative to use observables whose values are predicted reasonably accurately within the SM. The main source of the SM uncertainties is the hadronic matrix elements, whose theoretical cal-

culations often have errors of the order of tens of percent. We have handled this on many levels. First, we have tried to identify observables that will not be very sensitive to the hadronic uncertainties. For example in $\bar{B}_d^0 \to \bar{K}\mu^+\mu^-$, the SM prediction for the forward-backward asymmetry is simply zero, independent of any hadronic elements. Also, while the differential branching ratios may be strongly dependent on the hadronic matrix elements, the forward-backward asymmetries are less so. Furthermore, the large-energy effective theory (LEET) limits can be used to control the uncertainties in the low-q^2 region for observables like A_{FB} and $A_T^{(2)}$. For example, certain observables, such as the zero-crossing of A_{FB} in $\bar{B}_d^0 \to \bar{K}^*\mu^+\mu^-$, can be shown to be robust under form-factor uncertainties in the LEET limit. The longitudinal-transverse asymmetry A_{LT} in $\bar{B}_d^0 \to \bar{K}^*\mu^+\mu^-$ also has a zero crossing in the SM with small hadronic uncertainties. These measurements can even be used to extract the parameters of the NP operators, to a very good approximation.

Also, we focus only on the situations where the NP contribution can be so significant that it will stand out even if the SM errors were magnified. Our figures show bands for SM predictions that include the form-factor uncertainties as quoted in the form-factor calculations, and these are overlaid with some examples of the allowed values of these observables when NP contributions are included. This allows the scaling of these uncertainties to be easily visualized. We identify and emphasize only those situations where the results with the NP can be significantly different from those without the NP, even if the hadronic uncertainties were actually much larger. Note that further inclusion of the NLO QCD corrections would affect the central values of the SM predictions to a small extent, while also decreasing the renormalization scale uncertainty. However, since our primary interest is looking for observables where the NP effects are large, a LO analysis is sufficient.

Our results are summarized in Table 4.1, for the cases where the NP has only one type of Lorentz structure: VA, SP or T. We note certain generic features of the influence of different NP Lorentz structures.

New VA operators are the ones that influence the observables strongly in most cases. They typically can interfere with the SM terms constructively or destructively, thus enhancing or suppressing the differential branching ratios by up to factors of 2 or 3. They also are able to enhance almost all the asymmetries, the notable exception being A_{FB} in $\bar{B}_d^0 \to \bar{K}\mu^+\mu^-$, where the VA operators cannot contribute. But for most other observables, this kind of NP can potentially be observed. This can be traced to the large magnitudes of the NP couplings still allowed by data, which in turn can be traced to the possibility of interference between the new VA operators with the SM operators that allows more freedom for the new VA couplings. Typically, the $R_{V,A}$ couplings are constrained more weakly than the $R'_{V,A}$ couplings, since the corresponding operators have the same structure as those of the SM, allowing strong destructive interferences. Consequently, the operators with $R_{V,A}$ couplings are more likely to show themselves over and above the SM background. We point out that the exception to this rule is

Observable	SM	Only new VA	Only new SP	Only new T
$B_s^0 \to \mu^+\mu^-$				
BR	$(3.35 \pm 0.32) \times 10^{-9}$	• Marginal E • Significant S	• Large E • Maximal S	No effect
$B_d^0 \to X_s\mu^+\mu^-$				
DBR		• E ($\times 2$) • S ($\div 2$)	• Marginal E	• E ($\times 2$)
A_{FB}	ZC$\approx$ 3.5 GeV^2	• E(30%) low q^2 • ZC shift / disappearence	• Marginal S	• Marginal S
f_L	• $0.9 \to 0.3$ (low$\to$high q^2)	• Large S at low q^2	• Marginal S	• Marginal E
$\bar{B}_s^0 \to \mu^+\mu^-\gamma$				
DBR		• E ($\times 2 - \times 3$) • S (low q^2)	No effect	• E ($\times 3$)
A_{FB}	ZC$\approx$ 4.3 GeV^2	• ZC shift / disappearence	No effect	• Large S
$B_d^0 \to K\mu^+\mu^-$				
DBR		• E ($\times 2$) • Marginal S	• E at high q^2	• Small effect
A_{FB}	Vanishes	• No effect	• E at low q^2 • No ZC	• E at high q^2 • No ZC
$B_d^0 \to K^*\mu^+\mu^-$				
DBR		• E ($\times 2$) • S ($\div 2$)	No effect	• E ($\times 2$)
A_{FB}	ZC$\approx$ 3.9 GeV^2	• E at low q^2 • ZC shift / disappearence	No effect	• Significant S • ZC shift
f_L	• $0.9 \to 0.3$ (low$\to$high q^2)	• Large S	No effect	• Significant S
$A_T^{(2)}$	• $\uparrow$ with q^2 • No ZC	• E ($\times 2$) • ZC possible	No effect	• Significant S
A_{LT}	• ZC at low q^2 • more -ve at large q^2	• Significant S • ZC shift / disappearence	No effect	• Significant S

Table 4.1: The effect of NP couplings on observables. E($\times n$): enhancement by up to a factor of n, S($\div n$): suppression by up to a factor of n, ZC: zero crossing.

the A_{FB} in $\bar{B}^0_d \to \bar{K}^* \mu^+ \mu^-$ at large q^2, where the $R'_{V,A}$ couplings can cause a larger enhancement.

The SP operators, on the other hand, are handicapped by the stringent constraints from the upper bound on $B(\bar{B}^0_s \to \mu^+ \mu^-)$. If only $R_{S,P}$ or $R'_{S,P}$ couplings are present, the constraints become even more severe. It is for this reason that, even when the SP contributions are unsuppressed by m_μ/m_b, they are not often large enough to stand apart from the SM background.

The couplings of the T operators, viz. C_T and C_{TE}, are not as suppressed as those of the SP operators. Therefore, they typically contribute significantly to the DBRs. However, the interference terms of these operators with the SM operators often suffer from the m_μ/m_b helicity suppression, and hence they tend to suppress the magnitudes of the asymmetries.

The combination of multiple Lorentz structures in general gives rise to the combination of features of the individual Lorentz structures involved. In particular, if the VA operators appear in conjunction with another Lorentz structure, the effects of the VA operators typically dominate. The T operators can interfere with the SP operators without the m_μ/m_b helicity suppression, but the strong constraints on the SP operators hold them back. A remarkable exception is the combination of SP and T operators in the forward-backward asymmetry in $\bar{B}^0_d \to \bar{K} \mu^+ \mu^-$. This asymmetry, which vanishes in the SM, can be enhanced to $\sim 5\%$ at low q^2 with only SP operators, and can be enhanced to $\sim 30\%$ with T operators but only at $q^2 \approx m_B^2$. However, the presence of both SP and T operators allows the asymmetry to be $\sim 40\%$ in the whole high-q^2 region. A similar feature, though to a less-spectacular extent, is observed in A_{FB} of $\bar{B}^0_d \to \bar{K}^* \mu^+ \mu^-$ [178].

With the large amount of data expected from the LHC experiments and B-factories in the coming years, we may be able to detect confirmed NP signals in the above processes. In that case, a combined analysis of all these decay modes, as carried out in this chapter, would enable us to identify the Lorentz structure of the NP operators. This will be important in establishing precisely what type of NP is present.

Appendix

I Details of the $\bar{B}^0_d \to X_s\mu^+\mu^-$ analysis

The differential branching ratio for $\bar{B}^0_d \to X_s\mu^+\mu^-$ in SM can be written as

$$\begin{aligned}\left(\frac{\mathrm{d}B}{\mathrm{d}z}\right)_{\rm SM} &= B_0\frac{8}{3}(1-z)^2\sqrt{1-\frac{4t^2}{z}}\times \\ &\left[(2z+1)\left(\frac{2t^2}{z}+1\right)|C_9^{\rm eff}|^2+\left(\frac{2(1-4z)t^2}{z}+(2z+1)\right)|C_{10}^{\rm eff}|^2\right. \\ &\left.+\,4\left(\frac{2}{z}+1\right)\left(\frac{2t^2}{z}+1\right)|C_7^{\rm eff}|^2+12\left(\frac{2t^2}{z}+1\right)\mathrm{Re}(C_7^{\rm eff}C_9^{\rm eff*})\right], \quad \text{(I.1)}\end{aligned}$$

Here $t \equiv m_\mu/m_b^{\rm pole}$ and $z \equiv q^2/(m_b^{\rm pole})^2$. The normalization constant B_0 is [144]

$$B_0 = \frac{3\alpha_{em}^2\, B(\bar{B}\to X_c e\bar{\nu})}{32\pi^2\, f(\hat{m}_c)\,\kappa(\hat{m}_c)}\frac{|V_{tb}V_{ts}^*|^2}{|V_{cb}|^2}\,, \quad \text{(I.2)}$$

where $\hat{m}_c \equiv m_c^{\rm pole}/m_b^{\rm pole}$. We use $\hat{m}_c = 0.29 \pm 0.02$ [148], $B(\bar{B}\to X_c e\bar{\nu}) = 0.1061 \pm 0.0017$ [193] and $|V_{tb}V_{ts}^*|/|V_{cb}| = 0.967 \pm 0.009$ [208]. Here $f(\hat{m}_c)$ is the lowest-order (i.e. parton-model) phase-space factor in $B(\bar{B}\to X_c e\bar{\nu})$:

$$f(\hat{m}_c) = 1 - 8\hat{m}_c^2 + 8\hat{m}_c^6 - \hat{m}_c^8 - 24\hat{m}_c^4\ln\hat{m}_c\,, \quad \text{(I.3)}$$

and the function $\kappa(\hat{m}_c)$ includes both the $O(\alpha_s)$ QCD corrections and the leading-order $(1/m_b^2)$ power correction to $B(\bar{B}\to X_c e\bar{\nu})$:

$$\kappa(\hat{m}_c) = 1 - \frac{2\alpha_s(m_b)}{3\pi}g(\hat{m}_c) + \frac{h(\hat{m}_c)}{2m_b^2}\,. \quad \text{(I.4)}$$

Here the two functions are [144]

$$\begin{aligned} g(\hat{m}_c) &= (\pi^2 - \frac{31}{4})(1-\hat{m}_c)^2 + \frac{3}{2}\,, \\ h(\hat{m}_c) &= \lambda_1 + \frac{\lambda_2}{f(\hat{m}_c)}\left[-9 + 24\hat{m}_c^2 - 72\hat{m}_c^4 + 72\hat{m}_c^6 - 15\hat{m}_c^8 - 72\hat{m}_c^4\ln\hat{m}_c\right]. \quad \text{(I.5)}\end{aligned}$$

After including all the NP interactions, and neglecting terms suppressed by m_μ/m_b and m_s/m_b, the total differential branching ratio $\mathrm{d}B/\mathrm{d}z$ can be written in the form

$$\left(\frac{\mathrm{d}B}{\mathrm{d}z}\right)_{\rm Total} = \left(\frac{\mathrm{d}B}{\mathrm{d}z}\right)_{\rm SM} + B_0\left[B_{SM\text{-}VA} + B_{VA} + B_{SP} + B_T\right], \quad \text{(I.6)}$$

where

$$
\begin{aligned}
B_{SM\text{-}VA} &= \frac{16}{3}(1-z)^2(1+2z)\left[\mathrm{Re}(C_9^{\mathrm{eff}}R_V^*)+\mathrm{Re}(C_{10}R_A^*)\right] \\
&\quad + 32\,(1-z)^2\,\mathrm{Re}(C_7^{\mathrm{eff}}R_V^*)\,, \qquad \text{(I.7)} \\
B_{VA} &= \frac{8}{3}(1-z)^2(1+2z)\Big[|R_V|^2+|R_A|^2+|R_V'|^2+|R_A'|^2\Big]\,, \qquad \text{(I.8)} \\
B_{SP} &= 4\,(1-z)^2\,z\Big[|R_S|^2+|R_P|^2+|R_S'|^2+|R_P'|^2\Big]\,, \qquad \text{(I.9)} \\
B_T &= \frac{128}{3}(1-z)^2(1+2z)\Big[|C_T|^2+4|C_{TE}|^2\Big]\,. \qquad \text{(I.10)}
\end{aligned}
$$

Note that here we have separated the contribution of the SM VA operators (subscript $SM\text{-}VA$) from that of the NP VA operators (subscript VA), for clarity.

The forward-backward asymmetry in $\bar{B}_d^0 \to X_s\mu^+\mu^-$ is

$$
A_{FB}(q^2) = \frac{\int_0^1 d\cos\theta_\mu \frac{d^2B}{dq^2 d\cos\theta_\mu} - \int_{-1}^0 d\cos\theta_\mu \frac{d^2B}{dq^2 d\cos\theta_\mu}}{\int_0^1 d\cos\theta_\mu \frac{d^2B}{dq^2 d\cos\theta_\mu} + \int_{-1}^0 d\cos\theta_\mu \frac{d^2B}{dq^2 d\cos\theta_\mu}}\,, \qquad \text{(I.11)}
$$

where θ_μ is the angle between the μ^+ and the $\bar{B}^0$ in the dimuon center-of-mass frame. We can write A_{FB} in the form

$$
A_{FB}(q^2) = \frac{N(z)}{\mathrm{d}B/\mathrm{d}z}\,, \qquad \text{(I.12)}
$$

where the numerator is given by

$$
N(z) = B_0\Big[N_{SM} + N_{SM\text{-}VA} + N_{VA} + N_{SP\text{-}T}\Big]\,, \qquad \text{(I.13)}
$$

with

$$
\begin{aligned}
N_{SM} &= -8\,C_{10}\,(1-z)^2\Big[2C_7^{\mathrm{eff}} + z\,\mathrm{Re}(C_9^{\mathrm{eff}})\Big]\,, \qquad \text{(I.14)} \\
N_{SM\text{-}VA} &= -8\,(1-z)^2\Big[z\,\mathrm{Re}\Big(C_{10}R_V^* + C_9^{\mathrm{eff}}R_A^*\Big) + 2C_7^{\mathrm{eff}}\mathrm{Re}(R_A^*)\Big]\,, \qquad \text{(I.15)} \\
N_{VA} &= -8\,z\,(1-z)^2\Big[\mathrm{Re}(R_V R_A^*) - \mathrm{Re}(R_V' R_A'^*)\Big]\,, \qquad \text{(I.16)} \\
N_{SP\text{-}T} &= -8\,z\,(1-z)^2\Big[\mathrm{Re}\Big\{(R_S+R_P)\,(C_T^* - 2C_{TE}^*)\Big\} \\
&\quad + \mathrm{Re}\Big\{(R_S'-R_P')\,(C_T^* + 2C_{TE}^*)\Big\}\Big]\,. \qquad \text{(I.17)}
\end{aligned}
$$

The expressions of Eqs. (I.7)-(I.17) are in agreement with Ref. [146].

The polarization fractions f_L and f_T are defined as

$$f_L = \frac{H_L(z)}{H_L(z) + H_T(z)} \ , \qquad\qquad f_T = \frac{H_T(z)}{H_L(z) + H_T(z)} \ , \tag{I.18}$$

where

$$H_L(z) = H_L^{SM}(z) + H_L^{SM-VA}(z) + H_L^{VA}(z) + H_L^{SP}(z) + H_L^{T}(z) \ , \tag{I.19}$$

$$H_T(z) = H_T^{SM}(z) + H_T^{SM-VA}(z) + H_T^{VA}(z) + H_T^{SP}(z) + H_T^{T}(z) \ . \tag{I.20}$$

The components of H_L and H_T functions are

$$H_L^{SM}(z) = \frac{8\,B_0'}{3}(1-z)^2\Big[\left|C_9^{\rm eff} + 2C_7^{\rm eff}\right|^2 + |C_{10}|^2\Big] \ , \tag{I.21}$$

$$H_T^{SM}(z) = \frac{16\,B_0'}{3}z(1-z)^2\Big[\left|C_9^{\rm eff} + \frac{2}{z}C_7^{\rm eff}\right|^2 + |C_{10}|^2\Big] \ , \tag{I.22}$$

$$H_L^{SM\text{-}VA}(z) = \frac{16\,B_0'}{3}(1-z)^2\Big[{\rm Re}\left(C_9^{\rm eff}\,R_V^* + C_{10}R_A^*\right) + 2{\rm Re}(C_7^{\rm eff}\,R_V^*)\Big] \ , \tag{I.23}$$

$$H_T^{SM\text{-}VA}(z) = \frac{32\,B_0'}{3}(1-z)^2\Big[z{\rm Re}\left(C_9^{\rm eff}\,R_V^* + C_{10}R_A^*\right) + 2{\rm Re}(C_7^{\rm eff}\,R_V^*)\Big], \tag{I.24}$$

$$H_L^{VA}(z) = \frac{8\,B_0'}{3}(1-z)^2\Big[|R_V|^2 + |R_A|^2 + |R_V'|^2 + |R_A'|^2\Big] \ , \tag{I.25}$$

$$H_T^{VA}(z) = \frac{16\,B_0'}{3}z(1-z)^2\Big[|R_V|^2 + |R_A|^2 + |R_V'|^2 + |R_A'|^2\Big] \ , \tag{I.26}$$

$$H_L^{SP}(z) = \frac{4\,B_0'}{3}z(1-z)^2\Big[|R_S|^2 + |R_P|^2 + |R_S'|^2 + |R_P'|^2\Big] \ , \tag{I.27}$$

$$H_T^{SP}(z) = \frac{8\,B_0'}{3}z(1-z)^2\Big[|R_S|^2 + |R_P|^2 + |R_S'|^2 + |R_P'|^2\Big] \ , \tag{I.28}$$

$$H_L^{T}(z) = \frac{64\,B_0'}{3}(2-z)(1-z)^2\Big[|C_T|^2 + 4|C_{TE}|^2\Big] \ , \tag{I.29}$$

$$H_T^{T}(z) = \frac{128\,B_0'}{3}z(1-z)^2\Big[|C_T|^2 + 4|C_{TE}|^2\Big] \ . \tag{I.30}$$

II Details of the $\bar{B}_s^0 \to \mu^+\mu^-\gamma$ analysis

The transition amplitude for $\bar{B}_s^0 \to \mu^+\mu^-\gamma$ is

$$
\begin{aligned}
i\mathcal{M}(\bar{B}_s^0 \to \mu^+\mu^-\gamma) = (-i)\frac{1}{2}\Bigg[-\frac{4G_F}{\sqrt{2}}\frac{\alpha_{em}}{4\pi}(V_{ts}^* V_{tb})\Bigg] \times \\
\Bigg\{ \quad \langle\gamma(k)|\bar{s}\gamma_\mu b|\bar{B}_s^0(p_B)\rangle \left[(C_9^{\rm eff} + R_V + R_V')L^\mu + (C_{10} + R_A + R_A')L^{\mu 5}\right] \\
+ \left\langle\gamma(k)|\bar{s}\gamma_\mu\gamma_5 b|\bar{B}_s^0(p_B)\right\rangle \left[-(C_9^{\rm eff} + R_V - R_V')L^\mu - (C_{10} + R_A - R_A')L^{\mu 5}\right] \\
+ \left\langle\gamma(k)|\bar{s}i\sigma_{\mu\nu}q^\nu b|\bar{B}_s^0(p_B)\right\rangle \left[-2m_b\frac{C_7^{\rm eff}}{q^2}L^\mu\right] \\
+ \left\langle\gamma(k)|\bar{s}i\sigma_{\mu\nu}\gamma_5 q^\nu b|\bar{B}_s^0(p_B)\right\rangle \left[-2m_b\frac{C_7^{\rm eff}}{q^2}L^\mu\right] \\
+ \left\langle\gamma(k)|\bar{s}\sigma_{\mu\nu} b|\bar{B}_s^0(p_B)\right\rangle \left[2C_T L^{\mu\nu} + 2iC_{TE}\epsilon^{\mu\nu\alpha\beta}L_{\alpha\beta}\right] \Bigg\} ,
\end{aligned}
\tag{II.31}
$$

where the L's are defined in Eq. (4.8).

In order to calculate the DBR, one needs the $\bar{B}_s^0 \to \gamma$ matrix elements and form factors. The matrix elements are given in Ref. [156][5]:

$$
\begin{aligned}
\left\langle\gamma(k)|\bar{s}\gamma_\mu b|\bar{B}_s^0(p_B)\right\rangle &= -e\,\epsilon_{\mu\nu\rho\sigma}\varepsilon^{*\nu}q^\rho k^\sigma\frac{f_V(q^2)}{m_{B_s}} , \\
\left\langle\gamma(k)|\bar{s}\gamma_\mu\gamma_5 b|\bar{B}_s^0(p_B)\right\rangle &= ie\left[\varepsilon_\mu^* k\cdot q - \varepsilon^*\cdot q k_\mu\right]\frac{f_A(q^2)}{m_{B_s}} , \\
\left\langle\gamma(k)|\bar{s}i\sigma_{\mu\nu}q^\nu b|\bar{B}_s^0(p_B)\right\rangle &= e\,\epsilon_{\mu\nu\rho\sigma}\varepsilon^{*\nu}q^\rho k^\sigma f_{TV}(q^2) , \\
\left\langle\gamma(k)|\bar{s}i\sigma_{\mu\nu}\gamma_5 q^\nu b|\bar{B}_s^0(p_B)\right\rangle &= ie\left[\varepsilon_\mu^* k\cdot q - \varepsilon^*\cdot q k_\mu\right] f_{TA}(q^2) ,
\end{aligned}
$$

$$
\begin{aligned}
\left\langle\gamma(k)|\bar{s}\sigma_{\mu\nu} b|\bar{B}_s^0(p_B)\right\rangle &= -ie\,\epsilon_{\mu\nu\rho\sigma}\Bigg[\frac{\{f_{TV}(q^2) - f_{TA}(q^2)\}}{q^2}\Big\{(q\cdot k)\,\varepsilon^{*\rho}\,q^\sigma + (\varepsilon^*\cdot q)\,q^\rho\,k^\sigma\Big\} \\
&- f_{TV}(q^2)\,\varepsilon^{*\rho}\,k^\sigma\Bigg] .
\end{aligned}
\tag{II.32}
$$

Here ε_μ is the four-vector polarization of the photon and $q = p_B - k$. For the $\bar{B}_s^0 \to \mu^+\mu^-\gamma$ form factors f_i $(i = V, A, TA, TV)$, we use the parameterization [156]

$$
f_i(q^2) = \beta_i\frac{f_{B_s}m_{B_s}}{\Delta_i + 0.5m_{B_s}\left(1 - q^2/m_{B_s}^2\right)} , \tag{II.33}
$$

[5] We use the convention $\epsilon^{0123} = +1$.

where the parameters β_i and Δ_i are given in Table II. These values of parameters ensure that the large energy effective theory (LEET) relations between form factors are satisfied to a 10% accuracy [156]. In our numerical analysis we take the errors in these form factors to be $\pm 10\%$.

Parameter	f_V	f_{TV}	f_A	f_{TA}
$\beta(\mathrm{GeV}^{-1})$	0.28	0.30	0.26	0.33
$\Delta(\mathrm{GeV})$	0.04	0.04	0.30	0.30

Table 2: The parameters for $\bar{B}_s^0 \to \gamma$ form factors, as defined in Eq. (II.33).

In terms of the dimensionless parameter $x_\gamma = 2E_\gamma/m_{B_s}$, where E_γ is the photon energy in the $\bar{B}_s^0$ rest frame, one can calculate the double differential decay rate to be

$$\frac{\mathrm{d}^2\Gamma}{\mathrm{d}x_\gamma \mathrm{d}(\cos\theta_\mu)} = \frac{1}{2m_{B_s}} \frac{2v\, m_{B_s}^2 x_\gamma}{(8\pi)^3} \mathcal{M}^\dagger \mathcal{M} \,, \tag{II.34}$$

where $v \equiv \sqrt{1 - 4m_\mu^2/[m_{B_s}^2(1-x_\gamma)]}$. From Eq. (II.34) we get the DBR to be

$$\begin{aligned} \frac{\mathrm{d}B}{\mathrm{d}x_\gamma} &= \tau_{B_s} \int_{-1}^{1} \frac{\mathrm{d}^2\Gamma}{\mathrm{d}x_\gamma \mathrm{d}(\cos\theta_\mu)} \,\mathrm{d}\cos\theta_\mu \\ &= \tau_{B_s} \left[\frac{1}{2m_{B_s}} \frac{2vm_{B_s}^2}{(8\pi)^3}\right] \left[\frac{1}{4}\, \frac{16G_F^2}{2}\, \frac{\alpha_{em}^2}{16\pi^2} |V_{tb}V_{ts}^*|^2 e^2\right] \Theta \,. \end{aligned} \tag{II.35}$$

Here the quantity Θ has the form

$$\Theta = \frac{2}{3}\, m_{B_s}^4\, x_\gamma^3 \Big[X_{VA} + X_T + X_{VA\text{-}T}\Big] \,, \tag{II.36}$$

where the X terms are

$$\begin{aligned} X_{VA} &= \Big(|A|^2 + |B|^2\Big) m_{B_s}^2 \left(3 - v^2\right)(1 - x_\gamma) + \Big(|C|^2 + |D|^2\Big) 2m_{B_s}^2 v^2 (1 - x_\gamma) \,, \\ X_T &= 4|E|^2(3 - v^2) + 4|F|^2 m_{B_s}^4 v^2 (1 - x_\gamma)^2 \\ &\quad + 16|G|^2 \left(3 - v^2\right) + 16|H|^2 m_{B_s}^4 \left(3 - 2v^2\right)(1 - x_\gamma)^2 \\ &\quad + 8m_{B_s}^2 v^2 (1 - x_\gamma) \mathrm{Re}\left(E^* F\right) + 32 m_{B_s}^2 (3 - 2v^2)(1 - x_\gamma) \mathrm{Re}\left(G^* H\right) \,, \\ X_{VA\text{-}T} &= -24 m_\mu \mathrm{Re}\left(A^* E\right) - 48 m_\mu \mathrm{Re}\left(B^* G\right) - 48 m_\mu m_{B_s}^2 (1 - x_\gamma) \mathrm{Re}\left(B^* H\right) \end{aligned} \tag{II.37}$$

Note that here, the VA subscript includes the SM operators. The parameters A–H are combinations of the Wilson coefficients, form factors and NP parameters, and are

given by

$$\begin{aligned}
A &= (C_9^{\rm eff} + R_V + R'_V)\,\frac{f_V(q^2)}{m_{B_s}} + \frac{2\,m_b C_7^{\rm eff}}{q^2}\,f_{TV}(q^2)\,,\\
B &= (C_9^{\rm eff} + R_V - R'_V)\,\frac{f_A(q^2)}{m_{B_s}} + \frac{2\,m_b C_7^{\rm eff}}{q^2}\,f_{TA}(q^2)\,,\\
C &= (C_{10}^{\rm eff} + R_A + R'_A)\,\frac{f_V(q^2)}{m_{B_s}}\,,\\
D &= (C_{10}^{\rm eff} + R_A - R'_A)\,\frac{f_A(q^2)}{m_{B_s}}\,,\\
E &= -2C_T f_{TV}(q^2)\,,\\
F &= 2C_T\frac{f_{TV}(q^2) - f_{TA}(q^2)}{q^2}\,,\\
G &= -2C_{TE} f_{TV}(q^2)\,,\\
H &= 2C_{TE}\frac{f_{TV}(q^2) - f_{TA}(q^2)}{q^2}\quad .
\end{aligned} \tag{II.38}$$

The normalized forward-backward asymmetry of muons in $\bar{B}_s^0 \to \mu^+\mu^-\gamma$ is defined as

$$A_{FB}(q^2) = \frac{\displaystyle\int_0^1 d\cos\theta_\mu \frac{d^2B}{dq^2 d\cos\theta_\mu} - \int_{-1}^0 d\cos\theta_\mu \frac{d^2B}{dq^2 d\cos\theta_\mu}}{\displaystyle\int_0^1 d\cos\theta_\mu \frac{d^2B}{dq^2 d\cos\theta_\mu} + \int_{-1}^0 d\cos\theta_\mu \frac{d^2B}{dq^2 d\cos\theta_\mu}}\,, \tag{II.39}$$

where θ_μ is the angle between the three-momentum vectors of the $\bar{B}_s^0$ and the μ^+ in the dimuon center-of-mass frame. The calculation of A_{FB} gives

$$A_{FB}(q^2) = \frac{1}{\Theta}\left(2m_{B_s}^4 v\; x_\gamma^3\right)\left[Y_{VA} + Y_{VA\text{-}T}\right]\,, \tag{II.40}$$

with the Y terms given by

$$\begin{aligned}
Y_{VA} &= \Big(\mathrm{Re}\,(A^*D) + \mathrm{Re}\,(B^*C)\Big)m_{B_s}^2(1-x_\gamma)\,,\\
Y_{VA\text{-}T} &= -4m_\mu\left(2\mathrm{Re}\,(C^*G) + 2m_{B_s}^2(1-x_\gamma)\mathrm{Re}\,(C^*H) + \mathrm{Re}\,(D^*E)\right)\,.
\end{aligned} \tag{II.41}$$

III Details of the $\bar{B}^0_d \to \bar{K}\mu^+\mu^-$ analysis

The transition matrix element for $\bar{B}^0_d \to \bar{K}\mu^+\mu^-$ is given by

$$
\begin{aligned}
i\mathcal{M}\,(\bar{B}^0_d \to \bar{K}\mu^+\mu^-) = (-i)\,\frac{1}{2}\,\left[-\frac{4\,G_F}{\sqrt{2}}\frac{\alpha_{em}}{4\pi}(V^*_{ts}V_{tb})\right]\times \\
\Bigg\{\;\langle K(p_2)\,|\bar{s}\gamma_\mu b|\,B(p_1)\rangle\,[(C_9^{\rm eff}+R_V+R'_V)L^\mu+(C_{10}+R_A+R'_A)L^{\mu 5}] \\
+\langle K(p_2)\,|\bar{s}b|\,B(p_1)\rangle\,[(R_S+R'_S)L+(R_P+R'_P)L^5] \\
+\langle K(p_2)\,|\bar{s}i\sigma_{\mu\nu}q^\nu b|\,B(p_1)\rangle\,[-2C_7^{\rm eff}(m_b/q^2)L^\mu] \\
+\langle K(p_2)\,|\bar{s}\sigma_{\mu\nu}b|\,B(p_1)\rangle\;\,[2C_T L^{\mu\nu}+2iC_{TE}\epsilon^{\mu\nu\alpha\beta}L_{\alpha\beta}]\;\Bigg\}\,,
\end{aligned}
\tag{III.42}
$$

where the L's are defined in Eq. (4.8).

The $\bar{B}^0_d \to \bar{K}$ matrix elements needed to calculate the decay rate and asymmetry in $\bar{B}^0_d \to \bar{K}\mu^+\mu^-$ are [161]

$$
\begin{aligned}
\left\langle \bar{K}(p_2)\,|\bar{s}\gamma_\mu b|\,\bar{B}^0_d(p_1)\right\rangle &= (2p_1-q)_\mu f_+(z)+(\frac{1-k^2}{z})\,q_\mu[f_0(z)-f_+(z)]\,, \\
\left\langle \bar{K}(p_2)\,|\bar{s}i\sigma_{\mu\nu}q^\nu b|\,\bar{B}^0_d(p_1)\right\rangle &= -\Big[(2p_1-q)_\mu q^2-(m_B^2-m_K^2)q_\mu\Big]\,\frac{f_T(z)}{m_B+m_K}\,, \\
\left\langle \bar{K}(p_2)\,|\bar{s}b|\,\bar{B}^0_d(p_1)\right\rangle &= \frac{m_B(1-k^2)}{\hat{m}_b}f_0(z)\,, \\
\left\langle \bar{K}(p_2)\,|\bar{s}\sigma_{\mu\nu}b|\,\bar{B}^0_d(p_1)\right\rangle &= i\Big[(2p_1-q)_\mu q_\nu-(2p_1-q)_\nu q_\mu\Big]\,\frac{f_T(z)}{m_B+m_K}\,,
\end{aligned}
\tag{III.43}
$$

where $k \equiv m_K/m_B$, $\hat{m}_b \equiv m_b/m_B$, $q_\mu = (p_1-p_2)_\mu = (p_+ + p_-)_\mu$, and $z \equiv q^2/m_B^2$. The form factors $f_{+,0,T}$ were calculated in the framework of QCD light-cone sum rules in Ref. [161]. The z dependence of these is parametrized by

$$
f(z) = f(0)\,\exp(c_1 z + c_2 z^2 + c_3 z^3)\,,
\tag{III.44}
$$

where the parameters $f(0), c_1$, c_2 and c_3 for each form factor are taken from Tables III, IV and V of Ref. [161]. Using these, the differential branching ratio is given by

$$
\frac{dB}{dz} = B'_0\,\phi^{1/2}\,\beta_\mu\left[X'_{VA}+X'_{SP}+X'_T+X'_{VA\text{-}SP}+X'_{VA\text{-}T}\right]\,,
\tag{III.45}
$$

where B'_0 is the normalization factor:

$$
B'_0 = \frac{G_F^2\alpha^2\tau_B}{2^{12}\pi^5}|V_{tb}V^*_{ts}|^2 m_B^5\,,
\tag{III.46}
$$

the phase factor ϕ is

$$\phi \equiv 1 + k^4 + z^2 - 2(k^2 + k^2 z + z) \,, \tag{III.47}$$

and the X' terms are given by

$$\begin{aligned}
X'_{VA} &= \phi \left(1 - \frac{1}{3}\beta_\mu^2\right) (|A'|^2 + |B'|^2) \,+\, 4\,\hat{m}_\mu^2\,|B'|^2\,(2 + 2k^2 - z) \\
&\quad + 4\,\hat{m}_\mu^2\,z\,|C'|^2 \,+\, 8\,\hat{m}_\mu^2\,(1 - k^2)\,\mathrm{Re}(B'C'^*) \,, \\
X'_{SP} &= \frac{z}{m_B^2}\,(|E'|^2 + \beta_\mu^2\,|D'|^2) \,, \\
X'_{T} &= \frac{4}{3}\,\phi\,z\,m_B^2\left[3|F'|^2 \,+\, 2\,\beta_\mu^2\,(2|G'|^2 - |F'|^2)\right] \,, \\
X'_{VA\text{-}SP} &= \frac{4\hat{m}_\mu}{m_B}\,(1 - k^2)\,\mathrm{Re}(B'E'^*) + \frac{4\hat{m}_\mu}{m_B}\,z\,\mathrm{Re}(C'E'^*) \,, \\
X'_{VA\text{-}T} &= 8\hat{m}_\mu\,m_B\phi\,\mathrm{Re}(A'F'^*) \,.
\end{aligned} \tag{III.48}$$

Here $\hat{m}_\mu \equiv m_\mu/m_B$ and $\beta_\mu \equiv \sqrt{1 - 4\hat{m}_\mu^2/z}$. The parameters A'–G' are combinations of the Wilson coefficients, form factors and NP parameters, and are given by

$$\begin{aligned}
A' &\equiv 2(C_9^{eff} + R_V + R'_V)\,f_+(z) + 4C_7^{eff}\hat{m}_b\frac{f_T(z)}{1+k} \,, \\
B' &\equiv 2(C_{10} + R_A + R'_A)\,f_+(z) \,, \\
C' &\equiv 2(C_{10} + R_A + R'_A)\,\frac{1 - k^2}{z}\Big[f_0(z) - f_+(z)\Big] \,, \\
D' &\equiv 2(R_S + R'_S)\frac{m_B(1 - k^2)}{\hat{m}_b} f_0(z) \,, \\
E' &\equiv 2(R_P + R'_P)\frac{m_B(1 - k^2)}{\hat{m}_b} f_0(z) \,, \\
F' &\equiv 4C_T\frac{f_T(z)}{m_B(1+k)} \,, \\
G' &\equiv -4C_{TE}\frac{f_T(z)}{m_B(1+k)} \,.
\end{aligned} \tag{III.49}$$

The limits on the kinematical variables z and $\cos\theta_\mu$ are

$$-1 \le \cos\theta_\mu \le 1 \quad , \qquad 4\hat{m}_\mu^2 \le z \le (1 - k)^2 \,. \tag{III.50}$$

Note that in the large energy (LEET) limit, there are relations between form factors that are valid up to α_s, $1/E_K$ and $1/m_b$ corrections [166, 167]. These are

$$\begin{aligned}
f_+(z) &= \zeta(m_B, E_P), \\
f_0(z) &= \Big(1 - \frac{q^2}{m_B^2 - m_P^2}\Big)\zeta(m_B, E_P), \\
f_T(z) &= \Big(1 + \frac{m_P}{m_B}\Big)\zeta(m_B, E_P) \,.
\end{aligned} \tag{III.51}$$

Thus, all form factors can be expressed in terms of a single universal soft form factor $\zeta(m_B, E_P)$ in this limit.

The normalized forward-backward asymmetry for the muons in $\bar{B}^0_d \to \bar{K}\mu^+\mu^-$ is defined as

$$A_{FB}(q^2) = \frac{\displaystyle\int_0^1 d\cos\theta_\mu \frac{d^2B}{dq^2 d\cos\theta_\mu} - \int_{-1}^0 d\cos\theta_\mu \frac{d^2B}{dq^2 d\cos\theta_\mu}}{\displaystyle\int_0^1 d\cos\theta_\mu \frac{d^2B}{dq^2 d\cos\theta_\mu} + \int_{-1}^0 d\cos\theta_\mu \frac{d^2B}{dq^2 d\cos\theta_\mu}} \,, \tag{III.52}$$

where θ_μ is the angle between the three-momenta of the $\bar{B}^0_d$ and the μ^+ in the dimuon center-of-mass frame. The calculation of $A_{FB}(q^2)$ gives

$$A_{FB}(q^2) = \frac{2B'_0\,\beta_\mu\,\phi}{dB/dz}\left[Y'_{VA\text{-}SP} + Y'_{VA\text{-}T} + Y'_{SP\text{-}T}\right] \tag{III.53}$$

where

$$\begin{aligned} Y'_{VA\text{-}SP} &= -\frac{\hat{m}_\mu}{m_B}\mathrm{Re}(A'D'^*) \\ Y'_{VA\text{-}T} &= -4m_\mu(1-k^2)\mathrm{Re}(B'G'^*) - 4zm_\mu\mathrm{Re}(C'G'^*) \\ Y'_{SP\text{-}T} &= -\frac{z}{4}\mathrm{Re}(D'F'^*) - 2z\mathrm{Re}(E'G'^*)\,. \end{aligned} \tag{III.54}$$

Note that only $Y'_{SP\text{-}T}$ term is unsuppressed by the muon mass.

IV Details of the $\bar{B}^0_d \to \bar{K}^*\mu^+\mu^-$ angular analysis

IV.a Matrix elements

The full transition amplitude for $\bar{B}(p_B) \to \bar{K}^*(p_{K^*}, \epsilon^*)\mu^+(p_\mu^+)\mu^-(p_\mu^-)$ is

$$\begin{aligned} i\mathcal{M}\,(\bar{B}^0_d \to \bar{K}^*\mu^+\mu^-) = (-i)\,\frac{1}{2}\left[-\frac{4\,G_F}{\sqrt{2}}\frac{\alpha_{em}}{4\pi}(V^*_{ts}V_{tb})\right]\times \\ \Bigg\{ \quad \langle K^*(p_{K^*},\epsilon)|\bar{s}\gamma_\mu b|B(p_B)\rangle\,[(C_9^{\rm eff} + R_V + R'_V)L^\mu + (C_{10} + R_A + R'_A)L^{\mu 5}] \\ + \quad \langle K^*(p_{K^*},\epsilon)|\bar{s}\gamma_\mu\gamma_5 b|B(p_B)\rangle[-(C_9^{\rm eff} + R_V - R'_V)L^\mu - (C_{10} + R_A - R'_A)L^{\mu 5}] \\ + \quad \langle K^*(p_{K^*},\epsilon)|\bar{s}i\sigma_{\mu\nu}q^\nu(1+\gamma_5)b|B(p_B)\rangle\,[-2C_7^{\rm eff}(m_b/q^2)L^\mu] \\ + \quad \langle K^*(p_{K^*},\epsilon)|\bar{s}b|B(p_B)\rangle\,[(R_S + R'_S)L + (R_P + R'_P)L^5] \\ + \quad \langle K^*(p_{K^*},\epsilon)|\bar{s}\gamma_5 b|B(p_B)\rangle\,[(R_S - R'_S)L + (R_P - R'_P)L^5] \\ + \quad \langle K^*(p_{K^*},\epsilon)|\bar{s}\sigma_{\mu\nu}b|B(p_B)\rangle\,[2C_T L^{\mu\nu} + 2iC_{TE}\epsilon^{\mu\nu\alpha\beta}L_{\alpha\beta}] \Bigg\}\,, \end{aligned} \tag{IV.55}$$

where the L's are defined in Eq. (4.8). Here $q = p_B - p_{K^*} = p_\mu^+ + p_\mu^-$. This can be written in the form

$$\begin{aligned} i\mathcal{M}(\bar{B}_d^0 \to \bar{K}^* \mu^+ \mu^-) &= (-i)\frac{1}{2}\left[\frac{4\,G_F}{\sqrt{2}}\frac{\alpha_{em}}{4\pi}(V_{ts}^* V_{tb})\right] \times \\ & [M_{V\mu} L^\mu + M_{A\mu} L^{\mu 5} + M_S L + M_P L^5 + M_{T\mu\nu} L^{\mu\nu} + i M_{E\mu\nu} L_{\alpha\beta} \epsilon^{\mu\nu\alpha\beta}] \\ & , \end{aligned} \tag{IV.56}$$

with

$$\begin{aligned} M_{V\mu} &= -A'' \epsilon_{\mu\nu\alpha\beta} \varepsilon^{*\nu} p_{K^*}^\alpha q^\beta + i B'' \varepsilon_\mu^* + i C'' \varepsilon^*.q (p_B + p_{K^*})_\mu + i D'' \varepsilon^*.q q_\mu, \\ M_{A\mu} &= -E'' \epsilon_{\mu\nu\alpha\beta} \varepsilon^{*\nu} p_{K^*}^\alpha q^\beta + i F'' \varepsilon_\mu^* + i G'' \varepsilon^*.q (p_B + p_{K^*})_\mu + i H'' \varepsilon^*.q q_\mu, \\ M_S &= i S'' \varepsilon^*.q, \\ M_P &= i P'' \varepsilon^*.q, \\ M_{T\mu\nu} &= C_T (i T_1'' \epsilon_{\mu\nu\alpha\beta} \varepsilon^{*\alpha} (p_B + p_{K^*})^\beta + i T_2'' \epsilon_{\mu\nu\alpha\beta} \varepsilon^{*\alpha} q^\beta - i T_3'' \epsilon_{\mu\nu\alpha\beta} \varepsilon^*.q p_{K^*}^\alpha q^\beta), \\ M_{E\mu\nu} &= C_{TE} (i T_1'' \epsilon_{\mu\nu\alpha\beta} \varepsilon^{*\alpha} (p_B + p_{K^*})^\beta + i T_2'' \epsilon_{\mu\nu\alpha\beta} \varepsilon^{*\alpha} q^\beta - i T_3'' \epsilon_{\mu\nu\alpha\beta} \varepsilon^*.q p_{K^*}^\alpha q^\beta)\ . \end{aligned} \tag{IV.57}$$

The quantities A'', B'', C'', D'',E'', F'', G'', S'', P'', and T_i'' (1=1,2,3) are related to the $\bar{B} \to \bar{K}^*$ form factors which are given below. The contribution to the transition amplitudes from the quantity $D''(q^2)$ vanishes and that from $H''(q^2)$ is suppressed because of the equation of motion of the muons.

IV.b Form factors

The form factors for the decay amplitude for $\bar{B}_d^0 \to \bar{K}^* \mu^+ \mu^-$ [Eq. (IV.55)] in terms of matrix elements of the quark operators are given by [161]

$$\begin{aligned} \langle K^*(p_{K^*}, \epsilon) | \bar{s} \gamma_\mu (1 \pm \gamma_5) b | B(p_B) \rangle &= \mp\, i q_\mu \frac{2 m_{K^*}}{q^2}\, \epsilon^* \cdot q \left[A_3(q^2) - A_0(q^2)\right] \\ & \pm\, i \epsilon_\mu^* (m_B + m_{K^*}) A_1(q^2) \mp\ i (p_B + p_{K^*})_\mu\, \epsilon^* \cdot q\, \frac{A_2(q^2)}{(m_B + m_{K^*})} \\ & -\, \epsilon_{\mu\nu\lambda\sigma} \epsilon^{*\nu} p_{K^*}^\lambda q^\sigma \frac{2 V(q^2)}{(m_B + m_{K^*})}\ , \end{aligned} \tag{IV.58}$$

where

$$A_3(q^2) = \frac{m_B + m_{K^*}}{2 m_{K^*}} A_1(q^2) - \frac{m_B - m_{K^*}}{2 m_{K^*}} A_2(q^2)\ . \tag{IV.59}$$

$$\langle K^*(p_{K^*},\epsilon)|\bar{s}\sigma_{\mu\nu}b|B(p_B)\rangle = i\epsilon_{\mu\nu\lambda\sigma}\Bigg\{ -T_1(q^2)\epsilon^{*\lambda}(p_B+p_{K^*})^\sigma + \frac{(m_B^2-m_{K^*}^2)}{q^2}\Bigg(T_1(q^2)-T_2(q^2)\Bigg)\epsilon^{*\lambda}q^\sigma - \frac{2}{q^2}\Bigg(T_1(q^2)-T_2(q^2)-\frac{q^2}{(m_B^2-m_{K^*}^2)}\,T_3(q^2)\Bigg)\epsilon^*\cdot q\, p_{K^*}^\lambda q^\sigma\Bigg\}\,. \quad \text{(IV.60)}$$

$$\langle K^*(p_{K^*},\epsilon)|\bar{s}i\sigma_{\mu\nu}q^\nu(1\pm\gamma_5)b|B(p_B)\rangle = 2\epsilon_{\mu\nu\lambda\sigma}\epsilon^{*\nu}p_{K^*}^\lambda q^\sigma\; T_1(q^2) \pm i\Bigg\{\epsilon_{*\mu}(m_B^2-m_{K^*}^2)-(p_B+p_{K^*})_\mu\,\epsilon^*\cdot q\Bigg\}\,T_2(q^2) \pm i\,\epsilon^*\cdot q\left\{q_\mu-\frac{(p_B+p_{K^*})_\mu q^2}{(m_B^2-m_{K^*}^2)}\right\}\,T_3(q^2)\,. \quad \text{(IV.61)}$$

$$\langle K^*(p_{K^*},\epsilon)|\bar{s}(1\pm\gamma_5)b|B(p_B)\rangle = \mp\, 2i\frac{m_{K^*}}{m_b}\,\epsilon^*\cdot q\,A_0(q^2)\,. \quad \text{(IV.62)}$$

Here we have neglected the strange-quark mass. The matrix elements are functions of 7 unknown form factors: $A_{0,1,2}(q^2)$, $V(q^2)$, $T_{1,2,3}(q^2)$.

The matrix elements $M_{V,A,S,P,T,E}$ appearing in Eq. (IV.57) can be written in terms

of these 7 form factors, coupling constants and kinematic variables as

$$
\begin{aligned}
A'' &= \Big[\frac{2V(q^2)(C_9^{eff}+R_V+R'_V)}{m_B+m_{K^*}}+\frac{4m_b}{q^2}C_7^{eff}T_1(q^2)\Big],\\
B'' &= -\Big[(m_B+m_{K^*})A_1(q^2)(C_9^{eff}+R_V-R'_V)+\frac{2m_b}{q^2}C_7^{eff}T_2(q^2)(m_B^2-m_{K^*}^2)\Big],\\
C'' &= \Big[\frac{A_2(q^2)}{m_B+m_{K^*}}(C_9^{eff}+R_V-R'_V)+\frac{2m_b}{q^2}C_7^{eff}\Big(T_2(q^2)+\frac{q^2T_3(q^2)}{(m_B^2-m_{K^*}^2)}\Big)\Big],\\
D'' &= \Big[\frac{2m_{K^*}}{q^2}(C_9^{eff}+R_V-R'_V)(A_3(q^2)-A_0(q^2))-\frac{2m_b}{q^2}C_7^{eff}T_3(q^2)\Big],\\
E'' &= \Big[\frac{2V(q^2)(C_{10}+R_A+R'_A)}{m_B+m_{K^*}}\Big],\\
F'' &= -\Big[(m_B+m_{K^*})A_1(q^2)(C_{10}+R_A-R'_A)\Big],\\
G'' &= \Big[\frac{A_2(q^2)}{m_B+m_{K^*}}(C_{10}+R_A-R'_A)\Big],\\
H'' &= \Big[\frac{2m_{K^*}}{q^2}(C_{10}+R_A-R'_A)(A_3(q^2)-A_0(q^2))\Big],\\
S'' &= \Big[-2(R_S-R'_S)\frac{m_{K^*}}{m_b}A_0(q^2)\Big],\\
P'' &= \Big[-2(R_P-R'_P)\frac{m_{K^*}}{m_b}A_0(q^2)\Big],\\
T_1'' &= -2T_1(q^2),\\
T_2'' &= \Big[\frac{2(m_B^2-m_{K^*}^2)}{q^2}(T_1(q^2)-T_2(q^2))\Big],\\
T_3'' &= \Big[\frac{4}{q^2}\Big(T_1(q^2)-T_2(q^2)-\frac{q^2T_3(q^2)}{m_B^2-m_{K^*}^2}\Big)\Big].
\end{aligned}
\tag{IV.63}
$$

Also, we define

$$
\begin{aligned}
T_0 &= \frac{1}{m_{K^*}}\Big(\sqrt{q^2}(E_{K^*}\sqrt{q^2}+2m_{K^*}^2)T_1''+q^2(E_{K^*}T_2''-|\vec{p}_{K^*}|^2\sqrt{q^2}T_3'')\Big)\ ,\\
T_+ &= (q^2+2E_{K^*}\sqrt{q^2})T_1''+q^2T_2''\ ,\quad T_-=2|\vec{p}_{K^*}|\sqrt{q^2}T_1''\ .
\end{aligned}
\tag{IV.64}
$$

IV.c Transversity amplitudes

We summarize the various transversity amplitudes that appear in the $\bar{B}_d^0\to\bar{K}^*\mu^+\mu^-$ angular distribution. The decay amplitude of $\bar{B}_d^0\to\bar{K}^*\mu^+\mu^-$ depends on the K^* polarization vector $\varepsilon(\lambda)$ with helicity λ $(0,\pm1)$. Hence, the decay amplitude can be decomposed into three components. Below we define the helicity amplitudes of various

operators with different Lorentz structures (V, A, S, P, T, TE) in Eq. (IV.55).

$$\begin{aligned}
A_V^0 &= \sqrt{q^2}\Big(\frac{E_{K^*}}{m_{K^*}}B'' + \frac{2|\vec{p}_{K^*}|^2\sqrt{q^2}}{m_{K^*}}C''\Big) , \quad A_V^{\pm} = \sqrt{q^2}(\pm|\vec{p}_{K^*}|\sqrt{q^2}A'' + B'') , \\
A_A^0 &= \sqrt{q^2}\Big(\frac{E_{K^*}}{m_{K^*}}F'' + \frac{2|\vec{p}_{K^*}|^2\sqrt{q^2}}{m_{K^*}}G''\Big) , \quad A_A^{\pm} = \sqrt{q^2}(\pm|\vec{p}_{K^*}|\sqrt{q^2}E'' + F'') , \\
A_S &= \frac{2|\vec{p}_{K^*}|q^2}{m_{K^*}}S'' , \qquad\qquad A_P = \frac{2|\vec{p}_{K^*}|q^2}{m_{K^*}}P'' , \\
A_T^0 &= T_0 C_T , \qquad\qquad A_T^{\pm} = T_{\pm} C_T , \\
A_{TE}^0 &= 2T_0 C_{TE} , \qquad\qquad A_{TE}^{\pm} = 2T_{\pm} C_{TE} , \\
A_{vt} &= -2|\vec{p}_{K^*}|\sqrt{q^2}(C_{10} + R_A - R_{A'})A_0 ,
\end{aligned} \tag{IV.65}$$

where the amplitude A_{vt} is related to the time-like component of the virtual K^*. In the transversity basis, the positive and negative helicity amplitudes are replaced by the transversity amplitudes as

$$A_{\parallel}^i = \frac{1}{2}(A_i^+ + A_i^-) , \quad A_{\perp}^i = \frac{1}{2}(A_i^+ - A_i^-) , \qquad \mathrm{i} = \mathrm{V, A, T, TE.} \tag{IV.66}$$

The left and right component of the transversity amplitudes of vector and axial-vector currents in [177] can be written as

$$A_{0,VA}^{L,R} = A_V^0 \mp A_A^0 \, , A_{\parallel,VA}^{L,R} = (A_{\parallel}^V \mp A_{\parallel}^A) \, , A_{\perp,VA}^{L,R} = (A_{\perp}^V \mp A_{\perp}^A) \, . \tag{IV.67}$$

Note that in the notation of Ref. [177], we have the correspondence $A_{(0,\parallel,\perp),VA}^{L,R} = (\sqrt{q^2}/N)A_{(0,\parallel,\perp)}^{L,R}$. The amplitudes $A_{S,P,vt}$ remain the same, while $A_S = -(\sqrt{q^2}/N)A_S^{L,R}$.

IV.d Angular coefficients

The expressions for the twelve angular coefficients (I's) in the $\bar{B}_d^0 \to \bar{K}^*\mu^+\mu^-$ angular distribution are summarized here according to K^* helicity combinations $\lambda_1\lambda_2$. The

longitudinal I^0's ($\lambda_1\lambda_2 = 00$) are given by

$$
\begin{aligned}
I_1^0 &= 2\Big[\frac{1}{2}(|A_{0,VA}^L|^2 + |A_{0,VA}^R|^2) + \frac{1}{2}(\beta_\mu^2|A_S|^2 + |A_P|^2) + 4\beta_\mu^2(|A_T^0|^2 + |A_{TE}^0|^2) \\
&\quad + \frac{4m_\mu^2}{q^2}\Big(\mathrm{Re}[A_{0,VA}^L A_{0,VA}^{R*}] + 2|A_{vt}|^2 + 8|A_{TE}^0|^2\Big) \\
&\quad + \frac{4m_\mu}{\sqrt{q^2}}\Big(2\mathrm{Re}[(A_{0,VA}^L + A_{0,VA}^R)A_{TE}^{0*}] - \mathrm{Re}[A_{vt}A_P^*]\Big)\Big] \ , \\
I_2^0 &= \beta_\mu^2\Big[-(|A_{0,VA}^L|^2 + |A_{0,VA}^R|^2) + 8(|A_T^0|^2 + |A_{TE}^0|^2)\Big] \ , \\
I_3^0 &= 2\beta_\mu\Big[4(-\mathrm{Re}[A_{TE}^0 A_S^*] + \mathrm{Re}[A_T^0 A_P^*]) - \frac{4m_\mu}{\sqrt{q^2}}\Big(\frac{1}{2}\mathrm{Re}[(A_{0,VA}^L + A_{0,VA}^R)A_S^*] \\
&\quad + 4\mathrm{Re}[A_{vt}A_T^{0*}]\Big)\Big] \ . \qquad \text{(IV.68)}
\end{aligned}
$$

The transverse I^T's ($\lambda_1\lambda_2 = ++, --, +-, -+$) are given by

$$
\begin{aligned}
I_1^T &= \Big[\frac{2+\beta_\mu^2}{2}\Big(|A_\parallel^V|^2 + |A_\perp^V|^2 + |A_\parallel^A|^2 + |A_\perp^A|^2\Big) - 4(-2+\beta_\mu^2)\Big(|A_\parallel^T|^2 + |A_\perp^T|^2 + |A_\parallel^{TE}|^2 \\
&\quad + |A_\perp^{TE}|^2\Big) + \frac{4m_\mu^2}{q^2}\Big(|A_\parallel^V|^2 + |A_\perp^V|^2 - |A_\parallel^A|^2 - |A_\perp^A|^2 - 16(A_\parallel^T A_\perp^{T*} - A_\parallel^{TE}A_\perp^{TE*})\Big) \\
&\quad + 16\frac{m_\mu}{\sqrt{q^2}}\Big(\mathrm{Re}[A_\perp^V(A_\parallel^{T*} - A_\perp^{T*})] + \mathrm{Re}[A_\parallel^V(A_\parallel^{TE*} + A_\perp^{TE*})]\Big)\Big] \ , \\
I_2^T &= \beta_\mu^2\Big[\frac{1}{2}\Big(|A_\parallel^V|^2 + |A_\perp^V|^2 + |A_\parallel^A|^2 + |A_\perp^A|^2\Big) - 4\Big(|A_\parallel^T|^2 + |A_\perp^T|^2 + |A_\parallel^{TE}|^2 + |A_\perp^{TE}|^2\Big)\Big] \ , \\
I_3^T &= -4\beta_\mu\Big[\mathrm{Re}[A_\perp^V A_\parallel^{A*} + A_\parallel^V A_\perp^{A*}] + 4\frac{m_\mu}{\sqrt{q^2}}\mathrm{Re}[A_\parallel^A(A_\parallel^{T*} - A_\perp^{T*}) + A_\perp^A(A_\parallel^{TE*} + A_\perp^{TE*})]\Big] \ , \\
I_4^T &= \beta_\mu^2\Big[\Big(|A_\perp^V|^2 - |A_\parallel^V|^2 + |A_\perp^A|^2 - |A_\parallel^A|^2\Big) + 16\Big(A_\parallel^T A_\perp^{T*} + A_\parallel^{TE}A_\perp^{TE*}\Big)\Big] \ , \\
I_5^T &= 2\beta_\mu^2\mathrm{Im}[A_\parallel^{V*}A_\perp^V + A_\parallel^{A*}A_\perp^A] \ . \qquad \text{(IV.69)}
\end{aligned}
$$

The mixed I^{LT}'s ($\lambda_1\lambda_2 = 0\pm, \pm 0$) are given by

$$
\begin{aligned}
I_1^{LT} &= \beta_\mu^2\Big[\frac{1}{\sqrt{2}}\mathrm{Re}[A_{0,VA}^R(A_\parallel^{V*}+A_\parallel^{A*})+A_{0,VA}^L(A_\parallel^{V*}-A_\parallel^{A*})] \\
&\quad -4\sqrt{2}\Big(A_T^0(A_\parallel^{T*}+A_\perp^{T*})+A_{TE}^0(A_\parallel^{TE*}+A_\perp^{TE*})\Big)\Big] \ , \\
I_2^{LT} &= \frac{1}{\sqrt{2}}\beta_\mu^2\mathrm{Im}[A_{0,VA}^R(A_\perp^{V*}+A_\perp^{A*})+A_{0,VA}^L(A_\perp^{V*}-A_\perp^{A*})] \ , \\
I_3^{LT} &= \sqrt{2}\beta_\mu\Big[\mathrm{Re}[A_{0,VA}^L(A_\perp^{V*}-A_\perp^{A*})-A_{0,VA}^R(A_\perp^{V*}+A_\perp^{A*})]+2\mathrm{Re}[(A_\parallel^{TE}+A_\perp^{TE})A_S^*] \\
&\quad -2\mathrm{Re}[(A_\parallel^T+A_\perp^T)A_P^*]+2\frac{m_\mu}{\sqrt{q^2}}\mathrm{Re}[A_\parallel^V A_S^*]\Big] \ , \\
I_4^{LT} &= \sqrt{2}\beta_\mu\Big[\mathrm{Im}[A_{0,VA}^L(A_\parallel^{V*}-A_\parallel^{A*})-A_{0,VA}^R(A_\parallel^{V*}+A_\parallel^{A*})] \\
&\quad +2\mathrm{Im}[(A_\parallel^T-A_\perp^T)A_S^*]+2\mathrm{Im}[(A_\parallel^{TE}-A_\perp^{TE})A_P^*]-2\frac{m_\mu}{\sqrt{q^2}}\mathrm{Im}[A_\perp^V A_S^*]\Big] \ . \quad \text{(IV.70)}
\end{aligned}
$$

Bibliography:

[116] A. K. Alok, A. Datta, A. Dighe, M. Duraisamy, D. Ghosh and D. London, "New Physics in $b \to s\mu^+\mu^-$: CP-Conserving Observables," JHEP **1111**, 121 (2011) [arXiv:1008.2367 [hep-ph]].

[117] In the latest update of the πK puzzle, it was seen that, although NP was hinted at in $B \to \pi K$ decays, it could be argued that the SM can explain the data, see S. Baek, C. W. Chiang and D. London, "The $B \to \pi K$ Puzzle: 2009 Update," *Phys. Lett.* **B 675**, 59 (2009).

[118] H. Y. Cheng, C. K. Chua and A. Soni, "CP-violating asymmetries in B^0 decays to $K^+K^-K_{S,L}^0$ and $K_S^0K_S^0K_{S,L}^0$," *Phys. Rev.* **D 72**, 094003 (2005) [hep-ph/0506268].

[119] G. Buchalla, G. Hiller, Y. Nir and G. Raz, "The pattern of CP asymmetries in $b \to s$ transitions," *JHEP* **0509**, 074 (2005) [hep-ph/0503151].

[120] E. Lunghi and A. Soni, "Hints for the scale of new CP-violating physics from B-CP anomalies," *JHEP* **0908**, 051 (2009) [arXiv/0903.5059 [hep-ph]].

[121] T. Aaltonen et al. (CDF Collaboration), V. M. Abazov et al. (DO Collaboration), "Combination of DO and CDF Results on $\Delta\Gamma_s$ and the CP-Violating Phase $\beta_s^{J/\psi\phi}$," CDF Note No. CDF/PHYS/BOTTOM/CDFR/9787, 2009; D0 Note No. 5928-CONF, 2009.

[122] B. Aubert *et al.* [BABAR Collaboration], "Rates, polarizations, and asymmetries in charmless vector-vector B meson decays," *Phys. Rev. Lett.* **91**, 171802 (2003) [arXiv:hep-ex/0307026].

[123] K. F. Chen *et al.* [Belle Collaboration], "Measurement of branching fractions and polarization in $B \to \phi K^{(*)}$ decays," *Phys. Rev. Lett.* **91**, 201801 (2003) [arXiv:hep-ex/0307014].

[124] V. M. Abazov *et al.* [The D0 Collaboration], "Evidence for an anomalous like-sign dimuon charge asymmetry," arXiv:1005.2757 [hep-ex].

[125] A. Dighe, A. Kundu and S. Nandi, "Enhanced B_s–$\bar{B}_s$ lifetime difference and anomalous like-sign dimuon charge asymmetry from new physics in $B_s \to \tau^+\tau^-$," arXiv:1005.4051 [hep-ph].

[126] A. Ishikawa *et al.*, "Measurement of forward-backward asymmetry and Wilson coefficients in $B \to K^*\ell^+\ell^-$," *Phys. Rev. Lett.* **96**, 251801 (2006) [hep-ex/0603018].

[127] J. T. Wei *et al.* [BELLE Collaboration], "Measurement of the Differential Branching Fraction and Forward-Backword Asymmetry for $B \to K^{(*)}\ell^+\ell^-$," *Phys. Rev. Lett.* **103**, 171801 (2009) [arXiv/0904.0770 [hep-ex]].

[128] B. Aubert *et al.* [BABAR Collaboration], "Measurements of branching fractions, rate asymmetries, and angular distributions in the rare decays $B \to K\ell^+\ell^-$ and $B \to K^*\ell^+\ell^-$," *Phys. Rev.* **D 73**, 092001 (2006) [hep-ex/0604007].

[129] B. Aubert *et al.* [BABAR Collaboration], "Angular Distributions in the Decays $B \to K^*\ell^+\ell^-$," *Phys. Rev.* **D 79**, 031102 (2009) [arXiv/0804.4412 [hep-ex]].

[130] LHCb collaboration, R. Aaij *et al.*, "Angular analysis of $B_d \to K^*\mu^+\mu^-$", LHCb-CONF-2011-038 (2011).

[131] W. Skiba and J. Kalinowski, "$B_s \to \tau^+\tau^-$ decay in a two Higgs doublet model," *Nucl. Phys.* **B 404**, 3 (1993).

[132] S. R. Choudhury and N. Gaur, "Dileptonic decay of B_s meson in SUSY models with large tanβ," *Phys. Lett.* **B 451**, 86 (1999) [arXiv:hep-ph/9810307].

[133] C. S. Huang, W. Liao, Q. S. Yan and S. H. Zhu, "$B_s \to \ell^+\ell^-$ in a general 2HDM and MSSM," Phys. Rev. D **63**, 114021 (2001) [Erratum-ibid. D **64**, 059902 (2001)] [arXiv:hep-ph/0006250].

[134] C. Bobeth, T. Ewerth, F. Kruger and J. Urban, "Analysis of neutral Higgs boson contributions to the decays $\bar{B}_s \to \ell^+\ell^-$ and $\bar{B} \to K\ell^+\ell^-$," *Phys. Rev.* **D 64**, 074014 (2001) [hep-ph/0104284].

[135] C. S. Huang and X. H. Wu, "$B_s \to \mu^+\mu^-$ and $B \to X_s\mu^+\mu^-$ in MSSM," Nucl. Phys. B **657**, 304 (2003) [arXiv:hep-ph/0212220].

[136] P. H. Chankowski and L. Slawianowska, "Effects of the scalar FCNC in $b \to s\ell^+\ell^-$ transitions and supersymmetry," *Eur. Phys. J.* **C 33**, 123 (2004) [hep-ph/0308032].

[137] A. K. Alok and S. U. Sankar, "New physics upper bound on the branching ratio of $B_s \to \ell^+\ell^-$," *Phys. Lett.* **B 620**, 61 (2005) [arXiv:hep-ph/0502120].

[138] M. Blanke, A. J. Buras, D. Guadagnoli and C. Tarantino, "Minimal Flavor Violation Waiting for Precise Measurements of ΔM_s, $S_{\psi\phi}$, A^s_{SL}, $|V_{ub}|$, γ and $B^0_{s,d} \to \mu^+\mu^-$", *JHEP* **0610**, 003 (2006) [arXiv:hep-ph/0604057].

[139] A. K. Alok and S. K. Gupta, "$B_s \to \mu^+\mu^-$ decay in the R-parity violating minimal supergravity," *Eur. Phys. J.* **C 65**, 491 (2010) [arXiv:0904.1878 [hep-ph]].

[140] A. J. Buras, B. Duling, T. Feldmann, T. Heidsieck, C. Promberger and S. Recksiegel, "Patterns of Flavour Violation in the Presence of a Fourth Generation of Quarks and Leptons," JHEP **1009**, 106 (2010) [arXiv:1002.2126 [hep-ph]].

[141] E. Golowich, J. Hewett, S. Pakvasa, A. A. Petrov and G. K. Yeghiyan, "Relating B_s Mixing and $B_s \to \mu^+\mu^-$ with New Physics," arXiv:1102.0009 [hep-ph].

[142] A. Ali, T. Mannel and T. Morozumi, "Forward backward asymmetry of dilepton angular distribution in the decay $b \to s\ell^+\ell^-$," *Phys. Lett.* **B 273**, 505 (1991).

[143] A. J. Buras and M. Munz, "Effective Hamiltonian for $B \to X_s\ell^+\ell^-$ beyond leading logarithms in the NDR and HV schemes," Phys. Rev. D **52**, 186 (1995) [arXiv:hep-ph/9501281].

[144] A. Ali, G. Hiller, L. T. Handoko and T. Morozumi, "Power corrections in the decay rate and distributions in $B \to X_s\ell^+\ell^-$ in the standard model," *Phys. Rev.* **D 55**, 4105 (1997) [arXiv:hep-ph/9609449].

[145] C. S. Huang, W. Liao and Q. S. Yan, "The promising process to distinguish supersymmetric models with large tan(beta) from the standard model: $B \to X_s\mu^+\mu^-$," Phys. Rev. D **59**, 011701 (1999) [arXiv:hep-ph/9803460].

[146] S. Fukae, C. S. Kim, T. Morozumi and T. Yoshikawa, "A Model independent analysis of the rare B decay $B \to X_s\ell^+\ell^-$," Phys. Rev. D **59**, 074013 (1999) [arXiv:hep-ph/9807254].

[147] C. Bobeth, M. Misiak and J. Urban, "Photonic penguins at two loops and m_t-dependence of BR($B \to X_s\ell^+\ell^-$)," *Nucl. Phys.* **B 574**, 291 (2000) [hep-ph/9910220].

[148] A. Ali, E. Lunghi, C. Greub and G. Hiller, "Improved model independent analysis of semileptonic and radiative rare B decays," *Phys. Rev.* **D 66**, 034002 (2002) [hep-ph/0112300];

[149] T. Huber, T. Hurth and E. Lunghi, "Logarithmically Enhanced Corrections to the Decay Rate and Forward Backward Asymmetry in $\bar{B} \to X_s \ell^+ \ell^-$," *Nucl. Phys.* **B 802**, 40 (2008) [arXiv:0712.3009 [hep-ph]].

[150] K. S. M. Lee, Z. Ligeti, I. W. Stewart and F. J. Tackmann, "Extracting short distance information from $b \to s\ell^+\ell^-$ effectively," Phys. Rev. D **75**, 034016 (2007) [arXiv:hep-ph/0612156].

[151] Z. Ligeti and F. J. Tackmann, "Precise predictions for $B \to X_s \ell^+ \ell^-$ in the large q^2 region," Phys. Lett. B **653**, 404 (2007) [arXiv:0707.1694 [hep-ph]].

[152] G. Eilam, C. D. Lu and D. X. Zhang, "Radiative dileptonic decays of B mesons," *Phys. Lett.* **B 391**, 461 (1997) [arXiv:hep-ph/9606444].

[153] T. M. Aliev, A. Ozpineci and M. Savci, "$B_q \to \ell^+\ell^-\gamma$ decays in light cone QCD," *Phys. Rev.* **D 55**, 7059 (1997) [arXiv:hep-ph/9611393].

[154] C. Q. Geng, C. C. Lih and W. M. Zhang, "Study of $B_{s,d} \to \ell^+\ell^-\gamma$ decays," *Phys. Rev.* **D 62**, 074017 (2000) [arXiv:hep-ph/0007252].

[155] Y. Dincer and L. M. Sehgal, "Charge asymmetry and photon energy spectrum in the decay $B_s \to \ell^+\ell^-\gamma$," *Phys. Lett.* **B 521**, 7 (2001) [arXiv:hep-ph/0108144].

[156] F. Kruger and D. Melikhov, "Gauge invariance and form factors for the decay $B \to \gamma\ell^+\ell^-$," *Phys. Rev.* **D 67**, 034002 (2003) [arXiv:hep-ph/0208256].

[157] D. Melikhov and N. Nikitin, "Rare radiative leptonic decays $B_{d,s} \to \ell^+\ell^-\gamma$," *Phys. Rev.* **D 70**, 114028 (2004) [arXiv:hep-ph/0410146].

[158] D. Melikhov, N. Nikitin and K. Toms, "Rare radiative leptonic decays $B_{d,s} \to \ell^+\ell^-\gamma$," *Phys. Atom. Nucl.* **68** (2005) 1842 [*Yad. Fiz.* **68**, 1904 (2005)].

[159] A. K. Alok and S. Uma Sankar, "New physics upper bound on the branching ratio of $B_s \to \ell^+\ell^-\gamma$," *Mod. Phys. Lett.* **A 22**, 1319 (2007) [arXiv:hep-ph/0603262].

[160] I. Balakireva, D. Melikhov, N. Nikitin and D. Tlisov, "Forward-backward and CP-violating asymmetries in rare $B_{d,s} \to (V, \gamma)\ell^+\ell^-$ decays," Phys. Rev. D **81**, 054024 (2010) [arXiv:0911.0605 [hep-ph]].

[161] A. Ali, P. Ball, L. T. Handoko and G. Hiller, "A comparative study of the decays $B \to (K, K^*)\ell^+\ell^-$ in standard model and supersymmetric theories", *Phys. Rev.* **D 61**, 074024 (2000) [arXiv:hep-ph/9910221].

[162] T. M. Aliev, M. K. Cakmak, A. Ozpineci and M. Savci, "New physics effects to the lepton polarizations in the $B \to K\ell^+\ell^-$ decay," *Phys. Rev.* **D 64**, 055007 (2001) [hep-ph/0103039].

[163] W. Bensalem, D. London, N. Sinha and R. Sinha, "Lepton polarization and forward backward asymmetries in $b \to s\tau^+\tau^-$," *Phys. Rev.* **D 67**, 034007 (2003) [hep-ph/0209228].

[164] C. Bobeth, G. Hiller and G. Piranishvili, "Angular Distributions of $B \to K\ell\ell$ Decays," *JHEP* **0712**, 040 (2007) [arXiv:0709.4174 [hep-ph]].

[165] A. K. Alok, A. Dighe and S. Uma Sankar, "Large forward-backward asymmetry in $B \to K\mu^+\mu^-$ from new physics tensor operators," *Phys. Rev.* **D 78**, 114025 (2008) [arXiv:0810.3779 [hep-ph]].

[166] J. Charles, A. Le Yaouanc, L. Oliver, O. Pene and J. C. Raynal, "Heavy-to-light form factors in the heavy mass to large energy limit of QCD," Phys. Rev. D **60**, 014001 (1999) [arXiv:hep-ph/9812358].

[167] M. Beneke and T. Feldmann, "Symmetry-breaking corrections to heavy-to-light B meson form factors at large recoil," Nucl. Phys. B **592**, 3 (2001) [arXiv:hep-ph/0008255].

[168] F. Kruger and E. Lunghi, "Looking for novel CP violating effects in $\bar{B} \to K^*\ell^+\ell^-$," *Phys. Rev.* **D 63**, 014013 (2001) [hep-ph/0008210].

[169] M. Beneke, T. Feldmann and D. Seidel, "Systematic approach to exclusive $B \to V\ell^+\ell^-, V\gamma$ decays," *Nucl. Phys.* **B 612**, 25 (2001) [hep-ph/0106067].

[170] Q. S. Yan, C. S. Huang, W. Liao and S. H. Zhu, "Exclusive semileptonic rare decays $B \to (K, K^*)\ell^+\ell^-$ in supersymmetric theories," Phys. Rev. D **62**, 094023 (2000) [arXiv:hep-ph/0004262].

[171] T. M. Aliev, V. Bashiry and M. Savci, "Double-lepton polarization asymmetries in the $B \to K\ell^+\ell^-$ decay beyond the standard model," *Eur. Phys. J.* **C 35**, 197 (2004) [hep-ph/0311294].

[172] T. M. Aliev, V. Bashiry and M. Savci, "Polarized lepton pair forward-backward asymmetries in $B \to K^*\ell^+\ell^-$ decay beyond the standard model," *JHEP* **0405**, 037 (2004) [hep-ph/0403282].

[173] F. Kruger and J. Matias, "Probing new physics via the transverse amplitudes of $B^0 \to K^{*0}(\to K^-\pi^+)\ell^+\ell^-$ at large recoil," *Phys. Rev.* **D 71**, 094009 (2005) [arXiv:hep-ph/0502060].

[174] E. Lunghi and J. Matias, "Huge right-handed current effects in $B \to K^*(K\pi)\ell^+\ell^-$ in supersymmetry," *JHEP* **0704**, 058 (2007) [hep-ph/0612166].

[175] A. Hovhannisyan, W. S. Hou and N. Mahajan, "$B \to K^*\ell^+\ell^-$ forward-backward asymmetry and new physics," *Phys. Rev.* **D 77**, 014016 (2008) [hep-ph/0701046].

[176] U. Egede, T. Hurth, J. Matias, M. Ramon and W. Reece, "New observables in the decay mode $\bar{B} \to \bar{K}^{*0}\ell^+\ell^-$," *JHEP* **0811**, 032 (2008) [arXiv/0807.2589 [hep-ph]].

[177] W. Altmannshofer, P. Ball, A. Bharucha, A. J. Buras, D. M. Straub and M. Wick, "Symmetries and Asymmetries of $B \to K^*\mu^+\mu^-$ Decays in the Standard Model and Beyond," *JHEP* **0901**, 019 (2009) [arXiv:0811.1214 [hep-ph]].

[178] A. K. Alok, A. Dighe, D. Ghosh, D. London, J. Matias, M. Nagashima and A. Szynkman, "New-physics contributions to the forward-backward asymmetry in $B \to K^*\mu^+\mu^-$," *JHEP* **1002**, 053 (2010) [arXiv:0912.1382 [hep-ph]].

[179] A. Soni, A. K. Alok, A. Giri, R. Mohanta and S. Nandi, "SM with four generations: Selected implications for rare B and K decays," Phys. Rev. D **82**, 033009 (2010) [arXiv:1002.0595 [hep-ph]].

[180] C. Bobeth, G. Hiller and D. van Dyk, "The Benefits of $B \to K^*\ell^+\ell^-$ Decays at Low Recoil," JHEP **1007**, 098 (2010) [arXiv:1006.5013 [hep-ph]].

[181] E. Lunghi and A. Soni, "An improved observable for the forward-backward asymmetry in $B \to K^*\ell^+\ell^-$ and $B_s \to \phi\ell^+\ell^-$," JHEP **1011**, 121 (2010) [arXiv:1007.4015 [hep-ph]].

[182] C. Bobeth, G. Hiller and D. van Dyk, "More Benefits of Semileptonic Rare B Decays at Low Recoil: CP Violation," arXiv:1105.0376 [hep-ph].

[183] A. Bharucha, W. Reece, Eur. Phys. J. **C69**, 623-640 (2010) [arXiv:1002.4310 [hep-ph]].

[184] G. Hiller and F. Kruger, "More model independent analysis of $b \to s$ processes," *Phys. Rev.* **D 69**, 074020 (2004) [hep-ph/0310219].

[185] A. K. Alok, A. Dighe and S. U. Sankar, "Tension between scalar/pseudoscalar new physics contribution to $B_s \to \mu^+\mu^-$ and $B \to K\mu^+\mu^-$," *Mod. Phys. Lett.* **A 25**, 1099 (2010) [arXiv:0803.3511 [hep-ph]].

[186] A. K. Alok, A. Dighe and S. U. Sankar, "Probing extended Higgs sector through rare $b \to s\mu^+\mu^-$ transitions," *Phys. Rev.* **D 78**, 034020 (2008) [arXiv:0805.0354 [hep-ph]].

[187] M. Beylich, G. Buchalla, T. Feldmann, "Theory of $B \to K^* \ell^+ \ell^-$ decays at high q^2: OPE and quark-hadron duality," Eur. Phys. J. **C71**, 1635 (2011). [arXiv:1101.5118 [hep-ph]].

[188] A. K. Alok, A. Datta, A. Dighe, M. Duraisamy, D. Ghosh and D. London, "New Physics in $b \to s\mu^+\mu^-$: CP-Violating Observables," arXiv:1103.5344 [hep-ph].

[189] B. Grinstein and D. Pirjol, "Symmetry-breaking corrections to heavy meson form-factor relations," Phys. Lett. B **533**, 8 (2002) [arXiv:hep-ph/0201298].

[190] B. Grinstein and D. Pirjol, "Precise $|V_{ub}|$ determination from exclusive B decays: Controlling the long-distance effects," Phys. Rev. D **70**, 114005 (2004) [arXiv:hep-ph/0404250].

[191] P. Gambino, U. Haisch and M. Misiak, "Determining the sign of the $b \to s\gamma$ amplitude," *Phys. Rev. Lett.* **94**, 061803 (2005) [hep-ph/0410155].

[192] T. Aaltonen *et al.* [CDF Collaboration], "Search for $B_s^0 \to \mu^+\mu^-$ and $B_d^0 \to \mu^+\mu^-$ decays with $2fb^{-1}$ of $p\bar{p}$ collisions," *Phys. Rev. Lett.* **100**, 101802 (2008) [arXiv:0712.1708 [hep-ex]].

[193] C. Amsler *et al.* [Particle Data Group], "Review of particle physics," *Phys. Lett.* **B 667**, 1 (2008).

[194] E. Barberio *et al.* [Heavy Flavor Averaging Group], "Averages of $b-$hadron and $c-$hadron Properties at the End of 2007," arXiv:0808.1297 [hep-ex], and online update at `http://www.slac.stanford.edu/xorg/hfag`

[195] B. Aubert *et al.* [BABAR Collaboration], "Measurement of the $B \to X_s \ell^+ \ell^-$ branching fraction with a sum over exclusive modes," *Phys. Rev. Lett.* **93**, 081802 (2004) [arXiv:hep-ex/0404006].

[196] M. Iwasaki *et al.* [Belle Collaboration], "Improved measurement of the electroweak penguin process $B \to X_s \ell^+ \ell^-$," *Phys. Rev.* **D 72**, 092005 (2005) [arXiv:hep-ex/0503044].

[197] T. Aaltonen *et al.* [CDF Collaboration], "Measurement of the Forward-Backward Asymmetry in the $B \to K^{(*)} \mu^+ \mu^-$ Decay and First Observation of the $B_s^0 \to \phi \mu^+ \mu^-$ Decay," *Phys. Rev. Lett.* **106**, 161801 (2011) [arXiv/1101.1028[hep-ex]].

[198] J. Laiho, E. Lunghi and R. S. Van de Water, "Lattice QCD inputs to the CKM unitarity triangle analysis," Phys. Rev. D **81**, 034503 (2010) [arXiv:0910.2928 [hep-ph]].

[199] M. Lenzi, "Rare B decays at LHCb," arXiv:0710.5056 [hep-ex].

[200] T. E. Browder, T. Gershon, D. Pirjol, A. Soni and J. Zupan, "New Physics at a Super Flavor Factory," arXiv:0802.3201 [hep-ph].

[201] B. Aubert *et al.* [BABAR Collaboration], "Measurements of branching fractions, rate asymmetries, and angular distributions in the rare decays $B \to K\ell^+\ell^-$ and $B \to K^*\ell^+\ell^-$", *Phys. Rev.* **D 73**, 092001 (2006) [arXiv:hep-ex/0604007].

[202] K. Ikado [Belle Collaboration], "Measurements of forward-backward asymmetry in $B \to K^*\ell^+\ell^-$ and evidence of $B^- \to \tau^-\bar{\nu}$", arXiv:hep-ex/0605067.

[203] C. Adorisio, [for ATLAS and CMS Collaboration], "Studies of Semileptonic Rare B Decays at ATLAS and CMS", Talk given at CERN Theory Institute, May 2008. `http://indico.cern.ch/conferenceOtherViews.py?view=standard&confId=31959`

[204] B. Adeva *et al.* [The LHCb Collaboration], "Roadmap for selected key measurements of LHCb," arXiv:0912.4179 [hep-ex].

[205] C. H. Chen and C. Q. Geng, "Analysis of $B \to K^*\ell^+\ell^-$ decays at large recoil," *Nucl. Phys.* **B 636**, 338 (2002) [arXiv:hep-ph/0203003].

[206] C. H. Chen and C. Q. Geng, "Probing new physics in $B \to K^*\ell^+\ell^-$ decays," *Phys. Rev.* **D 66**, 094018 (2002) [arXiv:hep-ph/0209352].

[207] C. Collaboration, "Search for $B_s \to \mu^+\mu^-$ and $B_d \to \mu^+\mu^-$ Decays with CDF II," arXiv:1107.2304 [hep-ex].

[208] J. Charles *et al.* [CKMfitter Group], "CP violation and the CKM matrix: Assessing the impact of the asymmetric B factories," Eur. Phys. J. C **41**, 1 (2005) [arXiv:hep-ph/0406184].

Chapter 5

New Physics in $b \to s\mu^+\mu^-$: CP-Violating Observables

5.1 Introduction

The B factories have taken us to the luminosity frontier with more than a billion B^+/B_d mesons, and the Tevatron experiments have provided us with invaluable data on B_s mesons. We have now entered the precision era of B physics. The Standard Model (SM) has been successful in explaining most of the data to date. However, this is now the time to look forward to precision tests, with the ATLAS and CMS experiments already running, the LHCb expected to start recording data soon, and the Super-B factories on their way. One can now be ambitious and not only look for new-physics (NP) effects, but also try to identify the kind of NP involved.

Though there is no unambiguous signal of NP so far in all of the B decays we have observed, some possible hints of NP have recently surfaced in modes involving $b \to s$ transitions. These include measurements of CP-averaged quantities such as the large transverse polarization in $B \to \phi K^*$ [210, 211], and the anomalous forward-backward asymmetry in $B \to K^*\mu^+\mu^-$ [212–214]. There are also measurements of CP-violating quantities such as the difference between the mixing-induced CP asymmetries seen in $b \to s$ penguin decays and in $B_d \to J/\psi K_S$ [215–217], the large CP asymmetry in $B_s \to J/\psi\phi$ [218], and the anomalous CP asymmetry in like-sign dimuon signals [219].

In the previous chapter, we performed a general analysis with all possible Lorentz structures of NP in the transition $b \to s\mu^+\mu^-$. We included NP vector-axial vector (VA), scalar-pseudoscalar (SP), and tensor (T) $b \to s\mu^+\mu^-$ operators, and explored their possible effects on the decays $\bar{B}_s^0 \to \mu^+\mu^-$, $\bar{B}_d^0 \to X_s\mu^+\mu^-$, $\bar{B}_s^0 \to \mu^+\mu^-\gamma$,

This chapter is based on JHEP **1111**, 122 (2011) by Ashutosh Kumar Alok, Alakabha Datta, Amol Dighe, Murugeswaran Duraisamy, Diptimoy Ghosh and David London [209]. The analytic expressions for some of the CP-violating asymmetries existed partly (for a subset of new operators) in the literature. I have brought all the earlier results together in a consistent notation and completed them using all the Lorentz Structures. All the numerical analysis for the modes $\bar{B}_s^0 \to \mu^+\mu^-\gamma, \bar{B}_d^0 \to \bar{K}\mu^+\mu^-$, and $\bar{B}_d^0 \to X_s\mu^+\mu^-$ were performed by me with some initial help from Ashutosh Kumar Alok.

$\bar{B}_d^0 \to \bar{K}\mu^+\mu^-$, and $\bar{B}_d^0 \to \bar{K}^*\mu^+\mu^-$. We focused on CP-conserving observables such as differential branching ratios, forward-backward asymmetries, polarization fractions, and the asymmetries $A_T^{(2)}, A_{LT}$ in $\bar{B}_d^0 \to \bar{K}^*\mu^+\mu^-$. Because we only considered CP-conserving observables, all the NP couplings were taken to be real. We computed the effects of all NP operators, individually and in all combinations, on these observables.

The CP-violating observables in various $b \to s\mu^+\mu^-$ decays in the SM as well as in some NP models have been studied in Refs. [221–236] In this chapter, we explore the CP-violating quantities that may be measured in the same decay modes by allowing the new couplings to be complex. The introduction of complex couplings has two effects. First, some quantities which were taken to be CP-conserving above now display CP-violation, i.e. the quantities take different values in the CP-conjugate decays. The difference between the value of a measurement in a decay and in its CP-conjugate counterpart is then a CP-violating observable. Second, new observables appear which vanish in the CP-conserving limit. (These were not considered in Ref. [220] for this reason.) These essentially correspond to the CP-violating triple-product asymmetries $A_T^{(im)}$ and $A_{LT}^{(im)}$ in $\bar{B}_d^0 \to \bar{K}^*\mu^+\mu^-$, which may be obtained from the angular distribution in this decay. Our goal is to identify those quantities for which there may be large effects due to the presence of NP. In such cases, we try to find salient features of the effects of NP, which may help us identify the Lorentz structure of the NP involved.

Here we have taken the NP to be present only in the effective $b \to s\mu^+\mu^-$ operator. While this can, in principle, contribute to CP violation in B_d-$\bar{B}_d$ and B_s-$\bar{B}_s$ mixing, it is a higher-order effect, and hence negligible compared to the SM contribution. We therefore neglect mixing-induced (indirect) CP violation in this work, and focus only on CP violation in the decay. In the SM, such CP violation is expected to be close to zero in $b \to s$ transitions. A naive estimate indicates that this asymmetry will be $\sim 10^{-3}$ [229, 232], but even if next-to-leading order (NLO) QCD corrections and hadronic uncertainties are included, it is observed that the CP asymmetry will not exceed 1% [233,234,237]. Thus, if a large CP-violating effect, more than a few percent, is observed in any of the $b \to s\mu^+\mu^-$ channels, this will therefore be a clear signature of NP. In this chapter, we go further and explore the extent to which the Lorentz structure of NP can be ascertained from the CP-violating measurements.

The chapter is organized as follows. We begin in Sec. 5.2 by describing the effective Hamiltonian with NP operators and new couplings. Although the formalism is the same as that used in Ref. [220], the constraints on the NP couplings are now more relaxed since the couplings are allowed to be complex. We also present an overview of the types of CP-violating observables which are examined. In Sec. 5.3 we note that there are essentially no measurable CP-violating quantities in the mode $\bar{B}_s^0 \to \mu^+\mu^-$. We then consider the decays $\bar{B}_d^0 \to X_s\mu^+\mu^-$ (Sec. 5.4), $\bar{B}_s^0 \to \mu^+\mu^-\gamma$ (Sec. 5.5), and $\bar{B}_d^0 \to \bar{K}\mu^+\mu^-$ (Sec. 5.6). In these sections we examine the same observables as in Ref. [220], this time looking at the asymmetries between these processes and their CP-conjugates. In Sec. 5.7, we study the CP asymmetries in $\bar{B}_d^0 \to \bar{K}^*\mu^+\mu^-$ for the

observables considered in Ref. [220], and in addition we explore new observables that vanish in the CP-conserving limit (triple products). We summarize our findings in Sec. 5.8 and discuss their implications.

5.2 $b \to s\mu^+\mu^-$ Operators

In this chapter our formalism is identical to that used in section 4.2. But as we are interested in CP violating effects here, we take all NP couplings to be complex in our numerical analysis.

5.2.1 Constraints on NP couplings

The constraints on the NP couplings in $b \to s\mu^+\mu^-$ come mainly from the upper bound on the branching ratio $B(\bar{B}_s^0 \to \mu^+\mu^-)$ and the measurements of the total branching ratios $B(\bar{B}_d^0 \to X_s\mu^+\mu^-)$ and $B(\bar{B}_d^0 \to \bar{K}\mu^+\mu^-)$ [239–241]:

$$B(\bar{B}_s^0 \to \mu^+\mu^-) < 4.7 \times 10^{-8} \quad (90\%\ \text{C.L.})\ , \tag{5.1}$$

$$B(\bar{B}_d^0 \to X_s\mu^+\mu^-) = \begin{cases} (1.60 \pm 0.50) \times 10^{-6} & (\text{low } q^2) \\ (0.44 \pm 0.12) \times 10^{-6} & (\text{high } q^2) \end{cases}\ , \tag{5.2}$$

$$B(\bar{B}_d^0 \to \bar{K}\mu^+\mu^-) = \left(4.5^{+1.2}_{-1.0}\right) \times 10^{-7}\ , \tag{5.3}$$

where the low-q^2 and high-q^2 regions correspond to 1 GeV$^2 \le q^2 \le 6$ GeV^2 and $q^2 \ge 14.4$ GeV^2, respectively. Here q^2 is the invariant mass squared of the two muons.

We consider all the NP couplings R_i to be complex and parametrize them as

$$R_i = |R_i|\, e^{i\phi_{R_i}}\ , \tag{5.4}$$

where $i = V, A, S, P, T, TE$ and $-\pi \le \phi_{R_i} \le \pi$. The bounds on these couplings will in general depend on which operators are present. While we take the correlations in these constraints into account in our numerical calculations, for the sake of simplicity we only give the bounds when the NP operators (VA, SP, T) are present individually.

If the only NP couplings present are $R_{V,A}$, we obtain

$$\frac{|\text{Re}(R_V) + 2.8|^2}{(6.3)^2} + \frac{|\text{Im}(R_V)|^2}{(6.0)^2} \lesssim 1.0\ , \quad \frac{|\text{Re}(R_A) - 4.1|^2}{(6.1)^2} + \frac{|\text{Im}(R_A)|^2}{(6.0)^2} \lesssim 1.0\ . \tag{5.5}$$

If the only NP couplings present are $R'_{V,A}$, the constraints are

$$\frac{|\text{Re}(R'_V)|^2}{(3.5)^2} + \frac{|\text{Im}(R'_V)|^2}{(4.0)^2} \lesssim 1.0\ , \quad \frac{|\text{Re}(R'_A)|^2}{(3.5)^2} + \frac{|\text{Im}(R'_A)|^2}{(4.0)^2} \lesssim 1.0\ . \tag{5.6}$$

For the SP operators, the present upper bound on $B(\bar{B}_s^0 \to \mu^+\mu^-)$ provides the limit

$$|R_S - R'_S|^2 + |R_P - R'_P|^2 \lesssim 0.44^1 \ . \tag{5.7}$$

This constitutes a severe constraint on the NP couplings if only $R_{S,P}$ or $R'_{S,P}$ are present. However, if both types of operators are present, these bounds can be evaded due to cancellations between the $R_{S,P}$ and $R'_{S,P}$. In that case, $B(\bar{B}_d^0 \to X_s\mu^+\mu^-)$ and $B(\bar{B}_d^0 \to \bar{K}\mu^+\mu^-)$ can still bound these couplings. The stronger bound is obtained from the measurement of the latter quantity, which yields

$$|R_S|^2 + |R_P|^2 \lesssim 9 \ , \quad R_S \approx R'_S \ , \quad R_P \approx R'_P \ . \tag{5.8}$$

Finally, the constraints on the NP tensor operators come entirely from $B(\bar{B}_d^0 \to X_s\mu^+\mu^-)$. When only the T operators are present,

$$|C_T|^2 + 4|C_{TE}|^2 \lesssim 1.0 \ . \tag{5.9}$$

The constraints are not affected significantly if more than one type (VA, SP or T) of NP operators is present simultabeously.

5.2.2 CP-violating effects

All CP-violating effects are due to the interference of (at least) two amplitudes with a relative weak phase. In principle, there can be three types of interference: SM-SM, SM-NP, NP-NP. In the SM, all contributions to the $b \to s\mu^+\mu^-$ modes are proportional to the Cabibbo-Kobayashi-Maskawa (CKM) factors $V_{tb}^*V_{ts}$, $V_{cb}^*V_{cs}$, or $V_{ub}^*V_{us}$. The term $V_{cb}^*V_{cs}$ can be eliminated in terms of the other two using the unitarity of the CKM matrix. Furthermore, although $V_{ub}^*V_{us}$ has a large weak phase, its magnitude is greatly suppressed relative to that of $V_{tb}^*V_{ts}$. Thus, to a good approximation, all nonzero SM contributions have the same weak phase, and so all CP-violating effects are predicted to be tiny in the SM.

There are two types of CP violation. The first is direct CP-violating asymmetries. Suppose that a particular $\bar{B}$ decay has two contributing amplitudes: $i\mathcal{M}(\bar{B}\text{ decay}) = \mathcal{A}_1 + \mathcal{A}_2$. Each amplitude has both a weak and a strong phase. The matrix element $i\overline{\mathcal{M}}$ for the CP-conjugate decay is the same as $i\mathcal{M}$, except that the weak phases change signs. CP violation is indicated by a nonzero value of $|\mathcal{M}|^2 - |\overline{\mathcal{M}}|^2$. It is straightforward to show that this is proportional to $\sin\phi_w \sin\delta$, where ϕ_w and δ are, respectively, the relative weak and strong phases between $\mathcal{A}_1$ and $\mathcal{A}_2$. Direct CP-violating asymmetries therefore require that the interfering amplitudes have both a nonzero relative weak and strong phase.

[1](Written in July 2012) Note that, the latest LHCb data has strengthened this limit to $|R_S - R'_S|^2 + |R_P - R'_P|^2 \lesssim 0.04$. This will make the allowed contributions from the scalar and pseudoscalar operators extremely small.

The second type of CP violation is triple-product (TP) asymmetries. Suppose that the matrix element for the $\bar{B}$ decay takes the form $i\mathcal{M}(\bar{B}\text{ decay}) = \mathcal{A}_1 + i\mathcal{A}_2\epsilon_{\mu\nu\rho\sigma}p_{\bar{B}}^{\mu}v_1^{\nu}v_2^{\rho}v_3^{\sigma}$, where the v_i are spins or momenta of the final-state particles. The difference $|\mathcal{M}|^2 - |\overline{\mathcal{M}}|^2$ is proportional to $m_{\bar{B}}\vec{v}_1\cdot(\vec{v}_2\times\vec{v}_3)\sin\phi_w\cos\delta$. By measuring the TP $\vec{v}_1\cdot(\vec{v}_2\times\vec{v}_3)$ in both $\bar{B}$ and B decays, the TP asymmetry can be obtained. Note that the measurement of a nonzero TP in the $\bar{B}$ decay alone is not sufficient to establish CP violation, i.e. it does not necessarily imply a nonzero weak phase. A fake, CP-conserving TP can be produced if $\mathcal{A}_1$ and $\mathcal{A}_2$ have a relative strong phase. It is only by measuring the difference of TPs in $\bar{B}$ and B decays that the fake TP can be eliminated and a true, CP-violating signal produced [242].

Let us first turn to direct CP violation, which requires both a relative weak and strong phase between two interfering amplitudes. Now, strong phases are generated through the rescattering of the operators in the effective Hamiltonian. The NP strong phases involve only the (constrained) NP operators, and are therefore small [243]. Thus, direct CP asymmetries can never arise from NP-NP interference.

On the other hand, the SM strong phase is not so small. It is generated because the Wilson coefficient C_9^{eff}, which gets a contribution from a $c\bar{c}$ quark loop, has an imaginary piece. (C_9^{eff} also gets a contribution from a $u\bar{u}$ quark loop. But this is proportional to $V_{ub}^*V_{us}$, and hence negligible.) The quantity C_9^{eff} can be written as [234]

$$\begin{aligned} C_9^{\text{eff}} &= C_9(m_b) + h(z,\hat{m}_c)\left(\frac{4}{3}C_1 + C_2 + 6\,C_3 + 60\,C_5\right) \\ &\quad - \frac{1}{2}h(z,\hat{m}_b)\left(7C_3 + \frac{4}{3}C_4 + 76C_5 + \frac{64}{3}C_6\right) \\ &\quad - \frac{1}{2}h(z,0)\left(C_3 + \frac{4}{3}C_4 + 16\,C_5 + \frac{64}{3}C_6\right) + \frac{4}{3}C_3 + \frac{64}{9}C_5 + \frac{64}{27}C_6\ . \end{aligned} \tag{5.10}$$

Here $z \equiv q^2/m_b^2$, and $\hat{m}_q \equiv m_q/m_b$ for all quarks q. The function $h(z,\hat{m})$ represents the one-loop correction to the four-quark operators O_1-O_6 and is given by [232,234,244]

$$\begin{aligned} h(z,\hat{m}) &= -\frac{8}{9}\ln\frac{m_b}{\mu_b} - \frac{8}{9}\ln\hat{m} + \frac{8}{27} + \frac{4}{9}x \\ &\quad -\frac{2}{9}(2+x)|1-x|^{1/2}\begin{cases} \left(\ln\left|\frac{\sqrt{1-x}+1}{\sqrt{1-x}-1}\right| - i\pi\right), & \text{for } x \le 1\ , \\ 2\arctan\frac{1}{\sqrt{x-1}}, & \text{for } x > 1\ , \end{cases} \end{aligned} \tag{5.11}$$

where $x \equiv 4\hat{m}^2/z$. Thus, a nontrivial strong phase is generated when $z \ge 4\hat{m}^2$. This leads to the complex nature of C_9^{eff} in the SM. For example, typical values of C_9^{eff} in the low- and high-q^2 regions are $C_9^{\text{eff}}(m_b) = 4.75 + 0.09i$ $(z = 0.1)$, $C_9^{\text{eff}}(m_b) = 4.76 + 0.88i$ $(z = 0.7)$. C_9^{eff} therefore has a nontrivial imaginary component, which implies that direct CP asymmetries can arise due to SM-NP interference. Since the SM operator (C_9^{eff}) is of VA type, the NP operator must also be VA in order to generate

a significant direct CP asymmetry. Other NP operators can also interfere with the SM, but the effect is suppressed by m_μ/m_b, and hence very small. Note that, although this argument has used the total decay rate for illustration, we could have used (almost) any observable which is related to the square of the matrix element. This includes the differential branching ratio, forward-backward asymmetry, polarization asymmetries, etc.

The TP asymmetries, on the other hand, do not need a difference in strong phases between two amplitudes. Indeed, they are proportional to $\cos\delta$, though they do require a weak-phase difference. This means that a TP asymmetry can be produced by either SM-NP or NP-NP interference. Given that all SM operators are of VA type, the NP must also be VA if SM-NP interference is the reason for the TP. On the other hand, if NP-NP interference is involved, this can arise due to new SP and T operators (other NP-NP interference are possible, but the effects are suppressed by m_μ/m_b).

In this chapter, we explore both sources of CP asymmetries, direct CP violation and TPs. While we have checked the effects of SP and T NP operators on all the observables, we find them to be insignificant in most places (as expected from the arguments above), and we will mention them only during the discussion of TP asymmetries, where, in principle, they may play a significant role.

5.3 $\bar{B}_s^0 \to \mu^+\mu^-$

We begin by considering the direct CP asymmetry in $\bar{B}_s^0 \to \mu^+\mu^-$. Helicity conservation in the decay of B_s or $\bar{B}_s$ implies that the only final states can be $\mu_L^+\mu_L^-$ or $\mu_R^+\mu_R^-$, which are CP conjugates. The only CP-violating observables that can be constructed are then

$$\begin{aligned} A_{CP}^{RL}(t) &\equiv \frac{B(\bar{B}_s^0(t)\to\mu_R^+\mu_R^-) - B(B_s^0(t)\to\mu_L^+\mu_L^-)}{B(\bar{B}_s^0(t)\to\mu_R^+\mu_R^-) + B(B_s^0(t)\to\mu_L^+\mu_L^-)}\,, \\ A_{CP}^{LR}(t) &\equiv \frac{B(\bar{B}_s^0(t)\to\mu_L^+\mu_L^-) - B(B_s^0(t)\to\mu_R^+\mu_R^-)}{B(\bar{B}_s^0(t)\to\mu_L^+\mu_L^-) + B(B_s^0(t)\to\mu_R^+\mu_R^-)}\,. \end{aligned} \tag{5.12}$$

The CP asymmetry in the longitudinal polarization fraction A_{LP} may be written in terms of these two CP asymmetries. The measurement of either of these CP asymmetries requires the measurement of muon polarization, which will be an impossible task for the upcoming experiments [220]. And even if this were doable, the lack of any sources for different strong phases in the two CP-conjugate final states implies that the direct CP asymmetry would vanish even with NP. We therefore do not study CP violation in $\bar{B}_s^0 \to \mu^+\mu^-$.

5.4 $\bar{B}_d^0 \to X_s\mu^+\mu^-$

A model-independent analysis of the CP asymmetry in the differential branching ratio (DBR) of $\bar{B}_d^0 \to X_s\mu^+\mu^-$ was previously carried out in Ref. [223]. There, the CP asymmetry in the DBR was predicted for some specific values of the NP couplings. However, no experimental constraints on the parameters were used. In this chapter we study the CP asymmetry in the DBR, taking into account the constraints from the present measurements of other related observables. Moreover, in addition to the CP asymmetry in the DBR, we also study the CP asymmetry in the forward-backward asymmetry.

The CP asymmetry in DBR of $\bar{B}_d^0 \to X_s\mu^+\mu^-$ is defined as

$$A_{\rm CP}(q^2) = \frac{(dB/dz) - (d\overline{B}/dz)}{(dB/dz) + (d\overline{B}/dz)} \,, \tag{5.13}$$

where $z \equiv q^2/m_b^2$, and dB/dz and $d\overline{B}/dz$ are the DBRs of $\bar{B}_d^0 \to X_s\mu^+\mu^-$ and its CP-conjugate $B_d^0 \to X_s\mu^+\mu^-$, respectively. The expression for (dB/dz) has been given in Ref. [220].

The CP asymmetry in the forward-backward asymmetry A_{FB} is defined as

$$\Delta A_{FB}(q^2) \equiv A_{FB}(q^2) - \overline{A}_{FB}(q^2) \,, \tag{5.14}$$

where the definition of A_{FB} is given in Ref. [220], and $\overline{A}_{FB}$ is the analogous quantity for the CP-conjugate decay. Note that while the relevant angle θ in $\bar{B}_d^0 \to X_s\mu^+\mu^-$ is defined relative to the direction of μ^+, for the CP-conjugate decay one should define θ in relation to the direction of μ^-, and similarly for A_{FB} in other $b \to s\mu^+\mu^-$ decay modes below.

Fig. 5.1 shows $A_{\rm CP}(q^2)$ and $\Delta A_{FB}(q^2)$ for $\bar{B}_d^0 \to X_s\mu^+\mu^-$ in the presence of new VA couplings. We make the following observations:

- When only $R_{V,A}$ couplings are present, $A_{\rm CP}(q^2)$ can be enhanced up to 6% at low q^2. On the other hand, its value at high q^2 can be as high as 12%. $A_{\rm CP}(q^2)$ can have either sign at both low and high q^2. At high q^2, the magnitude of $A_{\rm CP}(q^2)$ is almost independent of q^2.

- When only $R'_{V,A}$ couplings are present, $A_{\rm CP}(q^2)$ cannot be enhanced above the SM value. This is because $R'_{V,A}$ couplings do not contribute to the numerator of $A_{\rm CP}(q^2)$ in Eq. (5.13). They can only affect the DBR, which may be enhanced by up to 50%, thus decreasing $A_{\rm CP}(q^2)$.

- In the presence of $R_{V,A}$ couplings, ΔA_{FB} can be enhanced up to 3% at low q^2. At high q^2, the enhancement can be up to 12%. The impact of $R'_{V,A}$ couplings is negligible ($< 1\%$).

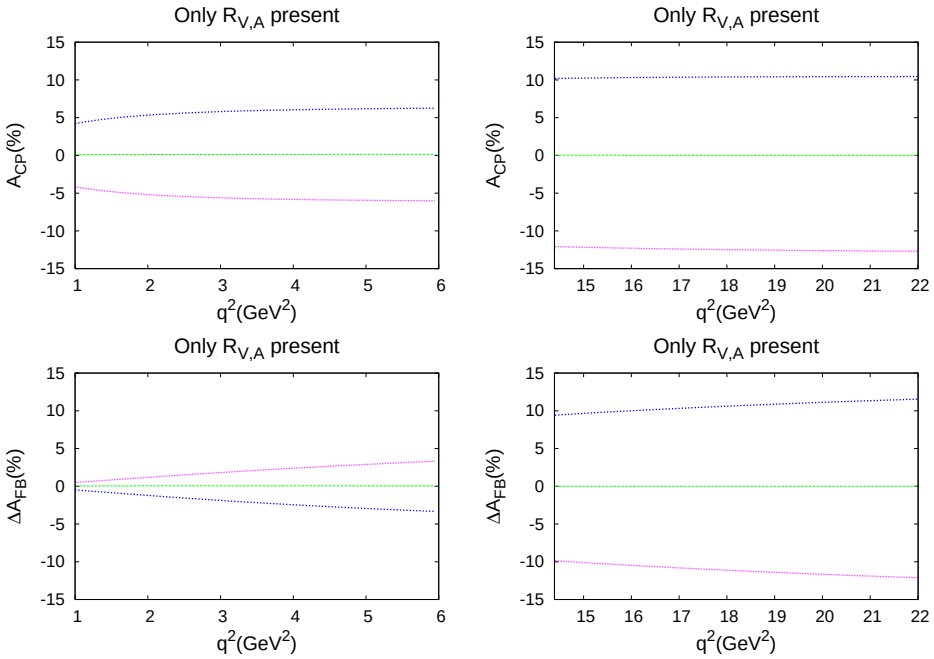

Figure 5.1: The left (right) panels of the figure show $A_{\rm CP}(q^2)$ and ΔA_{FB} for $\bar{B}^0_d \to X_s\mu^+\mu^-$ in the low-q^2 (high-q^2) region, in the scenario where only (R_V, R_A) couplings are present. The green line corresponds to the SM prediction. The other lines show predictions for some representative values of the NP parameters (R_V, R_A). For example, the blue curve in the low-q^2 and high-q^2 regions for the $A_{\rm CP}$ plot corresponds to $(5.68e^{i2.13}, 2.64e^{-i0.04})$ and $(4.29e^{i1.68}, 4.15e^{-i0.26})$, respectively, whereas the blue curve in the low-q^2 and high-q^2 regions for the $\Delta A_{\rm FB}$ plot corresponds to $(1.80e^{i2.91}, 5.45e^{i0.90})$ and $(1.69e^{-i3.08}, 6.83e^{-i0.91})$, respectively.

5.5 $\bar{B}^0_s \to \mu^+\mu^-\gamma$

Although $\bar{B}^0_s \to \mu^+\mu^-\gamma$ requires the emission of an additional photon as compared to $\bar{B}^0_s \to \mu^+\mu^-$, which suppresses the branching ratio (BR) by a factor of α_{em}, the photon emission also frees it from helicity suppression, making its BR much larger than $\bar{B}^0_s \to \mu^+\mu^-$. The SM prediction for the BR in the range $q^2 \leq 9.5$ GeV^2 and $q^2 \geq 15.9$ GeV^2 is $\approx 18.9 \times 10^{-9}$ [245]. As argued in Ref. [220], if we choose 2 GeV$^2 \leq q^2 \leq 6$ GeV^2 and 14.4 GeV$^2 \leq q^2 \leq 25$ GeV^2 as the low-q^2 and high-q^2 regions, respectively, then the dominating contribution comes from the diagrams in which the final-state photon is emitted either from the b or the s quark, and the $\bar{B}^0_s \to \mu^+\mu^-\gamma$ decay is governed by the same $b \to s\mu^+\mu^-$ effective Hamiltonian as the other decays considered in this chapter.

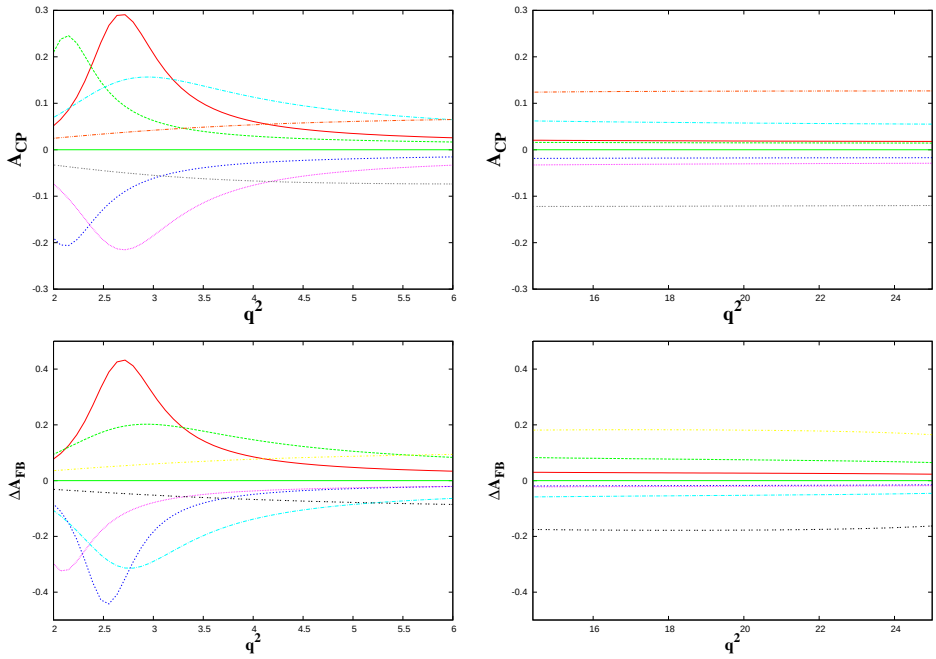

Figure 5.2: The left (right) panels of the figure show $A_{\rm CP}(q^2)$ and ΔA_{FB} for $\bar{B}_s^0 \to \mu^+\mu^-\gamma$ in the low-q^2 (high-q^2) region, in the scenario where only (R_V, R_A) couplings are present. For example, the blue curve in the low-q^2 and high-q^2 regions for the $A_{\rm CP}$ plot corresponds to $(2.95e^{-i0.38}, 4.56e^{-i0.04})$, whereas the blue curve in the low-q^2 and high-q^2 regions for the $\Delta A_{\rm FB}$ plot corresponds to $(1.60e^{-i0.08}, 4.14e^{-i0.12})$.

The CP asymmetry in $\bar{B}_s^0 \to \mu^+\mu^-\gamma$ is given in Eq. (5.13), where dB/dx_γ and $d\overline{B}/dx_\gamma$ are the DBRs of $\bar{B}_s^0 \to \mu^+\mu^-\gamma$ and its CP-conjugate $B_s^0 \to \mu^+\mu^-\gamma$, respectively. The expression for (dB/dx_γ) has been given in Ref. [220]. The CP asymmetry in A_{FB} is given in Eq. (5.14), where the definition of A_{FB} is given in Ref. [220], and $\overline{A}_{FB}$ is the analogous quantity for the CP-conjugate decay.

The CP asymmetry in the DBR of $B_s \to \mu\mu\gamma$ was studied in Refs. [226, 227], albeit only for the new-physics cases where $C_7 = -C_7^{\rm SM}, C_9 = -C_9^{\rm SM}$ and $C_{10} = -C_{10}^{\rm SM}$, and naturally only for VA operators. Here, we include a complete discussion of the possible enhancement of the asymmetry for all allowed values of C_9 and C_{10}, and in the presence of SP and T operators. In addition, we study the CP-violating asymmetry in A_{FB}, which also turns out to give possibly significant NP signals.

Fig. 5.2 shows $A_{\rm CP}(q^2)$ and $\Delta A_{FB}(q^2)$ for $\bar{B}_s^0 \to \mu^+\mu^-\gamma$ in the presence of new VA couplings. We make the following observations:

- When only $R_{V,A}$ couplings are present, at low q^2 the magnitude of $A_{\rm CP}(q^2)$ can be enhanced up to 30% at certain q^2 values. At high q^2, the magnitude of $A_{\rm CP}(q^2)$

is almost independent of q^2, and can be enhanced to about 13%. The asymmetry can have either sign at both low and high q^2.

- When only $R'_{V,A}$ couplings are present, $A_{\rm CP}(q^2)$ cannot be enhanced in magnitude to more than 1.5% at low q^2, or more than 3% at high q^2. The detection of NP of this kind is therefore expected to be very difficult in this channel. When both primed and unprimed VA couplings are present, the results are the same as those obtained with only $R_{V,A}$ couplings.

- The behaviour of $\Delta A_{FB}(q^2)$ is similar to that of $A_{CP}(q^2)$. This quantity can be enhanced up to 40% for some values in the low-q^2 region. It can be as high as 18% throughout the high-q^2 region. The impact of $R'_{V,A}$ couplings is negligible ($< 1\%$).

The new VA operators can therefore enhance the asymmetries $A_{\rm CP}(q^2)$ and $\Delta A_{FB}(q^2)$ in $\bar{B}_s^0 \to \mu^+\mu^-\gamma$ to $\sim$ 10% throughout the q^2 region. For a branching ratio of $O(2 \times 10^{-8})$, a measurement of a CP asymmetry of 10% at the 3σ level would require $\sim 10^{10}$ B mesons. It should therefore be possible to measure a CP asymmetry at the level of a few per cent at future colliders such as the Super-B factories [246–248].

5.6 $\bar{B}_d^0 \to \bar{K}\mu^+\mu^-$

The CP asymmetry in $\bar{B}_d^0 \to \bar{K}\mu^+\mu^-$ is defined in a manner similar to that in Eq. (5.13), where dB/dz and $d\overline{B}/dz$ are the DBRs of $\bar{B}_d^0 \to \bar{K}\mu^+\mu^-$ and its CP-conjugate $B_d^0 \to K\mu^+\mu^-$, respectively. The expression for (dB/dz) has been given in Ref. [220]. A model-independent analysis of the CP asymmetry in the DBR, with specific chosen values of VA operators, was carried out in Ref. [228]. However, the constraints on the NP operators, coming from the measured branching ratio of $\bar{B}_d^0 \to X_s\mu^+\mu^-$, were not taken into account. Here, in addition to taking these constraints into account, we also consider new SP and T operators, and extend the analysis to study the CP asymmetry in A_{FB}.

The CP asymmetry in A_{FB} is given in Eq. (5.14), where the definition of A_{FB} is as given in Ref. [220], while $\overline{A}_{FB}$ is the analogous quantity for the CP-conjugate decay. Now, the decay mode $\bar{B}_d^0 \to \bar{K}\mu^+\mu^-$ is unique because the forward-backward asymmetry of muons is predicted to vanish exactly in the SM. This is due to the fact that the $\bar{B}_d^0 \to \bar{K}$ hadronic matrix element does not have any axial-vector contribution. A_{FB} can therefore have a nonzero value only if it receives a contribution from new physics. However, even in the presence of NP, the expressions in Ref. [220] indicate that the only term contributing to $\Delta A_{FB}(q^2)$ is that with VA+SP NP operators, and this is suppressed by the factor m_μ/m_b. As a result, one does not expect a significant enhancement in ΔA_{FB} from any Lorentz structure of NP.

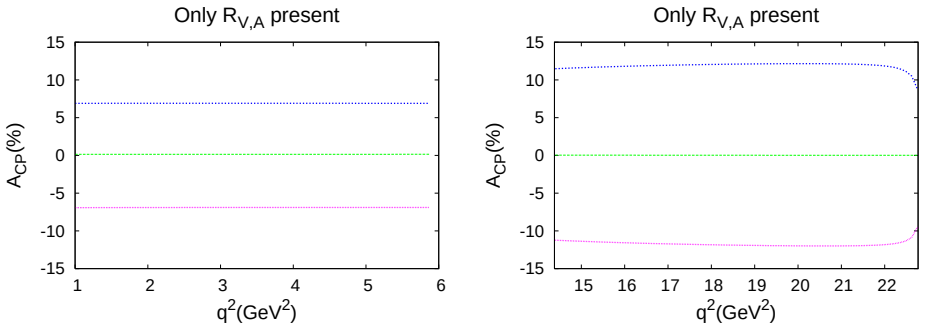

Figure 5.3: The left (right) panel of the figure shows $A_{\rm CP}(q^2)$ for $\bar{B}_d^0 \to \bar{K}\mu^+\mu^-$ in the low-q^2 (high-q^2) region, in the scenario where only (R_V, R_A) terms are present. The green line corresponds to the SM prediction. The other lines show predictions for some representative values of the NP parameters (R_V, R_A). For example, the blue curve in the low-q^2 and high-q^2 regions corresponds to $(5.97e^{i2.23}, 3.08e^{-i0.05})$ and $(6.47e^{i2.30}, 3.11e^{i0.48})$, respectively.

Fig. 5.3 shows $A_{\rm CP}(q^2)$ for $\bar{B}_d^0 \to \bar{K}\mu^+\mu^-$ in the presence of new VA couplings. We make the following observations:

- When only $R_{V,A}$ couplings are present, $A_{\rm CP}(q^2)$ can be enhanced up to 7% at low q^2. On the other hand, its value at high q^2 can be as high as 12%. $A_{\rm CP}(q^2)$ can have either sign at both low and high q^2, and its magnitude is almost independent of q^2 in these regions.

- When only $R'_{V,A}$ couplings are present, $A_{\rm CP}(q^2)$ can be enhanced up to 4% at low q^2. On the other hand, its value at high q^2 can be as high as 12%. $A_{\rm CP}(q^2)$ can have either sign at both low and high q^2, and its magnitude is almost independent of q^2 in these regions.

- When both primed and unprimed VA couplings are present, the results are the same as those obtained with only $R_{V,A}$ couplings.

For a $\bar{B}_d^0 \to \bar{K}\mu^+\mu^-$ branching ratio of $O(0.5 \times 10^{-6})$, a measurement of a CP asymmetry of 1% at the 3σ level would require $\sim 10^{11}$ B mesons. It should therefore be possible to measure a CP asymmetry at the level of a few per cent at future colliders such as the Super-B factories [246–248].

5.7 $\bar{B}_d^0 \to \bar{K}^*\mu^+\mu^-$

The complete three-angle distribution for the decay $\bar{B}^0 \to \bar{K}^{*0}(\to K^-\pi^+)\mu^+\mu^-$ in the presence of NP can be expressed in terms of q^2, two polar angles θ_μ and θ_K, and the

azimuthal angle ϕ between the planes of the dimuon and $K\pi$ decays:

$$\frac{d^4\Gamma^{\bar{B}}}{dq^2 d\cos\theta_\mu d\cos\theta_K d\phi} = N_F \times$$
$$\Big\{ \quad \cos^2\theta_K\Big(I_1^0 + I_2^0\cos 2\theta_\mu + I_3^0\cos\theta_\mu\Big) + \sin^2\theta_K\Big(I_1^T + I_2^T\cos 2\theta_\mu + I_3^T\cos\theta_\mu$$
$$+ I_4^T\sin^2\theta_\mu\cos 2\phi + I_5^T\sin^2\theta_\mu\sin 2\phi\Big) + \sin 2\theta_K\Big(I_1^{LT}\sin 2\theta_\mu\cos\phi$$
$$+ I_2^{LT}\sin 2\theta_\mu\sin\phi + I_3^{LT}\sin\theta_\mu\cos\phi + I_4^{LT}\sin\theta_\mu\sin\phi\Big)\Big\} \,. \tag{5.15}$$

The expressions for the normalization N_F and the I's are given in Ref. [220]. The I's are functions of the couplings, kinematic variables and form factors. The definitions of the angles in $\bar{B}_d^0 \to \bar{K}^*\mu^+\mu^-$ involve the directions of the μ^+ and $\overline{K}^*$. For the CP-conjugate decay $B^0 \to K^{*0}(\to K^+\pi^-)\mu^+\mu^-$, one defines these angles relative to the directions of the μ^- and K^*. The $\bar{I}$'s can be obtained from the I's by replacing $\theta_\mu \to \theta_\mu - \pi$ and $\phi \to -\phi$, and changing the signs of the weak phases.

The CP asymmetries in the branching ratio and forward-backward asymmetry were analyzed in Ref. [232] with the measurement of $B \to X_s\gamma$ and the limit on the $\bar{B}_d^0 \to \bar{K}^*\mu^+\mu^-$ branching ratio available then. An analysis of CP asymmetries in $\bar{B}_d^0 \to \bar{K}^*\mu^+\mu^-$ in the low-q^2 region was also performed earlier in Ref. [234]. We extend this analysis by including T operators, and present our results for all asymmetries, in both the low-q^2 and high-q^2 regions.

A detailed discussion of the CP-conserving observables in this decay distribution can be found in Ref. [220]. In this section we consider the direct CP asymmetries in the differential branching ratio (DBR), the forward-backward asymmetry A_{FB}, the longitudinal polarization fraction f_L, and the angular asymmetries $A_T^{(2)}$ and A_{LT}. We also examine the triple-product CP asymmetries $A_T^{(im)}$ and $A_{LT}^{(im)}$, which were not considered in Ref. [220] since they identically vanish in the CP-conserving limit (no strong or weak phases), regardless of the presence of NP.

5.7.1 Direct CP asymmetries in the DBR and A_{FB}

The direct CP asymmetry in the differential branching ratio is defined as

$$A_{CP}(q^2) \;=\; \frac{(d\Gamma^{\bar{B}}/dq^2) - (d\Gamma^B/dq^2)}{(d\Gamma^{\bar{B}}/dq^2) + (d\Gamma^B/dq^2)} \,, \tag{5.16}$$

where

$$\frac{d\Gamma^{\bar{B}}}{dq^2} \;=\; \frac{8\pi N_F}{3}(A_L^{\bar{B}} + A_T^{\bar{B}}) \,. \tag{5.17}$$

Here the longitudinal and transverse polarization amplitudes $A_L^{\bar{B}}$ and $A_T^{\bar{B}}$ are obtained from Eq. (5.15):

$$A_L^{\bar{B}} = \Big(I_1^0 - \frac{1}{3}I_2^0\Big), \quad A_T^{\bar{B}} = 2\Big(I_1^T - \frac{1}{3}I_2^T\Big) \ . \tag{5.18}$$

The expressions for A_L^B and A_T^B of the CP-conjugate mode can be obtained by replacing the I's with $\bar{I}$'s.

The forward-backward asymmetry in $\bar{B}_d^0 \to \bar{K}^*\mu^+\mu^-$ has recently been measured, and shows features that may indicate a deviation from the SM. This measured quantity is actually the CP-averaged forward-backward asymmetry A_{FB}. However, the difference between the measurement of this quantity in $\bar{B}_d^0 \to \bar{K}^*\mu^+\mu^-$ and its CP-conjugate mode may also reveal the presence of NP. This CP asymmetry is quantified as

$$\Delta A_{FB}(q^2) = A_{FB}^{\bar{B}}(q^2) + A_{FB}^{B}(q^2) \ , \tag{5.19}$$

where

$$A_{FB}^{\bar{B}(B)}(q^2) = \frac{\int_0^1 d\cos\theta_\mu \frac{d^2\Gamma^{\bar{B}(B)}}{dq^2 d\cos\theta_\mu} - \int_{-1}^0 d\cos\theta_\mu \frac{d^2\Gamma^{\bar{B}(B)}}{dq^2 d\cos\theta_\mu}}{\int_0^1 d\cos\theta_\mu \frac{d^2\Gamma^{\bar{B}(B)}}{dq^2 d\cos\theta_\mu} + \int_{-1}^0 d\cos\theta_\mu \frac{d^2\Gamma^{\bar{B}(B)}}{dq^2 d\cos\theta_\mu}} \ . \tag{5.20}$$

It can be obtained by integrating over the two angles θ_K and ϕ in Eq. (5.15).

Fig. 5.4 shows $A_{CP}(q^2)$ and $\Delta A_{FB}(q^2)$ for $\bar{B}_d^0 \to \bar{K}^*\mu^+\mu^-$ in the presence of new VA couplings. We make the following observations:

- If only $R_{V,A}$ couplings are present, $A_{CP}(q^2)$ can be enhanced up to 5% at low q^2, and up to 14 % at high q^2. $\Delta A_{FB}(q^2)$ can be enhanced up to 3% at low q^2, and up to 11 % at high q^2. Both $A_{CP}(q^2)$, and $\Delta A_{FB}(q^2)$ can have either sign at both low and high q^2.

- If only $R'_{V,A}$ couplings are present, $A_{CP}(q^2)$ can be enhanced up to 3% at low q^2, and up to 7% at high q^2. $\Delta A_{FB}(q^2)$ can be enhanced up to 1% at low q^2, and up to 4 % at high q^2. Both $A_{CP}(q^2)$, and $\Delta A_{FB}(q^2)$ can have either sign at both low and high q^2.

- When both primed and unprimed VA couplings are present, $A_{CP}(q^2)$ can be enhanced up to 9% at low q^2, and up to 14 % at high q^2. $\Delta A_{FB}(q^2)$ can be enhanced up to 6% at low q^2, and up to 19 % at high q^2. Both $A_{CP}(q^2)$, and $\Delta A_{FB}(q^2)$ can have either sign at both low and high q^2 (see Fig. 5.4).

These observations are consistent with the rough expectations in Ref. [232] about the effect of VA operators.

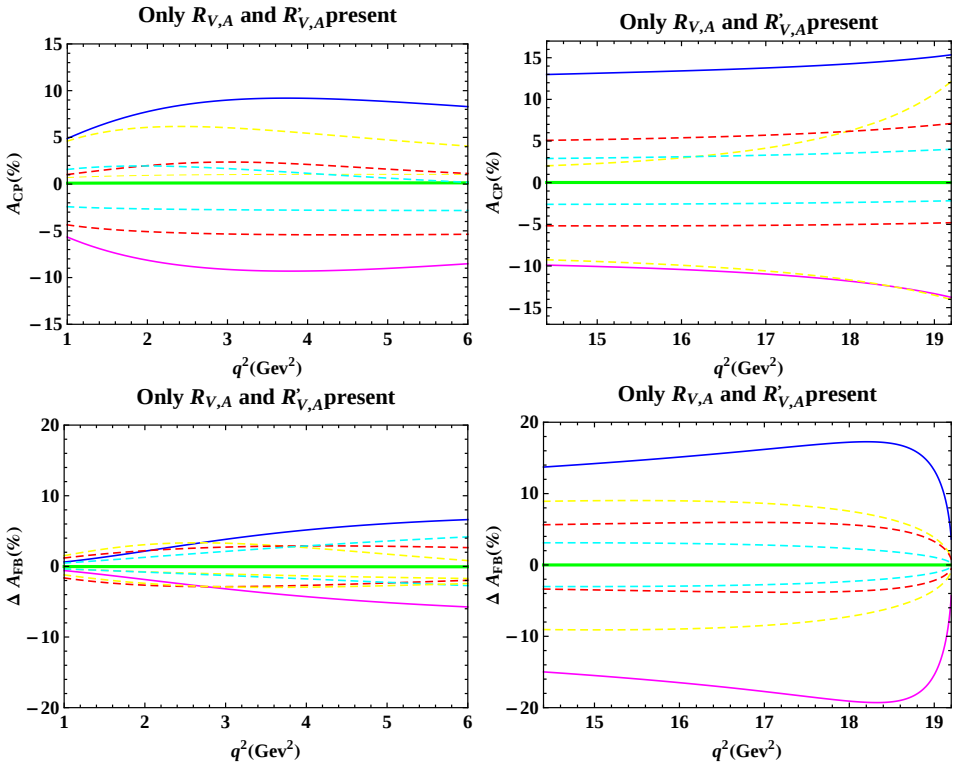

Figure 5.4: The left (right) panels of the figure show $A_{CP}(q^2)$ and $\Delta A_{FB}(q^2)$ for $\bar{B}^0_d \to \bar{K}^*\mu^+\mu^-$ in the low-q^2 (high-q^2) region, in the scenario where (R_V, R_A, R'_V, R'_A) terms are all present. The green line corresponds to the SM prediction. The other lines show predictions for some representative values of the NP parameters. For example, the blue curve for $A_{CP}(q^2)$ in the low-q^2 and high-q^2 regions corresponds to $(2.77e^{i1.83}, 2.08e^{i0.5}, 3.8e^{i0.08}, 1.23e^{-i2.74})$ and $(5.88e^{i2.29}, 1.66e^{i0.82}, 3.49e^{i0.36}, 1.02e^{i0.98})$, respectively. The blue curve for $\Delta A_{FB}(q^2)$ in the low-q^2 and high-q^2 regions corresponds to $(1.56e^{-i2.59}, 1.80e^{-i0.35}, 4.23e^{i0.67}, 1.29e^{i1.43})$ and $(3.21e^{i2.61}, 1.38e^{i2.26}, 5.55e^{i0.69}, 3.03e^{i1.92})$, respectively.

5.7.2 Direct CP asymmetry in the polarization fraction f_L

The CP asymmetry in the longitudinal polarization fraction f_L is defined as

$$\Delta f_L = f_L^{\bar{B}} - f_L^B \,, \tag{5.21}$$

where

$$f_L^{\bar{B}(B)} \;=\; \frac{A_L^{\bar{B}(B)}}{A_L^{\bar{B}(B)} + A_T^{\bar{B}(B)}} \,. \tag{5.22}$$

Fig. 5.5 shows $\Delta f_L(q^2)$ for $\bar{B}_d^0 \to \bar{K}^* \mu^+ \mu^-$ in the presence of new VA couplings. We make the following observations:

- If only $R_{V,A}$ couplings are present, $\Delta f_L(q^2)$ can be enhanced up to 2% at very low q^2. On the other hand, $\Delta f_L(q^2)$ is almost the same as the SM at high q^2. It can have either sign at both low and high q^2.
- If only $R'_{V,A}$ couplings are present, $\Delta f_L(q^2)$ can be enhanced up to 2% at both low and high q^2. It can have either sign at both low and high q^2.
- When both primed and unprimed VA couplings are present, $\Delta f_L(q^2)$ can be enhanced up to 9% at low q^2, and up to 6% at high q^2. It can have either sign at both low and high q^2 (see Fig. 5.5).

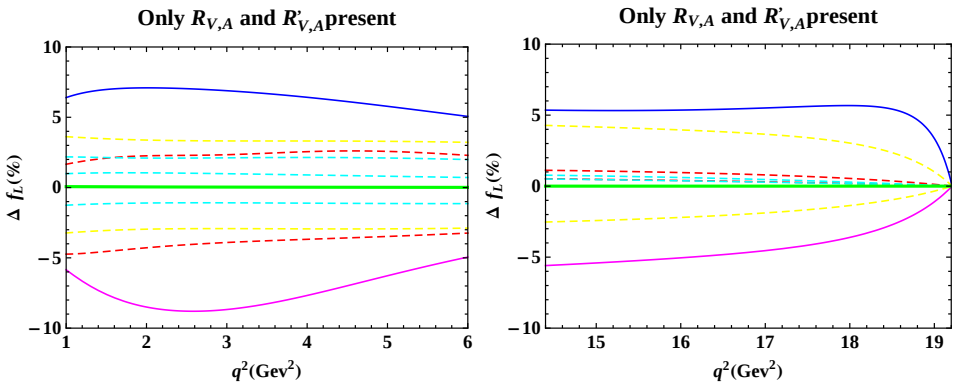

Figure 5.5: The left (right) panel of the figure shows $\Delta f_L(q^2)$ for $\bar{B}_d^0 \to \bar{K}^* \mu^+ \mu^-$ in the low-q^2 (high-q^2) region, in the scenario where (R_V, R_A, R'_V, R'_A) terms are all present. For example, the blue curve in the low-q^2 and high-q^2 regions corresponds to $(2.78e^{i2.98}, 2.19e^{-i0.77}, 6.91e^{-i0.29}, 3.34e^{-i0.56})$.

5.7.3 Direct CP asymmetries in the angular asymmetries $A_T^{(2)}$ and A_{LT}

The transverse asymmetry $A_T^{(2)\bar{B}(B)}$ is defined [249] through the double differential decay rate as

$$\frac{d^2\Gamma^{\bar{B}(B)}}{dq^2 d\phi} = \frac{1}{2\pi}\frac{d\Gamma^{\bar{B}(B)}}{dq^2}\Big[1 + f_T^{\bar{B}(B)}\left(A_T^{(2)\bar{B}(B)}\cos 2\phi + A_T^{(im)\bar{B}(B)}\sin 2\phi\right)\Big] \,. \quad (5.23)$$

It can be obtained by integrating Eq. (5.15) over the two polar angles θ_μ and θ_K. Here $A_T^{(im)\bar{B}(B)}$ is a triple product, and is discussed separately below. In terms of the coupling constants and matrix elements defined in Ref. [220], $A_T^{(2)\bar{B}(B)}$ can be expressed as

$$A_T^{(2)\bar{B}} = \frac{4I_4^T}{3A_T^{\bar{B}}}, \quad A_T^{(2)B} = \frac{4\bar{I}_4^T}{3A_T^B}. \tag{5.24}$$

While $A_T^{(2)\bar{B}}$ ($A_T^{(2)B}$) is finite even in the CP-conserving limit (and was discussed in Ref. [220]), a CP asymmetry may be defined through the difference

$$\Delta A_T^{(2)} \equiv A_T^{(2)\bar{B}} - A_T^{(2)B}. \tag{5.25}$$

Fig. 5.6 shows $\Delta A_T^{(2)}$ for $\bar{B}_d^0 \to \bar{K}^*\mu^+\mu^-$ in the presence of new VA couplings. We make the following observations:

- If only $R_{V,A}$ couplings are present, $\Delta A_T^{(2)}$ cannot be enhanced more than 1% at both low and high q^2. It can have either sign at both low and high q^2.
- If only $R'_{V,A}$ couplings are present, $\Delta A_T^{(2)}$ can be enhanced up to 4% at low q^2, and up to 6% high q^2. It can have either sign at both low and high q^2.
- When both primed and unprimed VA couplings are present, $\Delta A_T^{(2)}$ can be enhanced up to 11% at low q^2, and up to 12% at high q^2. It can have either sign at both low and high q^2 (see Fig. 5.6).

The longitudinal-transverse asymmetry $A_{LT}^{\bar{B}(B)}$ is defined through

$$\frac{d^2\Gamma_{LT}^{\bar{B}(B)}}{dq^2 d\phi} = \frac{d\Gamma^{\bar{B}(B)}}{dq^2}\left(A_{LT}^{(re)\bar{B}(B)}\cos\phi + A_{LT}^{(im)\bar{B}(B)}\sin\phi\right), \tag{5.26}$$

where

$$\frac{d^2\Gamma_{LT}^{\bar{B}(B)}}{dq^2 d\phi} = \int_0^1 d\cos\theta_K \frac{d^3\Gamma^{\bar{B}(B)}}{dq^2 d\cos\theta_K d\phi} - \int_{-1}^0 d\cos\theta_K \frac{d^3\Gamma^{\bar{B}(B)}}{dq^2 d\cos\theta_K d\phi}. \tag{5.27}$$

Here $A_{LT}^{(im)\bar{B}(B)}$ is a triple product, and is discussed separately below. In terms of the coupling constants and matrix elements defined in Ref. [220], $A_{LT}^{(re)\bar{B}(B)}$ can be expressed as

$$A_{LT}^{(re)\bar{B}} = \frac{I_3^{LT}}{4(A_L^{\bar{B}} + A_T^{\bar{B}})}, \quad A_{LT}^{(re)B} = -\frac{\bar{I}_3^{LT}}{4(A_L^B + A_T^B)}. \tag{5.28}$$

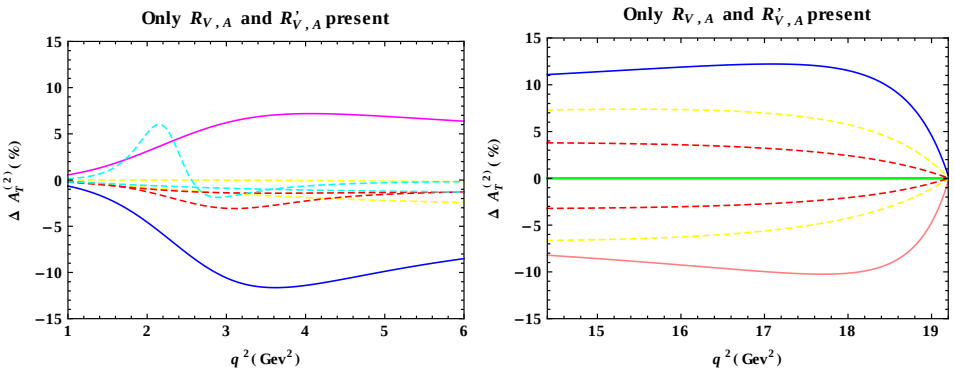

Figure 5.6: The left (right) panel of the figure shows $\Delta A_T^{(2)}(q^2)$ for $\bar{B}_d^0 \to \bar{K}^* \mu^+ \mu^-$ in the low-q^2 (high-q^2) region, in the scenario where (R_V, R_A, R'_V, R'_A) terms are all present. The green line corresponds to the SM prediction. The other lines show predictions for some representative values of the NP parameters. For example, the blue curve in the low-q^2 and high-q^2 regions corresponds to $(0.11e^{i2.18}, 2.66e^{-i1.31}, 4.3e^{i0.03}, 0.23e^{-i2.27})$ and $(2.32e^{i2.51}, 4.89e^{i1.27}, 3.12e^{i0.42}, 0.14e^{-i1.55})$, respectively.

Note that $A_{LT}^{(re)B} = -A_{LT}^{(re)\bar{B}}$ in the CP-conserving limit. Thus, a CP asymmetry may be defined through the sum

$$\Delta A_{LT}(q^2) \equiv A_{LT}^{(re)\bar{B}}(q^2) + A_{LT}^{(re)B}(q^2) \; . \tag{5.29}$$

We now assume the presence of new VA couplings. However, we find that these couplings cannot enhance $\Delta A_{LT}(q^2)$ to more than 3% at both low and high q^2.

Note that $\Delta A_{LT}(q^2)$ is related to the observable A_5^D in Ref. [233]: $\Delta A_{LT}(q^2) \approx A_5^D/4$. Our limit of 3% on the maximum value of $\Delta A_{LT}(q^2)$ is then consistent with the limit of 0.07 on the average value $\langle A_5^D \rangle$ over the low-q^2 region, as calculated in Ref. [233].

5.7.4 CP-violating triple-product asymmetries

In this subsection, we consider the triple products (TPs) in the decays $\bar{B}^0 \to \bar{K}^{*0}(\to K^- \pi^+)\mu^+\mu^-$ and $B^0 \to K^{*0}(\to K^+\pi^-)\mu^+\mu^-$. For the decaying $\bar{B}$ meson, the TP is proportional to $(\hat{n}_K \times \hat{n}_\mu) \cdot \hat{n}_z$ in its rest frame, where the unit vectors are given in terms of the momenta of the final-state particles as

$$\hat{n}_K \;=\; \frac{\hat{p}_{K^-} \times \hat{p}_{\pi^+}}{|\hat{p}_{K^-} \times \hat{p}_{\pi^+}|}, \quad \hat{n}_z = \frac{\hat{p}_{K^-} + \hat{p}_{\pi^+}}{|\hat{p}_{K^-} + \hat{p}_{\pi^+}|}, \quad \hat{n}_\mu = \frac{\hat{p}_{\mu^-} \times \hat{p}_{\mu^+}}{|\hat{p}_{\mu^-} \times \hat{p}_{\mu^+}|} \; . \tag{5.30}$$

In terms of the azimuthal angle ϕ, one gets

$$\cos\phi \;=\; \hat{n}_K \cdot \hat{n}_\mu \; , \quad \sin\phi = (\hat{n}_K \times \hat{n}_\mu) \cdot \hat{n}_z \; , \tag{5.31}$$

and hence the quantities that are coefficients of $\sin\phi$ (or of $\sin 2\phi = 2\sin\phi\cos\phi$) are the TPs.

As noted above, while the angular distribution for the $\bar{B}$ decay involves ϕ, for B it involves $-\phi$. Thus, the CP-violating triple-product asymmetry is proportional to the *sum* of $\bar{B}$ and B TPs.

The first TP is $A_T^{(im)\bar{B}(B)}$, introduced above in Eq. (5.23). In terms of the coupling constants and matrix elements defined in Ref. [220], $A_T^{(im)\bar{B}(B)}$ can be written as

$$A_T^{(im)\bar{B}} = \frac{4I_5^T}{3A_T^{\bar{B}}}, \quad A_T^{(im)B} = -\frac{4\bar{I}_5^T}{3A_T^B} . \tag{5.32}$$

We observe that $A_T^{(im)}$ depends only on the VA couplings. The CP-violating triple-product asymmetry is

$$A_T^{(im)} = \frac{1}{2}(A_T^{(im)\bar{B}} + A_T^{(im)B}) . \tag{5.33}$$

Fig. 5.7 shows $A_T^{(im)}(q^2)$ for $\bar{B}_d^0 \to \bar{K}^*\mu^+\mu^-$ in the presence of new VA couplings. We make the following observations:

- If only $R_{V,A}$ couplings are present, $A_T^{(im)}(q^2)$ can be enhanced up to 5% at low q^2 and can have either sign. On the other hand, $A_T^{(im)}(q^2)$ is almost same as the SM prediction ($\simeq 0$) at high q^2.

- If only $R'_{V,A}$ couplings are present, $A_T^{(im)}(q^2)$ can be enhanced up to 49% at low q^2, and up to 46% at high q^2. It can have either sign at both low and high q^2.

- When both primed and unprimed VA couplings are present, the results for $A_T^{(im)}(q^2)$ are almost the same as those obtained with only $R'_{V,A}$ couplings (see Fig. 5.7).

The second TP is $A_{LT}^{(im)\bar{B}(B)}$, introduced above in Eq. (5.26). In terms of the coupling constants and matrix elements defined in Ref. [220], $A_{LT}^{(im)\bar{B}(B)}$ can be written as

$$A_{LT}^{(im)\bar{B}} = \frac{I_4^{LT}}{4(A_L^{\bar{B}} + A_T^{\bar{B}})} , \quad A_{LT}^{(im)B} = \frac{\bar{I}_4^{LT}}{4(A_L^B + A_T^B)} . \tag{5.34}$$

We observe that A_{LT} depends on the VA couplings, as well as on V-S and SP-T interference terms. The CP-violating triple-product asymmetry is

$$A_{LT}^{(im)} = \frac{1}{2}(A_{LT}^{(im)\bar{B}} - A_{LT}^{(im)B}) . \tag{5.35}$$

Fig. 5.8 shows $A_{LT}^{(im)}(q^2)$ for $\bar{B}_d^0 \to \bar{K}^*\mu^+\mu^-$ in the presence of new VA couplings. We make the following observations:

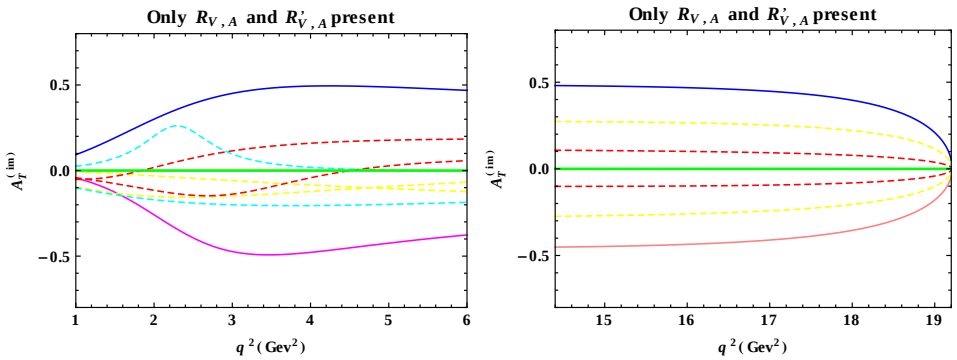

Figure 5.7: The left (right) panel of the figure shows $A_T^{(im)}(q^2)$ for $\bar{B}_d^0 \to \bar{K}^* \mu^+ \mu^-$ in the low-q^2 (high-q^2) region, in the scenario where (R_V, R_A, R'_V, R'_A) terms are all present. The green line corresponds to the SM prediction. The other lines show predictions for some representative values of the NP parameters. For example, the blue curve in the low-q^2 and high-q^2 regions corresponds to $(1.33e^{-i2.96}, 0.78e^{i2.47}, 0.83e^{-i0.27}, 3.15e^{i1.75})$ and $(2.15e^{-i2.77}, 0.7e^{-i2.43}, 8.20e^{-i0.16}, 4.8e^{-i1.62})$, respectively.

- If only $R_{V,A}$ couplings are present, $A_{LT}^{(im)}(q^2)$ can be enhanced up to 6% at very low q^2, and is almost same as the SM prediction (≈ 0) at high q^2. It can have either sign at both low and high q^2.

- If only $R'_{V,A}$ couplings are present, $A_{LT}^{(im)}(q^2)$ can be enhanced up to 8% at low q^2 and is almost same as the SM prediction (≈ 0) at high q^2. It can have either sign at both low and high q^2.

- When both primed and unprimed VA couplings are present, $A_{LT}^{(im)}(q^2)$ can be enhanced up to 10% at low q^2 and up to 0.5% at high q^2. It can have either sign at both low and high q^2 (see Fig. 5.8).

Note that $A_{LT}^{(im)}(q^2)$ is related to the observable A_7^D in Ref. [233]: $A_{LT}^{(im)}(q^2) \approx A_7^D/8$. Our limit of 10% on the maximum value of $A_{LT}^{(im)}(q^2)$ is then consistent with the limit of 0.76 on the average value $\langle A_7^D \rangle$ over the low-q^2 region, as calculated in Ref. [233]. However, in addition we present the full q^2-dependence of this quantity.

In principle, $A_{LT}^{(im)\bar{B}(B)}$ can be generated due to NP SP-T interference. However, we find that the effect is tiny: $A_{LT}^{(im)}(q^2)$ can be enhanced up to 0.4% at low q^2 and can have either sign; $A_{LT}^{(im)}(q^2)$ is same as the SM ($\simeq 0$) at high q^2.

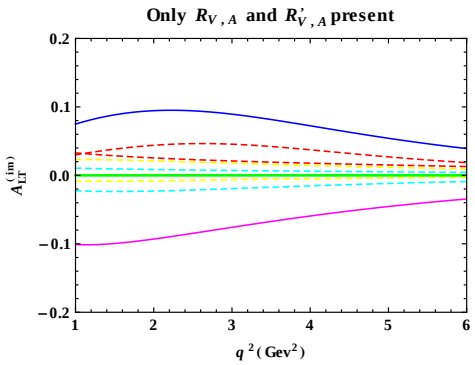

Figure 5.8: The figure shows $A_{LT}^{(im)}(q^2)$ for $\bar{B}_d^0 \to \bar{K}^*\mu^+\mu^-$ in the low-q^2 region, in the scenario where (R_V, R_A, R'_V, R'_A) terms are all present. The green line corresponds to the SM prediction. The other lines show predictions for some representative values of the NP parameters. For example, the blue curve corresponds to $(1.68e^{i1.92}, 2.27e^{i0.53}, 4.22e^{i0.28}, 0.14e^{-i1.91})$.

5.8 Discussion and summary

Even after the successful start of the LHC that will search for new physics (NP) at the TeV scale and beyond, B decays still remain one of the best avenues of detecting indirect NP signals. The copious amount of data on B decays, expected from future experiments like the LHC and super-B factories, will allow us to explore in detail many decay modes that are currently considered to be rare. The combined analysis of many such decay modes will allow us to look for NP in a model-independent manner. We consider all possible Lorentz structures of new physics (NP) in the $b \to s\mu^+\mu^-$ transition, and analyze their effects on the CP-violating observables in (i) $\bar{B}_s^0 \to \mu^+\mu^-$, (ii) $\bar{B}_d^0 \to X_s\mu^+\mu^-$, (iii) $\bar{B}_s^0 \to \mu^+\mu^-\gamma$, (iv) $\bar{B}_d^0 \to \bar{K}\mu^+\mu^-$, (v) $\bar{B}_d^0 \to \bar{K}^*\mu^+\mu^-$, and their CP-conjugate modes. These are the same modes we explored in the previous chapter, where we considered only CP-conserving quantities. We find that for $\bar{B}_s^0 \to \mu^+\mu^-$, the only CP-violating quantities that can be constructed even in principle require the measurement of muon polarization, a task not possible in foreseeable detectors. Therefore, we do not dwell on this mode further. For the rest of the modes, we focus on asymmetries in the branching ratios and forward-backward asymmetries. In $\bar{B}_d^0 \to \bar{K}^*\mu^+\mu^-$, we also explore the direct CP asymmetries in the longitudinal polarization fraction f_L and the angular asymmetries $A_T^{(2)}$ and A_{LT}, as well as the triple-product CP asymmetries $A_T^{(im)}$ and $A_{LT}^{(im)}$. We find that, in almost all cases, the CP-violating observables are sensitive only to new physics which involves VA operators. The VA new physics may therefore be unambiguously identified by a combined analysis of future measurements of these CP-violating observables. Our results are summarized in

Observable	SM	Only new VA	Only new SP	Only new T
$\bar{B}^0_d \to X_s\mu^+\mu^-$				
$A_{\rm CP}$	• $10^{-3} \to 10^{-4}$ (low→high q^2)	• $(6 \to 12)\%$ (low→high q^2)	• Marginal S	• Marginal S/E
ΔA_{FB}	$10^{-4} \to 10^{-5}$ (low→high q^2)	• $(3 \to 12)\%$ (low→high q^2)	• $< 1\%$	No effect
$\bar{B}^0_s \to \mu^+\mu^-\gamma$				
$A_{\rm CP}$	• $10^{-3} \to 10^{-4}$ (low→high q^2)	• $(30 \to 13)\%$ (low→high q^2)	No effect	• $< 1\%$
ΔA_{FB}	$10^{-4} \to 10^{-5}$ (low→high q^2)	• $(40 \to 18)\%$ (low→high q^2)	No effect	• $< 1\%$
$\bar{B}^0_d \to \bar{K}\mu^+\mu^-$				
$A_{\rm CP}$	• $10^{-3} \to 10^{-4}$ (low→high q^2)	• $(7 \to 12)\%$ (low→high q^2)	• Marginal S	• Marginal S/E
ΔA_{FB}	Zero	No effect	• $< 1\%$	No effect
$\bar{B}^0_d \to \bar{K}^*\mu^+\mu^-$				
$A_{\rm CP}$	• $10^{-3} \to 10^{-4}$ (low→high q^2)	• $(9 \to 14)\%$ (low→high q^2)	No effect	• $< 1\%$
ΔA_{FB}	• $10^{-4} \to 10^{-6}$ (low→high q^2)	• $(6 \to 19)\%$ (low→high q^2)	No effect	• $< 1\%$
Δf_L	• $10^{-4} \to 10^{-7}$ (low→high q^2)	• $(9 \to 16)\%$ (low→high q^2)	No effect	• $< 1\%$
$\Delta A_T^{(2)}$	Zero	• $\sim 12\%$	No effect	No effect
ΔA_{LT}	Zero	• $< 3\%$	No effect	No effect
$A_T^{(im)}$	Zero	• $\sim 50\%$	No effect	No effect
$A_{LT}^{(im)}$	Zero	• $\sim 10\%$	No effect	No effect

Table 5.1: The effect of NP couplings on observables. E: enhancement, S: suppression. The numbers given are optimistic estimates.

Table 5.1. We determine the constraints on the coupling constants in the effective NP operators by using the currently available data. On the basis of these limits and general arguments, we expect that the CP-violating quantities in most of the modes can only

be sensitive to the vector-axial vector (VA) couplings, while the scalar-pseudoscalar (SP) and the tensor (T) NP operators can only contribute, if at all, to certain TP asymmetries. Our later detailed exploration of the allowed parameter space for all the NP couplings vindicates this argument. The effects of SP and T NP operators are therefore discussed only briefly in this chapter.

Bibliography:

[209] A. K. Alok, A. Datta, A. Dighe, M. Duraisamy, D. Ghosh and D. London, "New Physics in $b \to s\mu^+\mu^-$: CP-Violating Observables," JHEP **1111**, 122 (2011) [arXiv:1103.5344 [hep-ph]].

[210] B. Aubert *et al.* [BABAR Collaboration], "Rates, polarizations, and asymmetries in charmless vector-vector B meson decays," *Phys. Rev. Lett.* **91**, 171802 (2003) [arXiv:hep-ex/0307026].

[211] K. F. Chen *et al.* [Belle Collaboration], "Measurement of branching fractions and polarization in $B \to \phi K^{(*)}$ decays," *Phys. Rev. Lett.* **91**, 201801 (2003) [arXiv:hep-ex/0307014].

[212] J. T. Wei *et al.* [BELLE Collaboration], "Measurement of the Differential Branching Fraction and Forward-Backword Asymmetry for B $B \to K^* l^+ l^-$," *Phys. Rev. Lett.* **103**, 171801 (2009) [arXiv/0904.0770 [hep-ex]].

[213] B. Aubert *et al.* [BABAR Collaboration], "Angular Distributions in the Decays $B \to K^*\ell^+\ell^-$," *Phys. Rev.* **D 79**, 031102 (2009) [arXiv/0804.4412 [hep-ex]].

[214] A. K. Alok, A. Dighe, D. Ghosh, D. London, J. Matias, M. Nagashima and A. Szynkman, "New-physics contributions to the forward-backward asymmetry in $B \to K^*\mu^+\mu^-$," *JHEP* **1002**, 053 (2010) [arXiv:0912.1382 [hep-ph]].

[215] H. Y. Cheng, C. K. Chua and A. Soni, "CP-violating asymmetries in B^0 decays to $K^+K^-K^0(S)(L)$ and $K^0(S)K^0(S)K^0(S)(L)$," *Phys. Rev.* **D 72**, 094003 (2005) [hep-ph/0506268].

[216] G. Buchalla, G. Hiller, Y. Nir and G. Raz, "The pattern of CP asymmetries in $b \to s$ transitions," *JHEP* **0509**, 074 (2005) [hep-ph/0503151].

[217] E. Lunghi and A. Soni, "Hints for the scale of new CP-violating physics from B-CP anomalies," *JHEP* **0908**, 051 (2009) [arXiv/0903.5059 [hep-ph]].

[218] T. Aaltonen et al. (CDF Collaboration), V. M. Abazov et al. (DO Collaboration), "Combination of DO and CDF Results on $\Delta\Gamma_s$ and the CP-Violating Phase $\beta_s^{J/\psi\phi}$," CDF Note No. CDF/PHYS/BOTTOM/CDFR/9787, 2009; D0 Note No. 5928-CONF, 2009.

[219] V. M. Abazov *et al.* [The D0 Collaboration], "Evidence for an anomalous like-sign dimuon charge asymmetry," arXiv:1005.2757 [hep-ex].

[220] A. K. Alok, A. Datta, A. Dighe, M. Duraisamy, D. Ghosh, D. London and S. U. Sankar, *"New Physics in $b \to s\mu^+\mu^-$: CP-Conserving Observables"*, arXiv:1008.2367 [hep-ph].

[221] D. S. Du and M. Z. Yang, "CP violation for $B \to X_s\, \ell^+\ell^-$ including long distance effects," Phys. Rev. D **54**, 882 (1996) [arXiv:hep-ph/9510267].

[222] T. M. Aliev, D. A. Demir, E. Iltan and N. K. Pak, "The CP Asymmetry in $b \to s l^+ l^-$ Decay," Phys. Rev. D **54**, 851 (1996) [arXiv:hep-ph/9511352].

[223] S. Fukae, "CP asymmetry of $B \to X_s l^+ l^-$ in low invariant mass region," Phys. Rev. D **64**, 054010 (2001) [arXiv:hep-ph/0102041].

[224] A. K. Alok, A. Dighe and S. Ray, "CP asymmetry in the decays $B \to (X_s, X_d)\mu^+\mu^-$ with four generations," Phys. Rev. D **79**, 034017 (2009) [arXiv:0811.1186 [hep-ph]].

[225] A. Soni, A. K. Alok, A. Giri, R. Mohanta and S. Nandi, "SM with four generations: Selected implications for rare B and K decays," Phys. Rev. D **82**, 033009 (2010) [arXiv:1002.0595 [hep-ph]].

[226] I. Balakireva, D. Melikhov, N. Nikitin and D. Tlisov, "Forward-backward and CP-violating asymmetries in rare $B_{d,s} \to (V, \gamma) l^+ l^-$ decays," Phys. Rev. D **81**, 054024 (2010) [arXiv:0911.0605 [hep-ph]].

[227] I. Balakireva, N. Nikitin and D. Tlisov, "Asymmetries in Rare Radiative Leptonic and Semileptonic Decays of B-Mesons," Yad. Fiz. **73**, 1762 (2010) [Phys. Atom. Nucl. **73**, 1713 (2010)].

[228] T. M. Aliev, S. R. Choudhury, A. S. Cornell and N. Gaur, "CP violation in the $B \to K l^+ l^-$ decay," Eur. Phys. J. C **49**, 657 (2007) [arXiv:hep-ph/0506188].

[229] F. Kruger, L. M. Sehgal, N. Sinha and R. Sinha, "Angular distribution and CP asymmetries in the decays $\bar{B} \to K^-\pi^+e^-e^+$ and $\bar{B} \to \pi^-\pi^+e^-e^+$," Phys. Rev. D **61**, 114028 (2000) [Erratum-ibid. D **63**, 019901 (2001)] [arXiv:hep-ph/9907386].

[230] T. M. Aliev, D. A. Demir and M. Savci, "Probing the sources of CP violation via $B \to K^* \ell^+ \ell^-$ decay," Phys. Rev. D **62**, 074016 (2000) [arXiv:hep-ph/9912525].

[231] G. Buchalla, G. Hiller and G. Isidori, "Phenomenology of nonstandard Z couplings in exclusive semileptonic $b \to s$ transitions," Phys. Rev. D **63**, 014015 (2000) [arXiv:hep-ph/0006136].

[232] F. Kruger and E. Lunghi, *"Looking for novel CP violating effects in* $\bar{B} \to K^* \ell^+$ *lepton-"*, *Phys. Rev.* **D 63**, 014013 (2001) [hep-ph/0008210];

[233] C. Bobeth, G. Hiller and G. Piranishvili, "CP Asymmetries in bar $B \to \bar{K}^*(\to \bar{K}\pi)\bar{\ell}\ell$ and Untagged $\bar{B}_s$, $B_s \to \phi(\to K^+K^-)\bar{\ell}\ell$ Decays at NLO," JHEP **0807**, 106 (2008) [arXiv:0805.2525 [hep-ph]].

[234] W. Altmannshofer, P. Ball, A. Bharucha, A. J. Buras, D. M. Straub and M. Wick, "Symmetries and Asymmetries of $B \to K^* \mu^+ \mu^-$ Decays in the Standard Model and Beyond," *JHEP* **0901**, 019 (2009) [arXiv:0811.1214 [hep-ph]].

[235] U. Egede, T. Hurth, J. Matias, M. Ramon and W. Reece, "New physics reach of CP violating observables in the decay $B \to K^* l^+ l^-$," PoS E **PS-HEP2009**, 184 (2009) [arXiv:0912.1349 [hep-ph]].

[236] U. Egede, T. Hurth, J. Matias, M. Ramon and W. Reece, "New physics reach of the decay mode $\bar{B} \to \bar{K}^{*0} \ell^+ \ell^-$," JHEP **1010**, 056 (2010) [arXiv:1005.0571 [hep-ph]].

[237] C. Bobeth, G. Hiller, D. van Dyk, JHEP **1107**, 067 (2011). [arXiv:1105.0376 [hep-ph]].

[238] C. Bobeth, M. Misiak and J. Urban, "Photonic penguins at two loops and m_t-dependence of BR($B \to X_s l^+ l^-$)," *Nucl. Phys.* **B 574**, 291 (2000) [hep-ph/9910220].

[239] C. Amsler *et al.* [Particle Data Group], "Review of particle physics," *Phys. Lett.* **B 667**, 1 (2008).

[240] E. Barberio *et al.* [Heavy Flavor Averaging Group], "Averages of $b-$hadron and $c-$hadron Properties at the End of 2007," arXiv:0808.1297 [hep-ex], and online update at `http://www.slac.stanford.edu/xorg/hfag`

[241] T. Huber, T. Hurth and E. Lunghi, "Logarithmically Enhanced Corrections to the Decay Rate and Forward Backward Asymmetry in $\bar{B} \to X_s \ell^+ \ell^-$," *Nucl. Phys.* **B 802**, 40 (2008) [arXiv:0712.3009 [hep-ph]].

[242] See, for example, A. Datta and D. London, "Triple-product correlations in $B \to V_1 V_2$ decays and new physics," Int. J. Mod. Phys. A **19**, 2505 (2004) [arXiv:hep-ph/0303159].

[243] A. Datta and D. London, "Measuring new-physics parameters in B penguin decays," Phys. Lett. B **595**, 453 (2004) [arXiv:hep-ph/0404130].

[244] A. J. Buras and M. Munz, *"Effective Hamiltonian for $B \to X_s l^+ l^-$ beyond leading logarithms in the NDR and HV schemes"*, Phys. Rev. D **52**, 186 (1995) [arXiv:hep-ph/9501281].

[245] D. Melikhov and N. Nikitin, "Rare radiative leptonic decays $B_{d,s} \to l^+ l^- \gamma$," *Phys. Rev.* **D 70**, 114028 (2004) [arXiv:hep-ph/0410146].

[246] T. E. Browder, T. Gershon, D. Pirjol, A. Soni and J. Zupan, *"New Physics at a Super Flavor Factory"*, arXiv:0802.3201 [hep-ph].

[247] M. Bona *et al.*, *"SuperB: A High-Luminosity Asymmetric e^+e^- Super Flavor Factory. Conceptual Design Report"*, arXiv:0709.0451 [hep-ex].

[248] B. O'Leary *et al.* [SuperB Collaboration], "SuperB Progress Reports – Physics," arXiv:1008.1541 [hep-ex].

[249] F. Kruger and J. Matias, "Probing new physics via the transverse amplitudes of $B_0 \to K_0^*(\to K^-\pi^+) l^+ l^-$ at large recoil," *Phys. Rev.* **D 71**, 094009 (2005) [arXiv:hep-ph/0502060].

Chapter 6

The $B^+ \to \tau^+ \nu_\tau$ anomaly and constraints on Supersymmetric Models

6.1 Introduction

Now that the CERN Large Hadron Collider (LHC) has commenced its long-awaited run and the first physics results have been analyzed and made public [251,252], there is an atmosphere of palpable suspense in the high energy physics community as to what physics results will come out as more and more data are collected and studied, and most importantly, as to whether these results will indicate new physics (NP) beyond the Standard Model (SM). The experimental programme is more or less clear: more statistics will be accumulated, and the results will be compared with the predictions of the SM. Deviations from the latter would imply some sort of NP, and one can refer to existing theoretical studies to indicate what kind of NP is indicated by the observed deviation. It is true that theorists have not succeeded in providing an unequivocal prediction in this regard. This is because there exist several rival possibilities for NP, each with good arguments both for and against it. However, for several technical and aesthetic reasons, of which tractable ultraviolet behavior and the natural appearance of chiral fermions are perhaps the most important, supersymmetry (SUSY) has always been the pick of these NP models. At the dawn of the LHC era, it still remains the first option for any study of NP predictions.

Elegant as SUSY may be as an abstract idea, it is well known that it presents a very different face when it comes to constructing realistic models at low energies. Any phenomenologically viable SUSY model must necessarily include a large number of soft SUSY-breaking parameters. A count of the number of free phenomenological parameters in the so-called minimal supersymmetric standard model (MSSM) [253–256] runs to over 100, including masses, coupling constants, and mixing angles for the large number of supersymmetric partners, or sparticles, in the model. This proliferation of

This chapter is based on Phys.Rev.D83:094026, 2011 by Biplob Bhattacherjee, Amol Dighe, Diptimoy Ghosh and Sreerup Raychaudhuri [250]. All the numerical results in this chapter have been obtained by me with some initial help from Biplob Bhattacherjee, using the software packages SuperIso, micrOMEGAs, SuSpect and SUSY-HIT.

parameters may be directly traced to the fact that the MSSM does not include a specific mechanism for the breaking of SUSY, and hence, the numerous SUSY-breaking parameters are essentially put in by hand. Although such a model can exist, at least in principle, a theory with a hundred odd free parameters is a phenomenologist's nightmare, since it leads to very few clear predictions at the empirical level. At the LHC, for example, this leads to a wide landscape of possible signals which would leave an experimentalist with hard data to compare with a bewildering variety of options [257]. It is also difficult to believe that the breaking of SUSY is a sheer accident brought on by a proliferation of arbitrary nonzero parameters. One would rather argue that there is a definite mechanism for SUSY breaking [258], and when we know it, we will also know the parameters in question. Once again, however, theorists have failed to come up with an unambiguous mechanism for SUSY breaking – there exist quite a few different suggestions [259], beginning with minimal supergravity (mSUGRA) models, through gauge-mediated SUSY breaking (GMSB), anomaly mediated SUSY breaking (AMSB) and so on, each with a very different pattern for the parameters in question. Each of these models has different predictions for LHC signals, and hence, in effect, the chaotic situation within the subset of SUSY models becomes a cameo of the general NP scenario.

The oldest, and perhaps the most restrictive, of these SUSY models where a specific mechanism for SUSY breaking is considered, is the so-called "constrained" MSSM (cMSSM), which is based on an underlying mSUGRA [260–266] scenario[1]. In this scenario, supergravity is broken spontaneously in a so-called "hidden" sector consisting of fields which do not have strong or electroweak couplings to the MSSM fields. However, gravity, which necessarily couples to all fields so long as they carry energy and momentum, acts as a mediator between the hidden sector and the MSSM sector, giving rise to the soft SUSY-breaking parameters. It is this circumstance that leads to a dramatic reduction in the number of parameters, since gravity is blind to all flavor and color quantum numbers, though it can sense the spin of a particle. As a result, the mSUGRA model has just five free parameters, viz. (i) a universal scalar mass m_0, (ii) a universal fermion mass $m_{1/2}$, (iii) a universal trilinear (scalar) coupling A_0, (iv) the ratio of vacuum expectation values of the two Higgs doublets, parametrized as $\tan\beta$, and (v) the Higgsino mixing parameter μ. This universality of the masses and couplings is valid at the scale where the SUSY-breaking parameters are generated, which is usually identified with the scale of grand unification (GUT scale)[2], i.e., above 10^{16} GeV. While running down to low energies using the renormalization group (RG)

[1]This mechanism, by invoking supergravity, gives up the good ultraviolet behavior, unless, indeed, the supergravity model is equivalent to, or embedded in, a string theory. Aficionados of the cMSSM would, of course, argue that gravity must eventually be included anyway.

[2]There exists a symbiotic relation between SUSY and grand unified theory (GUT) ideas, since SUSY solves the hierarchy problem in GUT , and a GUT is natural at the scale where SUSY breaking is generated.

equations, however, the various soft SUSY-breaking parameters evolve differently, and lead to a specific mass spectrum at the electroweak scale. In particular, one of the Higgs-mass-squared parameters is driven to a negative value, ensuring that the electroweak symmetry is spontaneously broken. The requirement that the electroweak symmetry be broken at precisely the right scale leads to a further constraint, which effectively fixes the magnitude of μ in terms of the other parameters, though its sign is still indeterminate. This version of the mSUGRA model, which depends on four parameters and a sign, viz. $\{m_0, m_{1/2}, A_0, \tan\beta, \text{sgn } \mu\}$, is called the cMSSM. Being more constrained, this model is also more predictive and hence is more readily testable. There exists, therefore, a vast amount of literature on this model, which has been studied with regard to (a) collider signals [267–274], (b) low-energy processes, such as decays of K, D, and B mesons [275–282], and (c)dark-matter constraints arising from the fact that the relic density of the lightest SUSY particle (LSP) can be identified with the dark-matter content of the Universe [283–290]. In this chapter, therefore, we shall focus on this model, though a simple extension will also figure into our analysis.

It is now common knowledge that null results from direct searches have pushed up the masses of sparticles into the regime of 100 GeV or above. However SUSY models can still make substantial contributions to low-energy processes, particularly those which are mediated by weak interactions. Among these, flavor-changing neutral current (FCNC) processes, with the famed Glashow-Iliopoulos-Maiani (GIM) cancellation, constitute a favored ground to look for SUSY effects (or any NP effects, for that matter). However, barring a few little hiccups, the SM rules supreme in the area of flavor physics, leaving very little room for NP theories, including SUSY and the cMSSM. Year by year, as the measurements of the FCNC processes grow better and better, the lower bounds on masses of new particles (including sparticles) have been creeping further and further up in order to squeeze the NP contributions into the ever-narrowing band of experimental errors in these measurements.

In this chapter, we consider one such recent low-energy experimental result, viz., the measurement of the branching ratio $B^+ \to \tau^+\nu_\tau$. It directly constrains all models with minimal flavor violation (MFV), viz., models where all flavor-changing transitions are entirely governed by the Cabibbo-Kobayashi-Maskawa (CKM) matrix with no new phases beyond the CKM phase δ. We find constraints on general NP with MFV that involves a charged Higgs boson. As the cMSSM (and almost any viable SUSY model) belongs to this category, we apply these constraints to the cMSSM and find a rather dramatic impact on the parameter space of the model. It turns out when we combine the results of the measurement in question with other low-energy measurements, such as the anomalous magnetic moment of the muon, and radiative and leptonic B decays, most of the cMSSM parameter space is disfavored at the 95% confidence level (C.L.). What survives all the constraints is a small patch in the four-dimensional parameter space $(m_0, m_{1/2}, A_0, \tan\beta)$ of the model, for a positive sign of μ. This is very different from the kind of constraints derived from earlier, less restrictive measurements of $B^+ \to$

$\tau^+\nu_\tau$, where wide areas of the cMSSM parameter space were allowed.

As mentioned above, one of the attractive features of SUSY is that it provides a dark-matter candidate, viz., the lightest supersymmetric particle (LSP). This carries a conserved quantum number (R parity) which forbids its decay[3]. One can, therefore, study the evolution of the Universe in a SUSY model, and check whether the relic density of LSP's matches with the observed density of dark-matter as indicated by the cosmic microwave background radiation (CMBR) data [294]. Obviously, this matching will happen for only a small part of the parameter space of the model. It is encouraging that the dark-matter-allowed region in the cMSSM overlaps the small patch allowed by low-energy measurements quite substantially. We can say, therefore, that there exists a rather specific set of parameters which is simultaneously consistent with the low-energy data as well as with the hypothesis that LSP's form the dark- matter content of the Universe. With this specific set of parameters, we generate the mass spectrum of sparticles, and find reasonably unequivocal indications as to the kind of signals expected at the LHC. No detailed analysis is necessary at this stage, for the relevant signals have already been considered in comprehensive studies by the ATLAS and CMS Collaborations [295, 296]. Comparing their results with our parameter choice, we find that the 7 TeV run of the LHC may provide a weak indication of SUSY [297–301], which could be verified comprehensively even in the very early stages of the 14 TeV run. Going further, we may even say that if SUSY is indeed the correct NP option, then the LHC may eventually turn out to be the hoped-for SUSY factory, claimed in the literature [302].

This chapter is organized as follows. In Sec.II we discuss the recent bounds on $B^+ \to \tau^+\nu_\tau$ and how they affect MFV models. This is followed by Sec.III, where we discuss other low-energy measurements which constrain the cMSSM parameter space. The combined constraints are displayed and discussed in Sec.IV, where we also discuss the possible LHC signals which could arise therefrom. Sec.V discusses the so-called nonuniversal Higgs-mass (NUHM) model, a variant of the cMSSM, and some of its consequences. A critical summary of our results forms the substance of the concluding Sec.VI.

6.2 The decay $B^+ \to \tau^+\nu_\tau$

On purely theoretical grounds, the leptonic decay $B^+ \to \tau^+\nu_\tau$ is a clean decay mode, since the final state consists only of leptons and hence the usually troublesome strong rescattering phases are absent. Indeed, in the SM, the branching ratio of $B^+ \to \tau^+\nu_\tau$

[3]Once again, this is not written in stone, for R-parity violation can happen and has been extensively studied [291–293].

is given by the tree-level formula

$$\mathrm{BR}(B^+ \to \tau^+\nu_\tau)_{\mathrm{SM}} = \frac{G_F^2 m_B m_\tau^2}{8\pi}\left(1 - \frac{m_\tau^2}{m_B^2}\right)^2 f_B^2 \left|V_{ub}\right|^2 \tau_B \ , \tag{6.1}$$

where G_F is the Fermi constant, τ_B is the B^+ lifetime, $f_B = 192.8 \pm 9.9$ MeV [303] is the B^+ decay constant, and m_B, m_τ are the masses of B^+, τ^+, respectively. Here

$$|V_{ub}| = (3.52 \pm 0.11) \times 10^{-3} \tag{6.2}$$

is the relevant CKM matrix element, obtained through the combined fit [304, 305] to all the data excluding the $B^+ \to \tau^+\nu_\tau$ measurements. The SM prediction, including higher-order corrections, is

$$\mathrm{BR}(B^+ \to \tau^+\nu_\tau)_{\mathrm{SM}} = (0.81 \pm 0.15) \times 10^{-4} \ . \tag{6.3}$$

As recently as 2008, the experimental average value of this parameter [306] was

$$\mathrm{BR}(B^+ \to \tau^+\nu_\tau)_{2008} = (1.41 \pm 0.43) \times 10^{-4} \ , \tag{6.4}$$

which was just about consistent with Eq. (6.3) at 1 standard deviation. At that time, it was shown [307] that corresponding constraints on the parameter space of the cMSSM (such as we discuss in this work) are rather minor.

Very recently (2010), however, new measurements of the branching ratio $\mathrm{BR}(B^+ \to \tau^+\nu_\tau)$ from B factories have changed the experimental value quite significantly. The most recent experimental measurements are [308–311]

$$\begin{aligned}
\text{Babar (semileptonic tag)}: \quad & \mathrm{BR}(B^+ \to \tau^+\nu_\tau) = \ (1.70 \pm 0.82) \times 10^{-4} \ , \\
\text{(hadronic tag)}: \quad & \mathrm{BR}(B^+ \to \tau^+\nu_\tau) = \ (1.80 \pm 0.61) \times 10^{-4} \ , \\
\text{Belle (semileptonic tag)}: \quad & \mathrm{BR}(B^+ \to \tau^+\nu_\tau) = \ (1.54 \pm 0.48) \times 10^{-4} \ , \\
\text{(hadronic tag)}: \quad & \mathrm{BR}(B^+ \to \tau^+\nu_\tau) = \ (1.79 \pm 0.71) \times 10^{-4} \ .
\end{aligned} \tag{6.5}$$

These results are quite consistent with each other. Combining these measurements, one gets the world average [312]

$$\mathrm{BR}(B^+ \to \tau^+\nu_\tau)_{\mathrm{exp}} = (1.68 \pm 0.31) \times 10^{-4} \ . \tag{6.6}$$

Clearly, this measurement deviates significantly from the SM prediction given in Eq. (6.3). Defining $R^{\mathrm{exp}}_{\tau\nu_\tau}$ to be [313, 314]

$$R^{\mathrm{exp}}_{\tau\nu_\tau} \equiv \frac{\mathrm{BR}(B^+ \to \tau^+\nu_\tau)_{\mathrm{exp}}}{\mathrm{BR}(B^+ \to \tau^+\nu_\tau)_{\mathrm{SM}}} \ , \tag{6.7}$$

and using Eqs. (6.3) and (6.6), we get

$$R^{\mathrm{exp}}_{\tau\nu_\tau} = 2.07 \pm 0.54 \ , \tag{6.8}$$

which indicates a $\sim 2\sigma$ deviation. Deviations at this level frequently arise from statistical fluctuations in small data samples, or from the use of ill-determined theoretical quantities, and often disappear when more data are analyzed, or when more rigorous calculations are performed. In this case, however, the mismatch may not disappear so easily. For neither are the current measurements of $\mathrm{BR}(B^+ \to \tau^+\nu_\tau)$ based on a small statistics sample (see Refs. [308–311]), nor should one expect the SM prediction to change much, since the formula in Eq. (6.1) involves quantities that are already known pretty accurately. It appears, therefore, that it is sensible to at least explore the ability of NP beyond the SM to resolve the observed discrepancy.

Following Ref. [313], we characterize the NP models that could potentially explain this anomaly by a quantity $R^{\mathrm{NP}}_{\tau\nu_\tau}$, defined as

$$R^{\mathrm{NP}}_{\tau\nu_\tau} \equiv \frac{\mathrm{BR}(B^+ \to \tau^+\nu_\tau)_{\,\mathrm{SM+NP}}}{\mathrm{BR}(B^+ \to \tau^+\nu_\tau)_{\mathrm{SM}}}\,, \tag{6.9}$$

where the subscript SM+NP represents the net branching ratio in the NP scenario, including the SM contribution. The 95% C.L. allowed range for $R^{\mathrm{NP}}_{\tau\nu_\tau}$ then works out to

$$0.99 < R^{\mathrm{NP}}_{\tau\nu_\tau} < 3.14\,, \tag{6.10}$$

which essentially means that NP models with positive contributions are favored by the data and those with negative contributions are quite strongly disfavored.

There exist, of course, a wide variety of models of NP which could provide extra contributions to the branching ratio of $B^+ \to \tau^+\nu_\tau$. However, we focus only on the MFV models. For a large class of MFV models that involve a charged Higgs boson H^+ – such as two-Higgs doublet models, of which the cMSSM is an example – the branching ratio of $B^+ \to \tau^+\nu_\tau$ is given by [315]

$$\mathrm{BR}(B^+ \to \tau^+\nu_\tau)_{\mathrm{NP}} = \frac{G_F^2 m_B m_\tau^2}{8\pi}\left(1-\frac{m_\tau^2}{m_B^2}\right)^2 f_B^2\,|\widetilde{V}_{ub}|^2\,\tau_B\left(1-\tan^2\beta\frac{m_B^2}{M_+^2}\right)^2 \tag{6.11}$$

at the tree level, where M_+ is the mass of the charged Higgs boson. Here NP stands specifically for the MFV model, but we retain the notation "NP" in the interests of simplicity[4].

In the above formula $|\widetilde{V}_{ub}|$ is the value of $|V_{ub}|$ obtained in the context of the NP model, which in general will be different from $|V_{ub}|$ obtained from the data in the context of the SM. In order to get rid of this uncertainty in the CKM parameter, we restrict ourselves to the determination of $|V_{ub}|$ through only those measurements that are independent of NP. Such a fit is called the fit to the universal unitarity triangle (UUTfit) [316], and it uses only

[4] Note that our analysis for the MFV models in this section closely follows that of [304], with minor differences. Our constraints in the M_+–$\tan\beta$ parameter space naturally are almost identical. However, we present the detailed analysis here for the sake of completeness and clarification of our procedure.

- the measurements of $|V_{ub}/V_{cb}|$ from semileptonic B decays,
- the ratio of mass differences in the B_s and B_d systems: $|\Delta M_s/\Delta M_d|$, and
- the measurement of $\sin 2\beta$ from the time-dependent CP asymmetry in $B_d \to J/\psi K^{(*)}$.

The UUTfit value of $|V_{ub}|$ comes out as [304]

$$|V_{ub}|_{\rm UUTfit} = (3.50 \pm 0.12) \times 10^{-3} \,, \tag{6.12}$$

which is actually very close to the global fit in Eq. (6.2). Using this value, the SM prediction for the branching ratio of $B^+ \to \tau^+\nu_\tau$ changes slightly from Eq. (6.3) and becomes

$$\mathrm{BR}(B^+ \to \tau^+\nu_\tau)_{\rm SM} = (0.80 \pm 0.15) \times 10^{-4} \,. \tag{6.13}$$

Note that while the UUTfit [304] is obtained using the lattice prediction $f_B = 200 \pm 20$ MeV [317] of the LQCD Collaboration, we use the more recent, averaged value from lattice simulations, $f_B = 192.8 \pm 9.9$ MeV [303], which has a much smaller error[5], for the calculation of $\mathrm{BR}(B^+ \to \tau^+\nu_\tau)_{\rm SM}$. The 95% C.L. allowed range for $R^{\rm NP}_{\tau\nu_\tau}$ assumes the value

$$0.99 < R^{\rm NP}_{\tau\nu_\tau} < 3.19 \,, \tag{6.14}$$

which forms the basis of all subsequent analyses in this chapter. Once $|V_{ub}|$ is chosen in this "model-independent" way, we can take $|\widetilde{V}_{ub}| = |V_{ub}|_{\rm UUTfit}$, and hence the theoretical MFV prediction for $R^{\rm NP}_{\tau\nu}$ at the tree level becomes

$$R^{\rm NP}_{\tau\nu_\tau}|_{\rm tree} = \left(1 - \tan^2\beta \frac{m_B^2}{M_+^2}\right)^2 \,. \tag{6.15}$$

If higher-order corrections are included then this ratio gets modified [318] to a form

$$R^{\rm NP}_{\tau\nu_\tau} = \left(1 - \frac{\tan^2\beta}{1 + \tilde{\epsilon}_0 \, \tan\beta} \frac{m_B^2}{M_+^2}\right)^2 \,, \tag{6.16}$$

where $\tilde{\epsilon}_0$ encodes all the higher-order corrections, which, of course, will have some dependence on the free parameters of the MFV model. We take the range of $\tilde{\epsilon}_0$ to be $-0.01 \le \tilde{\epsilon}_0 \le 0.01$, as obtained in [319] by a scan over reasonable values of the MFV model parameters. When a specific model, such as the cMSSM, is considered, $\tilde{\epsilon}_0$ can be calculated explicitly.

The impact of the experimental data on MFV models with a charged Higgs boson, as discussed above, can be clearly discerned from Fig. 6.1(a), where we plot the value of

[5] Ideally, of course, the UUTfit needs to be performed again with the updated f_B value. We have assumed that the updated fit will not significantly affect the $|V_{ub}|$ value.

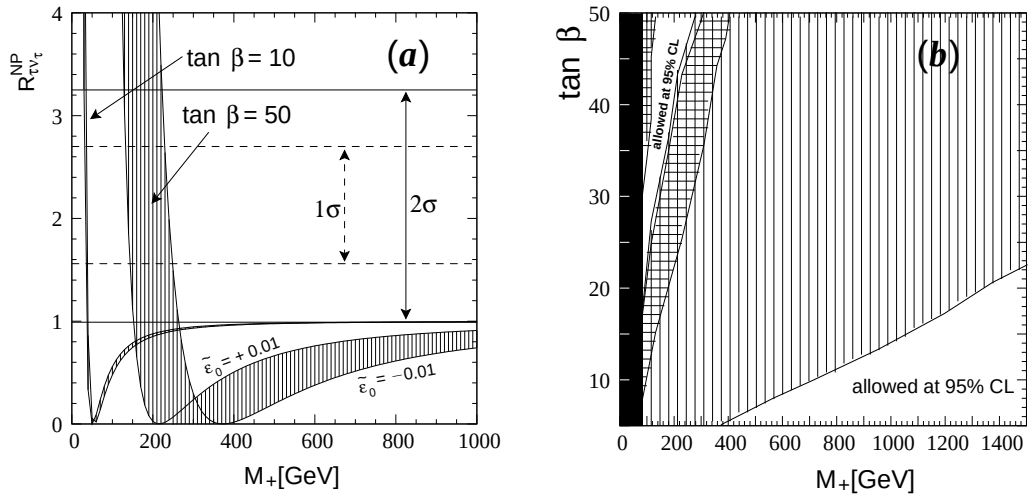

Figure 6.1: (a) The dependence of $R^{NP}_{\tau\nu_\tau}$ on the mass M_+ of the charged Higgs boson in MFV models for two values $\tan\beta = 10$ and 50, and (b) the 95% C.L. constraints on the M_+–$\tan\beta$ plane. The vertically hatched regions in (a) correspond to higher order corrections varying between $\tilde{\epsilon}_0 = -0.01$ and $+0.01$, while the 1σ (2σ) experimental measurements of $R^{NP}_{\tau\nu_\tau}$ are shown by horizontal broken (solid) lines. The dark band in (b) corresponds to the LEP bound. The large, vertically hatched region in (b) is disallowed by the recent (2010) $R^{NP}_{\tau\nu_\tau}$ constraint, while the horizontally hatched region is disallowed by the 2008 data.

$R^{NP}_{\tau\nu_\tau}$ as a function of the charged Higgs boson mass M_+. As Eq. (6.14) indicates, such a model should tend to make $R^{NP}_{\tau\nu_\tau}$ greater than unity, and there is very little room for $R^{NP}_{\tau\nu_\tau} < 1$. However, the negative sign on the right side of Eq. (6.16) indicates that unless the NP contribution is very large, the models in question have a tendency to diminish $R^{NP}_{\tau\nu_\tau}$ rather than augment its value. As a result, a model with a heavy charged Higgs boson *cannot* be considered as an explanation for the deviation of $\mathrm{BR}(B^+ \to \tau^+\nu_\tau)$ from its SM value. Instead, if we do have such a model, we would expect rather strong constraints on its parameters, since the NP contribution must be squeezed into the small tolerance below unity, as given in Eq. (6.14). Such a situation would naturally arise for large M_+, when the NP contribution becomes negligible, and $R^{NP}_{\tau\nu_\tau} \to 1$ for all $\tan\beta$ – though it always stays less than unity. This corresponds to the rising part of the curves, towards the right end of Fig. 6.1(a). A glance at the figure will, however, leave no doubt that this limiting case is barely allowed at 2σ for low $\tan\beta$ ($= 10$), but disallowed for high $\tan\beta$ ($= 50$). We surmise, therefore, that for high values of M_+, the $B^+ \to \tau^+\nu_\tau$ measurement favors low values of $\tan\beta$.

For low values of M_+, on the other hand, Eq. (6.16) tells us that it is possible for the NP contribution to be so large that it completely dominates the SM contribution,

and in this limit, it is possible to have $R^{NP}_{\tau\nu_\tau} \gtrsim 1$. The explicit condition is

$$\frac{\tan^2\beta}{1+\tilde{\epsilon}_0\tan\beta} \gtrsim \frac{2M_+^2}{m_B^2}\ . \tag{6.17}$$

However this can happen only for a very restricted set of $(M_+, \tan\beta)$ values, some of which are already constrained experimentally. For example, for $\tan\beta = 10$, one can have $R^{NP}_{\tau\nu_\tau}$ well inside the 2σ range only if M_+ is $\lesssim 50$ GeV, but such low M_+ values are ruled out by the LEP direct searches, which give $M_+ > 79.3$ GeV [320]. On the other hand, if $\tan\beta = 50$, the same LEP data permit 140 GeV$< M_+ <$ 220 GeV which can render $R^{NP}_{\tau\nu}$ well inside the 2σ range, as shown in Fig. 6.1(a). Thus, one may complement our earlier assertion by the statement that in the opposite limit, i.e. for low values of M_+, the $B^+ \to \tau^+\nu_\tau$ measurement favors high values of $\tan\beta$. This is also the limit in which the NP models contribute positively in accounting for the deviation of the experimental data from the SM predictions.

The two limits are made explicit in Fig. 6.1(b), which shows the 95% C.L. constraints on the M_+–$\tan\beta$ plane. The dark band represents the LEP constraint $M_+ > 79.3$ GeV and the vertically-hatched region is disallowed by the $B^+ \to \tau^+\nu_\tau$ measurement. This leaves only two small unshaded regions for low M_+ and high M_+, in accordance with the above discussion. Our result may be contrasted with the constraints obtained from the 2008 data, which are shown by horizontal hatching, and constrain only a small region with $M_+ < 400$ GeV and somewhat high $\tan\beta$. One may say, therefore, that the recent measurement of the branching ratio for $B^+ \to \tau^+\nu_\tau$ has considerably improved the constraints on MFV models with charged Higgs bosons. As the cMSSM belongs to this category, we should expect correspondingly severe constraints on the corresponding parameter space when we compare its predictions with this new experimental result.

6.3 Other constraints

When we consider an all-encompassing model like the cMSSM, with far-flung implications in almost all areas of electroweak physics, the constraints arising from $B^+ \to \tau^+\nu_\tau$ cannot be considered in isolation, but must be combined with other bounds – some of which are equally restrictive, at least at the 2σ level. These constraints can be classified as follows.

1. *Theoretical constraints.*– arising from requirements of internal consistency of the model. In particular, if the Higgs-mass parameter which should be driven negative by RG running remains positive, we cannot explain electroweak symmetry breaking (EWSB) in this model. There is also a substantial region where the model predicts that the charged stau $\widetilde{\tau}_1$ is the LSP, and is therefore precluded by the absence of a large relic density of charged particles.

2. *Collider bounds.*– arising from the nondiscovery in direct searches [320] at the CERN LEP and Fermilab Tevatron of predicted particles, most notably the light Higgs boson h^0 and the lighter chargino $\widetilde{\chi}_1^+$. While the chargino couplings are large enough for the experimental bounds to practically saturate the kinematic reach of these machines, the light Higgs boson mass in SUSY models is generally sensitive to higher-order corrections, where there is a theoretical uncertainty of around 3–4 GeV at the next-to-next-to-leading order (NNLO) and higher [321]. To take care of this, we consider a softer lower bound of 111 GeV, rather than the kinematic bound of 114.4 GeV usually applied to the SM Higgs boson.

3. *Indirect bounds.*–arising from measurements of low-energy processes where new particles and interactions in NP models can also contribute. In the context of the cMSSM, the most important of these are the measurements of (a) the anomalous magnetic moment of the muon, (b) the rate of the radiative decay $B_d \to X_s\gamma$, and (c) the BR for the leptonic decay $B_s \to \mu^+\mu^-$. Here we have assumed that the NP is of the MFV kind, and that it survives the measurements other than those explicitly mentioned above. In particular, the large B_s–$\overline{B}_s$ mixing phase, or the $A_{CP}(B \to K\pi)$ measurements, cannot be explained by any MFV models, and we assume that these anomalies will disappear with more data or with better theoretical calculations.

Of the above, the theoretical and direct search constraints may be considered firm constraints, as they are unlikely to be changed by inclusion of further types of NP along with the cMSSM or whatever model is being studied. On the other hand, constraints from indirect measurements are not so robust, as they can easily change if some new effect is postulated. Before we proceed to apply these constraints to the cMSSM parameter space, therefore, a brief discussion of the actual measurements used in our analysis is called for. This forms the remaining part of this section.

- *The anomalous magnetic moment of the muon, $a_\mu = (g-2)/2$:* This is one of the most compelling indicators of NP and it is well known as a major constraint for NP theories such as supersymmetry or extra dimensions. The latest measured value [322] for a_μ is

$$a_\mu^{\rm exp} = (11659208.0 \pm 6.3) \times 10^{-10} \; . \tag{6.18}$$

  In the recent past, the SM prediction [316] for a_μ has undergone numerous vicissitudes with respect to the experimental data, occasionally being consistent with it and occasionally deviating at the level of 2σ-3σ. Much of the difficulty in making this prediction accurate lies in the fact that the experimental measurement is sensitive to two-loop corrections where some nonperturbative QCD effects due to the low mass scale are involved. The latter have to be obtained by fitting

experimental data, whose errors then feed into the theoretical uncertainty. The most recent SM prediction is [323]

$$a_\mu^{\rm SM} = (11659178.5 \pm 6.1) \times 10^{-10}. \tag{6.19}$$

The discrepancy between the SM and experiment is, therefore,

$$\Delta a_\mu^{\rm exp} = a_\mu^{\rm exp} - a_\mu^{\rm SM} = (29.5 \pm 8.8) \times 10^{-10} \ . \tag{6.20}$$

This is at the somewhat high level of $\sim 3.4\sigma$, but is not normally considered a "smoking gun" signal for NP for reasons stated above. Nevertheless, in order to check if this discrepancy *can* be explained with the cMSSM, we use a procedure [324] that does not calculate the two-loop SUSY corrections, but includes them in the theoretical errors, to obtain a 95% C.L. range

$$11.5 \times 10^{-10} < \Delta a_\mu^{\rm NP} < 47.5 \times 10^{-10} \ , \tag{6.21}$$

where $\Delta a_\mu^{\rm NP}$ is the extra contribution due to NP. In our analysis, the NP in question will be the cMSSM, or a variant, but we choose, as in the previous section, to retain the label "NP".

Obviously, in the cMSSM, the value of $\Delta a_\mu^{\rm NP}$ will depend on all the free parameters of the model. However, it is known that the sign of the cMSSM contribution is directly sensitive to the sign of the μ parameter [325, 326]: for $\mu < 0$, the cMSSM contribution is negative, while for $\mu > 0$, a positive contribution is predicted by some regions of the cMSSM parameter space. Since the 95% C.L. range of $\Delta a_\mu^{\rm NP}$ indicated in Eq. (6.21) is entirely positive, it indicates that the sign $\mu < 0$ is disallowed by the measurement of the muon anomalous magnetic moment, and even with $\mu > 0$, there are strong constraints on the remaining parameters of the cMSSM.

- *The radiative decay $B_d \to X_s\gamma$:* In the SM, the BR of the radiative decay $B_d \to {\rm X}_s\gamma$ has been calculated [327–330] to NNLO in QCD to be

$${\rm BR}({\rm B}_d \to {\rm X}_s\gamma)_{\rm SM} = (3.15 \pm 0.23) \times 10^{-4} \ . \tag{6.22}$$

The current experimental average for the BR by the Heavy Flavor Averaging Group (HFAG) [331] is

$${\rm BR}({\rm B}_d \to {\rm X}_s\gamma)_{\rm exp} = (3.55 \pm 0.26) \times 10^{-4} \ , \tag{6.23}$$

which is consistent with the SM prediction within 1 standard deviation, leaving very little room for NP contributions. As a result, this measurement has a tremendous impact on MFV models involving a charged Higgs boson H^+, essentially pushing up the mass M_+ to very large values. Of all such models, the

constraints on SUSY models can be more relaxed because of large cancellations between the charged Higgs boson contributions and the chargino contributions which are the hallmark of SUSY models. Nevertheless, there do exist bounds on the cMSSM arising from the residual contribution, especially for light M_+, and these have to be taken into consideration.

In our analysis, after including the theoretical uncertainties in the cMSSM following the method outlined in [314], we set the 95% C.L. range for the branching ratio to be

$$2.05 \times 10^{-4} \leq \mathrm{BR}(\mathrm{B}_d \to \mathrm{X}_s\gamma) \leq 5.05 \times 10^{-4} \,. \tag{6.24}$$

It turns out that the $\mathrm{B}_d \to \mathrm{X}_s\gamma$ constraint is also extremely sensitive to the sign of μ. For $\mu < 0$, it eliminates a large part of the parameter space [332], while for $\mu > 0$ the constraint is comparatively weaker. Neither of these constraints is as strong as those arising from the muon $(g-2)/2$; however, they are complementary to it.

- *The leptonic decay $B_s \to \mu^+\mu^-$:* Within the SM, the fully leptonic decay $B_s \to \mu^+\mu^-$ is chirally suppressed; the SM prediction is

$$\mathrm{BR}(\mathrm{B}_s \to \mu^+\mu^-)_{\mathrm{SM}} = (3.19 \pm 0.35) \times 10^{-9} \,. \tag{6.25}$$

The uncertainty in the BR comes principally from the decay constant $f_{B_s} = 238.8 \pm 9.5$ MeV [303] and from the CKM element $|V_{ts}| = 0.041 \pm 0.001$ [320]. The current experimental upper bound by the CDF Collaboration is [333]

$$\mathrm{BR}(\mathrm{B}_s \to \mu^+\mu^-)_{\mathrm{CDF}} < 4.3 \times 10^{-8} \text{ (95\% C.L.)} \,. \tag{6.26}$$

After including the theoretical uncertainties, we get the 95% C.L. upper limit

$$\mathrm{BR}(\mathrm{B}_s \to \mu^+\mu^-) < 4.8 \times 10^{-8}. \tag{6.27}$$

Inclusion of charged Higgs bosons, whose left- and right-chiral couplings depend on $\cot\beta$ and $\tan\beta$, respectively, has a direct impact on the BR for $B_s \to \mu^+\mu^-$, which gets enhanced considerably above the SM prediction, and easily saturates the upper bound, especially for low values of M_+ and large $\tan\beta$. Indeed, for large $\tan\beta$, the cMSSM contribution is known [334] to scale as $\tan^6\beta/(M_+^2 - M_W^2)^2$. Thus, this process also constrains MFV models with a charged Higgs boson. It turns out that for the cMSSM, these constraints are not more severe than the combination of all other constraints; however, we shall demonstrate later that they do have an impact if the assumptions of the cMSSM are relaxed.

In this section, we have listed the major constraints, apart from the new data on $B^+ \to \tau^+\nu_\tau$, on the parameter space of SUSY models, of which the cMSSM will be showcased in the following section. It may be noted in passing that this list is not fixed for all time, as there are several other low-energy processes and direct search bounds which also constrain the SUSY parameter space. Current data on these rule out patches of the parameter space which are subsumed in the disallowed regions arising from the constraints which we have listed above. However, it is entirely possible that a future measurement – including some LHC searches – could rule out wider patches of the SUSY parameter space, and then the relevant processes would have to be taken into consideration. With this caveat, we now turn to the explicit constraints on the cMSSM parameter space, and the impact of the $B^+ \to \tau^+\nu_\tau$ measurement on this analysis.

6.4 Constraining the cMSSM

As mentioned in the Introduction, the parameter space of the cMSSM has four unknowns, viz. m_0, $m_{1/2}$, A_0, $\tan\beta$, that can take real values. The sign of the μ parameter is also undetermined, but as indicated in the previous section, the muon $(g-2)/2$ constraint disfavors $\mu < 0$. We therefore restrict ourselves to $\mu > 0$ and, hence, consider a simply connected parameter space of four dimensions.

The theoretical ranges of the parameters m_0, $m_{1/2}$, and A_0 are, in principle, completely undetermined, but the region of interest is clearly that which would lead to sparticle masses kinematically accessible to current accelerators such as the LHC. Keeping this in mind, we scan the ranges

$$0 \leq m_0 \leq 2 \text{ TeV} , \qquad 0 \leq m_{1/2} \leq 1 \text{ TeV} , \qquad -2 \text{ TeV} \leq A_0 \leq 2 \text{ TeV} . \tag{6.28}$$

The range of the remaining parameter $\tan\beta$ is determined mainly by its impact on the scalar Higgs sector of the cMSSM, where, indeed, it arises. For very low values of $\tan\beta$ (~ 1), one tends to predict the lightest Higgs boson h^0 to have a small mass, which is already ruled out by the LEP constraints. On the other hand, if $\tan\beta > m_t/m_b$, the couplings of the charged Higgs boson to a $t\bar{b}$ pair begin to enter the nonperturbative regime. We have chosen, therefore, the reasonable range

$$4 \leq \tan\beta \leq 50 . \tag{6.29}$$

Using these parameters, we perform a numerical scan over the cMSSM parameter space, using (*a*) SuSpect [335] to generate the mass spectrum (this also takes care of the theoretical and direct search constraints), (*b*) SuperIso [336, 337] to calculate the variables listed as indirect constraints in the previous section, and, finally, (*c*) micrOMEGAs [338, 339] to calculate the dark-matter relic density. All of these are state-of-the-art software in the public domain, guaranteed to include higher-order

corrections as available at the moment, which have been tested in multifarious applications, as the literature testifies.

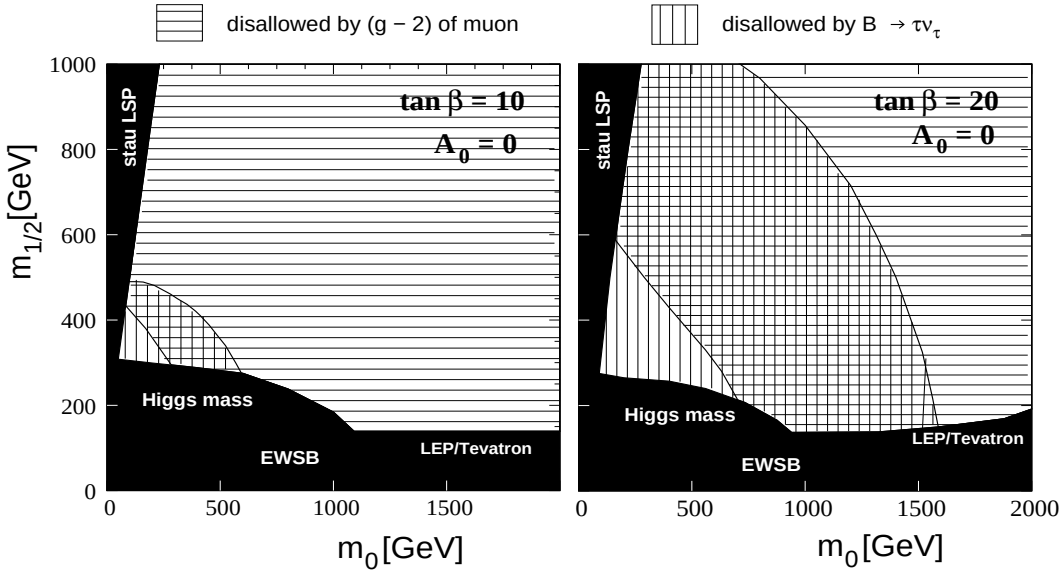

Figure 6.2: The 95% C.L. constraints on the m_0–$m_{1/2}$ plane, for $A_0 = 0$ and $\tan\beta = 10$ (left panel) and $\tan\beta = 20$ (right panel). Horizontal (vertical) hatching indicates regions ruled out by the measurement of the muon $(g-2)/2$ [$BR(B^+ \to \tau^+\nu_\tau)$] and the cross-hatched region represents their overlap. The constraint from $B \to X_s\gamma$ is subsumed in that from the lower bound on the Higgs mass from direct searches, and hence is invisible in these plots. We take $\mu > 0$ in this and all subsequent plots.

In Fig. 6.2, we present the constraints on the cMSSM parameter space in the m_0–$m_{1/2}$ plane, where the tension between various measurements appears quite clearly. For this figure, we have set $A_0 = 0$, which is an assumption commonly made for simplicity. We take $\mu > 0$ as required by the muon $(g-2)/2$ constraint. The panel on the left (right) corresponds to $\tan\beta = 10$ (20). The dark areas are ruled out by the theoretical and direct search constraints explained in the previous section, with the approximate areas highlighted in white lettering[6]. Focusing on the left panel, it is clear that the muon $(g-2)/2$ constraint (indicated by horizontal hatching) is very stringent, ruling out almost all the region considered, and allowing only a small patch with low values of m_0 and $m_{1/2}$. This patch, however, is disallowed by the new measurement of $B^+ \to \tau^+\nu_\tau$, as can be seen from the vertical hatching. The overlap between the disallowed regions is indicated by cross-hatching. It is quite clear, therefore, that for $\tan\beta = 10$, there is *no* region in the parameter space shown that is at once consistent (to 95% C.L.) with both the anomalous muon magnetic moment and the $B^+ \to \tau^+\nu_\tau$

[6]Following common practice, we do not delineate separate patches in the firmly disallowed (dark) region in detail, as that would not be germane to the present discussion.

branching ratio. We have checked that even if we take $\tan\beta$ down to values as small as $\tan\beta = 4$, the two measurements, taken together with the firm constraints, do not allow for a simultaneously allowed parameter space. At higher value of $\tan\beta$, the situation is even worse. This is apparent from the right panel, where our results are plotted for $\tan\beta = 20$. Here it is true that a larger region is permitted by the muon $(g-2)/2$ measurement, but the region disallowed by the $B^+ \to \tau^+\nu_\tau$ branching ratio is also much larger and covers the entire region allowed by $(g-2)/2$. The region disallowed by $B^+ \to \tau^+\nu_\tau$ grows for larger value of $\tan\beta$, as may be guessed from Fig. 6.1(b), and for values of $\tan\beta \sim 50$, it would cover the whole of the parameter space shown in the panels of Fig. 6.2. Thus, for $A_0 = 0$, one may say that these two measurements alone are enough to ensure that the full mSUGRA parameter space is strongly disfavored.

It may be noted in passing that among the other constraints from the low-energy data, the patch disallowed by $B_d \to X_s\gamma$ is subsumed in that from the Higgs-mass bound, and, likewise, the patch inconsistent with $B_s \to \mu^+\mu^-$ is overlaid by the dark region corresponding to the firm constraints. We have not, therefore, shown these disallowed regions in Fig. 6.2.

The above result, disappointing as it may appear, is by no means the end of the road for the cMSSM, for it has been obtained only on the slice of parameter space for which $A_0 = 0$. The situation changes when we permit A_0 to vary. This affects the running of the charged Higgs boson mass, and we find that for large negative values of A_0, for a given $\tan\beta$, the Higgs-mass M_+ is driven to larger values than what one would obtain by setting $A_0 = 0$. In the context of Fig. 6.1(b), this effect then pushes the model horizontally in the M_+–$\tan\beta$ plane, eventually penetrating into the "allowed" region. The $B^+ \to \tau^+\nu_\tau$ constraint, therefore, can be quite considerably weakened by choosing large negative values of A_0. We do not expect such a significant change in the muon $(g-2)/2$ constraint, but some relaxation is not unreasonable to expect when A_0 is varied over a wide range. Large negative values of A_0 also tend to increase the mass of the lightest Higgs boson h^0, thereby relaxing somewhat the LEP bounds arising from Higgs boson mass considerations [340]. Accordingly, we repeat our analysis of the constraints on the m_0–$m_{1/2}$ plane, keeping A_0 floating between -2 TeV and $+2$ TeV. In our analysis, a point in the m_0–$m_{1/2}$ plane, for a given $\tan\beta$, is taken to be allowed at 95% C.L. by a given constraint if we can find any value of A_0, lying in the range $-2 \text{ TeV} \leq A_0 \leq 2 \text{ TeV}$, for which the given constraint is satisfied. Our results are exhibited in Fig. 6.3, which follows the notations and conventions of Fig. 6.2 closely. In addition to the constraints shown therein, the one from $B_d \to X_s\gamma$ now makes its appearance as a small region hatched with slanting lines, indicating that this constraint is now stronger than the weakened Higgs-mass bound from collider machines. However, it is not strong enough to rule out any portion which is not already disallowed by the other constraints.

Even a cursory examination of the dark and hatched regions in Fig. 6.3 will indicate that, while the qualitative features of the regions disfavored by the muon $(g-2)/2$ and

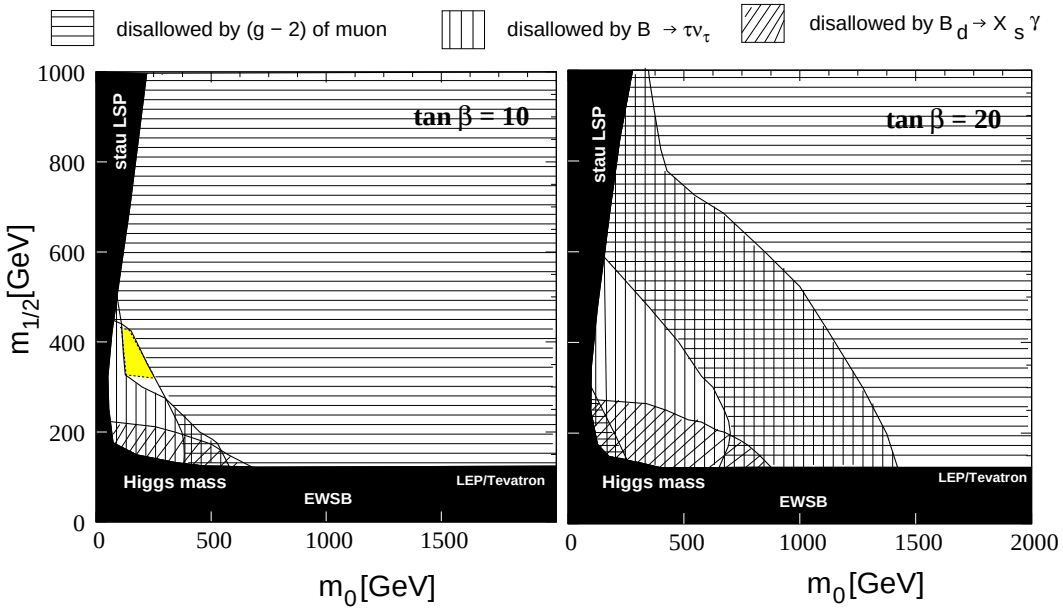

Figure 6.3: The same as in Fig. 6.2, except that the trilinear coupling A_0 is kept floating over the range $(-2, +2)$ TeV, and regions are considered disallowed only if they remain disallowed for all values of A_0 in the given range. This weakens the constraints enough for a small allowed region to appear in the left panel ($\tan\beta = 10$). The yellow/light gray region is simultaneously consistent with *all* constraints at 95% C.L.

the $B^+ \to \tau^+\nu_\tau$ measurements stay the same, somewhat larger areas in the plane are "allowed" by each constraint individually. This, by itself, is not surprising, but it has the exciting consequence that now the left panel ($\tan\beta = 10$) exhibits a small patch, roughly triangular in shape, which satisfies each of the constraints individually for *some* value of A_0, and moreover, there is a subset of this region where all the constraints are satisfied simultaneously for the *same* value of A_0. This subregion, which represents the actual parameter space consistent with all the measurements individually at 95% C.L., is denoted by yellow/light gray shading. It is on this "allowed" region that we focus our interest in the subsequent discussion.

If we glance at the right panel of Fig. 6.3, where $\tan\beta = 20$, we see that there is no allowed region at all, the disallowed regions showing substantial overlap and covering the whole of the plot area. Once again, we surmise that high values of $\tan\beta$ are disfavored, whatever value of A_0 is chosen, and that the allowed region in the cMSSM parameter space must lie in the neighborhood of $\tan\beta = 10$. We have already mentioned that consistency with the $B^+ \to \tau^+\nu_\tau$ constraint requires large negative values of the A_0 parameter, which can drive M_+ to higher values even for the low $\tan\beta$ (≈ 10). In order to see this, we plot, in the left panel of Fig. 6.4, the same constraints in the plane of A_0 and $m_{1/2}$, keeping m_0 fixed at the value $m_0 = 150$ GeV, for $\tan\beta = 10$.

This particular value of m_0 has been chosen since in the left panel of Fig. 6.3, it lies more-or-less near the center of the allowed triangle (yellow/light gray shading) and is roughly the value for which the maximum range of $m_{1/2}$ appears to be allowed. The dimensions of this allowed triangle also encourage us, in Fig. 6.4, to "zoom in" on the range $m_{1/2} = 300$–500 GeV, outside which we get disallowed regions. However, A_0 is varied between -1.5 TeV and $+1.5$ TeV, to adequately cover the whole range allowed by the firm constraints, as is apparent from the left panel of Fig. 6.4.

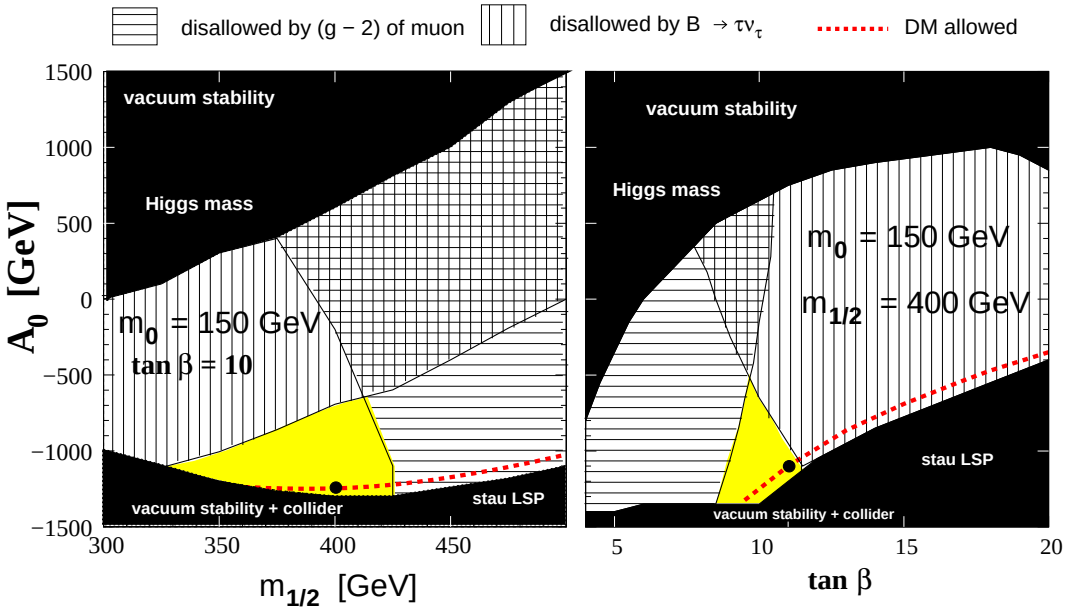

Figure 6.4: Further constraints on the cMSSM parameter space. The left panel shows constraints on the $m_{1/2}$–A_0 plane, for $m_0 = 150$ GeV and $\tan\beta = 10$. The right panel shows, similarly, constraints on the $\tan\beta$–A_0 plane for $m_0 = 150$ GeV and $m_{1/2} = 400$ GeV. Notations and conventions are the same as in Figs. 6.2 and 6.3. The dotted (red) line represents the dark-matter-compatible region, and the black dot superposed on it is a benchmark point chosen for LHC studies.

It is immediately apparent from the left panel of Fig. 6.4 that about half of the region with positive values of A_0 is ruled out by the firm constraints, and the remaining half by the $B^+ \to \tau^+\nu_\tau$ measurement. The latter has a severe impact on the $A_0 < 0$ region as well, essentially forcing us to consider large negative values of A_0 for small values of $m_{1/2}$. Including the muon $(g-2)/2$ constraint, which disfavors large values of $m_{1/2}$, then clinches the issue, permitting only another small wedge-shaped (yellow/light gray) region allowed by all the constraints. The maximum range of $m_{1/2}$ permitted by all the constraints is around 325–425 GeV, which matches tolerably well with the vertical limits of the allowed triangle in Fig. 6.3, as should be the case. The value A_0, on the other hand, is quite strictly restricted to the approximate range -625 GeV to

-1.4 TeV.

Of course, the above results are only for a fixed value $\tan\beta = 10$. Though we have already seen that jumping to a much larger value $\tan\beta = 20$ does not lead to any allowed region, it is interesting to 'zoom in' to the $\tan\beta$–A_0 plane and see the impact of all these constraints there. This is shown in the right panel of Fig. 6.4, where we set $m_0 = 150$ GeV as before, and $m_{1/2} = 400$ GeV, which lies close to its value on the left panel for which the allowed range of A_0 is maximum. Once again, the combined constraints predict a small allowed region, with a maximum range of $\tan\beta$ lying roughly between 8 and 12. If we now refer to Fig. 6.1(b), this means that the charged Higgs boson is predicted to have a mass $M_+ > 600$ GeV.

Combining all these results, therefore, we obtain a roughly polyhedral allowed region in the four-dimensional parameter space, which is enclosed in a rather small hypercube with sides approximately at

$$\begin{aligned} 100 \text{ GeV} \lessapprox \quad & m_0 \quad \lessapprox 225 \text{ GeV} , \\ 375 \text{ GeV} \lessapprox \quad & m_{1/2} \quad \lessapprox 425 \text{ GeV} , \\ -1.4 \text{ TeV} \lessapprox \quad & A_0 \quad \lessapprox -625 \text{ GeV} , \\ 8 \lessapprox \quad & \tan\beta \quad \lessapprox 12 . \end{aligned} \tag{6.30}$$

The volume of the actual allowed region is considerably smaller than that of the hypercube, given that the two-dimensional projections shown in the previous two figures are roughly triangular in shape. Compared to the large regions considered in traditional work on the cMSSM, this constitutes a rather specific region of parameter space, and encourages us to make specific predictions based on this model. One can easily argue that the qualitative features of the mass spectrum and couplings will not undergo dramatic changes from one end to the other of so small a box as this one, unless, indeed, it encloses some point(s) of instability. This is unlikely, for none of the many studies of the cMSSM parameter space have ever shown such a possibility.

The very first prediction one would naturally demand from a specific point or region in the cMSSM parameter space is whether this can adequately explain the dark-matter content of the Universe as a relic density of LSP's. The CMBR data indicate a relic density $\Omega h^2 = 0.1123 \pm 0.007$ at 95% C.L. [294]. In general, SUSY models with a low-lying mass spectrum, such as the one in question, tend to predict too large a density of LSP's unless these are coannihilated by some reaction with a substantial crosssection. This leads to a restriction on the cMSSM parameter space, which, given the accuracy of the CMBR data, confines us, more or less, to a line passing through the four-dimensional parameter space. The dark-matter requirement is known to favor large negative values of A_0 [341–348], and it is rather gratifying to see that this line passes right through the allowed region in the parameter space discovered in this work – which seems to indicate that a SUSY explanation of dark-matter may indeed be the

correct one. The line consistent with the dark-matter requirement[7] is shown by red dots on both panels in Fig. 6.4 and may be seen to pass clearly through the allowed region, favoring a narrow range of A_0 around -1.25 TeV and $\tan\beta$ in the range $9-11$. This region is rather close to the forbidden stau LSP region, as is apparent in both panels of Fig. 6.4. In the allowed region, the lighter stau $\widetilde{\tau}_1$ is rendered very light due to the presence of a large negative $m_\tau A_\tau$ in the off-diagonal terms in the stau mixing matrix; however it is marginally heavier than the neutralino $\widetilde{\chi}_1^0$ LSP. This permits stau coannihilation with neutralinos, and reduces the relic density so that it is within the observed range.

We note that there does not seem to be any á priori reason for the region allowed by the low-energy constraints to match with the dark matter-compatible region, since the low-energy constraints come from processes quite different from those that control the relic density. Nevertheless, the fact that the two regions do show some overlap encourages us to argue that we are now converging on the correct region in the hitherto-unknown parameter space. We may, therefore, make bold as to venture some predictions regarding the collider signals for this range of parameter space, especially in the context of the LHC.

In order to make a clear prediction about the LHC signals, we choose the following benchmark point in the cMSSM parameter space:

$$m_0 = 150 \text{ GeV} , \quad m_{1/2} = 400 \text{ GeV} , \quad A_0 = -1250 \text{ GeV} , \quad \tan\beta = 10 , \quad \mu > 0 . \tag{6.31}$$

Not only does this lie inside the hypercube marked out in Eq. (6.30), but it lies well within the allowed region, and right on the line corresponding to the dark-matter requirement. In Fig. 6.4, this benchmark point is indicated by a small black circle in both panels [on top of the dotted (red) line labeled "dark matter"]. The mass spectrum and signals expected for this "golden point" will be typical of the entire allowed region, which is, after all, rather small. At this benchmark point, we get the central values of the observables to be $\text{BR}(B \to X_s\gamma) = 2.64\times10^{-4}$, $R_{\tau\nu}^{NP} = 0.993$, and $a_\mu = 13.0\times10^{-10}$. Clearly, all of these are consistent with the measurements to within 2σ, though $R_{\tau\nu}^{NP}$ only barely survives the 2σ bound.

Let us first discuss the cMSSM mass spectrum expected with this benchmark point. We calculate[8] the mass spectrum and the branching ratios using the code SUSY-HIT [349] and taking $m_t = 173.1$ GeV. The lightest Higgs boson h^0 is predicted to have a mass around 119 GeV, which is consistent with current bounds, but lies precisely in the range where its detection is most problematic because of large QCD backgrounds at the LHC. In fact, a light Higgs boson of this mass range must be detected through the rare decay $h^0 \to \gamma\gamma$, which is unlikely in the 7 TeV run, and will

[7] We do not go so far as to call it a constraint, though this is not unheard of in the literature.

[8] The masses obtained using different RG evolution algorithms differ by a few GeV, and the errors from the calculation are difficult to quantify. Here we give the exact values obtained by SUSY-HIT.

require the accumulation of a fair amount of statistics even in the 14 TeV run. The heavy Higgs bosons, including the H^+, will lie in the range 835–840 GeV, which is again kinematically inaccessible in the 7 TeV run, but may be detectable at 14 TeV. We have already shown that for $\tan\beta = 10$, as taken for this benchmark point, this high value of M_+ is what allows us to evade the $B^+ \to \tau^+\nu_\tau$ constraint. Turning now to sparticles, the LSP $\widetilde{\chi}_1^0$ will have a mass of 164 GeV, with the next-to-LSP (NLSP) being, as expected, the $\widetilde{\tau}_1$ with a mass of 171 GeV. As explained above, the closeness in these masses permits the coannihilation of stau, so that the relic density is controlled. In this scenario, this stau and the lightest neutralino are the only sparticles with masses below that of the top quark, all other particles being heavier. The nearly degenerate lighter chargino $\widetilde{\chi}_1^+$ and second neutralino $\widetilde{\chi}_2^0$ lie at 315 GeV, while the other sleptons and the sneutrinos have different masses in the 200–320 GeV range. The gluino mass, however, is as high as 934 GeV and the squark masses mostly populate the range 800–900 GeV, except for the $\widetilde{b}_1$, with mass around 719 GeV, and a light stop $\widetilde{t}_1$ which lies as low as 393 GeV.

An immediate consequence of these large squark and gluino masses is that the sparticle production cross section at the LHC will be on the low side: at 7 TeV it will be around 0.4 pb at the leading order (LO), while at 14 TeV, it will have the much healthier value of 5.2 pb at LO. About 60% of these crosssections come from squark pair production, of which roughly half is due to $\widetilde{t}_1\widetilde{t}_1^*$ production alone. The $\widetilde{t}_1$ will decay to a top quark and a neutralino with a BR $\sim 2/3$, and hence, a possible signal would be a top-enriched final state with large missing transverse energy (MET). However, the enormous $t\bar{t}$ background to this process must be taken into consideration when studying this signal. The other traditional signals for SUSY – cascade decays of the gluino or squarks to charginos and heavy neutralinos, ending up in multileptons, jets, and MET – in this case provide τ-rich final states because of the low-lying $\widetilde{\tau}_1$. However, τ's coming from the decay $\widetilde{\tau}_1 \to \tau + \widetilde{\chi}_1^0$ will generally be too soft for detection, because of the small splitting $M(\widetilde{\tau}_1) - M(\widetilde{\chi}_1^0) \simeq 7$ GeV. Final states involving other charged leptons will be suppressed. This indicates that the best option to seek SUSY with this benchmark point is the final state with four or more jets and substantial MET, which can arise from cascade decays involving only strongly interacting sparticles and the invisible LSP.

In Fig. 6.5 we show the allowed parameter space (yellow/light gray) in the m_0–$m_{1/2}$ plane for $\tan\beta = 10$ and floating A_0 (as in Fig. 6.3), and also the ATLAS 5σ discovery limit [350] at the 7 TeV run with an integrated luminosity of 1 fb^{-1}, using the four-jets + MET channel. It may be seen that the entire parameter space allowed by low-energy constraints at 95% C.L., including our golden point, lies just outside the 5σ discovery limit of ATLAS. The ATLAS study, in fact, has shown that at neighboring points, an overall crosssection of about 1 pb is required for a 5σ discovery using the four-jets + MET channel. Making a simpleminded scaling with the predicted crosssection of 0.4 pb at our benchmark point, *one may expect a signal in this channel at the level*

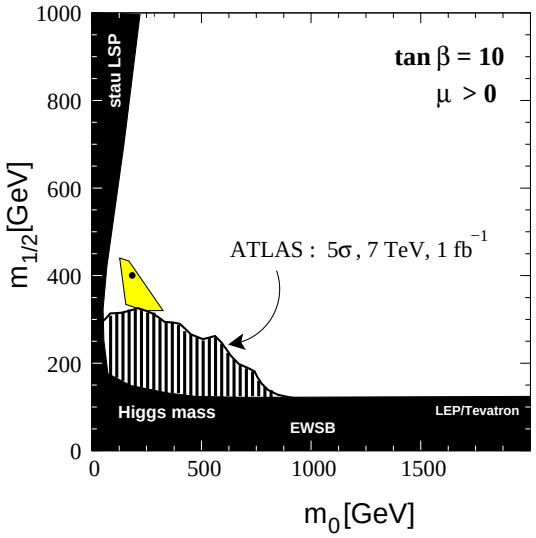

Figure 6.5: The m_0–$m_{1/2}$ plane in the cMSSM, showing the allowed region (yellow/light gray) for floating A_0, as well as the 5σ reach of the ATLAS detector at the 7 TeV run, using the jets + MET signal. The black dot inside the allowed region is the golden point discussed in the text. The entire nonshaded region inside this plot is accessible to the LHC with $\sqrt{s} = 14$ TeV with a luminosity of 10 fb^{-1}.

of about 2σ. The same conclusions can be reached using the CMS 95% exclusion plot for the 7 TeV run [296]. Thus, soon we may begin to see tantalizing hints of SUSY. [9] If this should occur, then, in the 14 TeV run, it will be easy to see a 5σ signal with even 1 fb^{-1} of data – which should collect within the first few months. Interestingly, some of the direct production modes for charginos, which are electroweak in nature, lie at the level of 5%–10% of the total crosssection. These may be difficult to detect in the 7 TeV run, but in the 14 TeV run, they are sure to provide additional signals for SUSY. With such copious production of sparticles, the LHC could indeed act as a SUSY factory, as mentioned in the Introduction.

6.5 NUHM : explaining $B^+ \to \tau^+\nu_\tau$

In the previous analysis, we have seen that the combination of constraints on the cMSSM parameter space leads to the prediction of a small value of $\tan\beta$ and hence, according to Fig. 6.1(b), the charged Higgs boson is necessarily heavy. Comparison with Fig. 6.1(a) readily shows that in this limit, the model is only just consistent with the $B^+ \to \tau^+\nu_\tau$ constraint at 95% C.L. However, if we take the position that the

[9] (Written in July 2012) Note that, the CMS [351] and ATLAS [352] collaborations have already ruled out the yellow/light gray region by 95% C.L..

2σ discrepancy between the SM and the experimental result should be *explained* by a positive NP contribution, then the cMSSM fails the test, for it actually tends to diminish the SM prediction, and barely survives exclusion in a decoupling limit. This bare survival, by the skin of its teeth, as it were, is the proximate cause of the stringent constraints on the cMSSM parameter space discussed in the previous section.

As the cMSSM is the SUSY model with the maximum number of simplifying assumptions (and hence the minimum number of free parameters), it is interesting to ask if the relaxation of one or more of these assumptions could lead to a SUSY model which actually explains, rather than merely remains consistent with, the $B^+ \to \tau^+\nu_\tau$ discrepancy. Since the NP effect in $B^+ \to \tau^+\nu_\tau$ involves the scalar sector of the cMSSM, an obvious option would be to consider a model where the parameters of the Higgs sector are given a greater degree of flexibility than in the highly constrained cMSSM. In this context, an obvious choice of model is the so-called nonuniversal Higgs-mass (NUHM) model, which is an extension of the cMSSM where the Higgs-mass parameters m_{H_1} and m_{H_2} are delinked from the universal scalar mass parameter m_0 at the GUT scale and are allowed to vary freely [353]. At the electroweak scale, these two extra parameters m_{H_1} and m_{H_2} are usually traded for the Higgsino mixing parameter μ and the pseudoscalar Higgs boson mass m_A. This model, therefore, has *six* parameters, viz. $m_0, m_{1/2}, \mu, M_A, A_0$ and $\tan\beta$.

NUHM models have been studied rather extensively, and various constraints on the six-dimensional parameter space have been found and exhibited in the literature [281,324,354–357]. What interests us here is the fact that M_A is a free parameter in the model, and it can be easily exchanged for M_+, to which it is related by the well-known SUSY relation

$$M_+^2 = M_A^2 + M_W^2 \ , \tag{6.32}$$

at tree level. We can accordingly fix m_0, $m_{1/2}$, A_0, etc. at whatever value is required to satisfy the other constraints in the cMSSM, and then claim an explanation for the $B^+ \to \tau^+\nu_\tau$ discrepancy by choosing a low M_+ and a high $\tan\beta$ – this freedom being allowed by the bigger parameter space in the theory. However, large values of $\tan\beta$ and small values of M_+ lead to large charged Higgs boson-mediated contributions to the FCNC process $B_s \to \mu^+\mu^-$, thus restricting the freedom in choosing parameter values. Here, as explained earlier, SUSY cancellations between the charged Higgs boson-mediated and the gaugino-mediated contributions come to the rescue: stringent bounds can be evaded if the gaugino masses are somewhat low, comparable to that of the light charged Higgs boson H^+. This, in turn, demands that the universal gaugino mass $m_{1/2}$ be somewhat small, compared with the other parameters, which are not so restricted.

While an exhaustive study of the NUHM parameter space vis-á-vis the present set of constraints would require a separate work in itself, it is interesting to see if the NUHM model can at all provide regions in parameter space which are consistent with all the constraints, and can simultaneously provide a NP explanation of the $B^+ \to \tau^+\nu_\tau$

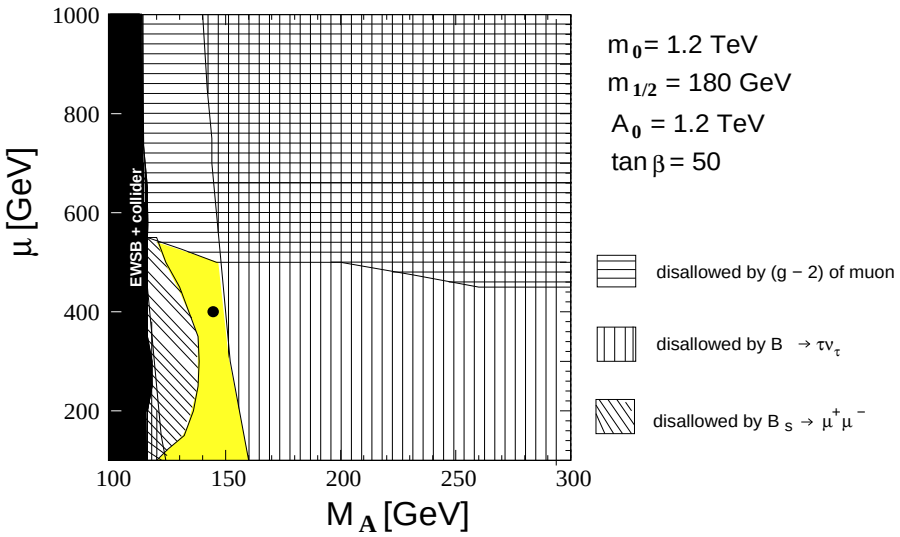

Figure 6.6: Constraints on the M_A–μ parameter space in the NUHM model. Notations and conventions are the same as in the previous plots, except that now there is a significant constraint from $B_s \to \mu^+\mu^-$ rather than $B_d \to X_s\gamma$. The yellow/light gray region is allowed by all the constraints, and the black dot inside it is a benchmark point chosen for LHC studies.

discrepancy [10]. To illustrate that this is, in fact, possible, we show in Fig. 6.6 the regions allowed by the different constraints in the m_A–μ plane, keeping all the other parameters fixed at

$$m_0 = 1.2 \text{ TeV} , \qquad m_{1/2} = 180 \text{ GeV} , \qquad A_0 = 1.2 \text{ TeV} , \qquad \tan\beta = 50 . \quad (6.33)$$

A glance at the figure will reveal that here, as in the cMSSM, there is a complementarity between the $B^+ \to \tau^+\nu_\tau$ constraint and the $(g-2)/2$ constraint, the former tending to rule out larger values of M_A and the latter tending to rule out larger values of μ, as a result of which only a small rectangular patch in the m_A–μ plane is allowed by both constraints taken together. A large portion of this remaining patch is again disallowed by the $B_s \to \mu^+\mu^-$ constraint, leaving a roughly sickle-shaped yellow/light gray region. In this region, M_A remains in the approximate range 100–150 GeV; i.e. M_+ lies roughly in the range 125–170 GeV, according to Eq. (6.32). Figure 6.1 then tells us that this is not only consistent with the experimental data, but it is precisely the range for which

[10](Written in July 2012) The constraint coming from the semileptonic decay $B \to D\tau\nu$ was not considered in this analysis because the branching ratio of $B \to \tau\nu$ was anyway in tension with that of $B \to D\tau\nu$. Therefore it is no surprise that the yellow/light gray region is not able to explain the $B \to D\tau\nu$ branching ratio which will need larger m_A or lower $\tan\beta$. It is worth mentioning that the BaBar Collaboration has recently published their updated results on the branching ratios of both $B \to D\tau\nu$ and $B \to D^*\tau\nu$ [358]. The low values for the charged Higgs mass which was required for a solution of the $B \to \tau\nu$ anomaly has also been ruled out by direct searches at the LHC [359].

the NP explanation saturates the gap between the SM prediction and the experimental central value.

As before, to be precise about the LHC signals, we choose a benchmark point, which has the fixed parameter choices of Eq. (6.33) as well as

$$M_A = 145 \text{ GeV} , \qquad \mu = 400 \text{ GeV} , \tag{6.34}$$

which is indicated in Fig. 6.6 by a small black dot in the middle of the allowed (yellow/light gray) patch. The central values of the observables at this point are $\text{BR}(B \to X_s\gamma) = 3.50 \times 10^{-4}, R_{\tau\nu}^{NP} = 1.24, \text{BR}(B_s \to \mu^+\mu^-) = 3.22 \times 10^{-8}, a_\mu = 12.8 \times 10^{-10}$, all of which are well within the 2σ range of the respective measurements. We note that the relic density of LSP's at this point is not enough to saturate the CMBR requirements, which means that this model is not ruled out by the latter, but is not a solution to that problem either.

The major features of the mass spectrum at this benchmark point are as follows: the lightest Higgs boson lies just beyond the LEP disallowed region, at 112 GeV, and, as in the cMSSM, this is a difficult mass range to search for the lightest Higgs boson. We would have to wait for enough statistics to accumulate at the 14 TeV run to see this Higgs boson in the $\gamma\gamma$ channel. The H^0 and A^0 lie at 145 GeV and may just be detectable through their decays to WW^* modes, while the charged Higgs boson H^+ lies at 170 GeV, where it will decay to $\tau^+\nu_\tau$. These may also be detectable fairly early in the 14 TeV run. The LSP, as before, is the lightest neutralino $\widetilde{\chi}_1$ with a mass of 71 GeV, which is permitted by the LEP direct search bound as applied to the NUHM [320]. The $\widetilde{\chi}_1^+$ and $\widetilde{\chi}_2^0$ lie at around 130 GeV, while the other gauginos are heavier than 400 GeV. The sleptons and squarks in this model are very heavy, lying in the range 700 GeV to 1.2 TeV, but the gluino $\widetilde{g}$ is comparatively light, having a mass of 511 GeV.

As a consequence of the low-lying gaugino states contrasted with heavy sfermions, the dominant sparticle production channels in this model turn out to be to chargino pairs $\widetilde{\chi}_1^+\widetilde{\chi}_1^-$ ($\sim 50\%$) and chargino-neutralino pairs $\widetilde{\chi}_1^\pm\widetilde{\chi}_2^0$ ($\sim 25\%$), with gluino pairs $\widetilde{g}\widetilde{g}$ bringing up the rear ($\sim 20\%$). The total crosssection in this model would be 4.4 pb at 7 TeV and 27.3 pb at 14 TeV, i.e. much larger than the earlier case of the cMSSM. The gluino production channel can give rise to the same jets + MET signal as before, as each gluino will undergo three-body decays through virtual squarks. The production crosssection for $\widetilde{g}\widetilde{g}$ pairs at 7 TeV is around 0.8 pb, which indicates that the jets + MET signal may actually be observable in the 7 TeV run at the 3σ–4σ level when 1 fb^{-1} of data have been collected. At 14 TeV, of course, a few hundred pb^{-1} of data would be enough to obtain a 5σ signal in this channel. Turning now to the chargino production modes, the rate of production of $\widetilde{\chi}_1^+\widetilde{\chi}_1^-$ indicates a crosssection for a dilepton + MET signal around 90 fb, which may not be discernible above the background, especially as the mass splitting $M(\widetilde{\chi}_1^+) - M(\widetilde{\chi}_1^0)$ is rather small. However, the $\widetilde{\chi}_1^\pm\widetilde{\chi}_2^0$ channel could lead to hadronically quiet trilepton + MET signals at the level of 74 fb, which have

smaller SM backgrounds and hence could probably be seen as more data are collected in the 7 TeV run, and would be a sure-shot option at the 14 TeV run.

Before concluding this section, we reiterate that NUHM models which explain the $B^+ \to \tau^+\nu_\tau$ discrepancy and, at the same time, remain consistent with the data on $B_s \to \mu^+\mu^-$, will generically come with light gauginos, and lead to collider signals somewhat similar to those discussed above. However, what we have studied is just one portion of the NUHM parameter space, inasmuch as we fixed m_0 and A_0 to very large values. A more comprehensive scan over the NUHM parameter space might reveal more patches consistent with all the constraints, and some of these may lead to collider signals which are different from those discussed in the context of our benchmark point. The detailed exploration of the NUHM parameter space in this context calls for a separate study.

6.6 Concluding remarks

With the commissioning of the LHC, the search for new physics beyond the Standard Model has assumed paramount importance in particle physics at the high scale. However, low-energy observables from flavor physics, like those from the decays of K, D, or B mesons, can offer indirect constraints on high scale physics. Indeed, with the high statistics available at the B factories BaBar and Belle, the freedom available for new physics has been substantially constrained. Most of the low- energy measurements have been consistent with the SM, and hence allow only a little leeway for NP. On the other hand, it is seen that the handful of measurements that indicate a $\sim 2\sigma$ deviation from the SM also restrain the NP parameters from taking arbitrary values.

The recent Belle and BaBar measurements of the branching ratio of $B^+ \to \tau^+\nu_\tau$ indicate a significant deviation from the standard model prediction. In this chapter, we have demonstrated that this measurement has a serious impact on models with minimal flavor violation involving a charged Higgs boson, ruling out a large portion of the currently allowed parameter space. In the constrained minimal supersymmetric standard model, this creates a tension between the measurements of $B^+ \to \tau^+\nu_\tau$ and the anomalous magnetic moment of the muon, unless $\tan\beta$ is small, $\mu > 0$, and A_0 takes a large negative value. In fact, a very small region of the parameter space of this model, with small values of m_0 and $m_{1/2}$, survives all the constraints at 95% C.L. It is remarkable that this specific region is still consistent with the lightest supersymmetric particle as the dark-matter. Moreover, it predicts observable supersymmetric signals in the early runs of the LHC, even perhaps at 7 TeV. We have also shown that a consistent explanation for the deviation of the $B^+ \to \tau^+\nu_\tau$ branching ratio from the standard model can be achieved in a nonuniversal Higgs-mass model, which could also predict early signals of supersymmetry at the LHC.

While we indicate a rather specific region of parameter space and specific signals

at the LHC, especially for the cMSSM, there are some caveats which need to be taken into consideration, even apart from theoretical issues in the construction of the cMSSM. The first is the issue of experimental errors on the low-energy measurements, which we have taken at the 2σ level. If these are given more latitude (e.g. taken at the 3σ level) the constraints from low-energy processes would be considerably relaxed. In particular, the $B^+ \to \tau^+\nu_\tau$ measurement would still allow wide regions in the cMSSM parameter space. However, it would still disfavor very large values of $\tan\beta \sim 50$. A more serious point is the asymptotic behavior $R^{\rm NP}_{\tau\nu_\tau} \to 1$ in the large M_+ limit, as compared to the 2σ bound $R^{\rm NP}_{\tau\nu_\tau} > 0.99$. The strong constraint on NP comes because one must squeeze the contribution of the charged Higgs bosons into the narrow region $0.99 - 1.00$. A small downward revision in the lower bound on $R^{\rm NP}_{\tau\nu_\tau}$ could allow large $\tan\beta$ values even for large M_+. Such deviations can come from a variety of sources, such as higher-order corrections, a slightly-changed value of f_B or $|V_{ub}|$, or a revised experimental result. On the other hand, a small upward revision of the allowed $R^{\rm NP}_{\tau\nu_\tau}$ band could rule out the entire gamut of MFV models with $M_+ > 200$ GeV. In particular, even the small leeway allowed for the cMSSM would then be closed. We note, therefore, that the bounds and predictions presented here are specific to the experimental limits mentioned in this chapter.

We have not made a very detailed study of the LHC signals, confining ourselves to generalities, because it is somewhat premature, at this stage, to make very definite predictions in this regard. Nevertheless, our work has highlighted the fact that if indeed we are to accept the cMSSM at face value, as most LHC studies do, then we should take the cMSSM in its entirety, i.e. all constraints from all sectors, including the low-energy sector. The next year and the years after it will be the most crucial in determining if our analysis, in fact, is on the right track.

Bibliography:

[250] B. Bhattacherjee, A. Dighe, D. Ghosh, and S. Raychaudhuri, Do new data on $B^+ \to \tau^+\nu_\tau$ decays point to an early discovery of supersymmetry at the LHC?, *Phys. Rev.* **D83** (2011) 094026, [arXiv:1012.1052].

[251] CMS Collaboration, https://twiki.cern.ch/twiki/bin/view/CMSPublic/PhysicsResults.

[252] ATLAS Collaboration, https://twiki.cern.ch/twiki/bin/view/Atlas/AtlasResults/Physics_Groups.

[253] H. P. Nilles, Supersymmetry, Supergravity and Particle Physics, *Phys. Rept.* **110** (1984) 1–162.

[254] H. E. Haber and G. L. Kane, The Search for Supersymmetry: Probing Physics Beyond the Standard Model, *Phys. Rept.* **117** (1985) 75–263.

[255] S. P. Martin, A Supersymmetry Primer, `hep-ph/9709356`.

[256] M. E. Peskin, Supersymmetry in Elementary Particle Physics, `arXiv:0801.1928`.

[257] P. Konar, K. T. Matchev, M. Park, and G. K. Sarangi, How to look for supersymmetry under the lamppost at the LHC, *Phys. Rev. Lett.* **105** (2010) 221801, [`arXiv:1008.2483`].

[258] J. Wess and J. Bagger, *Supersymmetry and Supergravity*. Princeton, 2nd ed., 1991.

[259] M. Dress, R. M. Godbole, and P. Roy, *Theory and Phenomenology of Sparticles*. World Scientific, Singapore, 2005.

[260] E. Cremmer et al., SuperHiggs Effect in Supergravity with General Scalar Interactions, *Phys. Lett.* **B79** (1978) 231.

[261] E. Cremmer et al., Spontaneous Symmetry Breaking and Higgs Effect in Supergravity Without Cosmological Constant, *Nucl. Phys.* **B147** (1979) 105.

[262] R. Barbieri, S. Ferrara, and C. A. Savoy, Gauge Models with Spontaneously Broken Local Supersymmetry, *Phys. Lett.* **B119** (1982) 343.

[263] A. H. Chamseddine, R. L. Arnowitt, and P. Nath, Locally Supersymmetric Grand Unification, *Phys. Rev. Lett.* **49** (1982) 970.

[264] L. J. Hall, J. D. Lykken, and S. Weinberg, Supergravity as the Messenger of Supersymmetry Breaking, *Phys. Rev.* **D27** (1983) 2359–2378.

[265] P. Nath, R. L. Arnowitt, and A. H. Chamseddine, Gauge Hierarchy in Supergravity Guts, *Nucl. Phys.* **B227** (1983) 121.

[266] N. Ohta, Grand Unified Theories based on local supersymmetry, *Prog. Theor. Phys.* **70** (1983) 542.

[267] C. F. Berger, J. S. Gainer, J. L. Hewett, and T. G. Rizzo, Supersymmetry Without Prejudice, *JHEP* **02** (2009) 023, [`arXiv:0812.0980`].

[268] J. Edsjo, E. Lundstrom, S. Rydbeck, and J. Sjolin, Early search for supersymmetric dark matter models at the LHC without missing energy, *JHEP* **03** (2010) 054, [`arXiv:0910.1106`].

[269] ATLAS and CMS collaboration Collaboration, N. Ozturk, Search for Supersymmetry Signatures at the LHC, arXiv:0910.2964.

[270] B. Bhattacherjee, A. Kundu, S. K. Rai and S. Raychaudhuri, "Multijet Discriminators for New Physics in Leptonic Signals at the LHC," Phys. Rev. D **81**, 035021 (2010) [arXiv:0910.4082 [hep-ph]].

[271] H. Baer, S. Kraml, A. Lessa, and S. Sekmen, Testing Yukawa-unified SUSY during year 1 of LHC: the role of multiple b-jets, dileptons and missing E_T, *JHEP* **02** (2010) 055, [arXiv:0911.4739].

[272] CMS and ATLAS collaboration Collaboration, M.-H. Genest, Prospects for R-Parity Conserving SUSY searches at the LHC, *PoS EPS-HEP2009* (2009) 221, [arXiv:0912.4378].

[273] D. Feldman, G. Kane, R. Lu, and B. D. Nelson, Dark Matter as a Guide Toward a Light Gluino at the LHC, *Phys. Lett.* **B687** (2010) 363–370, [arXiv:1002.2430].

[274] H. K. Dreiner, M. Kramer, J. M. Lindert, and B. O'Leary, SUSY parameter determination at the LHC using cross sections and kinematic edges, *JHEP* **04** (2010) 109, [arXiv:1003.2648].

[275] A. Djouadi, M. Drees, and J. L. Kneur, Constraints on the minimal supergravity model and prospects for SUSY particle production at future linear e^+e^- colliders, *JHEP* **08** (2001) 055, [hep-ph/0107316].

[276] J. R. Ellis, K. A. Olive, and Y. Santoso, Constraining supersymmetry, *New J. Phys.* **4** (2002) 32, [hep-ph/0202110].

[277] M. E. Gomez, G. Lazarides, and C. Pallis, Yukawa quasi-unification, *Nucl. Phys.* **B638** (2002) 165–185, [hep-ph/0203131].

[278] H. Baer et al., Updated constraints on the minimal supergravity model, *JHEP* **07** (2002) 050, [hep-ph/0205325].

[279] A. Djouadi, M. Drees, and J.-L. Kneur, Updated constraints on the minimal supergravity model, *JHEP* **03** (2006) 033, [hep-ph/0602001].

[280] S. Heinemeyer, X. Miao, S. Su, and G. Weiglein, B^- Physics Observables and Electroweak Precision Data in the CMSSM, mGMSB and mAMSB, *JHEP* **08** (2008) 087, [arXiv:0805.2359].

[281] O. Buchmueller et al., Likelihood Functions for Supersymmetric Observables in Frequentist Analyses of the CMSSM and NUHM1, *Eur. Phys. J.* **C64** (2009) 391–415, [arXiv:0907.5568].

[282] O. Buchmueller et al., Frequentist Analysis of the Parameter Space of Minimal Supergravity, arXiv:1011.6118.

[283] M. Drees and M. M. Nojiri, The Neutralino relic density in minimal $N = 1$ supergravity, *Phys. Rev.* **D47** (1993) 376–408, [hep-ph/9207234].

[284] G. Jungman, M. Kamionkowski, and K. Griest, Supersymmetric dark matter, *Phys. Rept.* **267** (1996) 195–373, [hep-ph/9506380].

[285] P. Nath and R. L. Arnowitt, Non-universal soft SUSY breaking and dark matter, *Phys. Rev.* **D56** (1997) 2820–2832, [hep-ph/9701301].

[286] V. D. Barger and C. Kao, Relic density of neutralino dark matter in supergravity models, *Phys. Rev.* **D57** (1998) 3131–3139, [hep-ph/9704403].

[287] G. Bertone, D. Hooper, and J. Silk, Particle dark matter: Evidence, candidates and constraints, *Phys. Rept.* **405** (2005) 279–390, [hep-ph/0404175].

[288] H. Baer, A. Mustafayev, E.-K. Park, S. Profumo, and X. Tata, Mixed higgsino dark matter from a reduced SU(3) gaugino mass: Consequences for dark matter and collider searches, *JHEP* **04** (2006) 041, [hep-ph/0603197].

[289] U. Chattopadhyay, D. Das, and D. P. Roy, Mixed Neutralino Dark Matter in Nonuniversal Gaugino Mass Models, *Phys. Rev.* **D79** (2009) 095013, [arXiv:0902.4568].

[290] S. Bhattacharya, U. Chattopadhyay, D. Choudhury, D. Das, and B. Mukhopadhyaya, Non-universal scalar mass scenario with Higgs funnel region of SUSY dark matter: a signal-based analysis for the Large Hadron Collider, *Phys. Rev.* **D81** (2010) 075009, [arXiv:0907.3428].

[291] G. Bhattacharyya, A brief review of R-parity-violating couplings, hep-ph/9709395.

[292] H. K. Dreiner, An introduction to explicit R-parity violation, hep-ph/9707435.

[293] S.-L. Chen, D. K. Ghosh, R. N. Mohapatra, and Y. Zhang, Dynamical R-parity Breaking at the LHC, arXiv:1011.2214.

[294] E. Komatsu et al., Seven-Year Wilkinson Microwave Anisotropy Probe (WMAP) Observations: Cosmological Interpretation, arXiv:1001.4538.

[295] ATLAS Collaboration ATL-PHYS-PUB-2010-010 (2010).

[296] CMS Collaboration, CMS NOTE 2010/008 (2010).

[297] H. Baer, V. Barger, A. Lessa, and X. Tata, Capability of LHC to discover supersymmetry with $\sqrt{s}$=7 TeV and 1 fb^{-1}, *JHEP* **06** (2010) 102, [arXiv:1004.3594].

[298] N. Bhattacharyya, A. Datta, and S. Poddar, SUSY darkmatter at the LHC - 7 TeV, *Phys. Rev.* **D82** (2010) 035003, [arXiv:1005.2673].

[299] B. Altunkaynak, M. Holmes, P. Nath, B. D. Nelson, and G. Peim, SUSY Discovery Potential and Benchmarks for Early Runs at $\sqrt{s} = 7$ TeV at the LHC, arXiv:1008.3423.

[300] N. Chen, D. Feldman, Z. Liu, P. Nath, and G. Peim, Low Mass Gluino within the Sparticle Landscape, Implications for Dark Matter, and Early Discovery Prospects at LHC-7, arXiv:1011.1246.

[301] S. Bornhauser, M. Drees, S. Grab, and J. S. Kim, Light Stop Searches at the LHC in Events with two b-Jets and Missing Energy, arXiv:1011.5508.

[302] G. Kane, The LHC: A 'why' machine and a supersymmetry factory, . In *Kane, Gordon (ed.) et al.: Perspectives on LHC physics* 1-11 (2008).

[303] J. Laiho, E. Lunghi, and R. S. Van de Water, Lattice QCD inputs to the CKM unitarity triangle analysis, *Phys. Rev.* **D81** (2010) 034503, [arXiv:0910.2928].

[304] UTfit collaboration Collaboration, M. Bona et al., An Improved Standard Model Prediction Of BR($B \to \tau\nu$) And Its Implications For New Physics, *Phys. Lett.* **B687** (2010) 61–69, [arXiv:0908.3470].

[305] CKMfitter Group Collaboration, J. Charles et al., CP violation and the CKM matrix: Assessing the impact of the asymmetric B factories, updated results and plots available at: http://ckmfitter.in2p3.fr , *Eur. Phys. J.* **C41** (2005) 1–131, [hep-ph/0406184].

[306] Heavy Flavor Averaging Group Collaboration, E. Barberio et al., Averages of $b-$hadron and $c-$hadron Properties at the End of 2007, arXiv:0808.1297.

[307] F. Mahmoudi, Flavor Data Constraints on the SUSY Parameter Space, *AIP Conf. Proc.* **1078** (2009) 243–246, [arXiv:0808.3952].

[308] BABAR collaboration Collaboration, B. Aubert et al., A Search for $B^+ \to \ell^+\nu_\ell$ Recoiling Against $B^- \to D^0\ell^-\bar{\nu}X$, *Phys. Rev.* **D81** (2010) 051101, [arXiv:0809.4027].

[309] The BABAR Collaboration Collaboration, P. del Amo Sanchez et al., Evidence for $B^+ \to \tau^+\nu_\tau$ decays using hadronic B tags, arXiv:1008.0104.

[310] Belle Collaboration Collaboration, K. Hara et al., Evidence for $B \to \tau^- \bar{\nu}$ with a Semileptonic Tagging Method, arXiv:1006.4201.

[311] Belle collaboration Collaboration, K. Ikado et al., Evidence of the purely leptonic decay $B \to \tau^- \bar{\nu}_\tau$, *Phys. Rev. Lett.* **97** (2006) 251802, [hep-ex/0604018].

[312] S. T'Jampens (CKMFitter Collaboration), Talk at ICHEP 2010,.

[313] G. Isidori and P. Paradisi, Hints of large tan(beta) in flavour physics, *Phys. Lett.* **B639** (2006) 499–507, [hep-ph/0605012].

[314] J. R. Ellis, S. Heinemeyer, K. A. Olive, A. M. Weber, and G. Weiglein, The Supersymmetric Parameter Space in Light of B- physics Observables and Electroweak Precision Data, *JHEP* **08** (2007) 083, [arXiv:0706.0652].

[315] W.-S. Hou, Enhanced charged Higgs boson effects in $B^- \to \tau\bar{\nu}$, $\mu\bar{\nu}$ and $b \to \tau\bar{\nu} + X$, *Phys. Rev.* **D48** (1993) 2342–2344.

[316] A. J. Buras, P. Gambino, M. Gorbahn, S. Jager, and L. Silvestrini, Universal unitarity triangle and physics beyond the standard model, *Phys. Lett.* **B500** (2001) 161–167, [hep-ph/0007085].

[317] V. Lubicz and C. Tarantino, Flavour physics and Lattice QCD: averages of lattice inputs for the Unitarity Triangle Analysis, *Nuovo Cim.* **B123** (2008) 674–688, [arXiv:0807.4605].

[318] A. G. Akeroyd and S. Recksiegel, The effect of H^{+-} on $B^{+-} \to \tau^{+-}\nu_\tau$ and $B^{+-} \to \mu^{+-}\nu_\mu$, *J. Phys.* **G29** (2003) 2311–2317, [hep-ph/0306037].

[319] A. J. Buras, P. H. Chankowski, J. Rosiek, and L. Slawianowska, $\Delta M_{d,s}, B^0_{d,s} \to \mu^+\mu^-$ and $B \to X_s\gamma$ in supersymmetry at large $\tan\beta$, *Nucl. Phys.* **B659** (2003) 3, [hep-ph/0210145].

[320] Particle Data Group Collaboration, C. Amsler et al., Review of particle physics, *Phys. Lett.* **B667** (2008) 1–1340.

[321] S. Heinemeyer, MSSM Higgs physics at higher orders, *Int. J. Mod. Phys.* **A21** (2006) 2659–2772, [hep-ph/0407244].

[322] Muon G-2 collaboration Collaboration, G. W. Bennett et al., Final report of the muon E821 anomalous magnetic moment measurement at BNL, *Phys. Rev.* **D73** (2006) 072003, [hep-ex/0602035].

[323] J. P. Miller, E. de Rafael, and B. L. Roberts, Muon g-2: Review of Theory and Experiment, *Rept. Prog. Phys.* **70** (2007) 795, [hep-ph/0703049].

[324] D. Eriksson, F. Mahmoudi, and O. Stal, Charged Higgs bosons in Minimal Supersymmetry: Updated constraints and experimental prospects, *JHEP* **11** (2008) 035, [arXiv:0808.3551].

[325] U. Chattopadhyay and P. Nath, Probing supergravity grand unification in the Brookhaven g-2 experiment, *Phys. Rev.* **D53** (1996) 1648–1657, [hep-ph/9507386].

[326] U. Chattopadhyay and P. Nath, Muon g-2 and implications for supersymmetry, *Phys. Atom. Nucl.* **65** (2002) 2101–2108, [hep-ph/0108250].

[327] E. Lunghi and J. Matias, Huge right-handed current effects in $B \to K^*(K\pi)l+l-$ in supersymmetry, *JHEP* **04** (2007) 058, [hep-ph/0612166].

[328] M. Misiak and M. Steinhauser, NNLO QCD corrections to the $B \to X_s\gamma$ matrix elements using interpolation in m_c, *Nucl. Phys.* **B764** (2007) 62–82, [hep-ph/0609241].

[329] M. Misiak et al., The first estimate of $B(\bar{B} \to X_s\gamma)$ at $O(\alpha_s^2)$, *Phys. Rev. Lett.* **98** (2007) 022002, [hep-ph/0609232].

[330] A. Freitas and U. Haisch, $\bar{B} \to X_s\gamma$ in two universal extra dimensions, *Phys. Rev.* **D77** (2008) 093008, [arXiv:0801.4346].

[331] Heavy Flavor Averaging Group Collaboration, D. Asner et al., Averages of b-hadron, c-hadron, and tau-lepton Properties, arXiv:1010.1589.

[332] P. Nath and R. L. Arnowitt, $b \to s\gamma$ decay in supergravity grand unification and dark matter, *Phys. Lett.* **B336** (1994) 395–401, [hep-ph/9406389].

[333] Search for $B_s^0 \to \mu^+\mu^-$ and $B_d^0 \to \mu^+\mu^-$ Decays in $3.7 fb^{-1}$ of $p\bar{p}$ collisions with CDF II, *CDF collaboration, CDF Public Note 9892* (2009).

[334] E. Lunghi, W. Porod, and O. Vives, Analysis of enhanced tan(beta) corrections in MFV GUT scenarios, *Phys. Rev.* **D74** (2006) 075003, [hep-ph/0605177].

[335] A. Djouadi, J.-L. Kneur, and G. Moultaka, SuSpect: A Fortran code for the supersymmetric and Higgs particle spectrum in the MSSM, *Comput. Phys. Commun.* **176** (2007) 426–455, [hep-ph/0211331].

[336] F. Mahmoudi, SuperIso: A program for calculating the isospin asymmetry of $B \to K^*\gamma$ in the MSSM, *Comput. Phys. Commun.* **178** (2008) 745–754, [arXiv:0710.2067].

[337] F. Mahmoudi, SuperIso v2.3: A Program for calculating flavor physics observables in Supersymmetry, *Comput. Phys. Commun.* **180** (2009) 1579–1613, [arXiv:0808.3144].

[338] G. Belanger, F. Boudjema, A. Pukhov, and A. Semenov, micrOMEGAs: A program for calculating the relic density in the MSSM, *Comput. Phys. Commun.* **149** (2002) 103–120, [hep-ph/0112278].

[339] G. Belanger, F. Boudjema, A. Pukhov, and A. Semenov, micrOMEGAs2.0: A program to calculate the relic density of dark matter in a generic model, *Comput. Phys. Commun.* **176** (2007) 367–382, [hep-ph/0607059].

[340] M. S. Carena and H. E. Haber, Higgs boson theory and phenomenology. ((V)), *Prog. Part. Nucl. Phys.* **50** (2003) 63–152, [hep-ph/0208209].

[341] V. A. Bednyakov, S. G. Kovalenko, H. V. Klapdor-Kleingrothaus, and Y. Ramachers, Is SUSY accessible by direct dark matter detection?, *Z. Phys.* **A357** (1997) 339–347, [hep-ph/9606261].

[342] V. A. Bednyakov, H. V. Klapdor-Kleingrothaus, and S. G. Kovalenko, Superlight neutralino as a dark matter particle candidate, *Phys. Rev.* **D55** (1997) 503–514, [hep-ph/9608241].

[343] A. Bottino, F. Donato, N. Fornengo, and S. Scopel, Probing the supersymmetric parameter space by WIMP direct detection, *Phys. Rev.* **D63** (2001) 125003, [hep-ph/0010203].

[344] V. A. Bednyakov, H. V. Klapdor-Kleingrothaus, and V. Gronewold, Squark-, slepton- and neutralino-chargino coannihilation effects in the low-energy effective MSSM, *Phys. Rev.* **D66** (2002) 115005, [hep-ph/0208178].

[345] J. R. Ellis, K. A. Olive, Y. Santoso, and V. C. Spanos, High-Energy Constraints on the Direct Detection of MSSM Neutralinos, *Phys. Rev.* **D69** (2004) 015005, [hep-ph/0308075].

[346] L. S. Stark, P. Hafliger, A. Biland, and F. Pauss, New allowed mSUGRA parameter space from variations of the trilinear scalar coupling A0, *JHEP* **08** (2005) 059, [hep-ph/0502197].

[347] L. Calibbi, Y. Mambrini, and S. K. Vempati, SUSY-GUTs, SUSY-Seesaw and the Neutralino Dark Matter, *JHEP* **09** (2007) 081, [arXiv:0704.3518].

[348] U. Chattopadhyay, D. Das, A. Datta, and S. Poddar, Non-zero trilinear parameter in the mSUGRA model - dark matter and collider signals at Tevatron and LHC, *Phys. Rev.* **D76** (2007) 055008, [arXiv:0705.0921].

[349] A. Djouadi, M. M. Muhlleitner, and M. Spira, Decays of Supersymmetric Particles: the program SUSY-HIT (SUspect-SdecaY-Hdecay-InTerface), *Acta Phys. Polon.* **B38** (2007) 635–644, [hep-ph/0609292].

[350] ATLAS collaboration Collaboration, J. Dietrich, The ATLAS discovery reach for SUSY models with early data, arXiv:1005.2034.

[351] CMS Collaboration, Physics Analysis Summary, Report No PAS-SUS-12-005 (2012).

[352] ATLAS Collaboration, Report No ATLAS-CONF-2012-033 (Moriond 2012).

[353] V. Berezinsky et al., Neutralino dark matter in supersymmetric models with nonuniversal scalar mass terms, *Astropart. Phys.* **5** (1996) 1–26, [hep-ph/9508249].

[354] J. R. Ellis, K. A. Olive, and Y. Santoso, The MSSM Parameter Space with Non-Universal Higgs Masses, *Phys. Lett.* **B539** (2002) 107–118, [hep-ph/0204192].

[355] J. R. Ellis, T. Falk, K. A. Olive, and Y. Santoso, Exploration of the MSSM with Non-Universal Higgs Masses, *Nucl. Phys.* **B652** (2003) 259–347, [hep-ph/0210205].

[356] H. Baer, A. Mustafayev, S. Profumo, A. Belyaev, and X. Tata, Direct, indirect and collider detection of neutralino dark matter in SUSY models with non-universal Higgs masses, *JHEP* **07** (2005) 065, [hep-ph/0504001].

[357] J. Ellis, K. A. Olive, and P. Sandick, Update on the Direct Detection of Dark Matter in MSSM Models with Non-Universal Higgs Masses, *New J. Phys.* **11** (2009) 105015, [arXiv:0905.0107].

[358] J. P. Lees *et al.* [BaBar Collaboration], "Evidence for an excess of $\bar{B} \to D^{(*)}\tau^-\bar{\nu}_\tau$ decays," arXiv:1205.5442 [hep-ex].

[359] S. Chatrchyan *et al.* [CMS Collaboration], Phys. Lett. B **713**, 68 (2012) [arXiv:1202.4083 [hep-ex]].

Chapter 7

Conclusions

Over the past decade, there have been many measurements of various B decays. To date, there is no discrepancy with the standard model (SM). However, there have been several results which show possible hints of physics beyond the SM, particularly in $b \to s$ transitions. In the most recent of these, the muon forward-backward asymmetry in $\bar{B}^0_d \to \bar{K}^* \mu^+ \mu^-$ has been found to deviate slightly from the SM predictions. If this is indeed due to the presence of new physics (NP), it implies that there is new physics in $b \to s \mu^+ \mu^-$ decays.

In this thesis, we consider all possible Lorentz structures of NP in the transition $b \to s \mu^+ \mu^-$. We perform a general analysis that includes NP vector-axial vector (VA), scalar-pseudoscalar (SP), and/or tensor (T) $b \to s \mu^+ \mu^-$ operators. If such new couplings are present, they will affect a number of decays: $\bar{B}^0_s \to \mu^+ \mu^-$, $\bar{B}^0_d \to X_s \mu^+ \mu^-$, $\bar{B}^0_s \to \mu^+ \mu^- \gamma$, $\bar{B}^0_d \to \bar{K} \mu^+ \mu^-$, $\bar{B}^0_d \to \bar{K}^* \mu^+ \mu^-$. Here we compute the effects of such NP operators, individually and in all combinations, on these decays.

Given that our aim is to find NP signals, and then, using them, to identify the Lorentz structure of the NP, it is crucial to use observables whose values are predicted precisely within the SM. That is, one must ensure that these predictions have small hadronic uncertainties. We follow this prescription throughout our analysis. For example, in $\bar{B}^0_d \to \bar{K}^* \mu^+ \mu^-$, we present the general angular analysis in the presence of NP operators. We note that there are several observables whose hadronic uncertainties in the SM are small. These include the well-known zero crossing of A_{FB} and the vanishing of $A_T^{(2)}$ for low q^2. We also define a new observable A_{LT} in $\bar{B}^0_d \to \bar{K}^* \mu^+ \mu^-$ that also has a zero crossing in the SM with small hadronic uncertainties.

In a similar vein, in $\bar{B}^0_d \to \bar{K} \mu^+ \mu^-$, where the SM prediction for the forward-backward asymmetry A_{FB} is zero, we find that NP can produce a large nonzero A_{FB}. We show that, in the low-q^2 region, A_{FB} for new-physics operators is independent of form factors in the large-energy limit. This indicates small hadronic uncertainties in the A_{FB} predictions and hence A_{FB} measurements in the low-q^2 region can be used to extract the parameters of the NP operators, to a very good approximation, without form-factor uncertainties.

As far as CP violating observables are concerned we consider

- CP violation in the differential branching ratio (A_{CP}), and

- CP violation in the forward-backward asymmetry (ΔA_{FB}).

In addition, for $\bar{B}^0_d \to \bar{K}^* \mu^+ \mu^-$, we analyze

- the CP asymmetry in the longitudinal polarization fraction (Δf_L),
- the CP asymmetries $\Delta A_T^{(2)}$ and ΔA_{LT} arising in the angular distributions, and
- the triple-product (TP) CP asymmetries $\Delta A_T^{(im)}$ and $\Delta A_{LT}^{(im)}$.

We determine the constraints on the coupling constants in the effective NP operators by using the currently available data. On the basis of these limits and general arguments, we expect that the CP-violating quantities in most of the modes can only be sensitive to the vector-axial vector (VA) couplings, while the scalar-pseudoscalar (SP) and the tensor (T) NP operators can only contribute, if at all, to certain TP asymmetries. Our later detailed exploration of the allowed parameter space for all the NP couplings vindicates this argument. The effects of SP and T NP operators are therefore discussed only briefly.

On the other hand, the VA operators can have a significant impact on the CP-violating observables. The SM predicts $A_{CP}(q^2) \lesssim 10^{-3}$ for all the modes, while VA NP operators allow this quantity to be as large as $\sim 10\%$ (for $\bar{B}^0_d \to X_s \mu^+ \mu^-$, $\bar{B}^0_d \to \bar{K} \mu^+ \mu^-$ and $\bar{B}^0_d \to \bar{K}^* \mu^+ \mu^-$) and even up to $\sim 30\%$ for $\bar{B}^0_s \to \mu^+ \mu^- \gamma$. Even ΔA_{FB}, expected to be $\lesssim 10^{-4}$ in the SM, can be enhanced up to $\sim 10\%$ (for $\bar{B}^0_d \to X_s \mu^+ \mu^-$) and up to $\sim 40\%$ (for $\bar{B}^0_s \to \mu^+ \mu^- \gamma$). While ΔA_{FB} in $\bar{B}^0_d \to \bar{K} \mu^+ \mu^-$ stays zero even with VA NP, its value in $\bar{B}^0_d \to \bar{K}^* \mu^+ \mu^-$ may be enhanced to $\sim 10\%$ from its SM expectation of $\lesssim 10^{-4}$.

In $\bar{B}^0_d \to \bar{K}^* \mu^+ \mu^-$ the SM predicts $\Delta f_L \lesssim 10^{-4}$, while VA NP operators allow this quantity to be enhanced up to $\sim 10\%$. $\Delta A_T^{(2)}$, ΔA_{LT}, $A_T^{(im)}$ and $A_{LT}^{(im)}$ are all zero in the SM. VA NP operators can enhance $\Delta A_T^{(2)}$ up to $\sim 12\%$, $A_T^{(im)}$ even up to $\sim 50\%$, and $A_{LT}^{(im)}$ up to $\sim 10\%$. ΔA_{LT} can not be enhanced more than $\sim 3\%$ even in the presence of VA NP operators. Note that while in almost all the cases the impact of the left-handed VA NP couplings $R_{V,A}$ is dominant, for the TP asymmetry $\Delta A_T^{(im)}$, the $R'_{V,A}$ couplings play a dominating role.

TP's can also be generated by NP-NP interference. However, we do not find large effects. The interference of new tensor C_{TE} and C_T operators can enhance $A_T^{(im)}(q^2)$ up to 3% at low q^2, while SP-T interference can increase $A_{LT}^{(im)}(q^2)$ up to only 0.2% at low q^2.

It is quite possible that if the NP is of the VA type, its presence would first be indicated through the CP-conserving/CP-averaged quantities. However, the CP-violating signals considered in this thesis are so robust (orders of magnitude more than the SM predictions) that these may be the ones that will unambiguously establish the presence of NP of the VA kind. Moreover, hadronic uncertainties play a very minor

role in the CP-violating asymmetries considered in this thesis. A combined analysis of CP-violating and CP-conserving signals may allow even the determination of the magnitudes and phases of the NP coupling constants, in addition to confirming the NP Lorentz structure.

In the last part of the thesis we have shown that the combined effect of low-energy measurements – those consistent with the SM (e.g. the branching ratios of $B_d \to X_s\gamma$ and $B_s \to \mu^+\mu^-$) as well as those showing deviations from the SM (e.g. the anomalous magnetic moment of the muon, and the branching ratio of the $B^+ \to \tau^+\nu_\tau$) – results not only in indicating new physics, but also in pinpointing the relevant new physics parameters. In particular, we have pointed out that the latest measurement of $B^+ \to \tau^+\nu_\tau$ branching ratio has a large impact on a large class of NP models, especially those which include a charged Higgs boson H^+. In fact, the decay $B^+ \to \tau^+\nu_\tau$, by itself, can constrain most of the models with minimal flavor violation that involve an H^+. This is because the latest measurement gives a branching ratio $\sim 2\sigma$ more than the SM prediction. If this discrepancy is to be explained by a MFV model, one needs very light charged Higgs bosons ($M_+ \lesssim 200$ GeV) and large $\tan\beta$ ($\gtrsim 20$). On the other hand, a heavy charged Higgs boson ($M_+ \gtrsim 300$ GeV) and a small $\tan\beta$ can be barely consistent with the data to within 2σ, but cannot be considered an explanation for the gap between theory and experiment. This is a general result that can be applied to any member of the MFV models, and we choose to apply it to the constrained MSSM, which is motivated by mSUGRA and is one of the most predictive SUSY models.

In cMSSM models, the charged Higgs boson is typically heavy, so that only the low $\tan\beta$ region survives the $B^+ \to \tau^+\nu_\tau$ measurement. When combined with the anomalous magnetic moment of the muon, the fate of even this region is in jeopardy: indeed, for a vanishing universal trilinear coupling A_0, there is no region in the cMSSM parameter space that is consistent with both these measurements to 95% C.L.. The situation can only be salvaged with a large and negative A_0, and that too for an extremely small region in the m_0–$m_{1/2}$ plane. The combined low-energy data thus pinpoint us to a very specific location (the golden point) in the five-dimensional parameter space of cMSSM: $\mu > 0,\ A_0 \approx -1.25$ TeV, $\tan\beta \approx 10$, $m_0 \approx 150$ GeV, $m_{1/2} \approx 400$ GeV. It is remarkable that for part of this specific region, including the golden point, the mass and coupling of the LSP are exactly such that it can account for all the dark-matter in the Universe. This may either be a coincidence, or an indication that we are on the right track in our quest.

If we indeed are on the right track, and the golden point of the cMSSM is actually the NP that we have all been looking for, then we may not have to wait too long for its discovery. Since the values of m_0 and $m_{1/2}$ at this point are rather small, at the LHC, one expects a weak 2σ signal in the jets + MET channel even in the 7 TeV run with 1 fb^{-1} of integrated luminosity, and a 5σ discovery early in the 14 TeV run with just 1 fb^{-1} of data.

While the above suggestive coincidence is quite appealing, and the prospects of the

detection of SUSY during the early parts of the 14 TeV run quite enticing, even at the golden point the model barely survives the 95% limit bounds and does not offer any help at all in explaining the $B^+ \to \tau^+\nu_\tau$ data – the absence of a light H^+ makes it impossible for the cMSSM to do so. We therefore explore a related but less constrained model, the NUHM, where the charged Higgs boson mass can be considered to be a free parameter. Here the presence of an extra parameter works wonders for explaining the low-energy data, covering the entire experimentally allowed region, including the central value. This model can also lead to rather spectacular trilepton + MET signals at the LHC, which may become detectable soon.

A word of caution while reading this thesis in in order. This thesis is based on papers written in 2010 and 2011. The experimental numbers used in this thesis have been updated by the LHC using larger data samples. Analyses of the various decay modes presented in this thesis with the new available data may result in improvements in the constraints on the NP operators. The impact of major updates have been pointed out in the footnotes.

We will finish by saying that the manifestation of New Physics, if any, in the dynamics of flavour transitions is likely to be highly non-generic and subtle. Thus the interpretation of any NP signal would require a large amount of data with high precision. If the New Physics scale is sufficiently low then it will be observed through the production of new quanta at the LHC. In that case we have to study the impact of such New Physics on flavour dynamics. It is not guaranteed that such new quanta will have any effect on flavour physics but even then this is an important piece of information. It might also be that no new particle will be discovered and no deviation from the SM predictions will be identified. Yet it does not invalidate the theoretical arguments and experimental evidence pointing to the incompleteness of the SM. It merely means that we have to increase the sensitivity of our probes, either at the future hadron colliders or a Super-flavour factory with a luminosity of order 10^{36} cm^{-2} s^{-1} or more. Such efforts are indispensable for our understanding of the true nature of the underlying microscopic dynamics.
